N° d'ordre : 4743

THÈSE

présentée à

L'UNIVERSITÉ BORDEAUX I

ÉCOLE DOCTORALE DES SCIENCES CHIMIQUES

par **Christopher SMITH**

pour obtenir le grade de

DOCTEUR

SPÉCIALITÉ : **POLYMÈRES**

****

Synthèse de polyuréthanes par organo-catalyse dans le dioxyde de carbone supercritique

****

Soutenue le 20 Décembre 2012

Après avis de :

JEROME Christine	Professeur, Université de Liège, CERM	**Rapporteur**
DESTARAC Mathias	Professeur, Université de Toulouse, LHFA	**Rapporteur**

Devant la commission d'examen formée de :

JEROME Christine	Professeur, Université de Liège, CERM	**Rapporteur**
DESTARAC Mathias	Professeur, Université de Toulouse, LHFA	**Rapporteur**
COSTA GOMES Margarida	Directrice de recherche, CNRS, ICCF	**Examinateur**
TATON Daniel	Professeur, Université de Bordeaux, LCPO	**Président**
TASSAING Thierry	Directeur de recherche, CNRS, ISM	**Directeur de thèse**
CRAMAIL Henri	Professeur, Université de Bordeaux, LCPO	**Directeur de thèse**
CLOUTET Eric	Directeur de recherche, CNRS, LCPO	**Invité**

Remerciements

Tout d'abord je voudrais remercier Christine Jérôme, Mathias Destarac, Margarida Costa Gomes et Daniel Taton pour l'intérêt qu'ils ont porté à ce travail et pour leurs commentaires pertinents.

Un grand merci à Henri Cramail, Thierry Tassaing et Eric Cloutet de m'avoir donné l'opportunité d'effectuer ce projet stimulant et pour leur aide, conseils et suggestions tout au long de ces trois ans. Merci de m'avoir initié à la chimie des polymères et à la spectroscopie vibrationnelle et de m'avoir transmis une vue panoramique du sujet.

Je voudrais également remercier tous les membres de l'ANR Polygreen avec lesquelles j'ai pu engager des discussions fructueuses, à savoir Yannick Landais, Frédéric Robert, Benoît Gadenne, Daniel Taton, Jérôme Alsarraf, Stéphanie Foltran, Lise Maisonneuve et Arvind More.

Il y a beaucoup de personnes qui permettent l'aboutissement d'une thèse à travers leur aide au jour le jour et je tiens à les remercier. Tout d'abord merci à Patrick Garrigues, Nicolas Guidolin et Anne-Laure Wirotius pour leur aide, respectivement avec la microscopie électronique à balayage, la GPC et la RMN. Dans le groupe spectroscopie merci à Thierry Buffeteau, Joseph Grondin, Nicolas Daugey et Sébastien Bonhommeau qui m'ont donné des conseils tant pour des manips spécifiques que pour des soucis informatiques. Dans les deux laboratoires je tiens à remercier également les gens qui ont permis le bon fonctionnement quotidien (Bernadette, Mimi, Loïc, Collette, Christian) et ceux qui ont facilité les démarches administratives (Catherine, Corinne, Nicole).

Last but not least, MERCI à tous les occupants du LCPO et du groupe spectroscopie de l'ISM pour la bonne ambiance dans les deux laboratoires, et plus particulièrement, Thomas, Lise, Na, Stéphanie, Flavio, Enora et Aude.

Abbreviations **2**

Introduction Générale **5**

Chapter I Background and Literature Review **9**

I-1 Synthesis of Polyurethanes **12**

I-1-1 Generalities 12

I-1-2 Isocyanate reactions in polyurethane chemistry 13

I-1-3 Catalysis 15

I-1-3-1 Amidines and Guanidines *17*

I-1-3-2 Amine N-oxides *19*

I-1-3-3 N-heterocyclic carbenes *20*

I-2 Carbon Dioxide as a Solvent for Chemical Processes **21**

I-2-1 Supercritical Carbon Dioxide 22

I-2-1-1 Properties of Supercritical CO_2 .... *23*

I-2-2 Polymers in CO_2 23

I-2-2-1 Solubility of polymers in CO_2 .... *23*

I-2-2-1-1 Fluorinated polymers 24

I-2-2-1-2 Silicones 25

I-2-2-1-3 Organic polymers 26

I-2-2-1-4 Effect of polymer end-group 27

I-2-2-2 Polymerisation in CO_2 .... *28*

I-2-2-2-1 Dispersion Polymerisation in CO_2 29

I-2-2-2-2 Dispersion Polymerisation of Polyurethanes 35

I-2-3 Organocatalysis in CO_2 37

I-3 Conclusions **43**

Chapter II Kinetic Studies of a Model Urethane Forming Reaction in Supercritical Carbon Dioxide **45**

II-1 Introduction **48**

II-2 Catalyst screening on a model reaction **48**

II-2-1 Reaction parameters 48

II-2-2 Choice of catalysts...49

II-2-2-1 pK_{BHX} database...*51*

II-2-3 IR spectra of the solvent, reactants and product 54

II-2-3-1 Carbon dioxide...*54*

II-2-3-2 n-Butanol..*55*

II-2-3-3 2,4-TDI...*56*

II-2-3-4 Dibutyl 4-methyl-1,3-phenylenedicarbamate..*57*

II-2-4 Reaction kinetics with 5 mol% catalyst..58

II-2-4-1 N-H peak shape...*61*

II-2-5 Reaction kinetics with 1 mol% catalyst..66

II-2-6 Reaction kinetics with phenyl isocyanate..68

II-2-7 NMR and Raman analysis of product residues 69

II-2-8 Robustness of organocatalysts versus DBTDL 79

II-2-8-1 The behaviour of amidines/guanidines in the presence of CO_2: an explanation of catalytic activity...*81*

II-2-9 Effect of CO_2 on the kinetics of reaction in organic solvent................................85

II-3 Conclusions 87

II-4 Experimental Section 88

II-4-1 Infrared Set-Up..88

II-4-2 Raman Spectroscopy 89

II-4-3 Materials..89

II-4-4 Kinetic Monitoring in $scCO_2$..90

II-4-5 NMR/Raman analysis of reaction residues 91

II-4-6 Kinetic monitoring in dichloromethane solution...91

II-4-7 CO_2 absorption experiments...91

Chapter III Polymerisation in Supercritical Carbon Dioxide.....................93

III-1 Introduction..96

III-2 Precipitation Polymerisation of Polyurethanes in $scCO_2$.....................................96

III-2-1 Analysis of the Polyurethanes 98

III-2-1-1 ^{1}H NMR Spectroscopy...98

III-2-1-2 ATR-FTIR Spectroscopy 101

III-2-1-3 Raman Spectroscopy..102

III-2-2 Conclusions of precipitation polymerisations 103

III-3 Dispersion Polymerisation of Polyurethanes using Macromonomer.................104

III-3-1 Functionalisation of PDMS-$(OH)_2$ to PDMS-$(NCO)_2$.......................................104

III-3-2 Polymerisation...105

III-3-2-1 ^{1}H NMR analysis of polyurethanes..113

III-3-2-2 Incorporation of PDMS 113

III-3-2-3 Raman Imaging...115

III-3-3 Conclusions of dispersion polymerisations using macromonomer...................116

III-4 Dispersion Polymerisation of Polyurethanes using Catasurfs...........................117

III-4-1 Synthesis of Organocatasurfs 117

III-4-1-1 Synthesis using a carbonate linker 117

III-4-1-2 Synthesis via a hydrosilylation reaction..122

III-4-1-3 Thermal Stability of the Catasurfs..127

III-4-2 Polymerisation...129

III-4-2-1 Incorporation of PDMS 138

III-4-2-2 Raman Imaging...139

III-4-3 Conclusions of dispersion polymerisation using organocatasurfs 140

III-5 Summary and Outlook 140

III-6 Experimental Section...141

III-6-1 Materials..141

III-6-2 Instrumentation..142

III-6-3 High pressure reactor 143

III-6-4 Experimental Procedures...144

III-6-4-1 Synthesis of PDMS-$(NCO)_2$ 144

III-6-4-2 Synthesis of Organocatasurfs 144

III-6-4-2-1 Typical Hydrosilylation Procedure...144

III-6-4-2-2 Typical Oxidation Procedure with mCPBA 144

III-6-4-2-3 Typical Oxidation Procedure with H_2O_2 145

III-6-4-3 Precipitation Polymerisations 145

III-6-4-4 Dispersion Polymerisations with Macromonomer 146

III-6-4-5 Dispersion Polymerisations with Catasurfs..146

Conclusions Générales...**149**

Appendix...**153**

A-1 Synthesis of model compounds 156

A-2 Calculation of PDMS content in polyurethane particles by NMR 161

A-3 Calculation of PDMS content in polyurethane particles by elemental analysis.....161

A-4 Calculation of the difference in PDMS content after dispersion/centrifugation in cyclohexane...162

References **165**

Abbreviations

4-PPY: 4-pyrrolidinopyridine

ASB: anchor-soluble balance

ATR: attenuated total reflectance

ATRP: atom transfer radical polymerisation

CDI: 1,1’-carbonyldiimadazole

CL: caprolactone

COSY: correlation spectroscopy

COV: composé organique volatile

DABCO: 1,4-diazabicyclo[2.2.2]octane

DBN: 1,5-diazabicyclo[3.4.0]non-5-ene

DBTDL: dibutyltin dilaurate

DBU: 1,8-diazabicyclo[5.4.0]undec-7-ene

DCC: dicyclohexylcarbodiimide

DMAP: 4-dimethylaminopyridine

DMF: dimethylformamide

DMSO: dimethylsulfoxide

DTG: differential thermogravimetric analysis

e.e.: enantiomeric excess

eq.: equivalent(s)

FTIR: Fourrier transform infrared

GPC: gel permeation chromatography

HDI: 1,6-hexane diisocyanate

HMDI: hydrogenated methylene diphenyl diisocyanate

HPLC: high-performance liquid chromatography

HSQC: heteronuclear single quantum correlation

IPDI: isophorone diisocyanate

IR: infrared

$\boldsymbol{J}_{\mathbf{crit}}$ **:** critical molecular weight for precipitation

LCST: lower critical solution temperature

MALDI-TOF: matrix-assisted laser desorption/ionisation – time-of-flight

mCPBA : meta-chloroperbenzoic acid

MDI: methylene diphenyl diisocyanate

Mes: Mesityl

MMA: methyl methacrylate

$\mathbf{M_n}$**:** number average molecular weight

MTBD: 7-methyl-1,5,7-triazabicyclo[4.4.0]dec-5-ene

$\mathbf{M_w}$**:** weight average molecular weight

NHC: N-heterocyclic carbene

NMO: *N*-methylmorpholine-*N*-oxide

NMP: nitroxide-mediated polymerisation

NMR: nuclear magnetic resonance

p: packing parameter

PBA: poly(butyl acrylate)

P_c: critical pressure

PCL: poly(caprolactone)

P_{cp}: cloud-point pressure

PDMS: polydimethylsiloxane

PEG: poly(ethylene glycol)

PFDA: poly(1,1,2,2-tetrahydroperfluorodecyl acrylate)

PFOA: poly(1,1-dihydroperfluorooctyl acrylate)

PMA: poly(methyl acrylate)

PMMA: poly(methyl methacrylate)

PS: polystyrene

PU/PUR: polyurethane

PVAc: poly(vinyl acetate)

r.t.: room temperature

RAFT: reversible addition-fragmentation chain transfer

ROMP: ring-opening metathesis polymerisation

ROP: ring-opening polymerisation

scCO$_2$: supercritical carbon dioxide

SCF: supercritical fluid

SEC: size exclusion chromatography

SEM: scanning electron microscopy

TBD: 1,5,7-triazabicyclo[4.4.0]dec-5-ene

T_c: critical temperature

TDI: toluene diisocyanate

T_g: glass transition temperature

TGA: thermogravimetric analysis

THF: tetrahydrofuran

UCST: upper critical solution temperature

UV: ultraviolet

VOC: volatile organic compound

Vibrational spectroscopy assignments

ν: stretching

δ: in-plane deformation

γ: out-of-plane deformation

Introduction Générale

Cette thèse s'inscrit dans un projet de synthèse de polyuréthanes plus respectueuse de l'environnement. Les polyuréthanes sont des matériaux polyvalents dont les applications s'étendent des mousses de rembourrage et d'isolation aux revêtements. Les synthèses de polyuréthanes emploient souvent des catalyseurs de type organo-étain, en particulier les dicarboxylates de dibutylétain[1] mais leurs potentiels effets toxicologiques[2] pourraient conduire à une limitation de leur utilisation. D'ailleurs, l'emploi de composés organo-étain pour les revêtements de bateaux est déjà interdite en Europe.[3] Dans ce contexte, l'organo-catalyse pourrait être une alternative prometteuse et les synthèses de polymères qui y recourent sont en fort développement.[4] Par ailleurs, ces composés peuvent promouvoir des mécanismes catalytiques différents et par conséquent une sélectivité en contraste de celle observée avec les catalyseurs métalliques. Des organo-catalyseurs de type amine tertiaire sont depuis longtemps utilisés par l'industrie pour la production de polyuréthanes,[5] mais leurs activités catalytiques restent modérées, limitant leurs usages. Ainsi, la recherche pour des organo-catalyseurs plus efficaces reste d'actualité.

Cette étude vise plus particulièrement la production de polyuréthanes sous la forme de microparticules de géométrie contrôlée, sujet relativement peu étudié et qui pourrait élargir le champ d'application de ces polymères. Ce type de morphologie est déjà très utilisé dans des domaines où la rhéologie et la formulation sont des paramètres importants, comme par exemple, les peintures, les adhésifs, les liants et les plastiques antichocs.[6] Ces microparticules peuvent être produites par des techniques de polymérisation hétérogène telles que les polymérisations en émulsion et en dispersion. Ces méthodes présentent des avantages pratiques par rapport aux polymérisations en masse (contrôle de l'exothermie de la réaction, faible viscosité du milieu réactionnel). Néanmoins, elles nécessitent une grande quantité de dispersant (eau ou solvant organique), ce qui entrainent des inconvénients environnementaux tel que le rejet d'eaux polluées ou l'émission de composés organiques volatils (COV). Dans ce contexte, le dioxyde de carbone pourrait offrir une alternative séduisante : celui-ci est non toxique et disponible à faible coût en tant que déchet d'autres processus chimiques. Le CO_2 peut être facilement éliminé du milieu réactionnel et ne laisse pas de résidu sur le polymère obtenu.

D'autre part, lors des réactions en milieu dispersé, des stabilisants stériques sont communément employés afin de prévenir la coagulation des particules. Dans le CO_2, ces stabilisants sont souvent à base de PDMS ou de polymères fluorés. Ces composés peuvent avoir un impact sur les propriétés du produit fini (hydrophobicité). Ainsi, le développement de stabilisants qui peuvent être aisément éliminés en fin de réaction, pourrait permettre d'augmenter le champ d'application des matériaux formés.

En conséquence, la stratégie défendue par ce manuscrit consiste à utiliser l'organo-catalyse pour la synthèse de polyuréthanes en dispersion dans le dioxyde de carbone supercritique. Un regard sera également porté sur la nature des stabilisants.

Le premier chapitre de cette thèse est une étude bibliographique organisée en deux parties. La première concerne les polyuréthanes : leur chimie y est exposée ainsi que les catalyseurs utilisés, avec une attention toute particulière pour les organo-catalyseurs. La seconde partie traite du CO_2. Tout d'abord, ses propriétés en tant que fluide supercritique y sont reportées, suivi des réactions où il est employé en tant que solvant. Enfin des exemples de réactions organo-catalysées dans le CO_2 terminent cette section.

Les deux chapitres suivants concernent les résultats expérimentaux obtenus au cours de cette thèse.

Un criblage d'organo-catalyseur sur une réaction modèle de synthèse d'uréthane dans le CO_2 supercritique constitue le second chapitre. Le suivi des réactions *in situ* par spectroscopie FTIR permet une discussion sur l'activité et la sélectivité des catalyseurs, ainsi que sur leur compatibilité avec le CO_2.

La synthèse de polyuréthanes dans le CO_2 supercritique fait l'objet du troisième et dernier chapitre. Celui-ci débute par une comparaison des organo-catalyseurs avec le DBTDL (catalyseur à base d'étain) lors de polymérisations par précipitation. Ensuite, l'étude se concentre sur les réactions en milieu dispersé où le stabilisant est un macromonomère de PDMS. L'effet de la concentration des organo-catalyseurs est alors examiné. Enfin, le développement de composés combinant les fonctions de catalyseur et de surfactant (« catasurfs ») est décrit. Les propriétés des polyuréthanes produits et les possibilités d'élimination et de récupération des catasurfs concluent ce manuscrit.

Chapter I

Background and Literature Review

Summary

I-1 Synthesis of Polyurethanes 12

I-1-1 Generalities 12

I-1-2 Isocyanate reactions in polyurethane chemistry 13

I-1-3 Catalysis 15

I-1-3-1 Amidines and Guanidines 17

I-1-3-2 Amine N-oxides 19

I-1-3-3 N-heterocyclic carbenes 20

I-2 Carbon Dioxide as a Solvent for Chemical Processes 21

I-2-1 Supercritical Carbon Dioxide 22

I-2-1-1 Properties of Supercritical CO_2 *........ 23*

I-2-2 Polymers in CO_2 23

I-2-2-1 Solubility of polymers in CO_2 *........ 23*

I-2-2-1-1 Fluorinated polymers 24

I-2-2-1-2 Silicones 25

I-2-2-1-3 Organic polymers 26

I-2-2-1-4 Effect of polymer end-group 27

I-2-2-2 Polymerisation in CO_2 *........ 28*

I-2-2-2-1 Dispersion Polymerisation in CO_2 29

I-2-2-2-2 Dispersion Polymerisation of Polyurethanes 35

I-2-3 Organocatalysis in CO_2 37

I-3 Conclusions 43

I-1 Synthesis of Polyurethanes

I-1-1 Generalities

Polyurethanes (PUs or PURs) represent an important class of materials and are used in a wide variety of applications including coatings, sealants, elastomers, adhesives, upholstery foams and insulation foams. In 2011, they represented around 7% by weight of the European polymer demand.[7] The term 'polyurethane' actually encompasses a wide range of materials with varied chemical structures, but all have the urethane linkage in common. To date, the only industrially relevant pathway to polyurethanes remains the original route proposed by Otto Bayer in 1937, involving the reaction of polyisocyanates and polyols (scheme 1).[8]

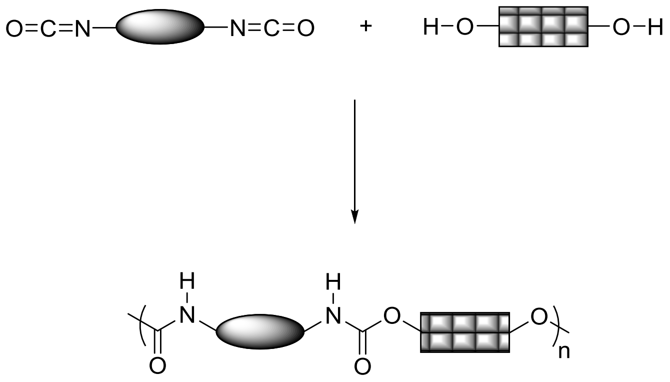

Scheme 1. Polyurethane synthesis from diisocyanates and diols.

The diisocyanate starting materials most commonly used in PUR synthesis are shown in scheme 2.[9] Aromatic diisocyanates toluene diisocyanate (TDI, often a mixture of the 2,4- and 2,6-isomers) and methylene diphenyl diisocyanate (MDI) are the most frequently employed. Aliphatic isocyanates such as isophorone diisocyanate (IPDI) are less reactive and are used in certain applications for example when yellowing of the polymer must be avoided.[10] Polyol structure can be very varied and includes short chain diols such as ethylene glycol and 1,4-butanediol as well as polymeric polyols including polyethers (e.g. poly(propylene glycol)), polyesters (e.g. poly(caprolactone)), and more recently poly(ether-carbonate)s from copolymerisation of epoxides with CO_2.[9, 11]

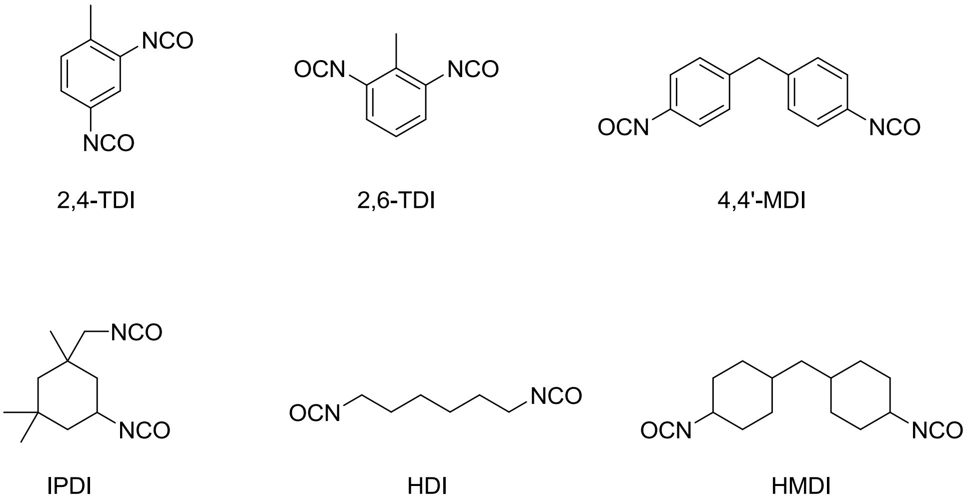

Scheme 2. Isocyanates commonly used in polyurethane synthesis.

I-1-2 Isocyanate reactions in polyurethane chemistry

Other than the primary urethane forming reaction between alcohols and isocyanates, there are many other reactions which are important in PUR chemistry (scheme 3). The extent of these reactions depends primarily on the catalyst used, the temperature of reaction and the ratio of NCO/OH groups.[12] The character of the isocyanate (aromatic/aliphatic) may also determine the products obtained.

The reaction of an isocyanate with water leads to an unstable carbamic acid. This product then decomposes to a primary amine with liberation of carbon dioxide. The amine can then react further with another molecule of isocyanate to produce a urea.[1a, 10] The carbon dioxide produced in urea formation contributes to the expansion process in polyurethane foams and this is hence often referred to as the “blow” reaction. In applications where water is not intentionally introduced into the reaction mixture, urea formation may limit the molecular weight of the polymer by decreasing the NCO/OH ratio below stoichiometry.[13]

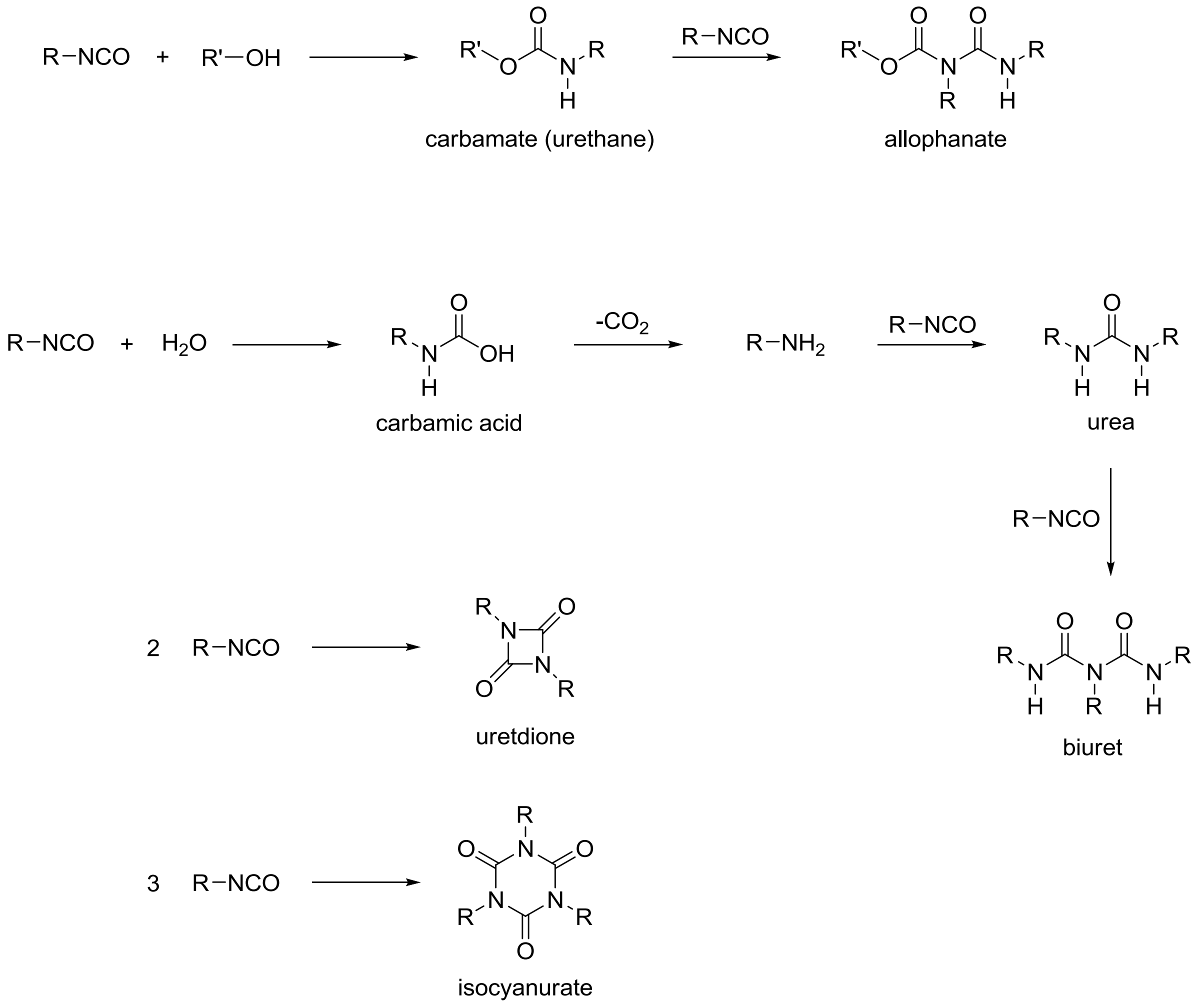
R−NCO
R'−OH
carbamate (urethane)
R−NCO
allophanate
R−NCO
H2O
carbamic acid
-CO2
R−NH2
R−NCO
urea
R−NCO
2 R−NCO
uretdione
biuret
3 R−NCO
isocyanurate

Scheme 3. Isocyanate reactions in polyurethane chemistry.

Urethanes and ureas can further react with isocyanates to produce allophanates or biurets respectively. In the absence of catalysts, aromatic isocyanates react with *O*-alkyl *N*-arylcarbamates at 125-140°C, although the reaction is reversible and the equilibrium constant is low at these high temperatures.[14] At lower temperatures the reaction can be catalysed efficiently by certain metal carboxylates.[15] The reaction can also be favoured by ammonium carboxylates and phenolates as well as certain tertiary amines but in this case the allophanate may serve as an intermediate for further reactions.[12a] Biuret is reported to form with a higher rate and equilibrium constant than allophanate.[12b]

Uretdiones (1,3-diazetidine-2,4-diones), the cyclodimers of isocyanates, are formed from isocyanates in an equilibrium reaction which is favoured at low temperatures. In the absence of catalyst the spontaneous dimerisation is extremely slow, but catalysts such as trialkylphosphines or pyridine can promote the process, particularly for aromatic isocyanates.[16] In the course of reactions between isocyanates and alcohols, uretdiones may be formed as by-products but they are generally consumed as the concentration of isocyanate falls and the equilibrium is shifted towards dissociation.[12a] They may also provide alternative routes to other products such as allophanates of isocyanurates.

The formation of isocyanurates, the cyclotrimers of isocyanates, is irreversible below about 200°C and they are the most thermodynamically stable products of isocyanate reactions below this temperature.[12a] Isocyanurates may be obtained by direct trimerisation of isocyanates in the presence of various catalysts (such as alkylphosphines and certain tertiary amines),[10, 16b] but it has been shown that formation may also be accelerated through a sequence of consecutive reactions of isocyanates with alcohols, urethanes and allophanates.[12a]

Urethane and urea formation lead to linear chain extension, while allophanate, biuret and isocyanurate formation lead to branching and cross-linking of the polymer. Some other products of isocyanate reactions are also possible, such as carbodiimides, uretimines and linear homopolymers,[1a] but these have little relevance under the usual conditions of polyurethane formation.

I-1-3 Catalysis

The most common catalysts for polyurethane synthesis are tertiary amines and organotin compounds.[1a, 17] A large variety of tertiary amine structures have been used in the polyurethane industry and many have been developed in order to control the selectivity in catalysing the isocyanate-water (“blow”) reaction or isocyanate-polyol (“gel”) reaction. Certain amines are also used to promote isocyanurate trimerization which imparts greater heat resistance to PUR foams.[10] Catalysts are often used in combination to obtain the desired properties of the material. The activity of tertiary amines generally increases with increasing basicity and decreasing steric hindrance around the nitrogen atom. For these reasons 1,4-diazabicyclo[2.2.2]octane (DABCO, scheme 4) is one of the most frequently employed catalysts.[1a, 17]

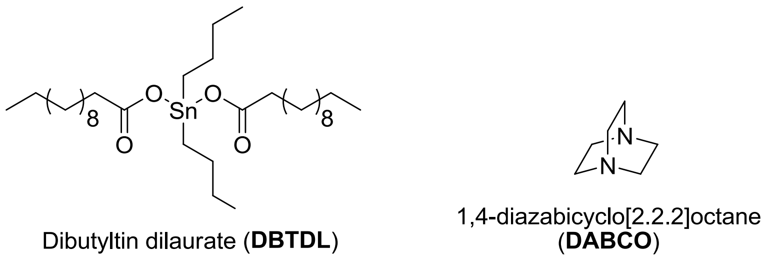
Sn
O
8
Dibutyltin dilaurate (**DBTDL**)
N
1,4-diazabicyclo[2.2.2]octane
(**DABCO**)

Scheme 4. Two of the most commonly employed polyurethane catalysts.

For tertiary amine catalysis, two possible general mechanisms are usually evoked, namely nucleophilic catalysis or base catalysis (scheme 5).[18] Nucleophilic catalysis involves the formation of an activated base-isocyanate complex, which then goes on to react with the alcohol. Alternatively, the base catalysis mechanism involves the formation of a base-alcohol complex with increased reactivity towards the isocyanate. Schwetlick *et al*. have proposed three more detailed mechanisms for base-catalysed reactions according to the basicity of the catalyst and the acidity of the alcohol (or phenol, amine, etc.).[19]

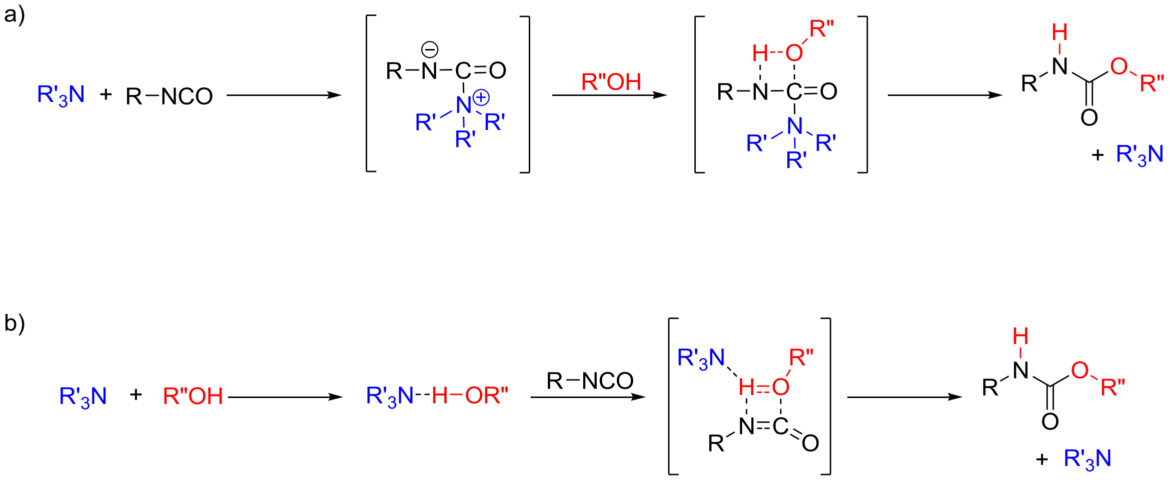

Scheme 5. Possible mechanisms of tertiary amine catalysis: a) nucleophilic catalysis; b) base catalysis.

Organotin compounds, such as dibutyltin dilaurate (DBTDL, scheme 4), show very high activity and are standard catalysts in the polyurethane industry. They are particularly useful for reactions with aliphatic isocyanates, which are less reactive than aromatic isocyanates.[1a] Tin catalysts are rather selective regarding both the polyol-isocyanate versus water-isocyanate reaction[1a, 18c] as well as urethane formation versus allophanate and isocyanurate formation.[12a] The mechanism of tin based catalysis is not firmly established and may involve activation of the isocyanate, the alcohol or both reaction partners.[1a, 20] Many other metal based catalysts exist, including compounds of zinc, lead, mercury, zirconium and bismuth.[1, 17] They are often adapted to specific applications such as delayed-action (latent) catalysis.

I-1-3-1 Amidines and Guanidines

Amidines and guanidines are strong bases with particularly high catalytic activity for the formation of urethanes (scheme 6). The earliest reports concerned acyclic guanidines (**4-6**, **8**)[18a, 21] but bicyclic guanidines (**9-10**) were later shown to give faster reaction rates.[18c] With regards to amidines, Katsamberis and Pappas equally reported much greater catalytic activity for the bicyclic substrate **1** compared to monocyclic derivatives **2** and **3**.[22] The size of the rings also has an influence on the catalyst performance with the best results obtained when the carbamimidoyl function (R_2N-C(=NR)-) is contained in a six or seven-membered ring.[18c] These findings suggest that conformational or steric factors could be important for catalytic activity.

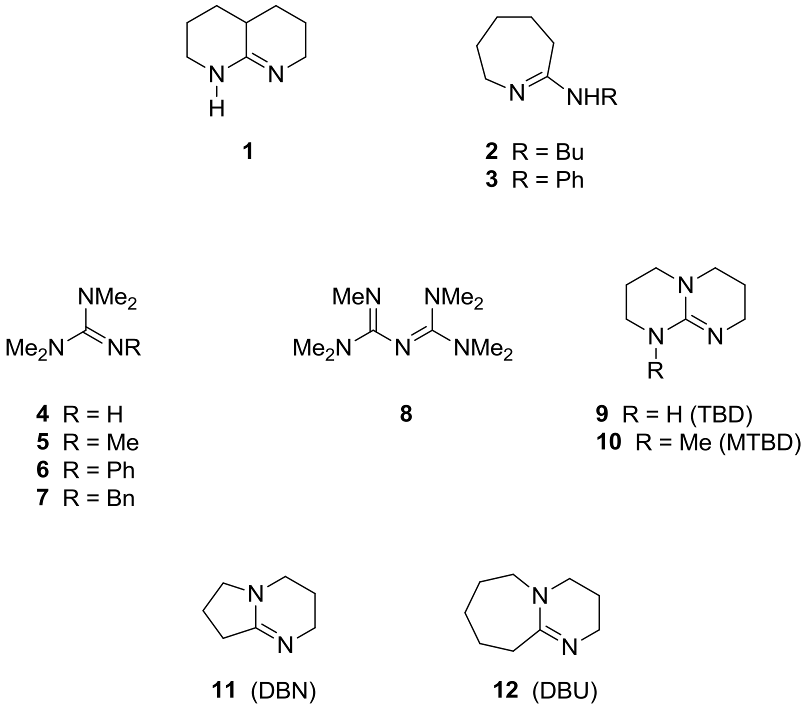

Scheme 6. Some amidines and guanidines that have been tested for their catalytic activity in urethane formation.

The bicylic amidine 1,8-diazabicyclo[4.5.0]undec-7-ene (DBU, **12**) has become a frequently employed catalyst in the polyurethane industry.[1a, 10] The salts of DBU with weak acids are also used, for example as heat sensitive catalysts. DBU and its salts are not particularly selective for the isocyanate-alcohol reaction, as demonstrated by their use in the manufacture of polyisocyanurate foams.[10] The results of kinetic studies by Schwetlick and Noack are also noteworthy; they suggested that DBU catalysis promoted a faster rate of reaction between phenyl isocyanate and butyl *N*-phenylcarbamate (allophanate formation) than between phenyl isocyanate and butanol (carbamate formation) in acetonitrile at 50°C (scheme 7).[12a]

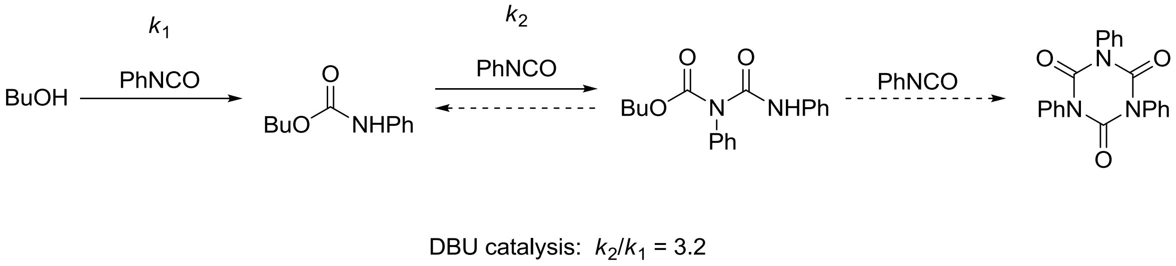

Scheme 7. Kinetic scheme for the reaction of butanol with phenyl isocyanate catalysed by DBU.

As regards bicyclic guanidines, 1,5,7-triazabicyclo[4.4.0]dec-5-ene (TBD, **9**) was found to show lower catalytic activity than the methyl substituted analogue (MTBD, **10**). This was attributed to initial reaction of the active hydrogen of TBD with isocyanate to form a less basic/nucleophilic carbamoylguanidine (scheme 8).[18c, 23] In contrast, the presence of a free N-H in acyclic guanidines has been found to give equivalent catalytic activity compared to peralkyl substrates.[53, 64a]

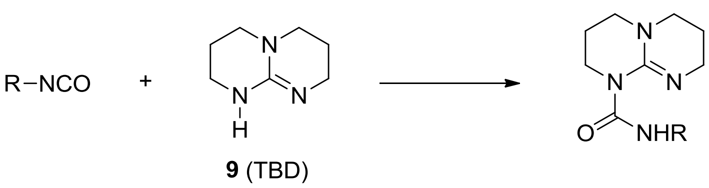

Scheme 8. The reaction of TBD with an isocyanate to form a carbamoylguanidine.

Mechanistic investigations of guanidine/amidine catalysis have cited the reactivity of these compounds with isocyanates as evidence to support a nucleophilic catalysis mechanism.[18a, 18c]

It has been known for some time that, in the absence of alcohols, amidines and guanidines form 1:2 cycloadducts with isocyanates, or in other cases, catalyse isocyanate dimerization and trimerization (scheme 9).[10, 24] Alsarraf and co-workers showed that the stability of some of the cycloadducts was substrate-dependent; while the adduct of MTBD with benzyl isocyanate could undergo alcoholysis at increased temperature, adducts of DBU or DBN could not, thus providing a possible mechanism of catalyst deactivation.[18c]

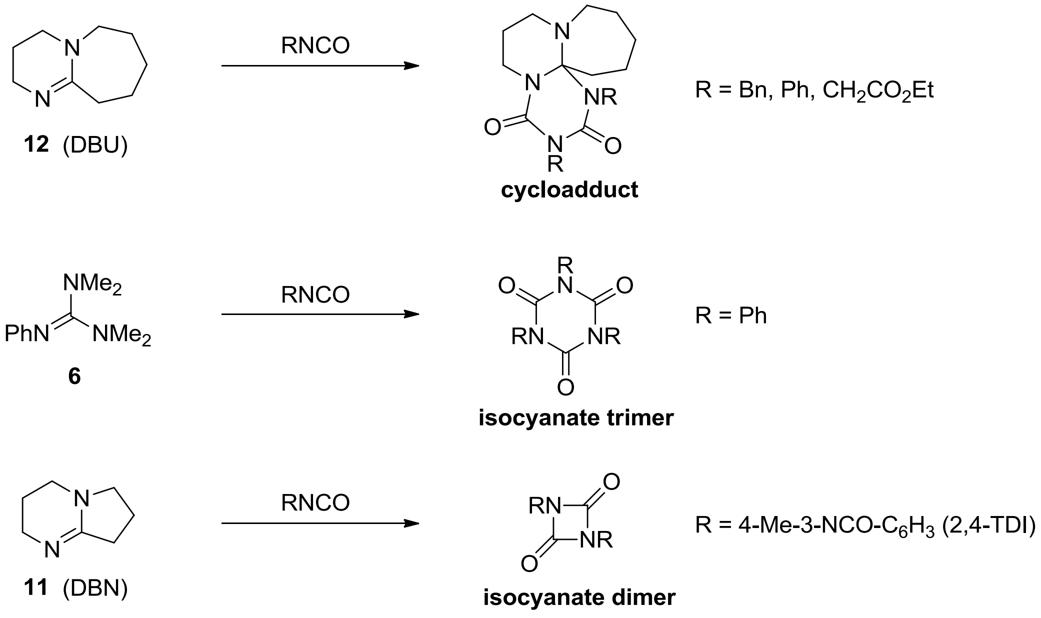

Scheme 9. Some reactions of amidines and guanidines with isocyanates.

I-1-3-2 Amine N-oxides

The rate of the isocyanate/alcohol reaction has been found to be accelerated by pyridine *N*-oxides[25], and yet more effectively, by aliphatic tertiary amine *N*-oxides.[25c] The activity of the amine oxides is greater than that of the parent amines. Considering the same two general mechanisms of catalysis as for tertiary amines, the fact that the amine oxides are less basic than the parent amines could suggest a nucleophilic rather than a base catalysis mechanism, but this fact has been accounted for by considering the greater hydrogen bonding basicity of amine oxides.[25b] On the other hand, in the absence of protic compounds, pyridine oxides are known to undergo nucleophilic addition to isocyanates (scheme 10)[26] while trimethylamine oxide catalyses trimerization,[27] implying a base-isocyanate complex.

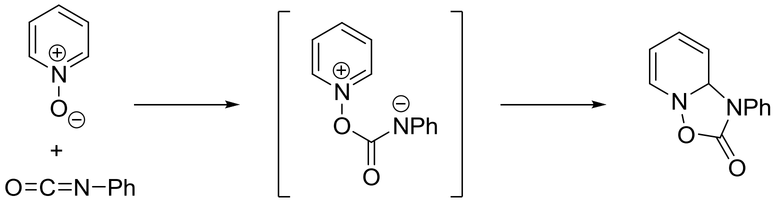

Scheme 10. The reaction of pyridine oxide with phenyl isocyanate.

I-1-3-3 N-heterocyclic carbenes

More recently an N-heterocyclic carbene (NHC, **13**, scheme 11) was shown to be an efficient catalyst for polyurethane formation.[28] However, the order of addition of the reactants was important to attain the best results and only moderate molecular weights could be obtained, suggesting deactivation of the catalyst during the polymerisation. This was attributed to a probable reaction of the catalyst with isocyanate. In the absence of alcohols, and sometimes even in their presence, NHCs can promote isocyanate dimer and trimer formation, depending on both the structure of the NHC and the nature of the isocyanate (aliphatic/aromatic).[28-29]

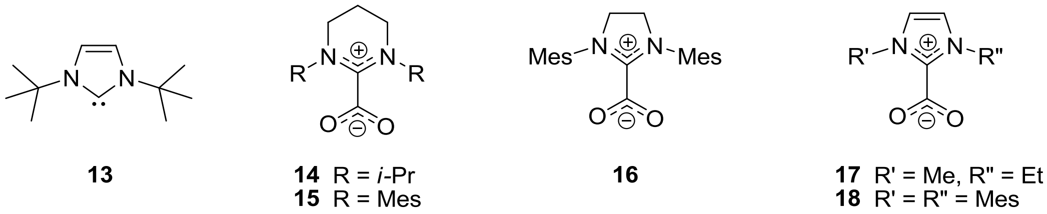

Scheme 11. NHCs and protected NHCs used in the preparation of polyurethanes.

CO_2 protected carbenes (**14**-**18**) or metal carbene complexes may also be used as latent catalysts for PUR formation.[29a, b] The CO_2-NHC adduct thermally degrades upon heating to liberate the free carbene, which may then deprotonate the alcohol. According to the proposed mechanism, the imidazolium alkoxide then catalyses PUR formation (scheme 12).

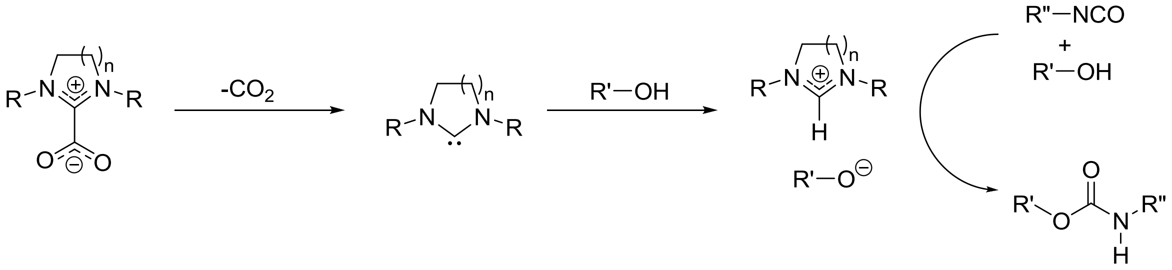

Scheme 12. The proposed mechanism for NHC catalysis of urethane formation.

NHCs thus take their place in the catalogue of organic catalysts that have been used to accelerate the formation of polyurethanes. These organocatalysts are generally highly basic compounds, but the mechanisms of catalysis remain somewhat debated. Organocatalysts are rarely as active or selective as organotin catalysts and may promote the formation of ureas, allophanates or isocyanate dimers and trimers. The application of organocatalysts to reactions conducted in CO_2 as solvent, as well as a more general examination of polymerisation in CO_2, will be considered in the next section.

I-2 Carbon Dioxide as a Solvent for Chemical Processes

Increasing environmental awareness and legislation have led a drive to develop more sustainable chemical processes. This includes a reduction in the utilization of organic solvents, which are a major contributor to the emission of volatile organic compounds (VOCs).[30] It is not surprising that carbon dioxide has attracted much attention as a replacement for conventional solvents due to a long list of advantages such as non-toxicity, non-flammability, availability at low cost and high purity, and relative chemical inertness.[30-31] In the synthesis of polymers, carbon dioxide is typically suited to heterogeneous polymerisation techniques, leading to the formation of particle morphologies. One of the major benefits of CO_2 is the ease of separation of the solvent from the reaction product. The solvent can be removed simply by depressurizing the reaction vessel, and can easily be recycled in a closed-loop cycle.[30-31] This avoids energy intensive drying steps to remove organic solvents and is also a notable advantage over other 'green' solvents such as water and ionic liquids, which may produce aqueous waste streams or where separation may be a concern.[30-31] According to the conditions of temperature and pressure, carbon dioxide may be employed as a solvent under liquid or supercritical fluid conditions. The opportunity to exploit some of the unique characteristics of supercritical fluids may therefore offer a further advantage to the use of this solvent.

I-2-1 Supercritical Carbon Dioxide

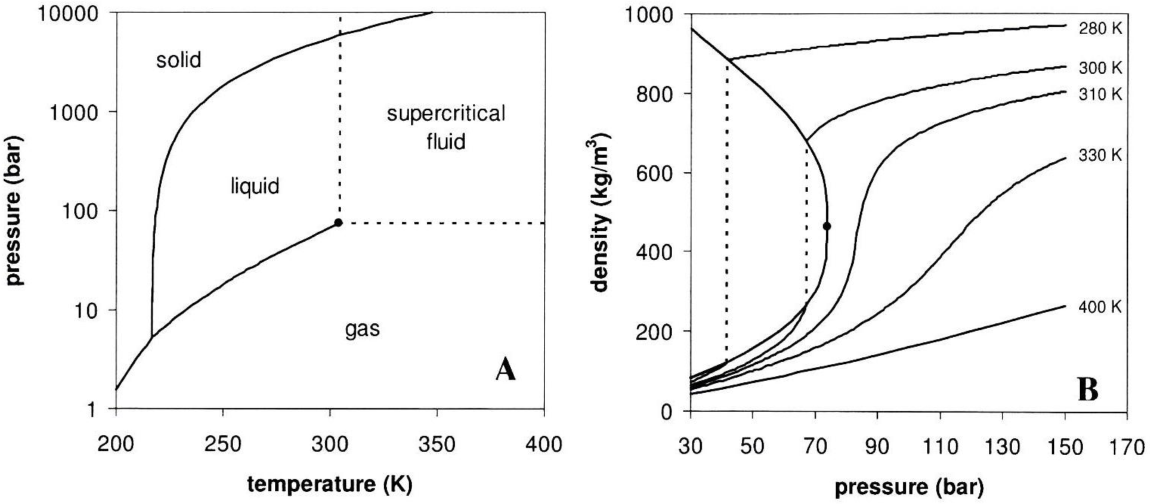

Figure 1. (A) Phase diagram of carbon dioxide showing the critical point (T_c, P_c) above which there is no longer a liquid-vapour equilibrium. (B) Density of carbon dioxide as a function of pressure at different temperatures (dashed lines mark the liquid-vapour equilibrium).[30]

The transition to a supercritical fluid can be visualised as an extension of the more common phase transitions between liquids and gases (figure 1A). Heating a liquid to its boiling point results in vaporisation, while pressurizing a gas leads to liquefaction (or solidification); we can therefore imagine that simultaneously raising both temperature and pressure of a substance will lead to opposing tendencies. If we follow the liquid-vapour co-existence curve of a substance with increasing temperature and pressure, the density of the liquid phase decreases while the density of the vapour increases. At a certain point, defined by a critical temperature (T_c) and a critical pressure (P_c), the densities of the liquid and gas converge and the two phases become indistinguishable (figure 1B). Under these conditions the substance is referred to as a supercritical fluid (SCF). The full definition of a supercritical fluid is thus "a compound, mixture or element above its critical pressure and critical temperature but below the pressure required to condense it into a solid".[32] The critical parameters of carbon dioxide are easily accessible with T_c = 31.1°C and P_c = 7.38 MPa.[31a]

I-2-1-1 Properties of Supercritical CO_2

The density of a supercritical fluid is intermediate between that of the liquid and the gas and the SCF shows somewhat ‘hybrid’ behaviour. For example, an SCF may be relatively dense and dissolve certain solids while at the same time remaining miscible with permanent gases.[31b] Another way of regarding this behaviour is to consider the inhomogeneity of the molecular distribution; on a scale of 10-100 Å, liquid-like molecular clusters are surrounded by less dense regions of compressed gas.[33] The transport properties of supercritical CO_2 (heat capacity, thermal conductivity and dynamic viscosity) vary between liquid-like or gas-like according principally to the density of the medium, with the exception of the region close to the critical point where there can be a pronounced divergence.[34] Small changes in pressure or temperature can lead to significant changes in fluid properties; CO_2 is thus considered to be a rather ‘tuneable’ solvent.[30, 31b] The favourable solvent properties of supercritical CO_2 include low viscosity, high diffusivity and excellent wetting characteristics (no surface tension).[30] It is worth noting that the use of supercritical rather than liquid CO_2 may not always result from a desire to take advantage of the specific properties of the supercritical fluid, but rather that the process in question may require a temperature above T_c, while high pressures may be necessary in order to maintain sufficient CO_2 density.[31b]

I-2-2 Polymers in CO_2

I-2-2-1 Solubility of polymers in CO_2

Since the 1990s a considerable amount of research has focused on the solubility of polymers in carbon dioxide as awareness has grown of the advantages of CO_2 as a low cost and environmentally friendly solvent for synthesis and processing. However, the solvent properties of CO_2 are difficult to assess. Carbon dioxide has a low polarizability, low dielectric constant and no permanent dipole moment, suggesting a similarity to methane or perfluoromethane.[30] On the other hand, carbon dioxide does have a considerable quadrupole moment, which acts over short distances,[35] and the possibility of specific Lewis acid-Lewis base type interactions.[31a] The solvent properties of CO_2 have been likened to toluene, acetone, hexane and pyridine according to different parameters, showing the complexity of categorizing its solvent power.[35-36] While most small molecules, whether polar or non-polar, are reasonably soluble in CO_2, many high molecular weight polymers require drastic conditions of temperature and pressure in order to dissolve.[30-31]

The solubility of polymers in CO_2 (as for any other solvent) is governed by the energy balance of the polymer-solvent interactions compared to the solvent-solvent and polymer-polymer interactions, as well as the entropy of mixing.[35] Attempts to design CO_2 soluble polymers have therefore aimed to produce polymers with low cohesive energy density (weak polymer-polymer interactions), functional groups capable of favourable interactions with CO_2, and, in order to maximise the entropy of mixing, high flexibility and free volume.[36-37] However, increasing the polymer-CO_2 interactions may also lead to an increase in polymer-polymer interactions and achieving the right balance of these factors is not straightforward. To date, only fluorinated polymers, polysiloxanes and a limited number of organic polymers have been shown to be soluble in CO_2 at easily accessible temperatures and pressures (< 100°C, < 40 MPa).[38]

Solubility in CO_2 is most commonly determined by cloud-point measurements. This involves raising the CO_2 pressure in a variable volume view cell containing a known amount of solute until a clear single-phase solution is obtained. The pressure is then decreased until the solution becomes cloudy, indicating the phase boundary.[37] Other methods of assessing solubility include high pressure FTIR measurements[39] and a gravimetric extraction technique.[40]

The solubility of polymers in CO_2 increases with pressure due to the resulting increase in solvent density. On the other hand, the solubility has a more complicated relationship with temperature, which is dependent not only on the 'usual' thermodynamic factors governing mixing but is also strongly influenced by the decreasing density of CO_2 with increasing temperature (at constant pressure).[38] This results in decreasing solvent power with increasing temperature to a first approximation. As with liquid solvents, polymer solubility is also strongly dependent on molecular weight, irrespective of chemical structure.

I-2-2-1-1 Fluorinated polymers

Fluorinated polymers such as fluorinated polyacrylates and polyethers have been shown to be readily soluble in CO_2 and some examples are shown in scheme 13 with their cloud-point pressures (P_{cp}). However, fluorination does not guarantee CO_2 solubility and some perfluorinated polymers such as poly(tetrafluoroethylene) actually have very poor solubility.[41] It may be important that fluorination imparts some polarity to the polymer.[36]

Much research has aimed to identify specific interactions between CO_2 and fluorine through FTIR, NMR or computational techniques.[36] Although the results may not have generated a consensus, favourable interactions may be due to van der Waals forces, dipole-quadrupole interactions, or Lewis acid-Lewis base interactions between carbon and fluorine as well as an H-bond between the oxygen of CO_2 and hydrogen atoms with increased acidity due to neighbouring fluorine.

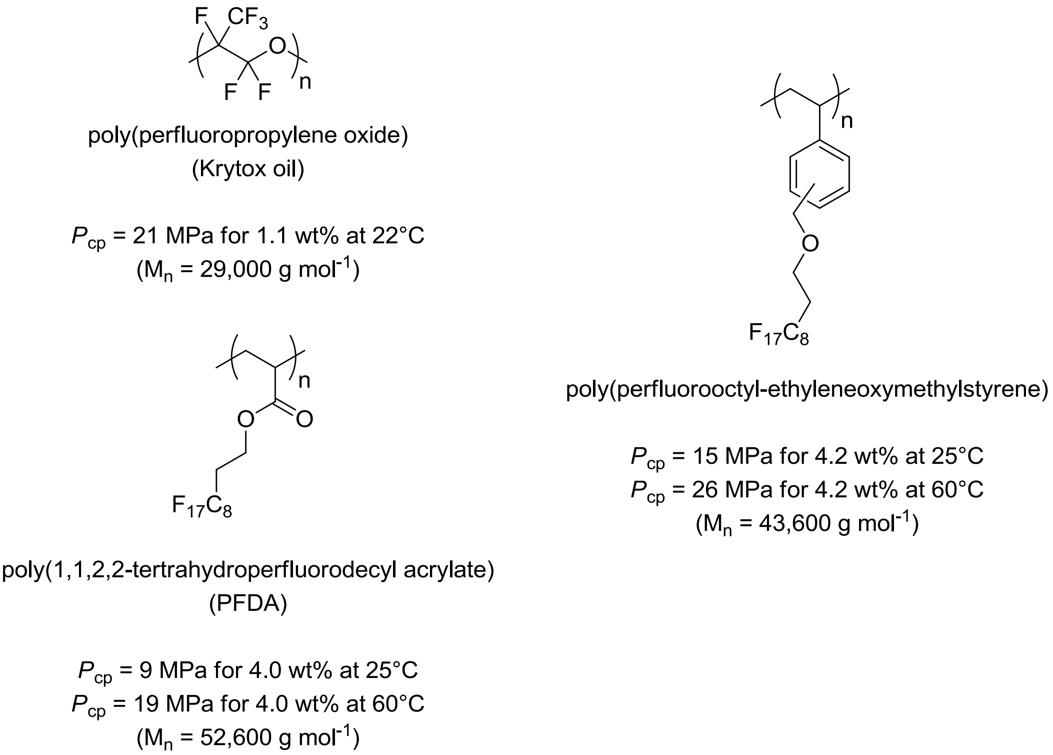
F CF3
O
n
F F
poly(perfluoropropylene oxide)
(Krytox oil)
Pcp = 21 MPa for 1.1 wt% at 22°C
(Mn = 29,000 g mol-1)
n
O O
F17C8
poly(1,1,2,2-tertrahydroperfluorodecyl acrylate)
(PFDA)
Pcp = 9 MPa for 4.0 wt% at 25°C
Pcp = 19 MPa for 4.0 wt% at 60°C
(Mn = 52,600 g mol-1)
n
O
F17C8
poly(perfluorooctyl-ethyleneoxymethylstyrene)
Pcp = 15 MPa for 4.2 wt% at 25°C
Pcp = 26 MPa for 4.2 wt% at 60°C
(Mn = 43,600 g mol-1)

Scheme 13. Fluorinated polymers with their corresponding cloud-point pressures in CO_2 (wt% vs. CO_2).

I-2-2-1-2 Silicones

Silicones are generally considered to be less CO_2-philic than fluorinated polymers and require higher pressures to dissolve in CO_2.[42] The phase behaviour of polydimethylsiloxane (PDMS) in CO_2 has been studied in some detail,[43] and differs in some respects to that of fluorinated polymers. Unlike fluorinated polymers, PDMS shows behaviour typical of a system with an upper critical solution temperature (UCST) (as well as a lower critical solution temperature (LCST)).[43a, 43d] Thus, at low temperatures there is a sharp increase in the demixing pressure (cloud-point pressure) with decreasing temperature (figure 2). The result of this is that the solubility of PDMS and fluorinated polymers become much closer at higher temperatures.[42]

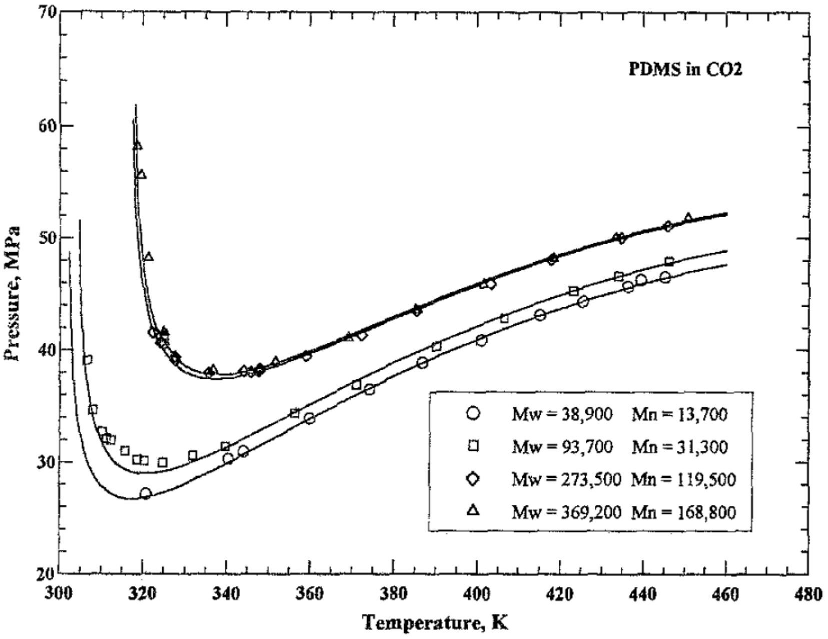

Figure 2. Demixing pressures of PDMS solutions (5 wt%) in $scCO_2$.[43a]

Although demixing pressures increase with increasing molecular weight, high molecular weight PDMS (M_w = 369,000 g mol^{-1}) can still be dissolved under moderate conditions (38 MPa for 5 wt% at 60°C).[43a] The solubility of PDMS in CO_2 is generally ascribed to its high flexibility and free volume.[35]

I-2-2-1-3 Organic polymers

The high cost of fluoropolymers and silicones and some environmental concerns have led to a drive to discover non-fluorous organic polymers which are soluble in CO_2. Poly(vinyl acetate) (PVAc) is the most CO_2 soluble organic homopolymer which has been found to date.[39a, 44] The solubility can further be improved by copolymerisation of vinyl acetate with bulky monomers such as vinyl butyrate,[45] dibutyl maleate[46] or vinyl pivalate.[47] Poly(ether-carbonate)s with greater solubility than the fluorinated krytox oil have also been synthesised successfully (scheme 14).[37] Several polymers of low molecular weight such as poly(propylene oxide), block copolymers of propylene oxide and ethylene oxide (commercialised under the trade name Pluronics), and poly(vinyl alkyl ethers) also show significant solubility in CO_2.[44a, 48]

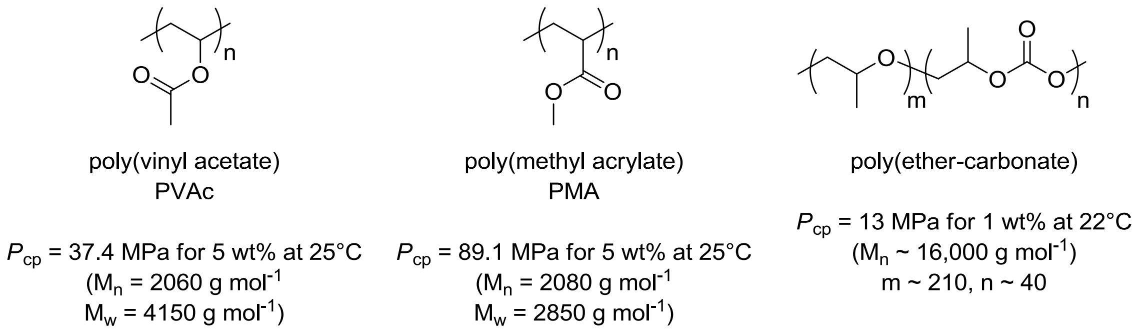
n
poly(vinyl acetate)
PVAc
Pcp = 37.4 MPa for 5 wt% at 25°C
(Mn = 2060 g mol-1
Mw = 4150 g mol-1)
n
poly(methyl acrylate)
PMA
Pcp = 89.1 MPa for 5 wt% at 25°C
(Mn = 2080 g mol-1
Mw = 2850 g mol-1)
m
n
poly(ether-carbonate)
Pcp = 13 MPa for 1 wt% at 22°C
(Mn ~ 16,000 g mol-1)
m ~ 210, n ~ 40

Scheme 14. The solubility of some organic polymers in CO_2.[37, 44a]

Organic polymers generally show a much sharper decrease in CO_2 solubility with increasing molecular weight compared to polysiloxanes or fluorinated polymers and molecular weights above 20,000 g mol^{-1} are essentially insoluble below 40 MPa.[40, 44a] Carbonyl groups and/or ether linkages are common motifs in CO_2 soluble organic polymers. The carbonyl group has been shown by FTIR[49] and computer modelling[50] to have specific interactions with CO_2 while ether linkages are expected to increase flexibility and free volume[37] and can also provide a site for favourable interactions with the solvent.[50a, b] However, small changes in structure can lead to large changes in solubility (e.g. poly(vinyl acetate) is much more soluble than the isomeric poly(methyl acrylate), see scheme 14) and the understanding of the relationship between molecular structure and CO_2 solubility remains limited.[50b] Microstructure/topology may be important as, for example, poly(ether-carbonate)s synthesised by statistical copolymerisation of propylene oxide with CO_2 are apparently much more soluble than polymers with a more regular structure produced by step growth polymerisation.[51] Bray and co-workers screened a library of polyesters in order to determine structure/solubility relationships in CO_2.[52] Branching with acyl chains brought the biggest increase to solubility but there were also significant effects brought about by more subtle changes such as an odd/even effect in the number of carbons in the diacid moiety, which could be related to chain packing and crystallinity in the polymer.

I-2-2-1-4 Effect of polymer end-group

The nature of polymer end-groups can sometimes have a significant effect on solubility. Polar end-groups such as hydroxyls are expected to decrease CO_2 solubility due to increased polymer self-association.[50b] Kilic and co-workers showed that capping poly(propylene oxide) hydroxyl functions with acetate groups led to a 3-7 MPa decrease in cloud-point pressures.[50b] However, in another study, conversion of the hydroxyl end-groups of PVAc oligomers to methylcarbonate functions showed the opposite effect.[53]

In order to take advantage of the characteristics of reversible addition fragmentation chain transfer (RAFT) polymerisation, Girard *et al.* employed a fluorinated RAFT agent in the polymerisation of vinyl acetate; the resulting fluorinated xanthate end-group noticeably increased the solubility of the polymer.[39a] In other work, Fink and Beckman reported on the synthesis of sodium sulfonate terminated PDMS surfactants. They found that surfactants with two PDMS tails were less soluble than those with only one; in this case molecular weight had a greater effect on solubility than the balance of CO_2-phile/CO_2-phobe (i.e. the relative influence of the end-group).[42] Thus, polymer end-groups may be a factor of secondary importance in determining CO_2 solubility.

I-2-2-2 Polymerisation in CO_2

Due to the limited solubility of the large majority of moderate to high molecular weight polymers in CO_2, most polymerisations in this medium are heterogeneous processes. There are a few exceptions for which homogenous solution polymerisation is possible, including the polymerisation of certain fluoropolymers or polymerisations where the conversion is limited to low values so that monomer may play the role of co-solvent.[31] Given that CO_2 is generally a good solvent for small molecules (monomers) but a poor solvent for polymers, precipitation and dispersion polymerisation are the most common heterogeneous processes. Dispersion polymerisation differs from precipitation polymerisation in that a surface-active molecule is present in order to prevent coagulation of the particles which form. In many cases, high conversions and molecular weights may be achieved by precipitation polymerisation, but in other systems, and when control of particle morphology is important, only dispersion polymerisation gives satisfactory results.[31b] Emulsion and suspension polymerisations in CO_2 are less common because these processes involve monomers which are not soluble in the continuous phase, but some examples exist such as the polymerisation or copolymerisation of lactide.[54] Water-in-CO_2 emulsion polymerisations have also been documented, where water soluble monomers are polymerised in a dispersed aqueous phase.[31b] Another important technique is melt polymerisation in the presence of carbon dioxide. CO_2 is a good plasticiser for many polymers and causes significant swelling of the polymer phase.[30-31] This lowers the glass transition temperature of the polymer (T_g) and may also lower the melting point temperature, leading to increased chain mobility. This may impart an increased reactivity to the polymer chain ends, improve the efficiency of condensate removal in polycondensations or otherwise lead to a reduction in the temperature required for the polymerisation.

The largest body of research on polymerisation in CO_2 concerns the free radical polymerisation of vinyl monomers. Early work related to classical radical polymerisation, but more recently there has been significant interest in controlled/living radical polymerisations such as nitroxide-mediated polymerisation (NMP), atom transfer radical polymerisation (ATRP) and reversible addition fragmentation chain transfer (RAFT) polymerisation.[34b, 55] Many other types of reaction have been investigated in CO_2 (mainly as precipitation polymerisations), including transition metal catalysed polymerisation of alkenes, ring opening polymerisation (ROP) of cyclic ethers and lactones, ring opening metathesis polymerisation (ROMP), cationic polymerisation of formaldehyde and substituted alkenes, and metal catalysed copolymerisation of CO_2 and epoxides.[31b] Various condensation polymerisations have also been investigated in the melt phase.

I-2-2-2-1 Dispersion Polymerisation in CO_2

The main advantage of dispersion polymerisation is that, under the appropriate conditions, the polymer product is obtained as a free flowing powder of spherical microparticles, which is easy to handle and process. Particle diameters are usually in the 100 nm - 10 µm range.[31b, 56] Increased molecular weight and conversion might also be achieved by this technique. The well established stabilisers/surfactants used for dispersions in organic media have been shown to be either insoluble[57] or have little activity in CO_2. Ionic surfactants are ineffective due to the low dielectric constant of the medium and only steric stabilisation is viable in this solvent.[31b, 34b] The desire to develop CO_2 based heterogeneous processes has thus required the conception of specially designed stabilisers for this medium. These stabilisers are usually made up of a CO_2-philic part, which almost always consists of a silicone or fluoropolymer chain, and a CO_2-phobic part or anchor which can be adsorbed or grafted to the polymer particles. This amphipathic character has been generated through a wide range of structural architectures including homopolymers, block, grafted and statistical copolymers and macromonomers. Molecules with a dual role of stabiliser and radical initiator, or stabiliser and chain transfer agent have also been elaborated (*vide infra*). More recently, stabilisers based entirely on organic polymers have been employed successfully, such as polymers and copolymers of vinyl alkylates.[47, 58]

The process of dispersion polymerisation in CO_2 is rather complex and has a number of features which may be general or system specific:[56, 59]

- The reaction medium is initially homogenous and polymerisation occurs in the continuous phase.
- Nucleation occurs when the polymer chains reach a certain molecular weight (J_{crit}) and precipitate from the continuous phase. The stabiliser molecules are adsorbed or grafted to the newly formed surface.
- Two reaction loci are present after this point; a polymer-rich dispersed phase and a CO_2-rich continuous phase. The various species present (monomers, polymers, initiator/catalyst…) will be partitioned between the two phases. Polymerisation in the continuous phase may be regarded as solution polymerisation without any diffusion limitations, while polymerisation in the particle phase is expected to resemble bulk polymerisation at high polymer content with reduced diffusivity.[56] Transport between the two phases should be fast for small molecules (monomers) but is expected to be reduced for molecules with higher molecular weight.
- The number of particles, the particle size and the total surface area may change as particles grow or coagulate.[59b]
- The stabiliser may be able to form micelles in the continuous phase, providing an alternative nucleation mechanism.[59c]
- The solvent characteristics of the continuous phase may change during the course of the polymerisation. For example, the monomer may act as a co-solvent for the polymer or stabiliser and in this case the solvent power of the continuous phase will be reduced as the reaction proceeds.[59a] A decrease in the dielectric constant of the medium may also enhance the van der Waals attractions between particles, encouraging flocculation.[60]
- An increase in CO_2 pressure is generally expected to increase the efficiency of stabilisation by increasing the solvent power of CO_2, leading to greater extension of the stabiliser.[60] On the other hand, the greater solvent power of CO_2 could result in an increase in J_{crit}, perhaps leading to a prolonged period of nucleation and a broader distribution of particle size.[61]

The complexity of the process and the difficulties in obtaining *in situ* measurements mean that there are fairly few fundamental studies of dispersion polymerisation in CO_2. Most reports in the literature aim to prove the efficacy of a given stabiliser and to find the optimal process conditions for the polymerisation under study. Some trends have nevertheless emerged from this work.

Poly(1,1-dihydroperfluorooctyl acrylate) (PFOA) was the first stabiliser to be used successfully for dispersion polymerisation in CO_2.[62] DeSimone et al. described the polymerisation of methyl methacrylate (MMA) with conversions in excess of 90% and molecular weights of 190,000 to 325,000 g mol^{-1}, much superior to those achieved in the analogous precipitation polymerisation. Spherical particles with an average diameter of 0.9 to 2.7 µm were formed. It was proposed that the stabiliser adsorbs to the PMMA particles via the hydrocarbon backbone while the fluorinated chains extend into the CO_2 phase. They tested PFOA stabilisers with different lengths (M_n = 11,000 and 200,000 g mol^{-1}) and found that, on an equivalent weight basis, the shorter stabiliser produced smaller particles although the size distribution was slightly broader.

Another system which has been studied quite extensively is the polymerisation of MMA with reactive PDMS-monomethacrylate macromonomers (PDMS-mMA, figure 3). In this case the macromonomer is expected either to form a block copolymer *in situ* or to graft directly onto the growing polymer particles. This gives rise to high yields of polymers with high molecular weights and particle sizes which are generally less than 3 µm (figure 4).[63]

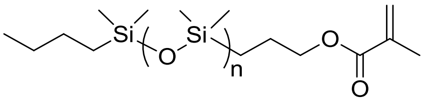

Figure 3. PDMS-monomethacrylate macromonomer.

Giles and co-workers investigated the effect of stabiliser molecular weight in this reaction by comparing masses of 2000, 5000 and 10,000 g mol^{-1}.[63b] In terms of the minimum concentration required to produce well-defined spherical morphology, they found that the smallest stabiliser was the most effective on a wt/wt basis but the 10,000 g mol^{-1} stabiliser was the most effective on a molar basis. The particle diameters were also about twice as big with the shorter stabiliser.

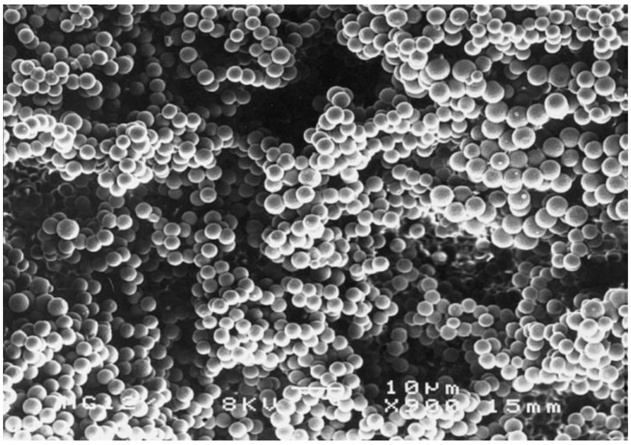

Figure 4. SEM micrograph of PMMA particles produced by dispersion polymerisation in the presence of 5 wt% PDMS-monomethacrylate macromonomer (M_n = 10,000 g mol^{-1}).[63b]

In general, the relationship between the molecular weight of the stabiliser and the stabilisation of the dispersion is not necessarily straightforward. For example, for an end-grafted stabiliser, two factors are presumably opposing each other; on an equal wt/wt basis, surface coverage should increase with decreasing molecular weight (more anchoring groups) but the thickness of the steric layer should decrease. An alternative anchoring mechanism, e.g. as for PFOA where the backbone of the stabiliser is expected to adsorb to the polymer particles, may result in different trends. Further complications arise from the fact that the solubility of the stabiliser in the continuous phase could be affected by its molecular weight, or that there may be an upper limit for the molecular weight above which the thickness of the steric layer has little importance.

Increasing the amount of stabiliser is expected to decrease the average particle size as an increased interfacial surface area can be supported. Stabiliser concentrations of between 2 to 15 wt% with respect to monomer are commonly used. The efficiency of the grafting or adsorption of the stabiliser is also important for increasing the surface coverage.[59] With block copolymers, the most favourable anchor-soluble balance is reportedly between 1:3 and 3:1.[61], while for PDMS-monomethacrylate macromonomers, the reduced stabilisation characteristics compared to PDMS-*b*-PMMA have been attributed to the low incorporation of the macromonomer (reduced reactivity compared to methyl methacrylate monomer).[59c, 63a] PDMS homopolymers without a particular anchoring mechanism are rather ineffective.[61, 63a] On the other hand, with just a single anchoring point ‘pseudo-grafted’ stabilisers can give good results. Christian and co-workers tested a perfluoropolyether functionalised with a carboxylic acid chain end (Krytox 157FSL, figure 5) and found that it was effective for the dispersion polymerisation of MMA down to very low concentrations (0.1 wt% vs. monomer).[64] They suggested that the stabiliser was bound to PMMA by hydrogen bonding interactions and the same stabiliser has proven to be much less efficient in the polymerisation of styrene.[65] It was later shown that stirring speeds above just 25 rpm could easily disrupt the stabilisation of these weakly-bound molecules, leading to coagulation and reduced molecular weights of PMMA.[66]

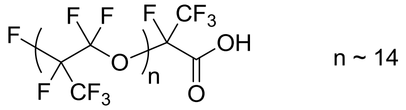

Figure 5. Carboxylic acid terminated perfluoropolyether, Krytox 157FSL.

Okubo and co-workers have pioneered the use of stabiliser molecules with dual function. The application of a commercially available PDMS-based azoinitiator ("inistab"- initiator and stabiliser, figure 6) to the radical polymerisation of methyl methacrylate led to PMMA particles with a diameter of around 200 nm.[67] In a similar manner, PDMS functionalised with a terminal bromo group has been used as an initiator for the ATRP of MMA,[68] while thiol-terminated PDMS has been used as a RAFT transfer agent ("transtab").[69]

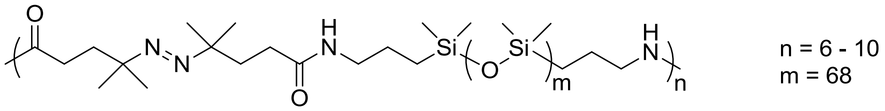

Figure 6. PDMS-based azoinitiator, VPS-0501.

In a further extension of this approach, an alkoxyamine "inistab" was employed in the dispersion NMP of styrene.[70] This stabiliser was based on a PS-PDMS-PS triblock copolymer, which was prepared from the PDMS-based azoinitiator and end-capped with nitroxide. In this case the particles obtained were not well defined, but better results were later achieved with a monofunctional rather than a telechelic initiator.[71]

A study by Grignard *et al.* is worth discussing as it is one of the few examples of dispersion polymerization in CO_2 which does not involve a free radical mechanism (scheme 15).[72] They investigated the dispersion polymerization of ε-caprolactone (CL) stabilised by diblock or triblock copolymers of poly(caprolactone) (PCL) and poly(1,1,2,2-tetrahydroperfluorodecyl acrylate) (PFDA). Dibutyltin dimethoxide was used to initiate the reaction.

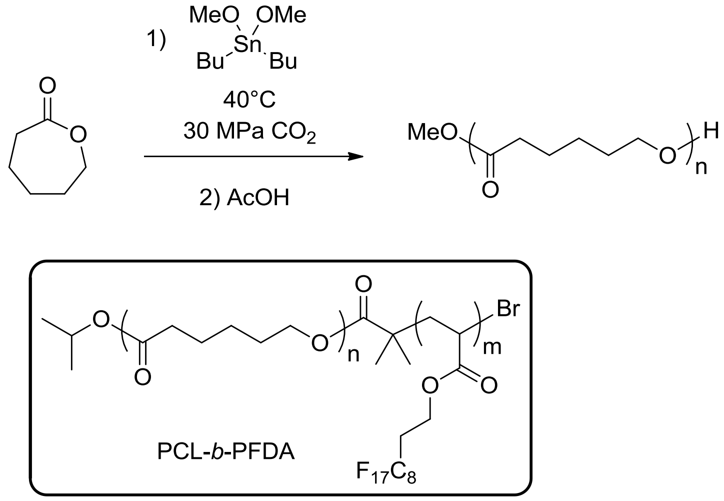

Scheme 15. Dispersion ring-opening polymerisation of ε-caprolactone in $scCO_2$.

The authors questioned whether stabilisation would prove problematic due to the change in reaction mechanism; in this system initiation is faster than propagation, all the chains grow simultaneously and could be expected to reach the critical molecular weight for precipitation (J_{crit}) at the same time. A large amount of stabiliser may therefore be required instantaneously. In the event, when a diblock copolymer with an anchor-soluble balance (ASB, $M_{n, PFDA}/M_{n, PCL}$) of 4.8 was used at 5 wt% vs. monomer, very large microspheres with a broad size distribution were obtained (mean diameter 245 ± 70 µm) (figure 7, left). However, increasing the stabiliser concentration to 10 wt% led a significant reduction in size (40 ± 17 µm) (figure 7, centre), and 5 wt% of a diblock copolymer with an ASB of 1.9 led to particles with a diameter of ~2 µm (although somewhat agglomerated) (figure 7, right). The influence of the CO_2 pressure was also studied and a drop in pressure from 30 to 15 MPa led to an increase in the particle size but decreased the extent of agglomeration. They suggested that higher pressures increased the efficiency of the stabiliser through improved solvation but might also increase the extent of plasticisation of the poly(caprolactone) facilitating agglomeration of the small particles.

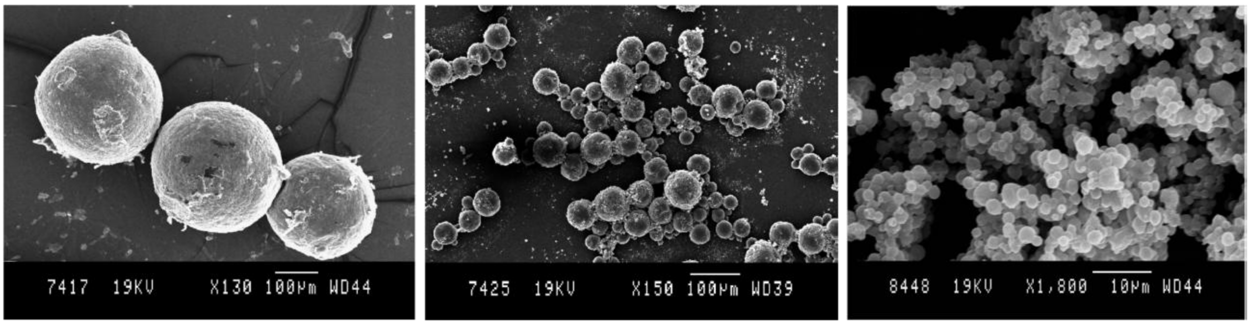
7417 19KV X130 100µm WD44
7425 19KV X150 100µm WD39
8448 19KV X1,800 10µm WD44

Figure 7. SEM micrographs of PCL particles prepared by dispersion polymerisation: particles prepared in the presence of 5 wt% PCL-*b*-PFDA with ASB = 4.8 (left), particles prepared in the presence of 10 wt% PCL-*b*-PFDA with ASB = 4.8 (centre), and particles prepared in the presence of 5 wt% PCL-*b*-PFDA with ASB = 1.9 (right).[72]

I-2-2-2-2 Dispersion Polymerisation of Polyurethanes

A number of studies have been undertaken by Cramail and co-workers to investigate the dispersion polymerisation of polyurethanes, originally in an organic medium and later in $scCO_2$. The first studies dealt with the DBTDL catalysed reaction of ethylene glycol and TDI in cyclohexane in the presence of polystyrene (PS) or poly(butyl acrylate) (PBA) based stabilisers.[73] One of the most important findings was that much greater stabilisation could be achieved by initial reaction of hydroxy-terminated macromonomers with diisocyanates, since the resulting isocyanate-terminated stabiliser (e.g. PBA-NCO, scheme 16) appeared to be more reactive. It was also shown that PBA end-functionalised with a diol group (PBA-$(OH)_2$) was more effective than the equivalent stabiliser with a single hydroxyl function, leading to smaller PUR particles with a narrower size distribution. This was attributed to more efficient nucleation and a better repartition of the stabiliser due to its grafting into the polyurethane chains.

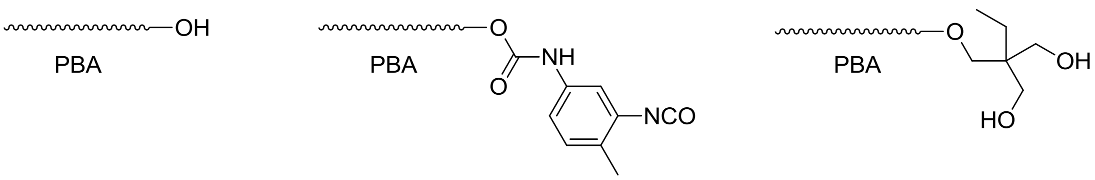

PBA-OH **PBA-NCO** **PBA-(OH)$_2$**

Scheme 16. Poly(butyl acrylate) stabilisers used for the dispersion polymerisation of polyurethanes in cyclohexane.

It was later found that PDMS based macromonomers were also effective stabilisers and that their use could be extended to CO_2-based dispersions.[74] Alkanol terminated PDMS stabilisers (PDMS-OH) led to coagulated polyurethane in $scCO_2$, but the use of pre-formed PDMS-NCO stabiliser gave spherical microparticles of 0.3 to 1.5 µm diameter. On the other hand, the molecular weight of the polymer remained rather limited (<10,000 g mol^{-1}). This work led on to a detailed study of polyurethane synthesis by dispersion polymerisation in $scCO_2$.[20, 75] A range of different stabilisers were tested based on PDMS or poly(1,1,2,2-tetrahydroperfluorodecyl acrylate) (PFDA) with various molecular weights. In line with previous results, the use of diol-terminated PDMS (PDMS-(OH)$_2$) or hydroxy-terminated PFDA (PFDA-OH) led to an agglomerated product. In all the other cases, with isocyanate-terminated stabilisers, discrete particles of micrometric size were obtained. PDMS terminated with two isocyanate functions (PDMS-(NCO)$_2$) led to a distinct reduction in the size of the particles and their size distribution compared to monoisocyanate functionalised PDMS with a similar molecular weight. PDMS stabilisers were also apparently more effective than their PFDA counterparts, producing smaller and more uniform particles. The concentration of PDMS stabilisers was additionally varied at 5, 10 or 17 wt% (with respect to the total mass of the system) with the optimal results obtained at 10 wt%.

Different diol monomers were tested in the reaction, which for solubility reasons were restricted to three short aliphatic diols, namely ethylene glycol, butanediol and a poly(ethylene glycol) (PEG) oligomer of 200 g mol^{-1}. The highest molecular weights of polyurethane were obtained with butanediol despite of the lower molecular weight of this diol compared to the PEG. Under the optimal conditions the (weight average) molecular weight of the polyurethane reached 90,000 g mol^{-1}. This greatly exceeded the molecular weights achieved in cyclohexane, suggesting that the urethanisation reaction was promoted in CO_2, and is perhaps related to an enhancement of the nucleophilicity of the diols due to specific interactions with the solvent.[20, 75a, b] Several reactions were also carried out without the presence of DBTDL catalyst. In this case the yield and molecular weight of the polymer were significantly reduced, while the particles formed where much larger and showed a broader size distribution. This was attributed to a prolonged period of nucleation and shows the importance of the catalyst in controlling the particle morphology. The replacement of DBTDL with an organocatalyst in this reaction is therefore not expected to be inconsequential.

I-2-3 Organocatalysis in CO_2

Many types of homogenously catalysed reactions have been carried out in carbon dioxide and the solvent has sometimes been shown to affect the rates, yields and selectivity of the reactions.[76] Carbon dioxide has even proven to be a suitable medium for enzymatic catalysis,[77] a methodology which has been extended to polymerisation.[78] However, only a minority of reports relate to organocatalysed reactions in CO_2.

Organic acid catalysis has been used in a range of reactions in CO_2 such as aldol,[79] alkylation,[80] cyclocondensation,[81] Friedel-Crafts,[82] esterification[79, 83] and methylenecyclopropane ring-opening[84] reactions. Fluorinated acids are generally selected because of their increased CO_2 solubility. Equally, there are a number of base catalysed reactions which have been documented (scheme 17), including triethylamine catalysed Henry reactions,[85] DABCO catalysed Baylis-Hillman reactions,[86] and an asymmetric Neber-type reaction catalysed with dihydroquinidine (in stoichiometric quantities or in catalytic quantities with K_2CO_3 as stoichiometric base).[87] The formation of tertiary amine-CO_2 complexes[88] did not appear to hinder these reactions.

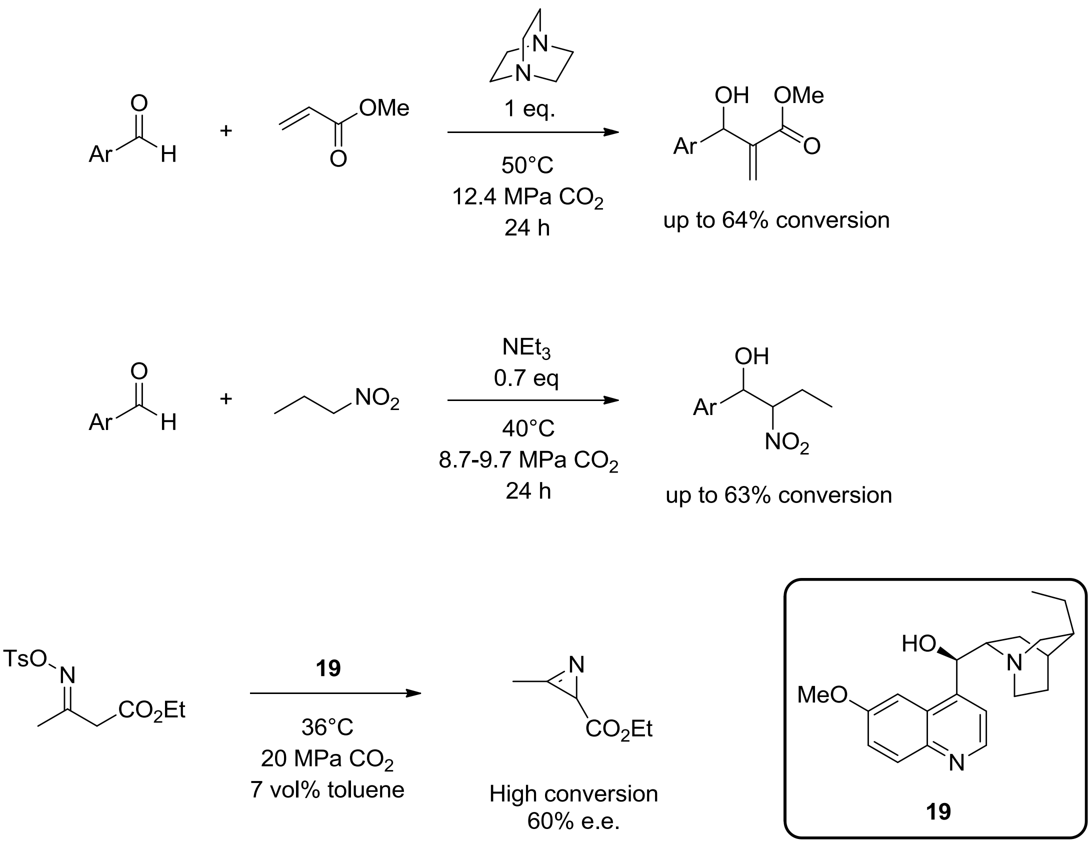
Ar
H
O
+
OMe
O
N
N
1 eq.
50°C
12.4 MPa CO2
24 h
OH
OMe
Ar
O
up to 64% conversion
Ar
H
O
+
NO2
NEt3
0.7 eq
40°C
8.7-9.7 MPa CO2
24 h
OH
Ar
NO2
up to 63% conversion
TsO
N
CO2Et
19
36°C
20 MPa CO2
7 vol% toluene
N
CO2Et
High conversion
60% e.e.
HO
MeO
N
N
19

Scheme 17. Organic base catalysed reactions in $scCO_2$.

Enantioselective Michael addition catalysed by Takemoto's catalyst (bifunctional tertiary amine-thiourea catalyst) has also been described (scheme 18).[89] This reaction shows specific solvent dependence since much greater stereoselectivity is achieved in aprotic solvents (including CO_2) and hydrogen bonding is considered to have a key role.

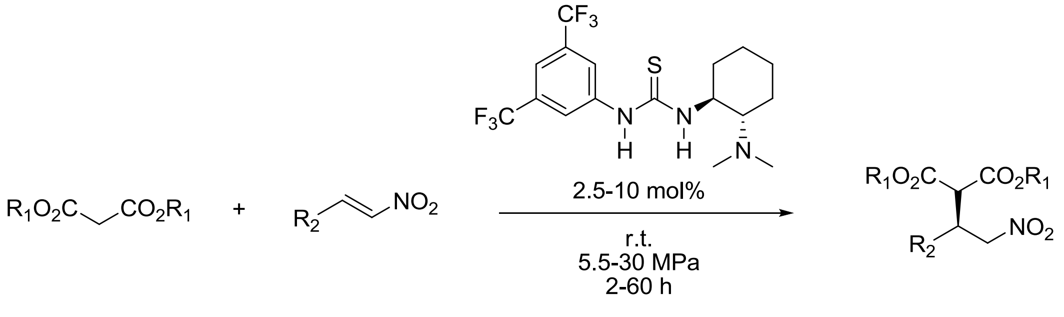
CF3
S
F3C
N
H
N
H
N
R1O2C
CO2R1
+
R2
NO2
2.5-10 mol%
r.t.
5.5-30 MPa
2-60 h
R1O2C
CO2R1
R2
NO2

Scheme 18. Asymmetric Michael reaction catalysed by Takemoto's catalyst in liquid CO_2.

As part of the growing interest in CO_2 as a green chemical feedstock for organic synthesis, organocatalysis has been applied to various reactions involving CO_2 fixation. Carbon dioxide is sometimes used as the solvent as well as the reactant in these processes, and in this context the formation of cyclic carbonates from epoxides and CO_2 (scheme 19) has been catalysed with peralkyl ammonium,[90] guanidinium[91] or phosphonium[92] salts as well as N-heterocyclic carbenes (NHCs)[93] amongst others.

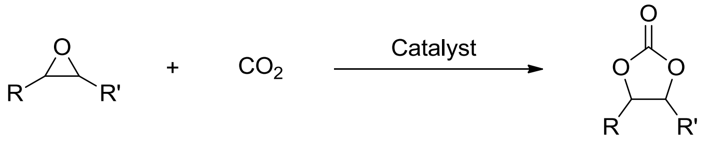

Scheme 19. Cyclic carbonate formation from addition of carbon dioxide to epoxides.

Another example is the carboxylative cyclization of propargylic alcohols (scheme 20), which can be catalysed by amidines/guanidines[94], NHCs[93] or tributylphosphine.[95] The first step of the amidine/guanidine catalysed reaction is presumed to be the formation of an alkyl carbonate salt from the alcohol, CO_2 and the strong base (scheme 20, upper pathway). Alternatively, in the NHC catalysed reaction, the NHC-CO_2 adduct is proposed to act as a nucleophile (scheme 20, lower pathway). A closely related reaction to this one is the carbonation of 2-aminobenzonitriles to 1*H*-quinazoline-2,4-diones catalysed by amine bases[96] or ionic liquids.[97]

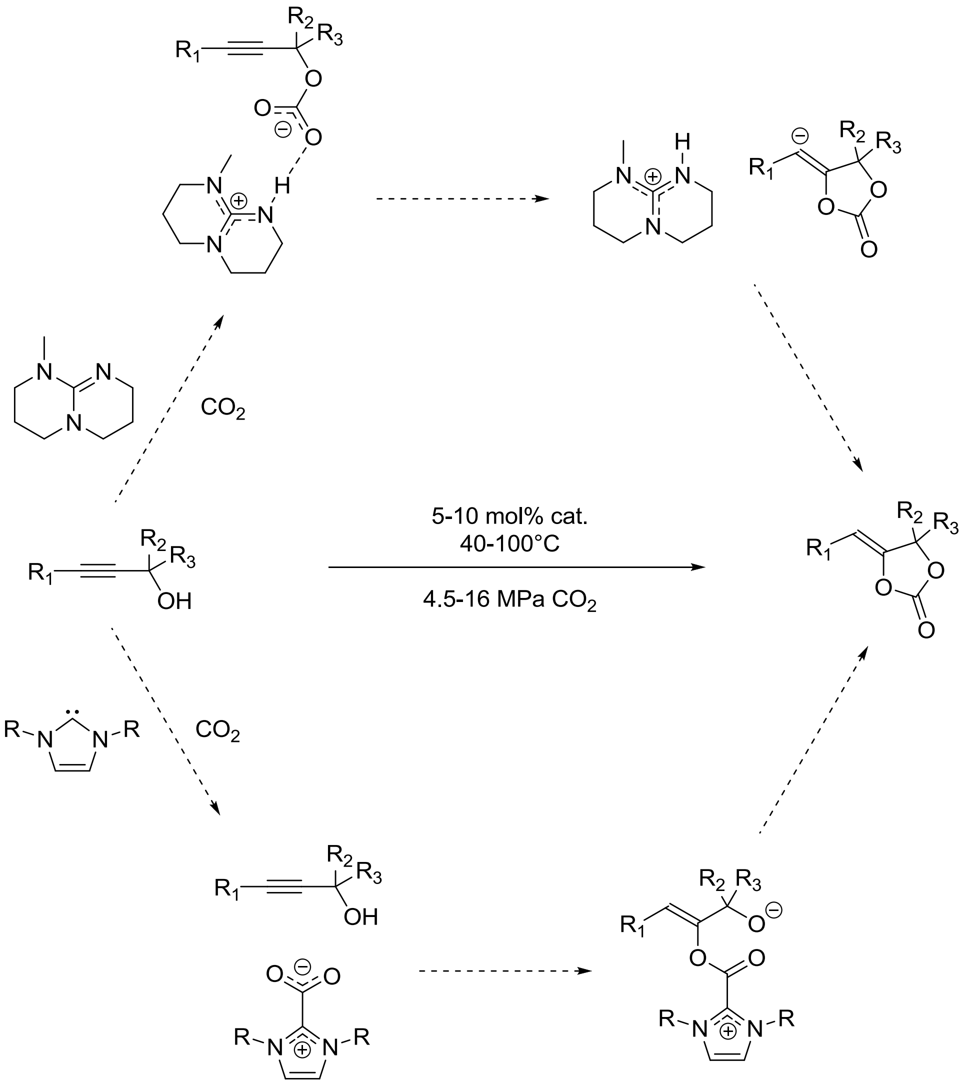

Scheme 20. Carboxylative cyclization of propargyl alcohols in $scCO_2$ catalysed by MTBD (upper pathway) or NHCs (lower pathway).

In the literature there are just a few examples of organocatalysed polymerisation reactions in $scCO_2$. Yoda *et al.* reported the condensation of poly(L-lactic acid) oligomers in $scCO_2$ using DCC (dicyclohexylcarbodiimide) as coupling agent and DMAP as catalyst (scheme 21).[98] The molecular weights were comparable to those obtained in dichloromethane solution and superior to those obtained in melt polymerisation without the presence of CO_2.

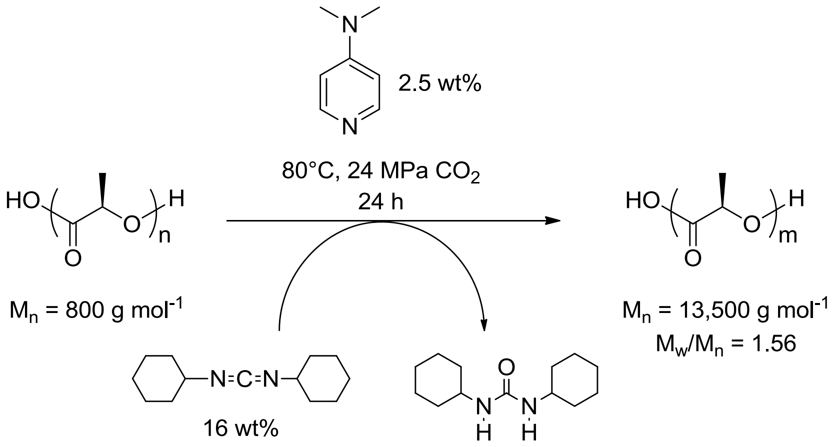

Scheme 21. Condensation of poly(L-lactic acid) oligomers in $scCO_2$ with dicyclohexylcarbodiimide as coupling agent and DMAP as catalyst.

In another polycondensation reaction in $scCO_2$, pyridine and triethylamine have been employed with the dual roles of catalyst and stoichiometric base for the esterification of aromatic diacid chlorides with diols (scheme 22). The use of pyridine, which showed higher solubility than triethylamine in CO_2, gave the highest molecular weights of polymer.

The DBU catalysed ring-opening polymerisation of lactide in $scCO_2$ has been documented by Blakey and co-workers (scheme 23).[99] They found that DBU was an efficient catalyst for the reaction, despite the fact that it can form carbonate salts with CO_2 in the presence of a proton source.[100] However, the rate of polymerisation was slower than in organic solvents.

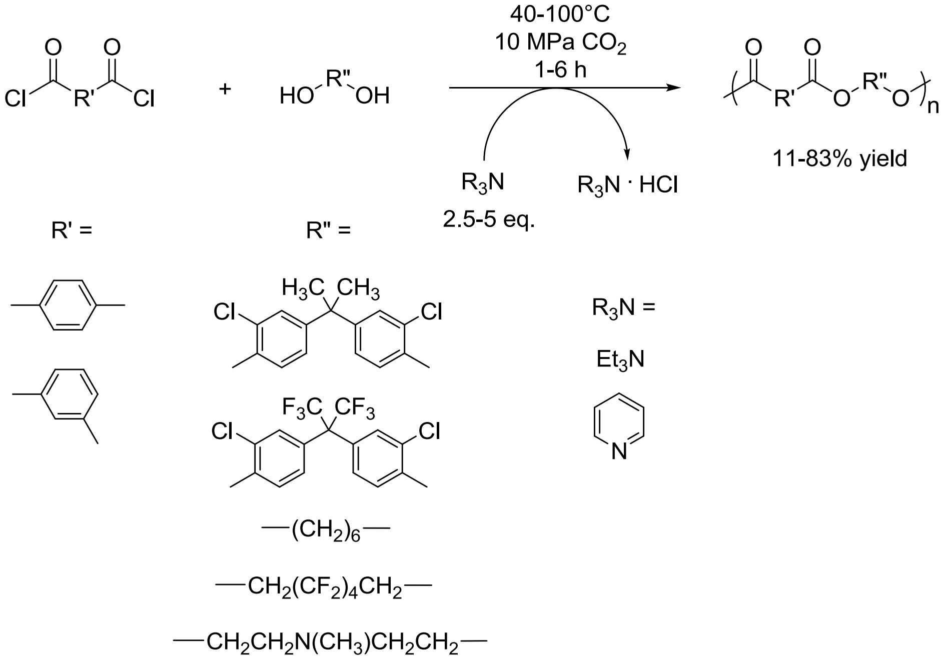
40-100°C
10 MPa CO2
1-6 h
R3N
2.5-5 eq.
R3N · HCl
11-83% yield
R' =
R'' =
R3N =
Et3N
—(CH2)6—
—CH2(CF2)4CH2—
—CH2CH2N(CH3)CH2CH2—

Scheme 22. Polycondensation of dicarboxylic acid chlorides and diols in $scCO_2$ in the presence of triethylamine or pyridine.

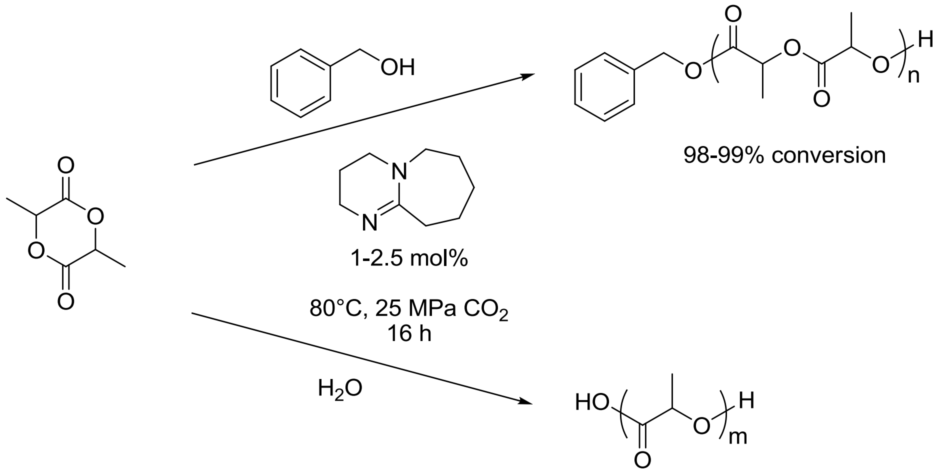
98-99% conversion
1-2.5 mol%
80°C, 25 MPa CO2
16 h
H2O

Scheme 23. Ring-opening polymerisation of lactide in $scCO_2$ catalysed by DBU.

Thus, a range of organocatalysts have successfully been used in the CO_2 medium and the results often rival those obtained under conventional conditions. Some organocatalysts are known to have specific reactivity with CO_2 (amidines/guanidines, NHCs) and have therefore been used to promote carbonation reactions. The effect of this reactivity when carbon dioxide is not a desired reactant remains largely unexamined.

I-3 Conclusions

Polymerisation in liquid or supercritical carbon dioxide has become a flourishing area of research, thanks to the environmental, economical, safety and possible processing advantages of this solvent. A number of polymeric stabilisers have been developed which allow the dispersion polymerisation of various monomers to produce well-defined microparticles. The chemical nature of the stabilisers and the mechanism by which they anchor to the growing particles can have a strong influence on the particle morphology. On the other hand, studies employing organocatalysts in the CO_2 medium remain relatively scarce. The existing data is encouraging since results are usually comparable to those obtained in conventional media, although questions remain concerning the compatibility of certain organocatalysts with CO_2. With respect to the synthesis of urethanes, some organocatalysts have also shown a tendency to promote secondary reactions, which could be a concern for the successful preparation of well-defined polyurethane microparticles in $scCO_2$.

Chapter II

Kinetic Studies of a Model Urethane Forming Reaction in Supercritical Carbon Dioxide

Summary

II-1 Introduction 48

II-2 Catalyst screening on a model reaction 48

II-2-1 Reaction parameters 48

II-2-2 Choice of catalysts 49

II-2-2-1 pK_{BHX} database *51*

II-2-3 IR spectra of the solvent, reactants and product 54

II-2-3-1 Carbon dioxide *54*

II-2-3-2 n-Butanol *55*

II-2-3-3 2,4-TDI *56*

II-2-3-4 Dibutyl 4-methyl-1,3-phenylenedicarbamate *57*

II-2-4 Reaction kinetics with 5 mol% catalyst 58

II-2-4-1 N-H peak shape *61*

II-2-5 Reaction kinetics with 1 mol% catalyst 66

II-2-6 Reaction kinetics with phenyl isocyanate 68

II-2-7 NMR and Raman analysis of product residues 69

II-2-8 Robustness of organocatalysts versus DBTDL 79

II-2-8-1 The behaviour of amidines/guanidines in the presence of CO_2: an explanation of catalytic activity *81*

II-2-9 Effect of CO_2 on the kinetics of reaction in organic solvent 85

II-3 Conclusions 87

II-4 Experimental Section 88

II-4-1 Infrared Set-Up 88

II-4-2 Raman Spectroscopy 89

II-4-3 Materials 89

II-4-4 Kinetic Monitoring in $scCO_2$ 90

II-4-5 NMR/Raman analysis of reaction residues 91

II-4-6 Kinetic monitoring in dichloromethane solution..91

II-4-7 CO_2 absorption experiments..91

II-1 Introduction

There is a wealth of studies in the literature on the kinetics of urethane forming reactions, with a range of different isocyanates and hydroxyl containing compounds under various conditions of temperature and concentration, in bulk or in solution.[9, 16a, 101] These studies set-out to determine the mechanisms of reaction or to compare the activity of different catalysts. Various methods have been used for reaction monitoring such as infrared[18b, 102], Raman[103] and NMR[104] spectroscopies, HPLC[12a, 105], and in earlier studies, back titration of unreacted isocyanates.[106] Each method has its own merits and limitations. Methods which measure only the concentration of isocyanate may overlook the formation of side products such as allophanates or isocyanurates. HPLC and NMR can give excellent resolution of the reaction components whereas in IR spectra absorption bands often overlap. The principal absorption bands in the IR spectra of isocyanates, alcohols and urethanes are well established (although the assignment of other peaks is not always rigorous and sometimes oversimplified). Most studies using IR spectroscopy follow the diminution of the strong isocyanate absorption around 2200 cm^{-1}, but the formation of products can be followed simultaneously, for example by the increase in intensity of the urethane C=O stretch at around 1700 cm^{-1}. *In situ* IR monitoring has the advantage that it is easy to obtain a large number of data points. The technique is particularly suited to reactions in supercritical CO_2 because it is otherwise difficult to sample the reaction mixture without changing the reaction conditions (pressure/concentration). The aim of this kinetic study is a comparison of catalyst performance in $scCO_2$ without further analysis to calculate reaction orders or rate constants.

II-2 Catalyst screening on a model reaction

II-2-1 Reaction parameters

In order to compare the efficacy of different catalysts for the formation of polyurethanes in supercritical CO_2, a suitable model reaction was chosen for *in situ* reaction monitoring by FTIR. This model was based on the reaction between an industrially relevant aromatic diisocyanate, toluenediisocyanate and a monofunctional alcohol, *n*-butanol (scheme 24). A monofunctional model was preferred over a polymerisation reaction in order to avoid the physical changes to the reaction environment associated with polymer growth and the eventual precipitation of polymer chains.

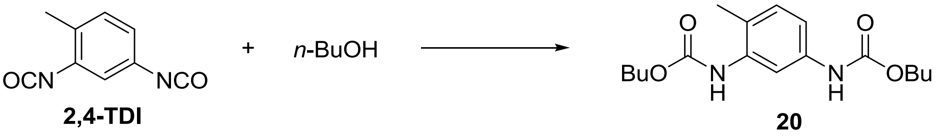

Scheme 24. Model reaction of urethane synthesis.

Although an 80:20 mixture of the 2,4- and 2,6-isomers of toluenediisocyanate is often used industrially (this mixture has a reduced tendency to crystallize), pure toluene-2,4-diisocyanate was used in this study in order to simplify the system. At 60°C and a typical polymerisation concentration of 2.5 wt% vs. CO_2, this diisocyanate is soluble above pressures of 17 MPa.[107] *n*-Butanol was chosen as an appropriate monofunctional model of the primary aliphatic polyols commonly used in polyurethane synthesis. *n*-Butanol was experimentally more practical to use than lower homologues (lower volatility and greater volume per OH group) and forms a single supercritical phase with CO_2 above 10 MPa at 60°C.[108]

Dilute conditions were used (10^{-2} mol dm^{-3} TDI) with the high-pressure cell configured for a large optical path length (5.05 mm) to ensure that the reactants and products were soluble, the agitation was unhindered and the absorbance of the urethane N-H band was in the linear region below 3 units. The concentration used was thus approximately ten times more dilute than for the polymerisation reactions performed in $scCO_2$. The temperature and pressure of 60°C and 24 MPa were selected to maintain good solubility and reaction rates. The reactions were followed up to 17 hours reaction time, which allowed the kinetic curve to reach a plateau in most cases.

II-2-2 Choice of catalysts

Organocatalysts of several different classes were chosen for investigation in this study (scheme 25).

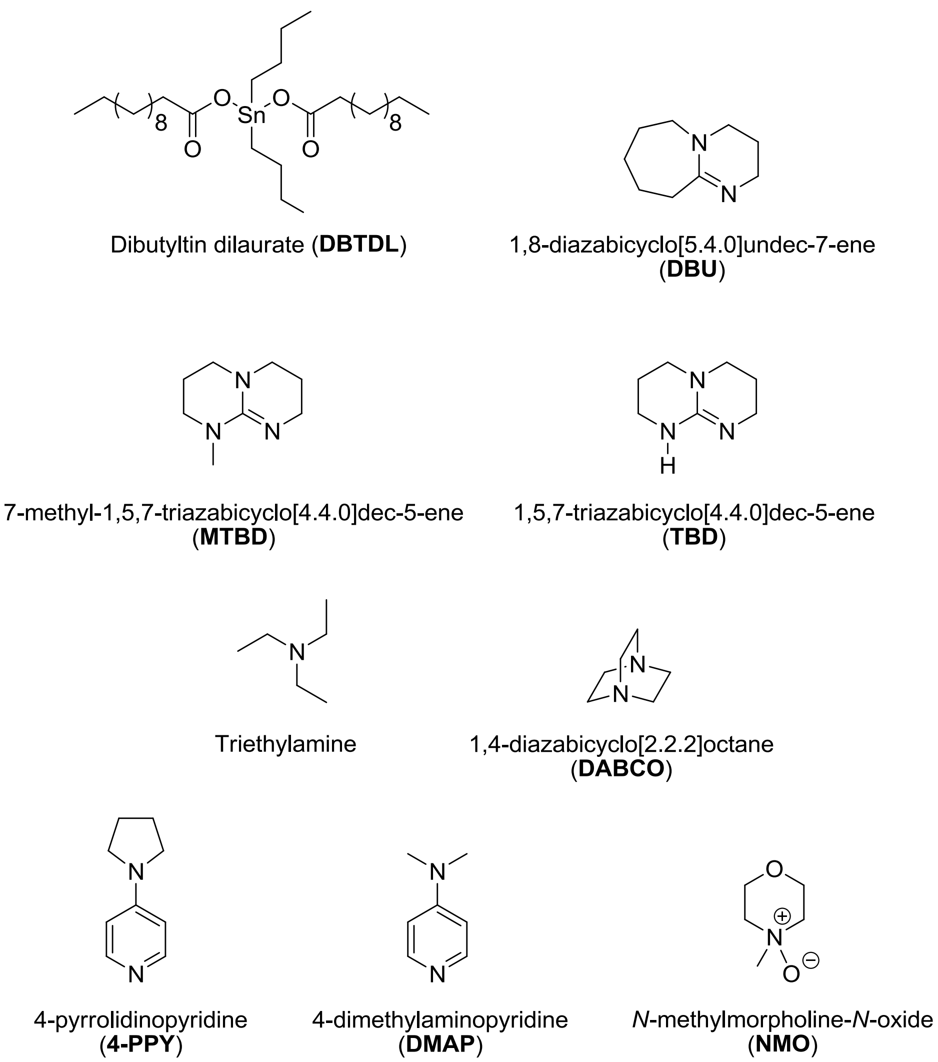
Dibutyltin dilaurate (**DBTDL**)
1,8-diazabicyclo[5.4.0]undec-7-ene (**DBU**)
7-methyl-1,5,7-triazabicyclo[4.4.0]dec-5-ene (**MTBD**)
1,5,7-triazabicyclo[4.4.0]dec-5-ene (**TBD**)
Triethylamine
1,4-diazabicyclo[2.2.2]octane (**DABCO**)
4-pyrrolidinopyridine (**4-PPY**)
4-dimethylaminopyridine (**DMAP**)
N-methylmorpholine-*N*-oxide (**NMO**)

Scheme 25. Catalysts screened for their activity in the isocyanate/alcohol reaction in $scCO_2$.

Tertiary amines are omnipresent in polyurethane foam applications. Triethylamine and 1,4-diazabicyclo[2.2.2]octane (DABCO) were selected as examples for this work and the latter is one of the most commonly used tertiary amine catalysts for polyurethane formation.[1a] Pyridine derivatives 4-dimethylaminopyridine and 4-pyrrolidinopyridine were also included due to their common use as nucleophilic acylation catalysts.[109]

The bicyclic guanidines and amidines TBD, MTBD and DBU are highly basic compounds which have seen a growing interest in organocatalysis,[4] and their efficiency in polyurethane synthesis has recently been highlighted.[18c]

Amine *N*-oxides are a family of highly polar molecules with some use as organocatalysts.[110] *N*-methylmorpholine-*N*-oxide (NMO) is an example which is readily available and relatively soluble in weakly polar solvents. Its inclusion in this study was a result of the observation that amine oxides reportedly show higher hydrogen bonding basicity than the highly active bicylic amidines and guanidines (see $\mathrm{p}K_{\mathrm{BHX}}$ database below). Furthermore, there is some existing literature showing that amine *N*-oxides are more active in the catalysis of isocyanate/alcohol reactions than the corresponding amines.[25a-c] It is also noteworthy that alkylamine *N*-oxides such as NMO have been found to be more active than pyridine *N*-oxides.[25c]

Dibutyltin dilaurate (DBTDL) is probably the most commonly used metal based catalyst for the urethane forming reaction[1, 17] and was included as a reference.

Industrially, tertiary amines typically make up 0.1 to 5 percent (by weight) of polyurethane formulations and are commonly used with aromatic isocyanates in foam applications. The more active DBTDL is used in urethane adhesives, coatings and sealants as well as foams and can give a rapid rate of reaction even at levels as low as 0.1 parts per hundred parts of polyol (~0.1 mol% vs OH functions for a polyol of $M_w = 1300$ g mol^{-1}). In this study, a catalyst loading of 5 mol% (vs OH functions) was chosen for the initial catalyst screening, in order to reach reaction completion within a short time period despite of the relatively dilute conditions.

In most cases, the preparation of catalyst solutions in butanol was necessary due to the minute quantities of catalyst required. It was important that the catalysts were premixed with the alcohol rather than the isocyanate in order to avoid the well-known self-addition reactions of isocyanates (e.g. dimerization, trimerization).

II-2-2-1 pK_{BHX} database

Various spectroscopic techniques have been used to probe the association of alcohols with bases in order to investigate the mechanisms of base catalysis. For example, Waymouth and Hedrick used NMR to highlight the activating effect of MTBD on alcohols for the ROP of lactones.[111] Equally, Baker and Gaunt used the evidence of IR spectra regarding alcohol-amine association to lend support to their proposed mechanism of the base-catalysed reaction of phenyl isocyanate with alcohols.[112] Indeed, the FTIR technique has been used to quantify hydrogen bond basicity and the $\mathrm{p}K_{\mathrm{BHX}}$ database is based on this technique. In the IR spectrum of an alcohol in dilute CCl_4 solution (4-fluorophenol and methanol are used as reference hydrogen bond donors), the ν(OH) absorption is observed as a sharp peak (dashed line, figure 8). Upon addition of a hydrogen bond acceptor, the intensity of this peak decreases while a new broad absorption is observed at lower wavenumbers (solid line, figure 8) corresponding to the ν(OH) absorption in hydrogen bonded associates.

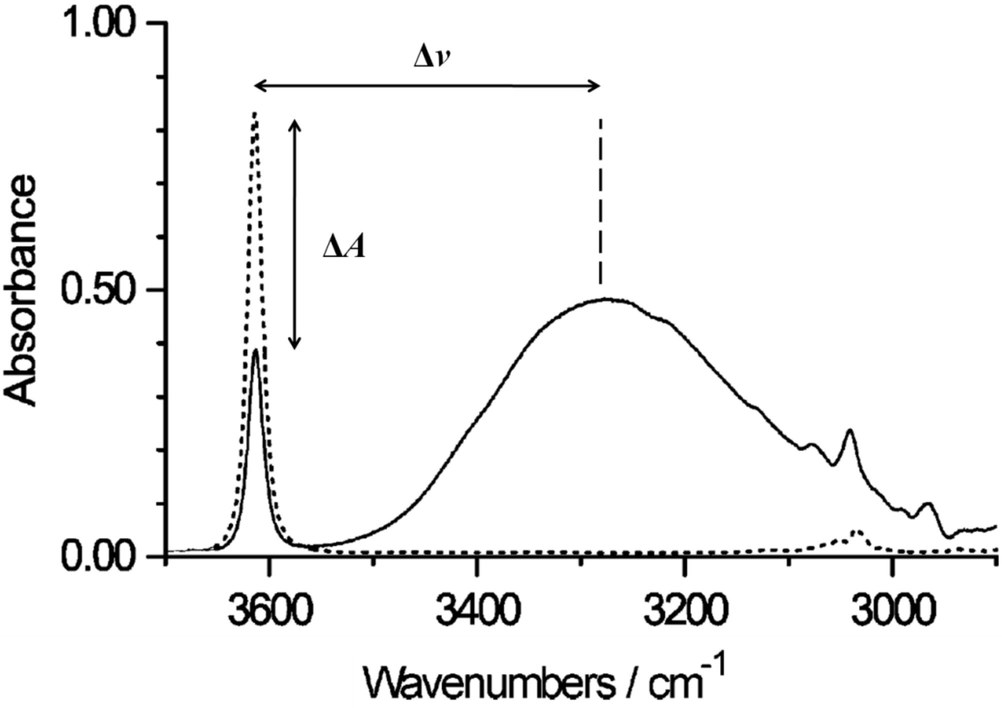

Figure 8. The ν(OH) absorption in the IR spectrum of an alcohol alone (dashed line) and in the presence of a hydrogen bond acceptor (solid line) in CCl_4 (figure adapted from [113]).

The pK_{BHX} is a measure of hydrogen bond association and is calculated from the change in the absorbance of ν(OH) of the free alcohol according to equations 1 to 3. The shift $\Delta\nu$(OH) is assumed to be dominated by the strength of the hydrogen bond.[114]

$$c = \frac{A}{\epsilon\, l} \tag{1}$$

(c is concentration, A is absorbance, ε is the extinction coefficient and l is the optical path length)

$$K = \frac{c_{\mathrm{BHX}}}{c_{\mathrm{B}} c_{\mathrm{HX}}} = \frac{c_{\mathrm{HX}}^{0} - c_{\mathrm{HX}}}{c_{\mathrm{HX}}(c_{\mathrm{B}}^{0} - c_{\mathrm{HX}}^{0} + c_{\mathrm{HX}})} \tag{2}$$

(K is the association constant, c is the equilibrium concentration, c^0 is the initial concentration, HX is the hydrogen bond donor (alcohol), B is the hydrogen bond acceptor and BHX is the hydrogen bonded complex)

$$\mathrm{p}K_{\mathrm{BHX}} = -\log K_{\mathrm{BHX}} = +\log K \tag{3}$$

Some values taken from the database are shown in scheme 26. The catalytically very active MTBD and DBU show large values of both $\mathrm{p}K_{\mathrm{BHX}}$ and $\Delta\nu$(OH). Other compounds from the database that show large values for both of these quantities include tetrabutylammonium acetate **21** and amine *N*-oxides **22** and **23**. Tetraalkylammonium carboxylates are reported to give a rapid rate of reaction in the formation of urethanes but favour even more so the reactions forming allophanates and isocyanurates.[12a] Also, as mentioned above, amine *N*-oxides are more active than their amine counterparts in urethane formation. Thus, there does seem to be a correlation between $\mathrm{p}K_{\mathrm{BHX}}$ and catalytic activity, which is perhaps more pertinent than for $\mathrm{p}K_{\mathrm{a}}$. A kinetic equation for the alcohol-isocyante reaction which takes account of hydrogen bonding basicity has already been proposed.[25b]

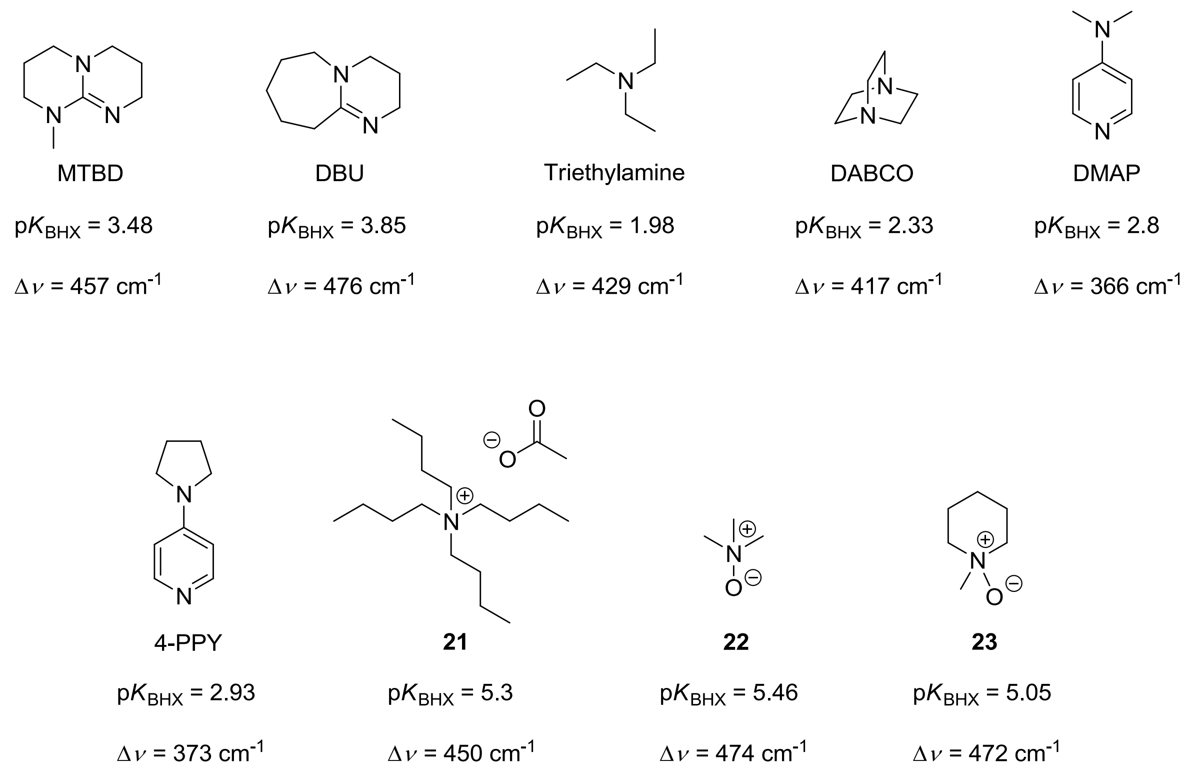
MTBD
pKBHX = 3.48
Δν = 457 cm-1
DBU
pKBHX = 3.85
Δν = 476 cm-1
Triethylamine
pKBHX = 1.98
Δν = 429 cm-1
DABCO
pKBHX = 2.33
Δν = 417 cm-1
DMAP
pKBHX = 2.8
Δν = 366 cm-1
4-PPY
pKBHX = 2.93
Δν = 373 cm-1
21
pKBHX = 5.3
Δν = 450 cm-1
22
pKBHX = 5.46
Δν = 474 cm-1
23
pKBHX = 5.05
Δν = 472 cm-1

Scheme 26. Selected entries from the pK_{BHX} database[114] ($\Delta\nu$ with respect to methanol).

II-2-3 IR spectra of the solvent, reactants and product

II-2-3-1 Carbon dioxide

The IR spectrum of supercritical CO_2 at 60°C and 24 MPa is shown in figure 9. The carbon dioxide molecule possesses three different vibrational modes, namely a symmetric stretch (ν_1), a two-fold degenerate bending mode (ν_2) and an asymmetric stretch (ν_3). The modes ν_2 and ν_3 show strong absorptions centred around 667 cm^{-1} and 2349 cm^{-1} respectively. The symmetric stretch does not cause a change in the dipole moment of the molecule and is thus theoretically forbidden, but it can nevertheless be observed in the spectrum of supercritical CO_2 (1387 cm^{-1}) when a large path length is used. Under these conditions a number of combination bands and overtones may also be observed, notably $2\nu_2$ (1267 cm^{-1}), $\nu_1 + \nu_2$ (2070 cm^{-1}), $2\nu_2 + \nu_3$ (3609 cm^{-1}) and $\nu_1 + \nu_3$ (3716 cm^{-1}). As a result of these numerous bands, the spectral regions between 600-800 cm^{-1}, 2200-2500 cm^{-1} and 3500-3800 cm^{-1} are saturated, preventing the observation of any solute molecule absorptions in these wavenumber ranges.

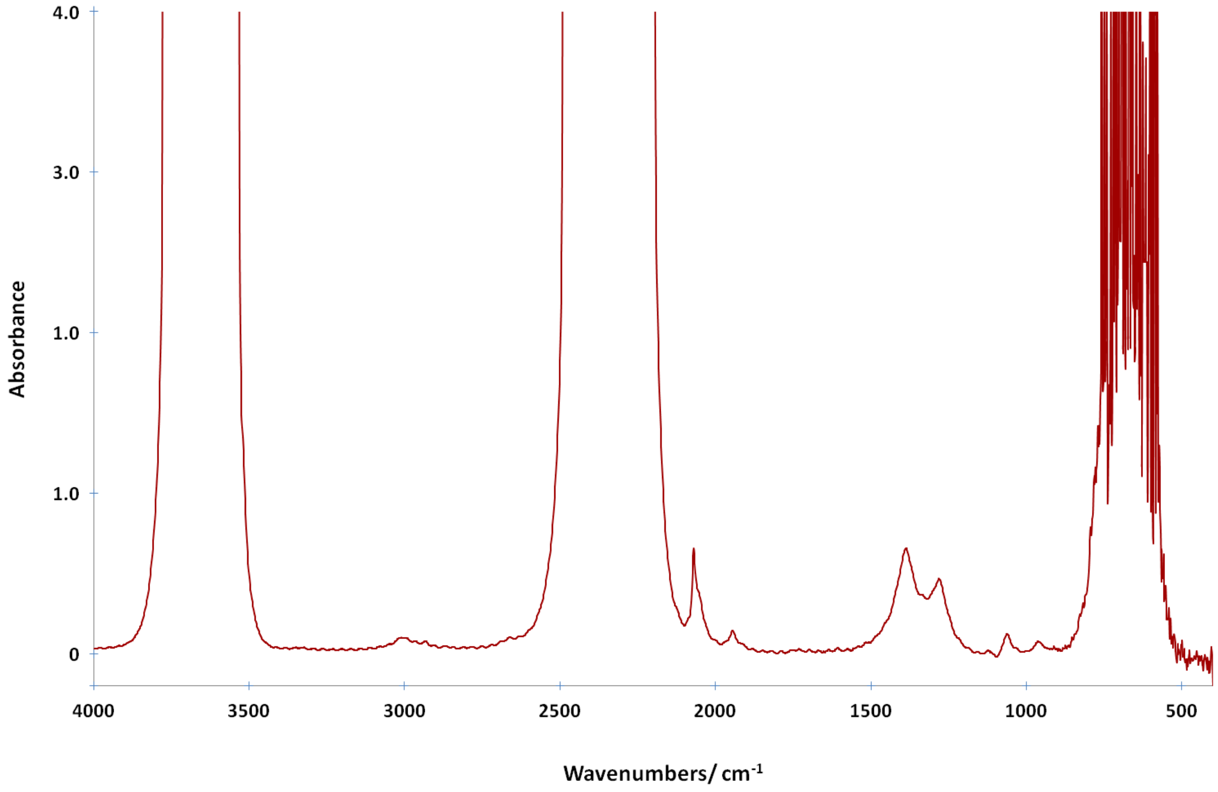

Figure 9. FTIR spectrum of $scCO_2$ (P = 24 MPa, T = 60°C)

II-2-3-2 n-Butanol

In the spectrum of *n*-butanol in $scCO_2$ (figure 10), the OH stretch band is masked by the CO_2 absorption at 3500-3800 cm^{-1}. The most intense band that can be observed in the spectrum, between 2850 cm^{-1} and 3000 cm^{-1}, corresponds to the C-H stretching modes.

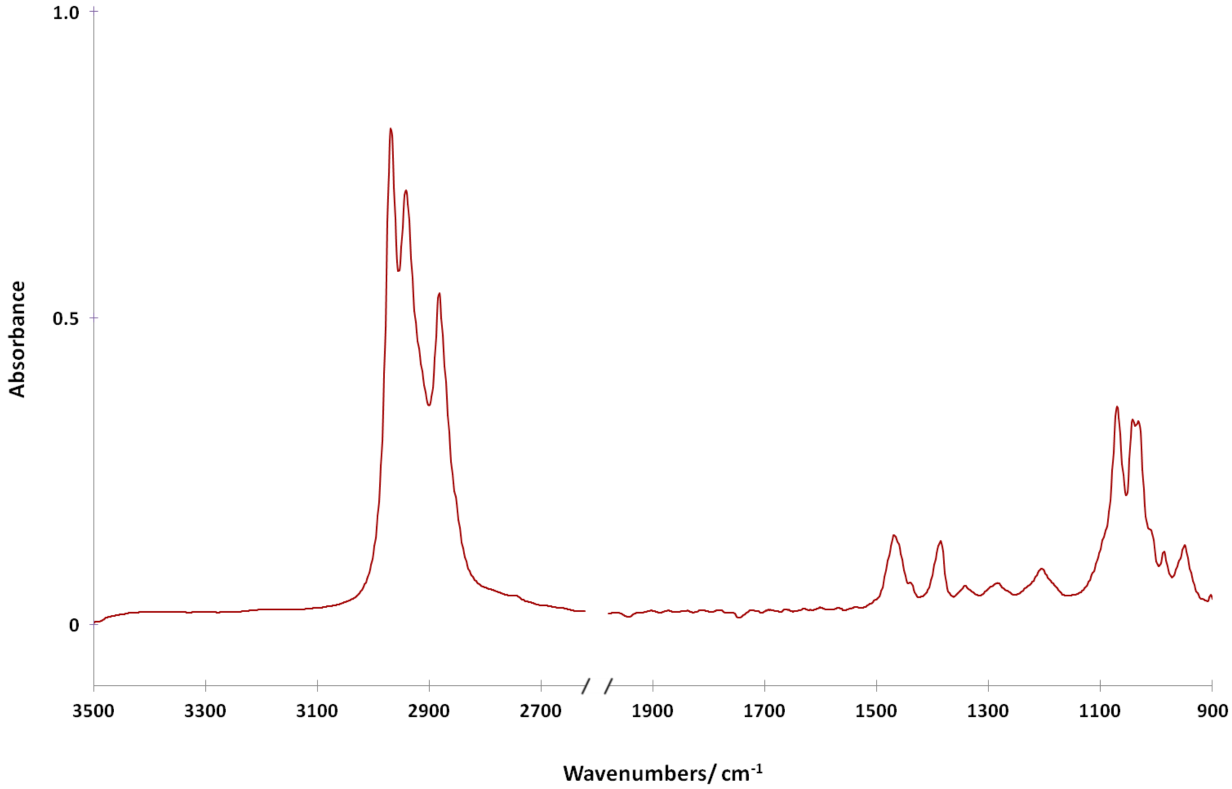

Figure 10. FTIR spectrum of *n*-butanol in $scCO_2$ (2.0 x 10^{-2} mol dm^{-3}, P = 20 MPa, T = 60°C)

II-2-3-3 2,4-TDI

The infrared spectrum of 2,4-TDI in $scCO_2$ is shown in figure 11. The spectrum is similar to that of the pure liquid and the bands have been assigned by analogy to similar compounds[115] or by theoretical simulation.[20] The intense peak centred around 2280 cm^{-1} in the spectrum of liquid TDI, corresponding to the asymmetric stretch of the isocyanate group and which is commonly followed during kinetic monitoring of isocyanate reactions, is masked by the spectrum of $scCO_2$. The isocyanate bending modes are also masked by CO_2 absorptions between 600 and 800 cm^{-1}. No evidence has been found for specific interactions between TDI and CO_2, on the basis that there is no change in frequency of the IR bands of TDI with increasing CO_2 pressure.[20]

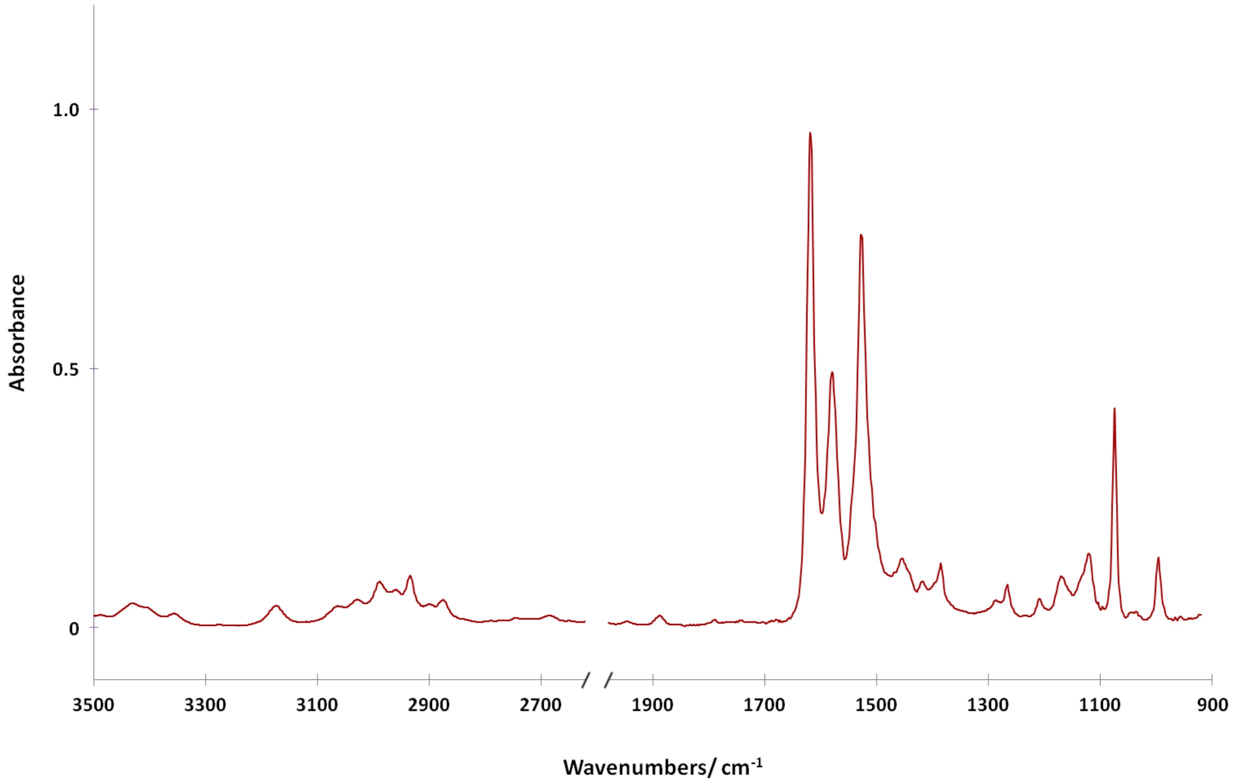

Figure 11. FTIR spectrum of 2,4-TDI in $scCO_2$ (1.0 x 10^{-2} mol dm^{-3}, P = 24 MPa, T = 60°C)

II-2-3-4 Dibutyl 4-methyl-1,3-phenylenedicarbamate

The infrared absorption bands of dimethyl 4-methyl-1,3-phenylenedicarbamate (the bis methyl carbamate of 2,4-TDI) have been assigned in accordance with theoretical calculations.[116] In $scCO_2$ (figure 12), the principal urethane bands of the di-*n*-butyl analogue (dibutyl 4-methyl-1,3-phenylenedicarbamate, **20**) are observed at 3456 cm^{-1} (amide A, ν(NH)), 1747 cm^{-1} (amide I, ν(C=O)), 1530 cm^{-1} (amide II, ν(CN) + δ(NH)) and 1210 cm^{-1} (amide III, ν(CO) + ν(CN) + δ(NH)).

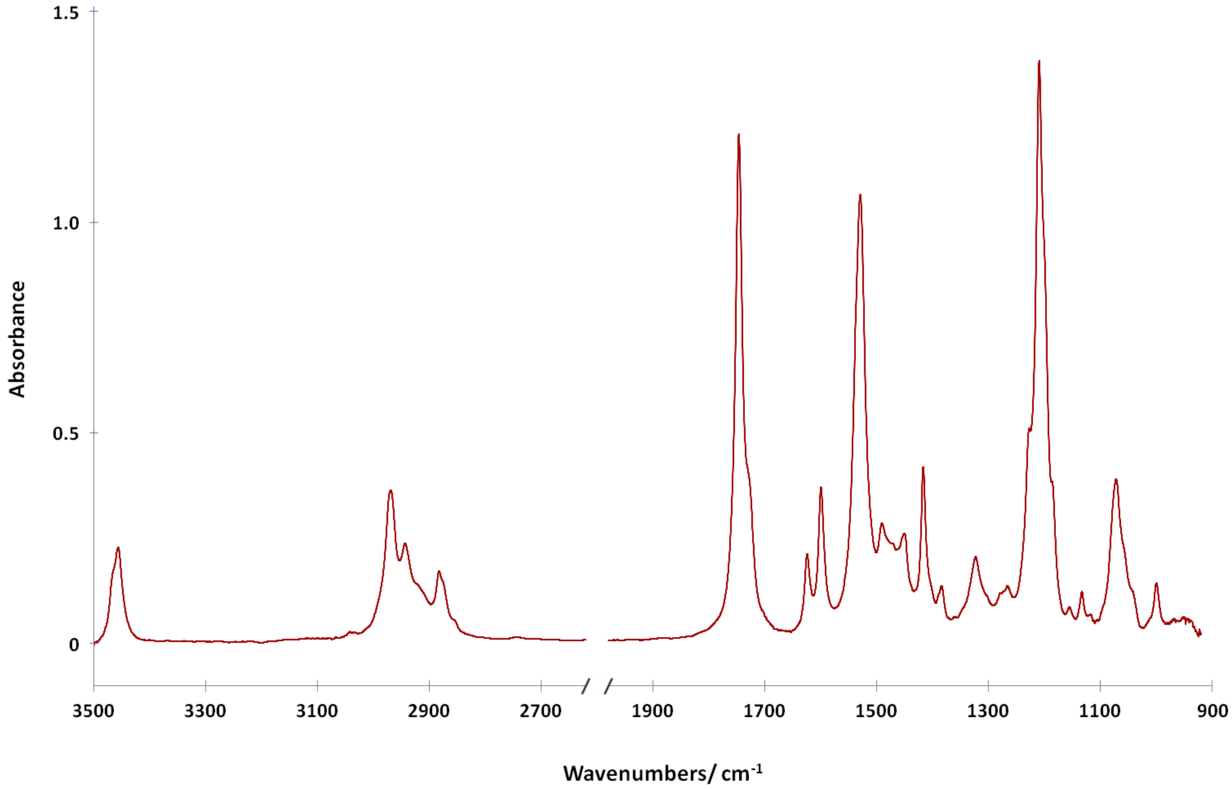

Figure 12. FTIR spectrum of dibutyl 4-methyl-1,3-phenylenedicarbamate (**20**) in $scCO_2$ (2.0 x 10^{-3} mol dm^{-3}, P = 24 MPa, T = 60°C)

II-2-4 Reaction kinetics with 5 mol% catalyst

In order to follow the reaction kinetics, a solution of the chosen catalyst in butanol was first dissolved in CO_2. The isocyanate was then injected by differential pressure and an initial IR spectrum was recorded immediately afterwards (t=0). Further spectra were recorded every two minutes thereafter, or every ten minutes once the reaction rate had diminished. As an example, figure 13 shows the evolution of the spectra with time for a reaction catalysed with triethylamine.

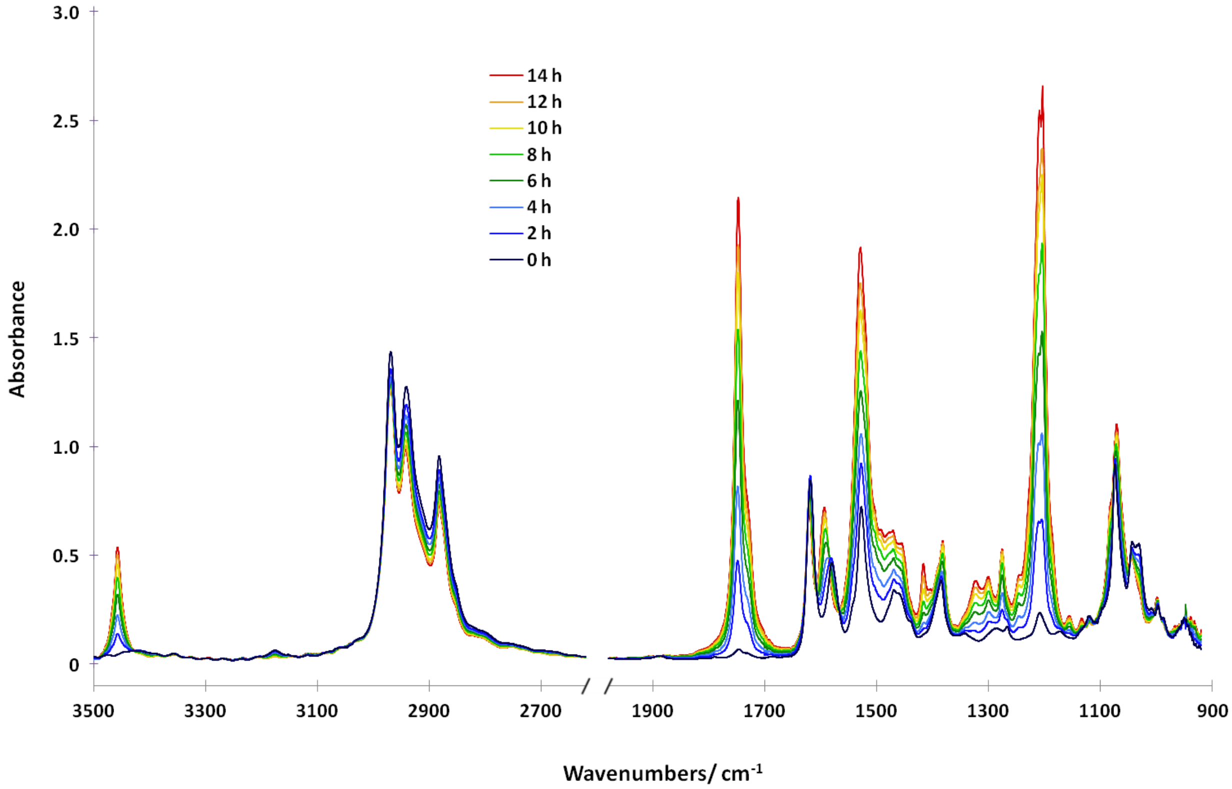

Figure 13. *In situ* IR spectra of the reaction between 2,4-TDI and *n*-butanol in $scCO_2$ catalysed by 5 mol% triethylamine at different reaction times.

A plot of the evolution of the area of the urethane N-H band with time in the presence of different catalysts at 5 mol% loading is shown in figure 14. With the reference tin based catalyst, DBTDL, there was a very rapid initial rate of reaction and the curve reached a plateau after approximately 60 minutes reaction time. The cyclic amidine DBU and guanidines MTBD and TBD also showed a rapid initial rate of reaction but the final values of the urethane peak absorbance (i.e. yields) were slightly lower. TBD was the only one of the catalysts to give a slightly “S” shaped kinetic curve, which presumably results from initial reaction of the active hydrogen of TBD with isocyanate (see scheme 27). The amine *N*-oxide NMO showed a similar kinetic profile to the amidine/guanidines although there appeared to be a slight decrease in the intensity of the urethane peak after it had rapidly reached a maximum. Tertiary amines (DABCO, NEt_3) and pyridine derivatives (DMAP, 4-pyrrolidinopyridine) showed a much slower rate of reaction and the curves had not reached a plateau after 17 hours reaction time. The value of the urethane peak area was only about 50-

60% of that achieved with DBTDL after this time. There was nevertheless a marked increase in the rate of reaction compared to the uncatalysed reaction, which was extremely sluggish.

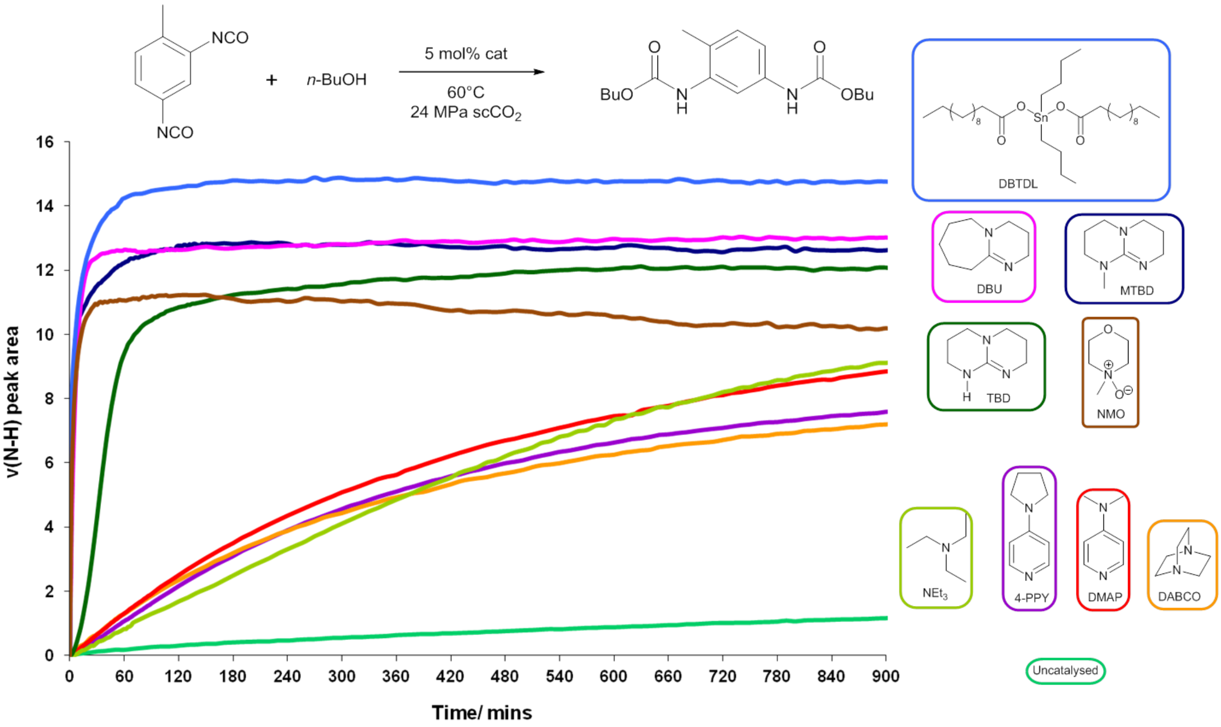

Figure 14. Kinetic curves for the reaction of 2,4-TDI with *n*-butanol in $scCO_2$ with 5 mol% catalyst.

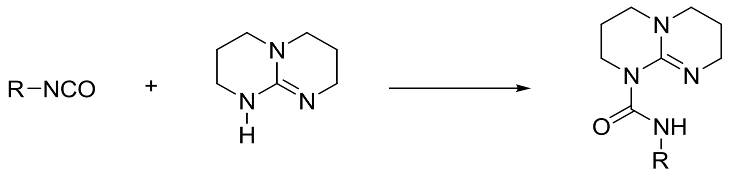

Scheme 27. Reaction of an isocyanate with TBD.

An absorbance calibration of the reaction product was carried out in order to allow direct conversion of absorbance into percentage yield. A purified sample of dibutyl 4-methyl-1,3-phenylenedicarbamate (**20**) was prepared and small portions of the product were weighed into the high pressure cell and dissolved in $scCO_2$ under the model reaction conditions, in order to plot the absorbance of the *v*(N-H) peak area (and *v*(C=O) peak height) as a function of concentration (figure 15). This allowed the absorbance recorded in the spectra of the model reactions to be converted into percentage yield. Accordingly, the reaction catalysed by DBTDL thus gave a yield of approximately 85%, which seemed surprising as the reaction was expected to be quantitative.

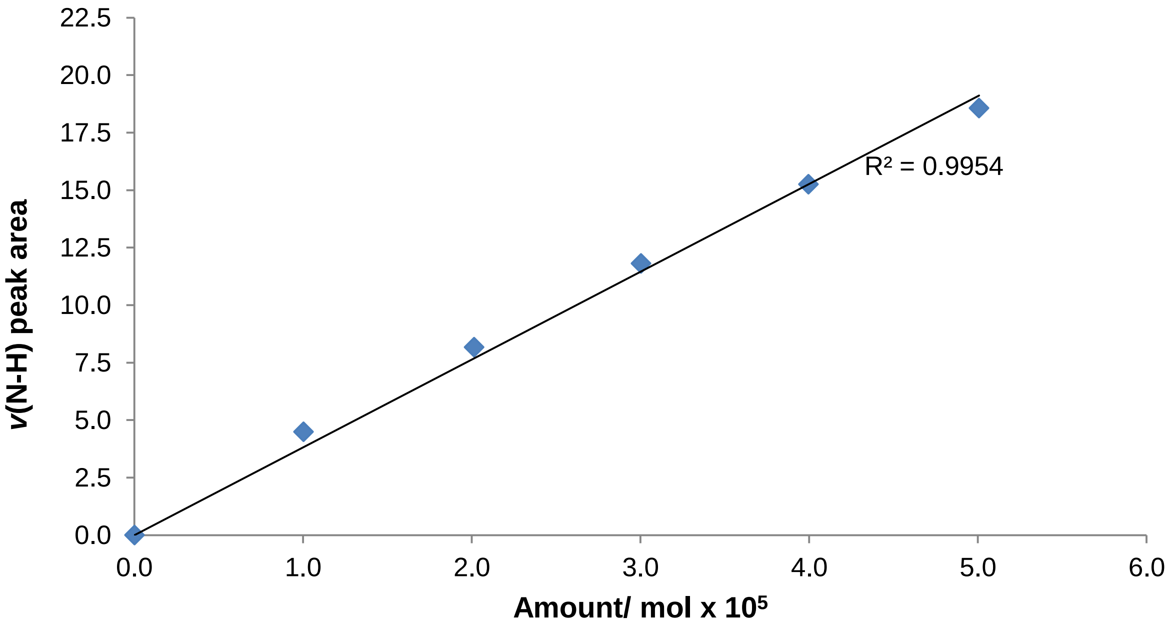

Figure 15. Plot of the *v*(N-H) peak area versus concentration in supercritical CO_2 at 60°C.

II-2-4-1 N-H peak shape

Analysis of the spectra recorded during kinetic monitoring showed a clear difference in the shape of the N-H peak depending on the catalyst employed. In the reactions with the more active catalysts (DBTDL, MTBD, TBD, DBU, NMO), two overlapping peaks could be observed by the end of the reaction, whereas with the less active catalysts (tertiary amines, pyridine derivatives) only a single peak was present (see figure 16). Given that both peaks are present in the spectrum of the pure product dibutyl 4-methyl-1,3-phenylenedicarbamate (**20**), the two peaks are logically assigned to the two different carbamate groups in this unsymmetrical molecule. This analysis is supported by theoretical calculations of the vibrational frequencies of dicarbamate derivatives of TDI, showing a separation of 11 cm^{-1} between the two N-H stretching vibrations.[116] In the solid state or in more concentrated solutions the N-H bands are broadened due to hydrogen bonding and the two different carbamate groups are indistinguishable.

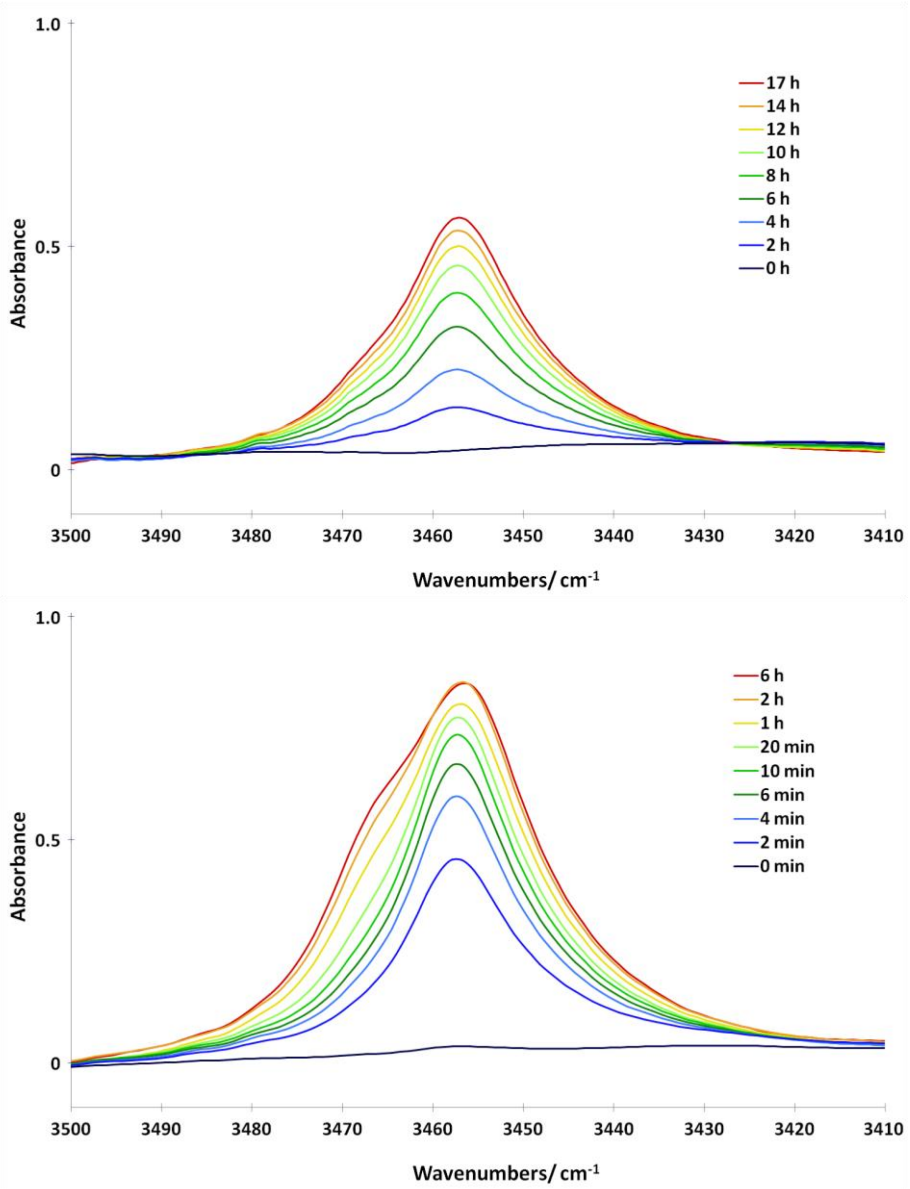

Figure 16. *In situ* IR spectra of the reaction between 2,4-TDI and *n*-butanol in $scCO_2$ showing the evolution of the urethane N-H stretch peak with time. *Top*, reaction catalysed with 5 mol% triethylamine; a single peak is observed with the less active catalysts, *bottom*, reaction catalysed with 1 mol% DBTDL; a second peak (shoulder) is observed with the more active catalysts.

The peak centred at 3457 cm^{-1} can reasonably be assigned to the para-carbamate group, as this peak is formed first and the greater reactivity of the para-isocyanate versus the ortho-isocyanate group in 2,4-TDI has been well documented.[117] The shoulder at 3466 cm^{-1} then corresponds to the ortho-carbamate group which is formed more slowly or hardly at all in the case of the less active catalysts.

The presence of two non-equivalent isocyanate groups actually leads to two possible reaction pathways with four associated reaction rates (scheme 28). Two factors influence the rate constants of these reaction steps. First of all, as mentioned above the ortho-isocyanate group is less reactive than the para-isocyanate group (i.e. $k_1 > k_2$, $k_4 > k_3$) due to the steric and/or electronic effects of the methyl group.[117b] Secondly, for a given isocyanate group, the reactivity is greater when the ring is substituted with another isocyanate group than with a carbamate group (i.e. $k_1 > k_4$, $k_2 > k_3$) due to the more electron withdrawing nature of the former. Several studies have attempted to calculate the relative rates of these four reaction steps by fitting kinetic data obtained through NMR, IR, HPLC, and/or back titration, and the results are summarised in table 1. Theoretical computations have also been used to calculate the reactivity ratios, finding values of 2.94 for k_1/k_2 and 22.65 and 6.65 for k_1/k_3 in the gas phase and benzene solutions respectively.[118]

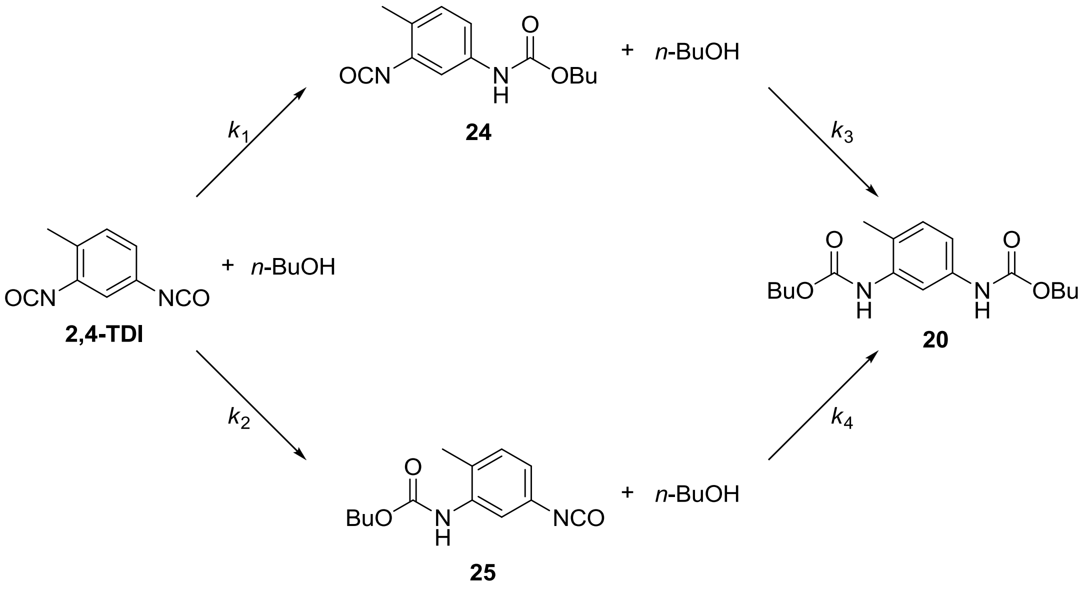

Scheme 28. The two possible reaction pathways for the reaction of 2,4-TDI with *n*-butanol.

Method	**Alcohol**	**Solvent**	**Temp.**	**Catalyst**	**Rate constants**				**Ref.**
					k_1	k_2	k_3	k_4	
NMR/IR	Methanol	CCl_4	50°C	-	69	10	1.0	2.9	104a
Titration/NMR/ HPLC	2-Hydroxyethyl acrylate	Bulk	40°C	-	79	13	1.0	54	105
Titration	*n*-Butanol	Xylene	80°C	-	15	2.7	1.0	8.3	106
IR	*n*-Propanol	CCl_4	R.T.	-	148	49	1.0	239	18b
				Caprolactam	19	10	1.0	17	
HPLC	*n*-Butanol	Bulk		-	18	4.4	1.0	4.2	101
NMR	Methanol	CCl_4	40°C	-	9.7	1.4	1.0	6.3	104b

Table 1. Summary of literature rate constants for the individual steps of the reaction of 2,4-TDI with hydroxyl containing compounds.

Given that k_1 is greater than k_2 and that all the reactions can be considered to be irreversible under the experimental conditions, the overall reaction passes predominantly through the intermediate **24**. Additionally, since k_4 is greater than or equal to k_2 (according to most authors), there should not be an accumulation of intermediate **25** during the reaction.

Other than the changes in the form of the N-H stretch peak during the reaction, changes to the absorption bands in the region between 1240 and 1440 cm^{-1} also appear to highlight the two-step reaction pathway. Figure 17 shows the evolution of the spectra with time in a reaction catalysed with 1 mol% DBTDL. Peaks at 1276, 1301 and 1382 cm^{-1} grow rapidly at the beginning of the reaction, reaching a maximum after about 10 minutes and then slightly diminish afterwards, while peaks at 1323 and 1417 cm^{-1} grow gradually throughout the reaction. The first three peaks thus presumably correspond to the intermediate **24**, while the other two peaks correspond to the final product **20**. In the reactions catalysed by the less active catalysts (triethylamine, DABCO, DMAP and 4-PPY), there appeared to be little formation of the ortho-carbamate group, and after 17 hours reaction time intermediate **24** appears to be the principal reaction product.

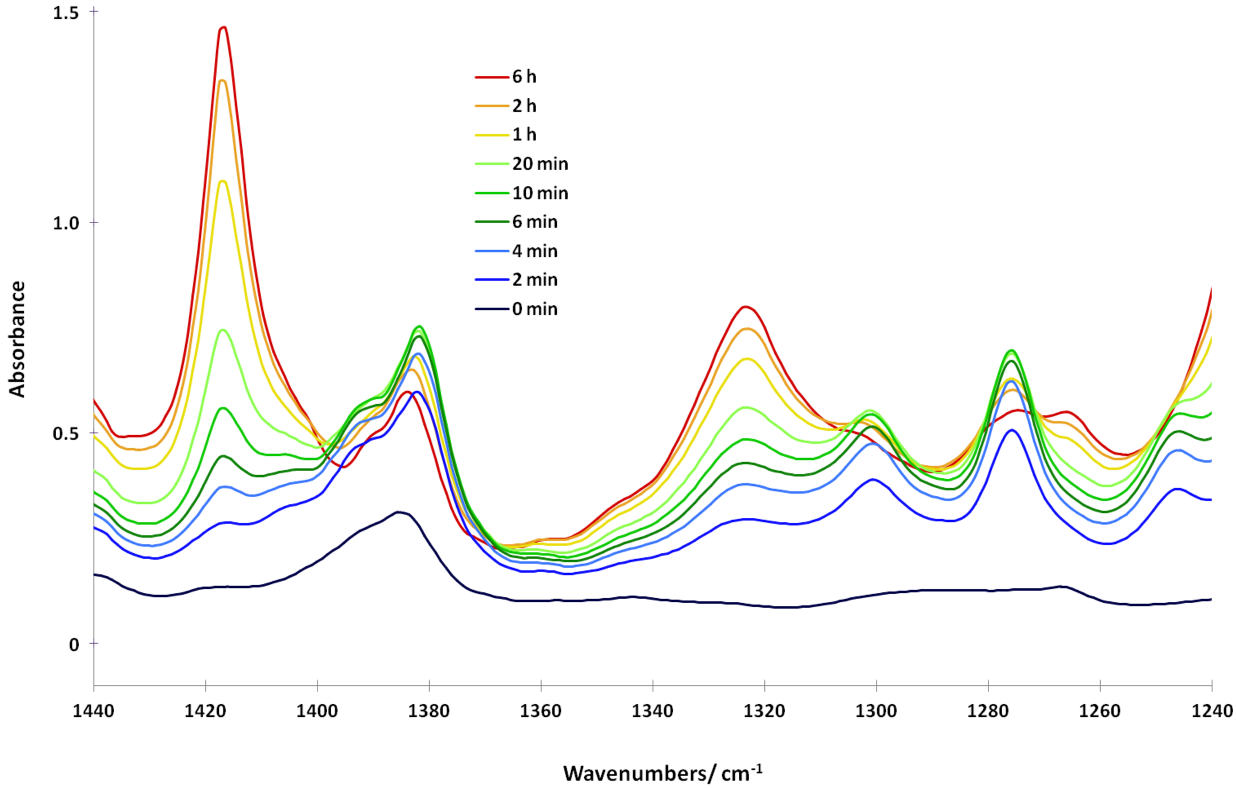

Figure 17. *In situ* IR spectra of the reaction between 2,4-TDI and *n*-butanol in scCO$_2$, catalysed with 1 mol% DBTDL: the evolution of bands in the region between 1240 and 1440 cm^{-1} with time.

The nature of any catalyst used clearly has an influence on the relative rates of the individual reaction steps. Boitsov and Trub found that organotin catalysts such as DBTDL enhanced the difference in reactivity between the ortho- and para-NCO groups of 2,4-TDI (k_1/k_2) compared to the uncatalysed reaction, while tertiary amines had an equalizing effect.[104b] In the spectra recorded in the present study, the relative selectivity of the different catalysts for the ortho- and para-isocyanate groups can be examined by comparing the shape of the N-H peak at low isocyanate conversion (figure 18). In the reaction catalysed by MTBD, the two isocyanate groups appear to react somewhat more simultaneously (greater intensity of the shoulder at 3466cm^{-1}) compared to the reaction catalysed by DBTDL. NMO and triethylamine show intermediate selectivity. DBU gave a similar result to that presented for MTBD. A more quantitative analysis of the reaction rates would appear to be difficult, considering the presence of three different carbamate species with overlapping absorptions.

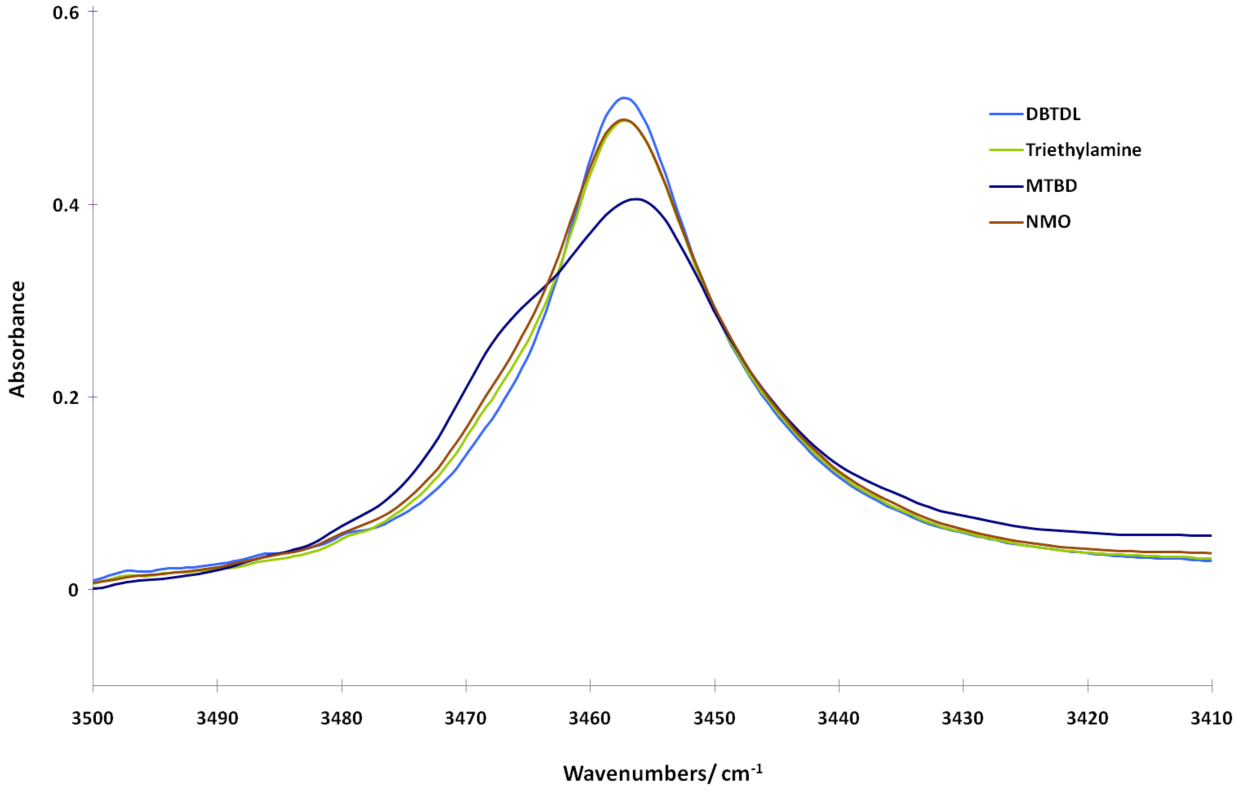

Figure 18. Carbamate N-H peak in the reaction of 2,4-TDI with *n*-butanol in $scCO_2$ at approximately 40% yield, showing the dependence of the peak shape on the catalyst used (5 mol%).

II-2-5 Reaction kinetics with 1 mol% catalyst

The best performing compounds from the initial catalyst screening were further tested at lower catalyst loading. With 1 mol% catalyst, the superior rate of reaction with DBTDL compared to MTBD, DBU and NMO was more marked (figure 19). Nevertheless, the initial reaction rate observed with the organocatalysts remained relatively rapid. NMO showed a marginally faster rate than MTBD and DBU. The most striking difference between DBTDL and the organocatalysts was in the final carbamate peak areas, i.e. yields of the reactions. With the organocatalysts, the kinetic curves quickly reached a plateau, but at much lower yield than with DBTDL, suggesting either a drop in catalytic activity or the consumption of reactants in a secondary reaction. In order to further investigate these possibilities, analyses of the reaction residues were carried out by NMR and/or Raman spectroscopies (vide infra).

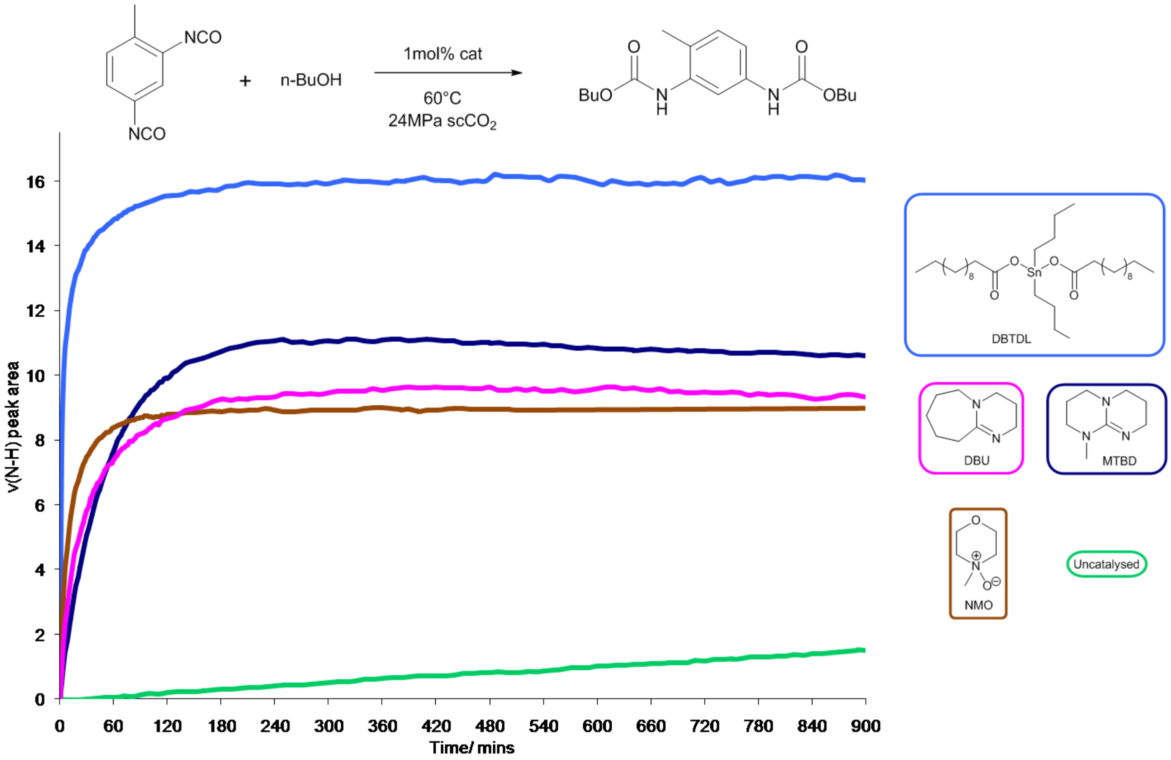

Figure 19. Kinetic curves for the reaction of 2,4-TDI with *n*-butanol in $scCO_2$ with 1 mol% catalyst.

An additional experiment aimed to test for the presence of remaining reactants; at the end of a reaction catalysed by 1 mol% MTBD, an additional 5 mol% DBTDL was added after the kinetic curve had reached a plateau (figure 20). This resulted in the reaction starting back up again with a second curve, showing that there were still unreacted starting materials in the mixture and thus that the catalyst may have been deactivated. However, the second plateau attained was not much higher than the first, and the apparent yield of the reaction was only approximately 60% of that achieved in the reaction catalysed solely by DBTDL. This suggests that secondary reactions may have occurred such as formation of allophanate or isocyanurate, which consume isocyanate.

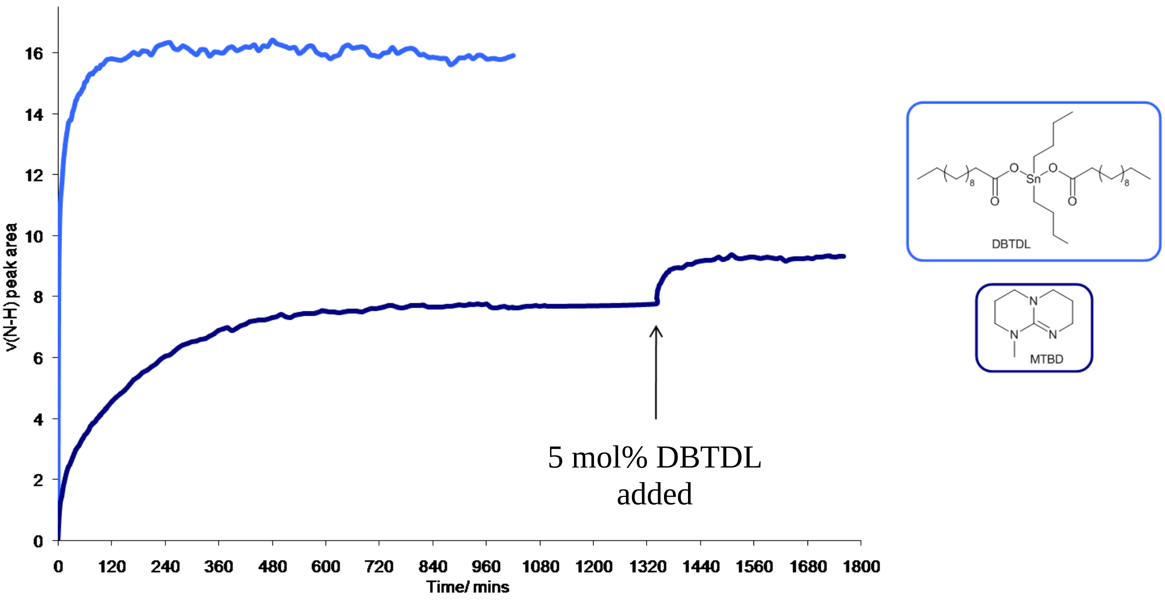

Figure 20. The kinetic curve for a reaction of 2,4-TDI with *n*-butanol in $scCO_2$ catalysed by 1 mol% MTBD, with subsequent addition of 5 mol% DBTDL after the reaction rate reached a plateau.

II-2-6 Reaction kinetics with phenyl isocyanate

A few kinetic runs were undertaken with phenyl isocyanate in the place of 2,4-TDI in order to compare the catalysts with a simpler monofunctional system (figure 21). DBTDL, MTBD and NMO were tested at 5 mol% and the organotin catalyst gave a somewhat faster rate of reaction than the organocatalysts (the difference in rate appeared to be greater with PhNCO than with TDI). The carbamate peak area (i.e. yield) was once again greater with DBTDL. With NMO, the carbamate peak area reached the same maximum as with MTBD but the rate of reaction was somewhat superior.

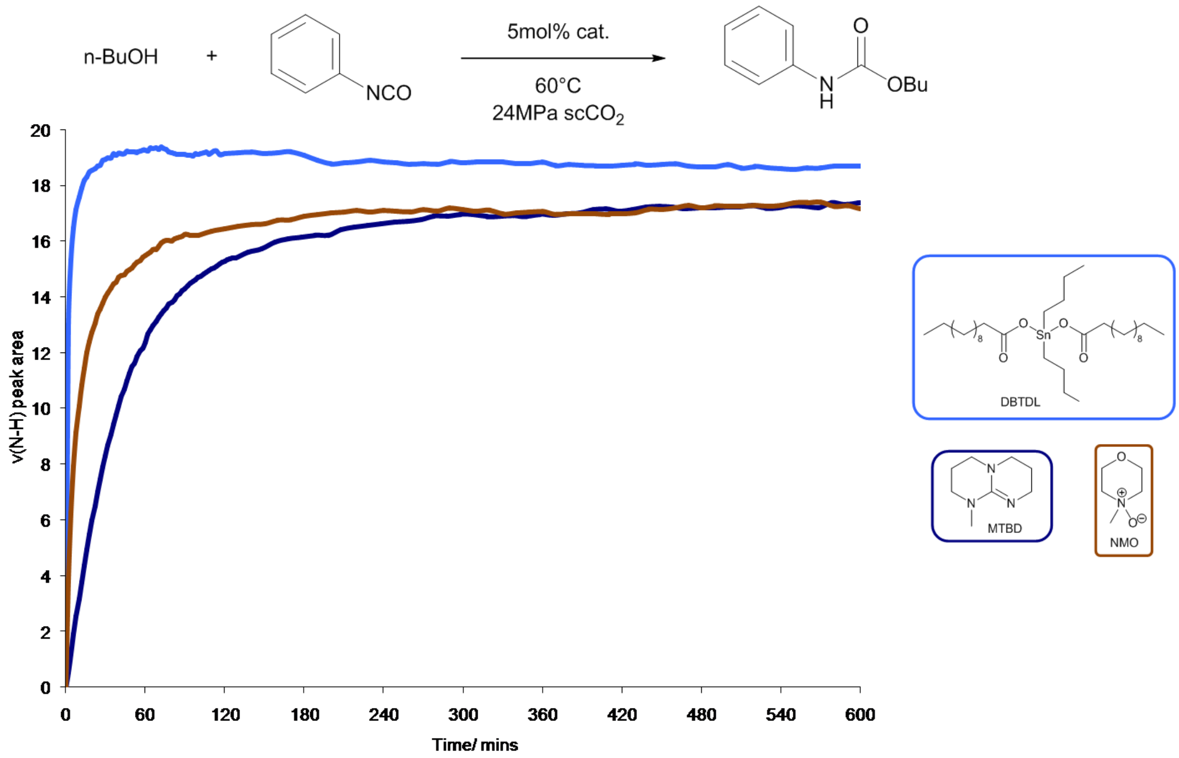

Figure 21. Kinetic curves for the reaction of phenyl isocyanate with *n*-butanol in $scCO_2$ with 5 mol% catalyst.

II-2-7 NMR and Raman analysis of product residues

Several of the kinetic runs were repeated with NMR and/or Raman analysis of the product residue in order to identify possible side-products. DMSO-d_6 was selected as the NMR solvent as there is already some existing data in the literature on the NMR of urethane derivatives of TDI in this solvent.[119] The NMR spectrum of the main reaction product dibutyl 4-methyl-1,3-phenylenedicarbamate **(20)** is shown in figure 22.

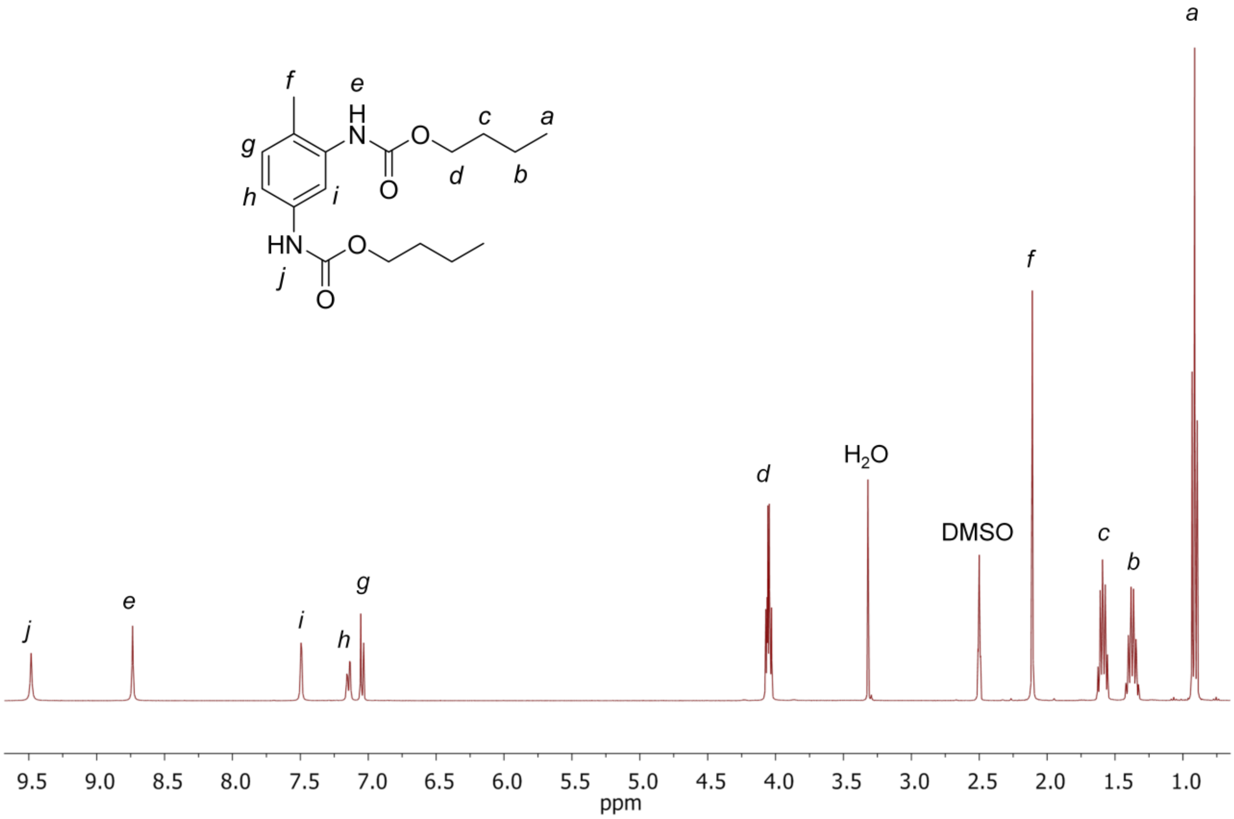

Figure 22. ^1H NMR spectrum of dibutyl 4-methyl-1,3-phenylenedicarbamate (**20**) in DMSO-d_6.

In the spectra of the reaction residues, several additional peaks could be identified other than those belonging to the principal product. The region around 2 ppm (containing the aromatic methyl singlets such as *f*) was particularly useful for the identification of the compounds present, by comparison with the spectra of model compounds (scheme 29, see appendix for synthesis and characterisation).

Amino substituted carbamates **26** and **27** (scheme 29) were clearly identified in all the spectra (CH_3 singlets at 2.02 and 1.96 ppm respectively). The amino groups are formed by reaction of the residual isocyanate groups with moisture present in the NMR solvent. These compounds thus represent unreacted isocyanate from the reactions in $scCO_2$ (compounds **24** and **25**).

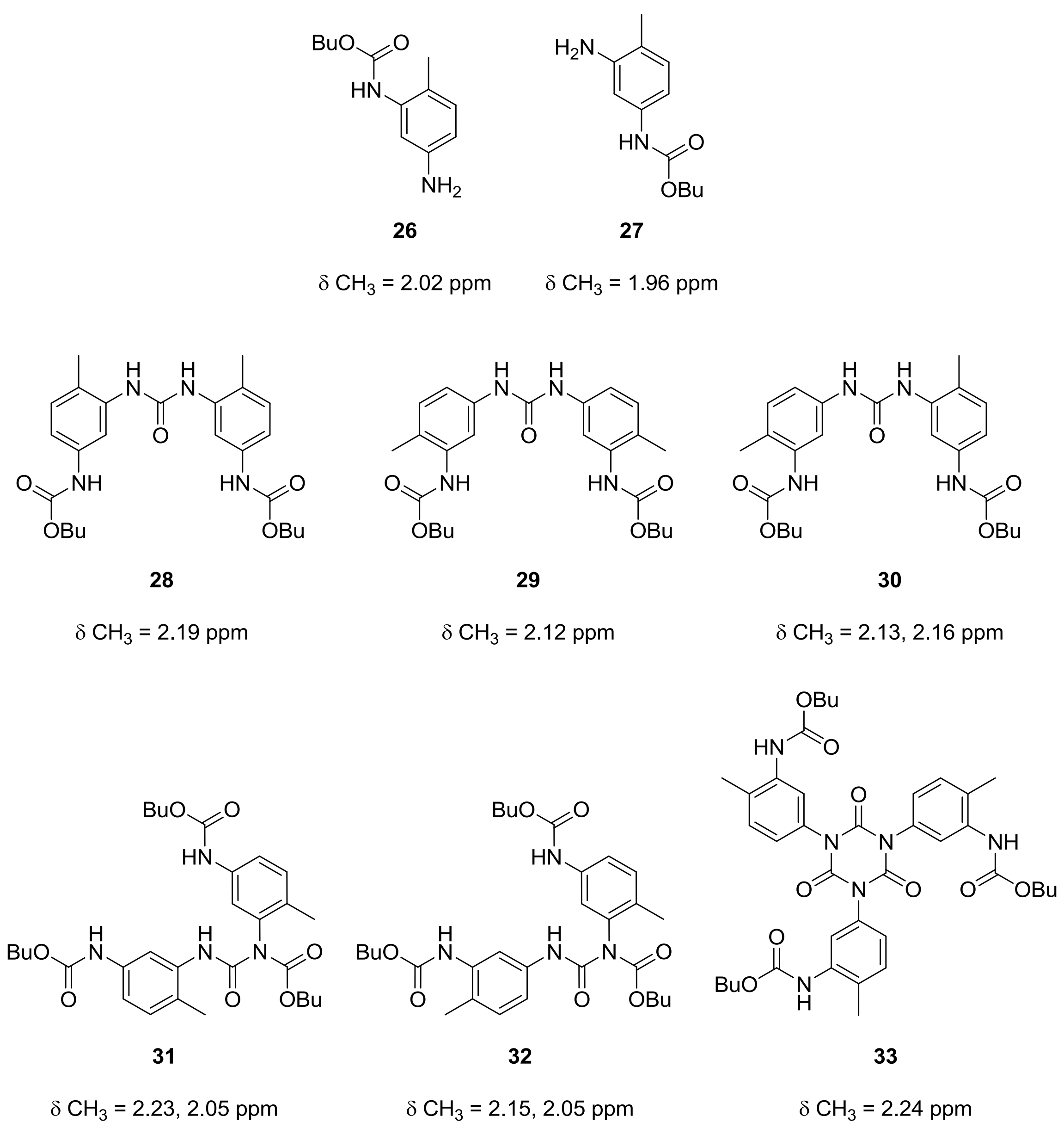

26 δ CH_3 = 2.02 ppm

27 δ CH_3 = 1.96 ppm

28 δ CH_3 = 2.19 ppm

29 δ CH_3 = 2.12 ppm

30 δ CH_3 = 2.13, 2.16 ppm

31 δ CH_3 = 2.23, 2.05 ppm

32 δ CH_3 = 2.15, 2.05 ppm

33 δ CH_3 = 2.24 ppm

Scheme 29. Possible side-products in the reaction of 2,4-TDI with *n*-butanol.

Several generally weak peaks could be observed between 2.12 and 2.19 ppm and appear to correspond to diarylureas **28**-**30**. Ureas are formed when an amine, generated from the reaction of water with an isocyanate, goes on to react with another isocyanate group. The three structural isomers each show different chemical shifts for the methyl singlets. It is difficult to assign all of these peaks with certainty in the spectra of the reaction residues due to their weak concentration. These ureas could be formed either during the reaction in $scCO_2$, or during the subsequent analysis, but the former seems more likely given the low concentration of isocyanate in the NMR solution (it can also be noted that in one of the analyses there is a relatively high amount of the amino substituted carbamate but nonetheless very little urea).

Two other types of expected side-products were isocyanurates (isocyanate trimers) and allophanates. The isocyanurate **33** and allophanates **31** and **32** were prepared as model compounds. The isocyanurate **33** showed a broad, highly shifted methyl singlet at 2.24 ppm. The allophanate **31** shows two different methyl singlets at 2.23 and 2.05 ppm and has a characteristic high field NH shift of 10.55 ppm. However, it was found that the allophanate linkage dissociated back to carbamate and isocyanate in DMSO-d_6 (or DMF-d_7). The isocyanate was then converted to the amino group by reaction with water. This was a surprising result considering that none of the literature NMR studies in these solvents had mentioned this as an issue. Additionally, Okuto[120] and Furukawa et al.[121] have reported that reactive amines are necessary in order to degrade allophante (and biuret) linkages in DMSO at low temperatures. Traces of peaks at 10.53 and 10.56 ppm were observed in the residues of reactions catalysed by 1 mol% MTBD, DBU and NMO (although not in reactions with 5 mol% catalyst). It is difficult to determine if only traces of allophanate were formed in the reactions in $scCO_2$ or if higher levels of allophanate were formed and only the remaining traces can be observed because of dissociation during the analysis. Biurets could also show peaks in this region and are reportedly more stable to dissociation.[12b, 122]

Further analysis of the NMR spectrum from each reaction is provided below and the associated kinetic curves are shown in figure 19 and figure 23. It is not always easy to account for the mass balance in these reactions, i.e. where the kinetic curve shows that the yield was less than quantitative, the corresponding amount of side-products or unreacted groups should be observed in the NMR spectrum. This could perhaps be explained by the elimination of a larger proportion of the more CO_2 soluble compounds on depressurisation. However, even if the analysis is not strictly quantitative, it provides good qualitative information on each reaction.

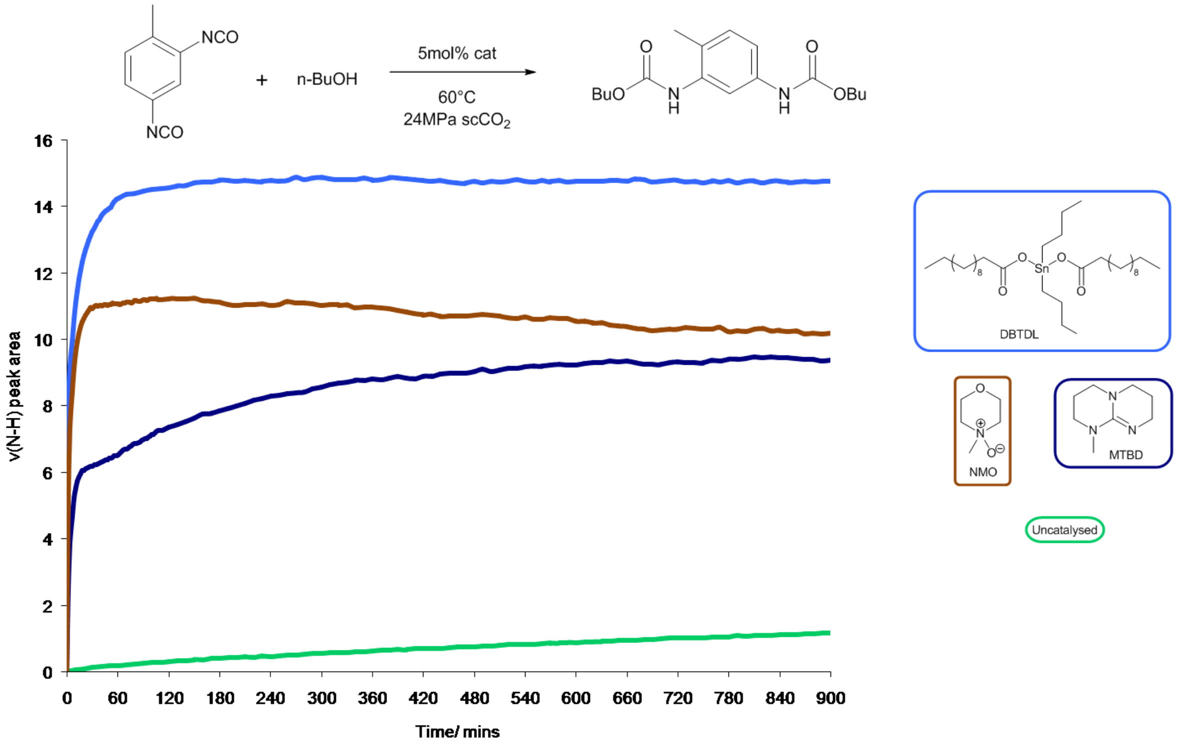

Figure 23. Kinetic curves for the reaction of 2,4-TDI with *n*-butanol in $scCO_2$ with 5 mol% catalyst (runs for which the reaction residue was analysed by NMR/Raman).

In the reaction catalysed with 5 mol% MTBD, the kinetic curve was somewhat different to that obtained in the original catalyst screening. There was an initial period of rapid reaction before the rate slowed suddenly, finally reaching a yield of around 60% of that observed with the DBTDL catalysed reaction. This ‘kinked’ curve shape was reproduced in a second repeat experiment.

In the NMR spectrum of the reaction residue (figure 24), small amounts of both the ortho- and para-amino substituted carbamates **26** and **27** were present, representing unreacted isocyanate groups. There appeared to be small amounts of the diarylureas, and more notably, an isocyanurate peak at 2.24 ppm.

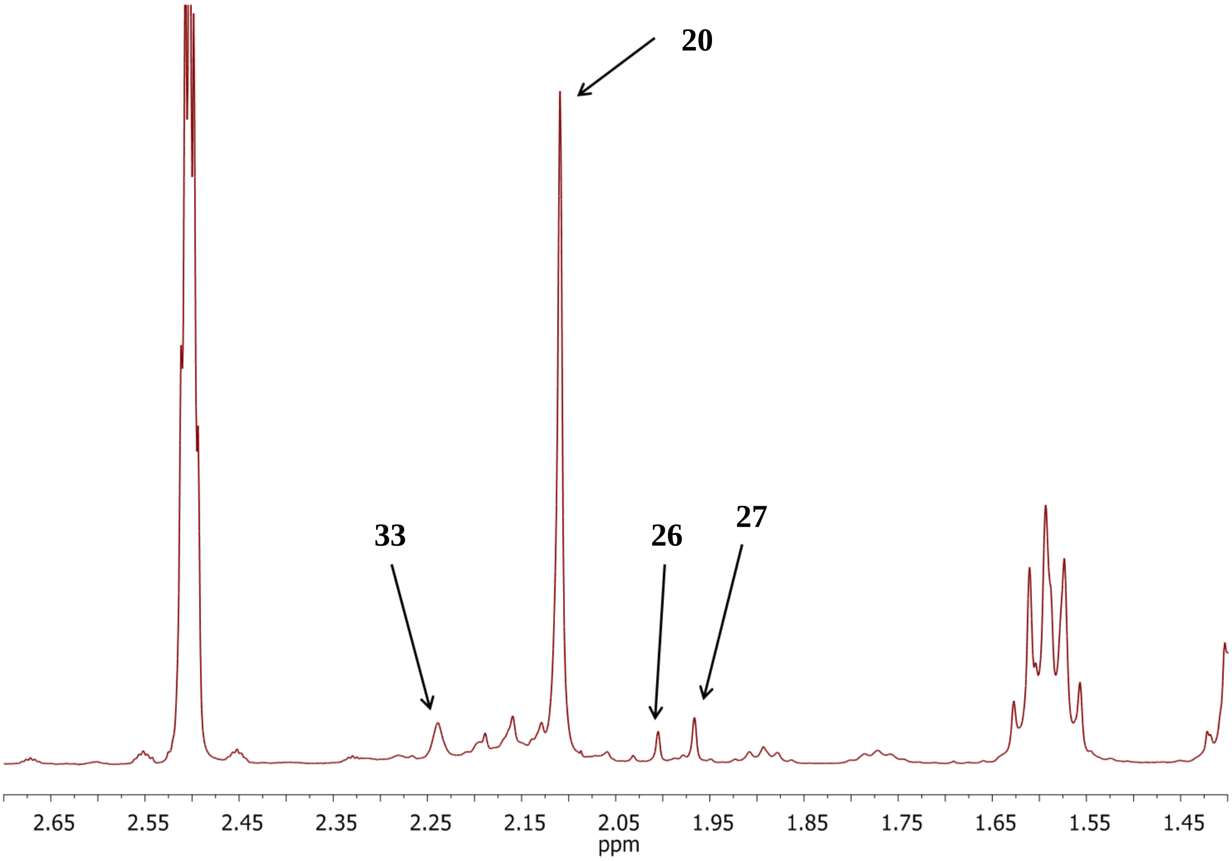

Figure 24. NMR spectrum of the reaction residue from the TDI/BuOH reaction catalysed by 5 mol% MTBD, showing the aromatic methyl group signals of various species present.

The presence of isocyanurate groups was confirmed by the presence of a peak at ~1780cm^{-1} in the Raman spectrum (figure 25). This band corresponds to the symmetric carbonyl vibration (A_1', ν(C=O)) which is not present in the IR spectra.[123] Thus, the reduced yield observed during *in situ* IR monitoring of this reaction seems primarily due to isocyanurate formation, which as well as consuming isocyanate groups could perhaps also render the carbamate groups attached to the isocyanurate ring unobservable due to poor solubility.

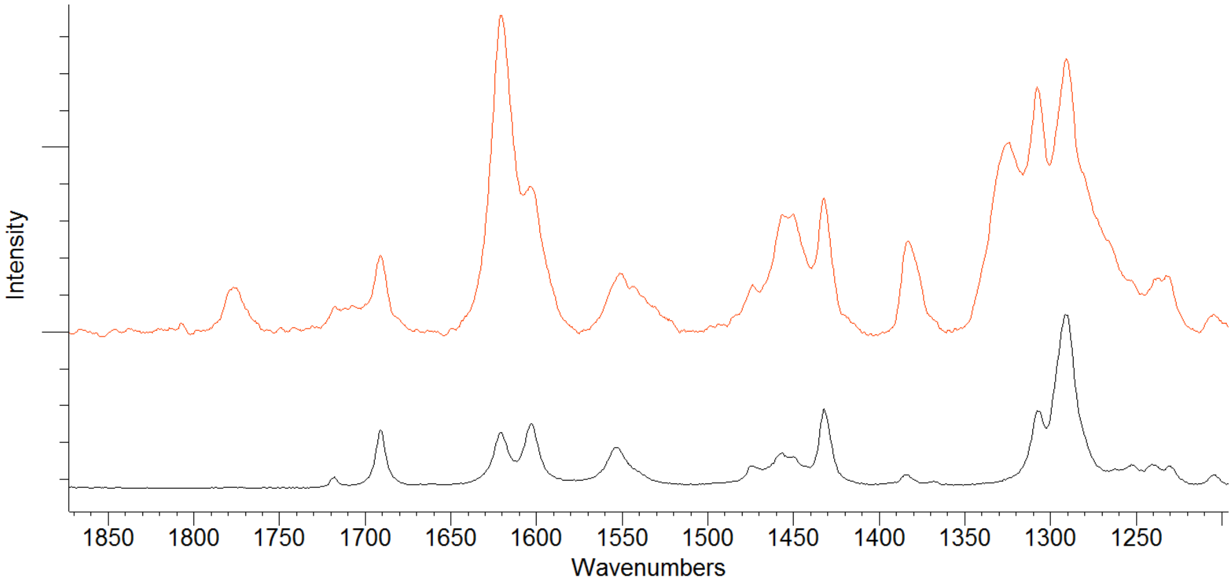

Figure 25. Raman spectra of dibutyl 4-methyl-1,3-phenylenedicarbamate (**20**, black) and the residue from the reaction of 2,4-TDI with *n*-butanol in $scCO_2$ catalysed by 5 mol% MTBD (red).

In the reaction catalysed by 1 mol% MTBD, although the initial rate of reaction was slower, there was no kink in the shape of the kinetic curve and the final yield was actually higher than that attained with 5 mol% catalyst loading.

In the NMR spectrum of the reaction residue (figure 26), a significant amount of the ortho-amino species **27** could be observed as well as a little of the diarylurea **28**. However, there appeared to be few other side-products present in the mixture, unlike the reaction with 5 mol% catalyst loading. The fact that the kinetic curve reached a plateau while there was still a significant amount of unreacted isocyanate groups remaining suggests that deactivation of the catalyst may have occurred. This could be due to the presence of traces of water (vide infra).

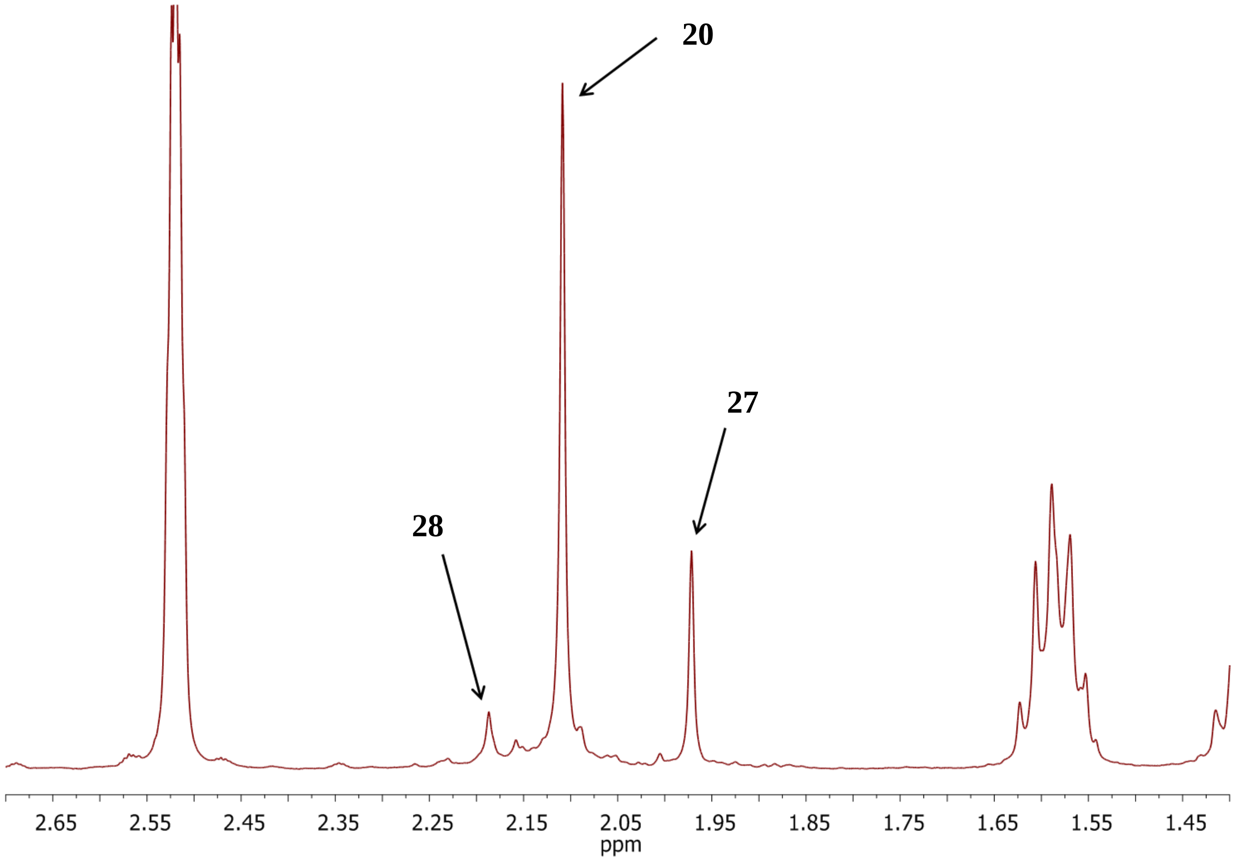

Figure 26. NMR spectrum of the reaction residue from the TDI/BuOH reaction catalysed by 1 mol% MTBD, in the aromatic methyl group region.

The reaction catalysed with 1 mol% DBU showed a similar rate of reaction to that catalysed with 1 mol% MTBD, with a marginally lower yield obtained. The NMR spectrum of the reaction residue (figure 27) showed a little of both the ortho- and para-amino species **26** and **27**, suggesting that catalysis with DBU is somewhat less selective than MTBD between the ortho- and para-isocyanate groups. There were few other side-product peaks observable in the spectrum and it seems difficult to account for the mass balance in this reaction.

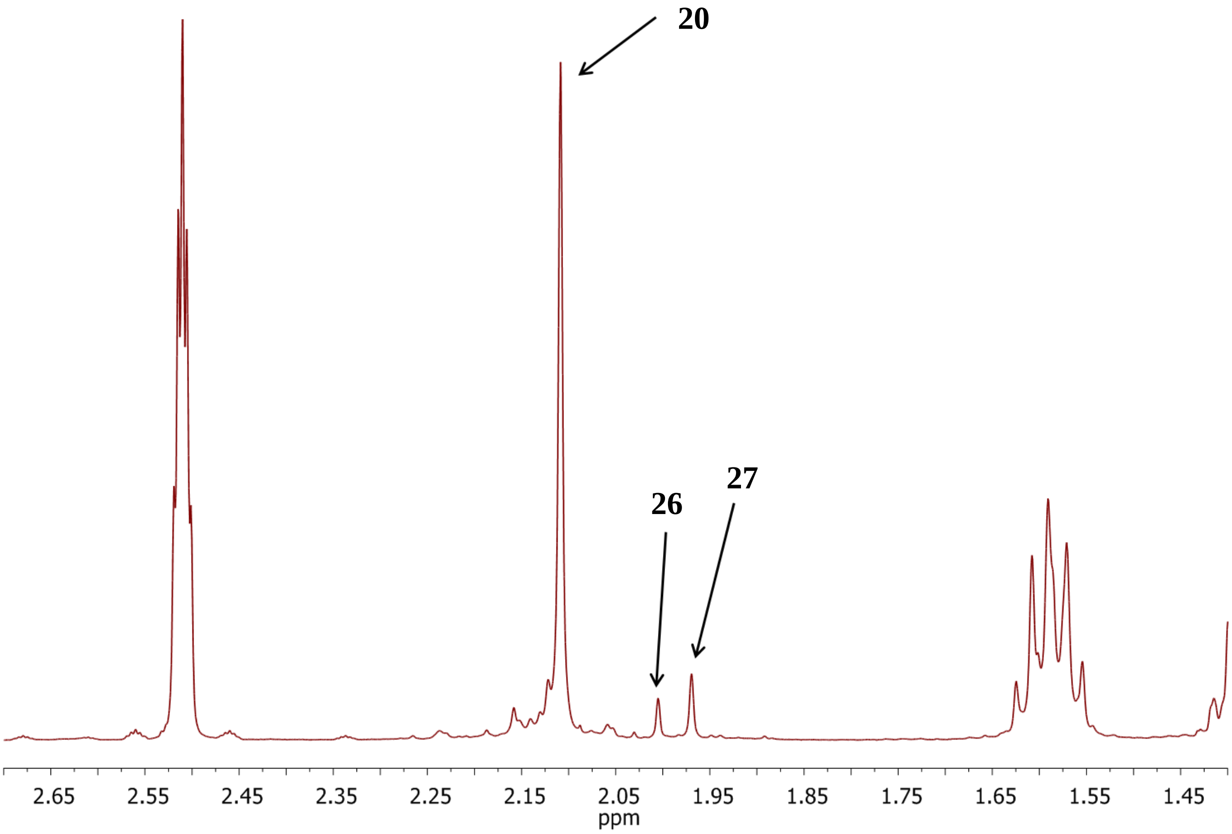

Figure 27. NMR spectrum of the reaction residue from the TDI/BuOH reaction catalysed by 1 mol% DBU, in the aromatic methyl group region.

In the reaction catalysed by 5 mol% NMO, the kinetic curve rapidly reached a plateau before descending slightly with prolonged reaction time. The final yield was greater than that achieved with 5 mol% MTBD but still significantly lower than that achieved with DBTDL. In the NMR spectrum of the reaction residue (figure 28) there was a reasonable amount of the ortho-amino species **27** present as well as the diarylurea **28**. The relatively high levels of diarylurea observed could be related to the highly hygroscopic nature of the amine oxide. As with MTBD at 1 mol% loading, the fact that the kinetic curve reached a plateau while there was still a significant amount of unreacted isocyanate groups remaining suggests that deactivation of the catalyst may have occurred. Small amounts of other side-products can be observed in the spectrum but are difficult to identify with certainty. It is interesting to note the absence of signals corresponding to residual NMO.

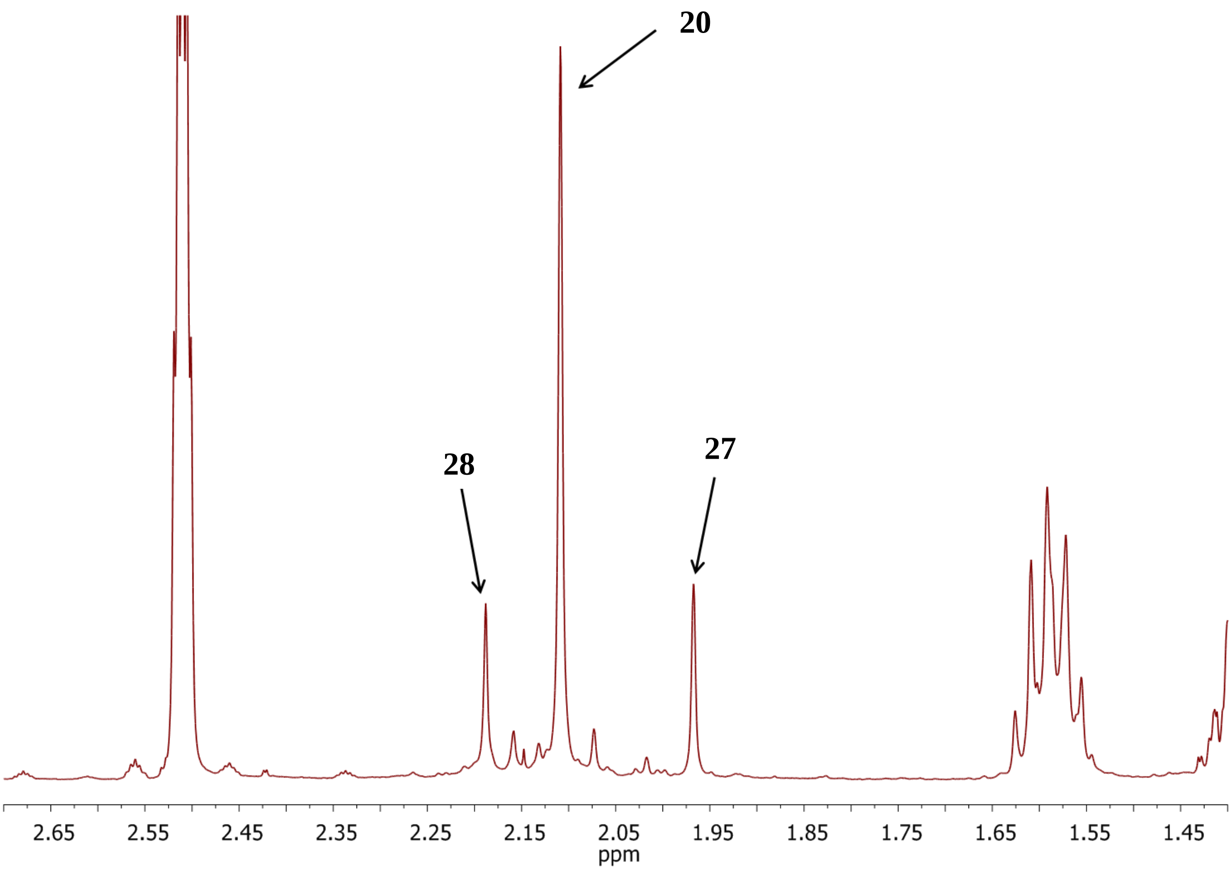

Figure 28. NMR spectrum of the reaction residue from the TDI/BuOH reaction catalysed by 5 mol% NMO, in the aromatic methyl group region.

In the reaction catalysed by 1 mol% NMO, the initial rate of reaction was greater than that for MTBD and DBU catalysts at the same loading, but the curve reached a plateau at a lower reaction yield. In the NMR spectrum of the reaction residue (figure 29), there was a ratio of approximately 1:1 of the dicarbamate **20** and the ortho-amino substituted species **27**, suggesting once again that the catalyst may have been deactivated. This also shows the strong selectivity for the para-isocyanate group.

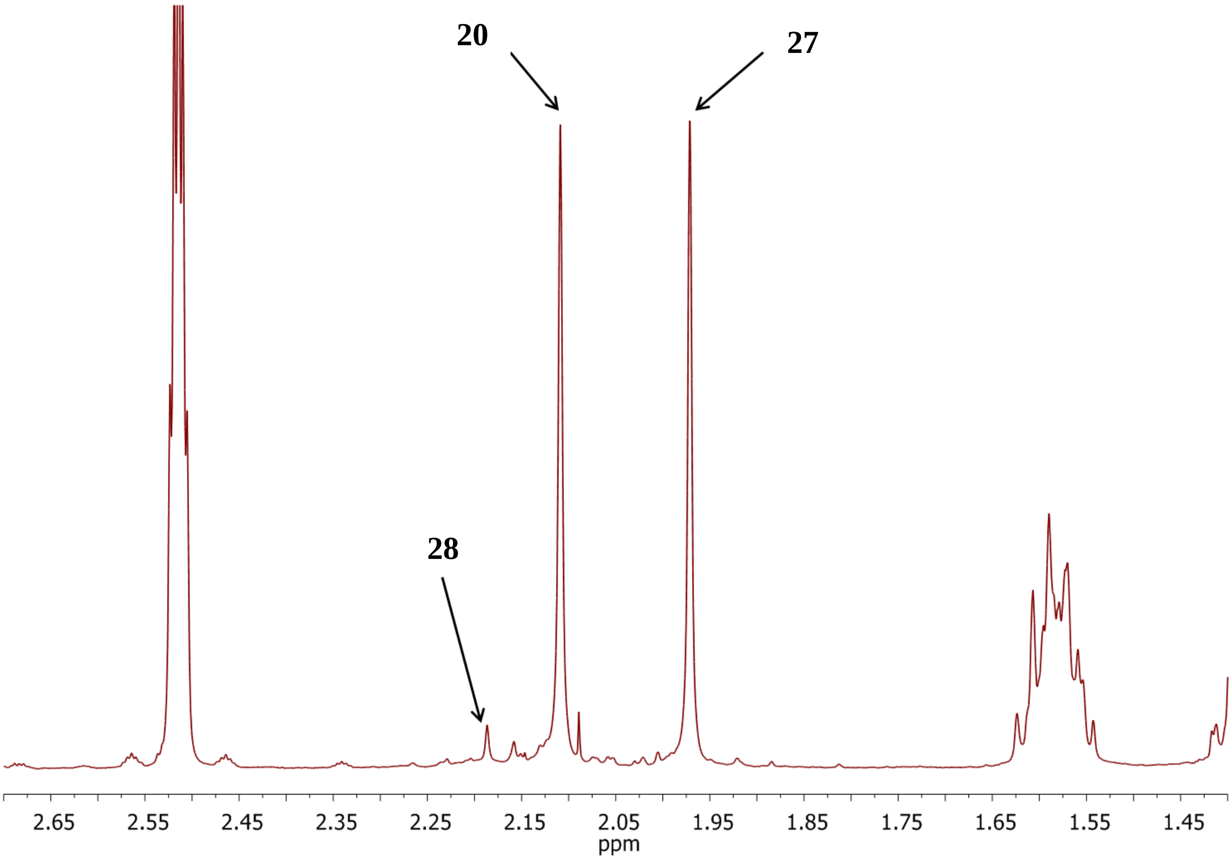

Figure 29. NMR spectrum of the reaction residue from the TDI/BuOH reaction catalysed by 1 mol% NMO, in the aromatic methyl group region.

II-2-8 Robustness of organocatalysts versus DBTDL

Some variability in the results of kinetic runs with the amidine/guanidine catalysts indicated that there might be some sensitivity to the reaction conditions. A series of experiments was thus undertaken to investigate the robustness of these organocatalysts compared to DBTDL.

First of all, the use of ordinary ‘wet’ butanol rather than anhydrous butanol led to a dramatic drop in the rate of the DBU catalysed reaction (figure 30, pink curves 1 and 2). In fact, after a reduced period of initial rapid reaction, the rate was similar to that of the uncatalysed reaction (green curve). A further drop in activity (pink curve 3) was observed when using standard industrial quality rather than N45 quality CO_2 (<7 ppm H_2O). Under the same conditions, MTBD showed no initial period of rapid reaction at all, although the rate remained greater than that of the uncatalysed reaction (dark blue curve 3). In comparison, the kinetic runs with

DBTDL were highly reproducible regardless of the dryness of the butanol or the quality of CO_2 employed.

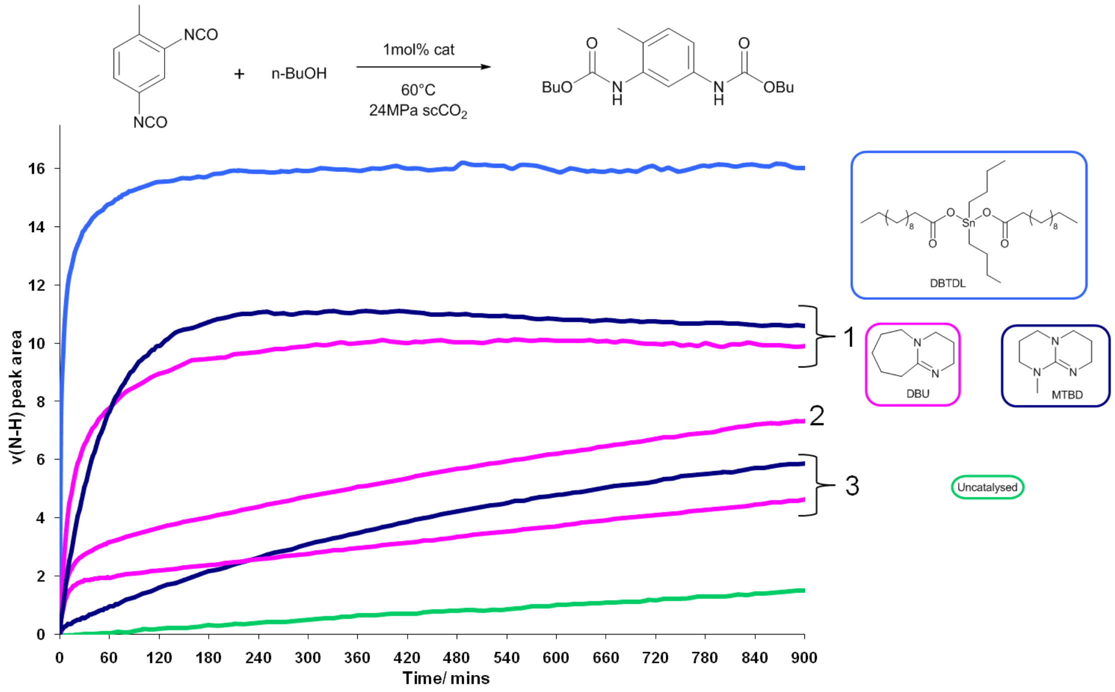

Figure 30. Kinetic curves for the reaction of 2,4-TDI with *n*-butanol in $scCO_2$ catalysed by 1 mol% catalyst under varied conditions; 1) anhydrous butanol and N45 quality CO_2, 2) standard 'wet' butanol and N45 quality CO_2, 3) standard 'wet' butanol and industrial quality CO_2.

In order to quantify somewhat the effect of water on the MTBD catalysed reaction, 10 mol% water was added to a reaction catalysed with 5 mol% MTBD (figure 31). This led to complete suppression of catalysis (dark blue curve marked with an asterisk), with the rate of reaction dropping down to that of the uncatalysed reaction. The same protocol was followed for a reaction catalysed by 5 mol% NMO and in this case resulted only in a reduction in yield with no obvious effect on the reaction rate (brown curve marked with an asterisk). Indeed, the reduced yield could just be due to the formation of (poorly soluble) ureas. The inhibiting effect of water on MTBD catalysis is undoubtedly due to the formation of a guanidinium bicarbonate salt resulting from the guanidine-CO_2- water ternary mixture.

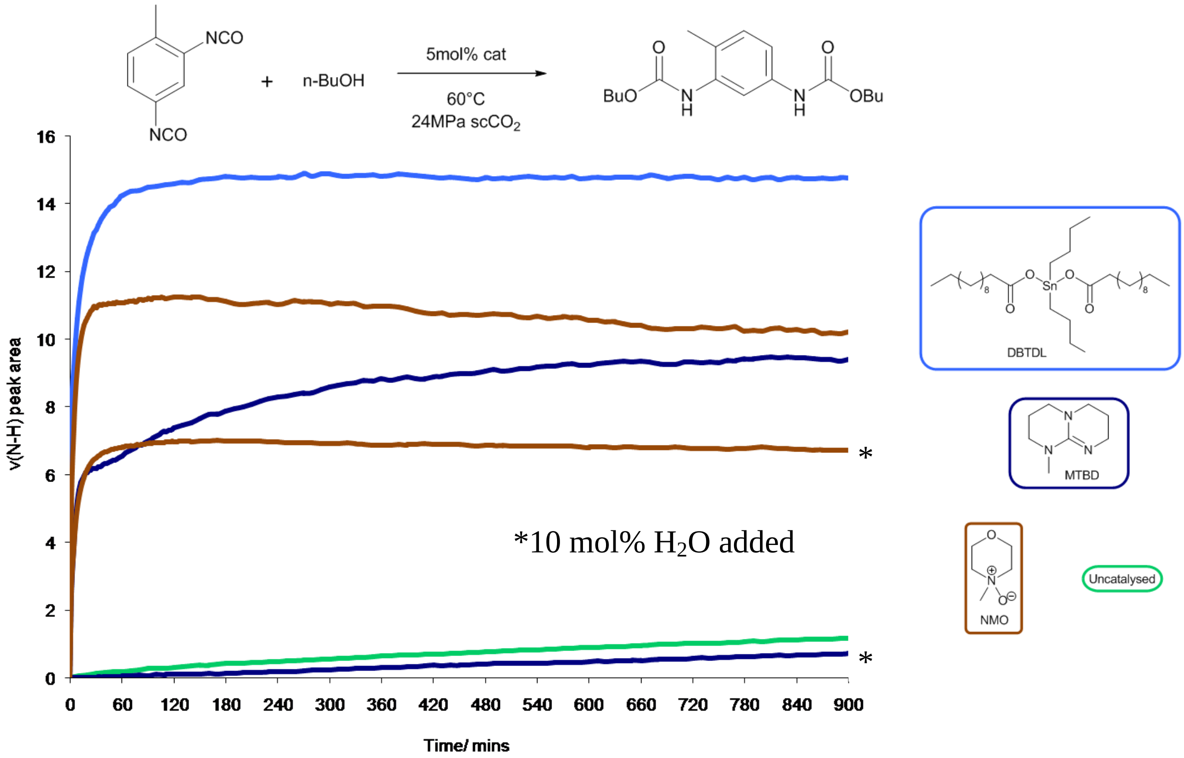

Figure 31. Kinetic curves for the reaction of 2,4-TDI with *n*-butanol catalysed by 5 mol% MTBD or NMO, in the presence and absence of 10 mol% water.

II-2-8-1 The behaviour of amidines/guanidines in the presence of CO_2: an explanation of catalytic activity

The interaction of guanidines or amidines with carbon dioxide has been the subject of a number of studies, aiming to elucidate the mechanism of CO_2 fixation (in CO_2 storage applications or synthetic transformations). There has been some debate as to whether binary CO_2-guanidine or CO_2-amidine adducts exist or if labile hydrogen containing compounds such as alcohols, amines or water are necessary in order to form a carbonate, carbamate or bicarbonate salt respectively.

Several reports of guanidine or amidine-CO_2 adducts have been published,[124] although the supporting experimental evidence is often limited. Jessop et al.[100b] cast doubt on their existence as they could obtain only a bicarbonate salt from DBU and CO_2 (and adventitious water), whilst under rigorously anhydrous conditions no adducts were observable. Recently however, the isolation of a TBD-CO_2 adduct has been achieved,[125] although its formation may be dependent on hydrogen bond stabilisation, which is not possible with peralkyl substrates such as DBU or MTBD. The crystal structure of the product pointed clearly to a zwitterionic adduct rather than a carbamic acid. However, CO_2 binding was somewhat transient as although the solid was stable under an inert atmosphere, it lost CO_2 on heating to 40°C under vacuum, and was transformed into the bicarbonate salt by ambient moisture in air, or by wet solvent in solution.

Analogously to the formation of bicarbonate salts in the presence of water, the formation of alkylcarbonate salts from guanidine/amidine and CO_2 in the presence of alcohol has also been documented.[100a, 100c, 126] These systems have been investigated for use as ‘switchable solvents’ and CO_2 capture agents, as the association of CO_2 is reversible with increased temperature. The system has also been used to catalyse the fixation of CO_2 into organic carbonates.[94, 127]

In this work, the formation of alkycarbonate salts could be conveniently followed by *in situ* FTIR spectroscopy. For example, when a stirred, equimolar solution of MTBD and methanol in acetonitrile was subjected to approximately 0.2 MPa CO_2 pressure, the methanol O-H stretch band centred at 3539 cm^{-1} disappeared while new peaks emerged corresponding to the methylcarbonate ion at 1675 cm^{-1} (C=O stretch), 1286 cm^{-1} and 1075 cm^{-1} (see figure 32). There was a reduction in intensity of the peak at 1511 cm^{-1} (C-N/C=N/C-C stretch combination of MTBD[128]), and the MTBD peak at 1606 cm^{-1} (C-N stretch combination[128]) was shifted to 1604 cm^{-1} and saw a significant increase in intensity (protonated MTBD shows two bands around 1600 cm^{-1} in dissociated salts, but a single band may be observed when it is involved in hydrogen bonding[129]). The appearance of a peak corresponding to dissolved carbon dioxide at 2342 cm^{-1} only *after* the complete formation of the methylcarbonate salt suggested that the process was rate limited by diffusion of CO_2 into the solution, in agreement with the findings of Heldebrant and co-workers.[100a] Equivalent results were obtained when MTBD was replaced by DBU. When normal ‘wet’ acetonitrile was used, the bicarbonate salt was formed and precipitated from the solution.

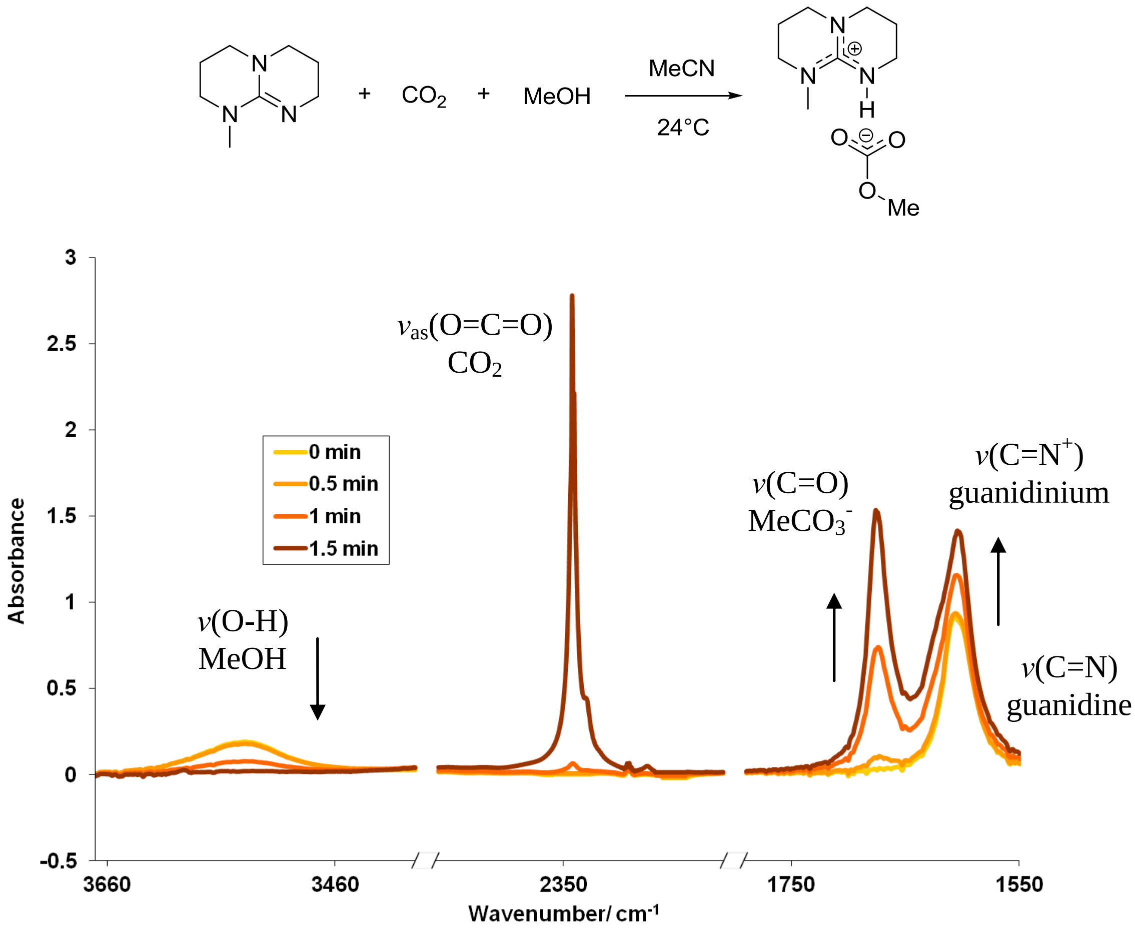

Figure 32. *In situ* IR spectra following the formation of the guanidinium alkylcarbonate salt from MTBD, methanol and CO_2 in anhydrous acetonitrile.

When the solution was heated under fixed volume conditions, the reversibility of the reaction could be established by following the decrease in intensity of the methylcarbonate peaks and the reappearance of the methanol O-H stretch peak. In figure 33, the absorbance of the methylcarbonate C=O stretch is plotted against temperature (data recorded while heating the solution from ambient temperature in red and data recorded while allowing the solution to cool in blue). The curves corresponding to heating and cooling are not exactly superimposed and there seems to be some loss of the methylcarbonate upon cooling. This is perhaps due to adventitious water replacing methanol to form the much less soluble guanidinium bicarbonate salt. At 60°C (the temperature used for the model reaction in $scCO_2$), the equilibrium ratio of guanidinium methylcarbonate to guanidine was approximately 70:30.

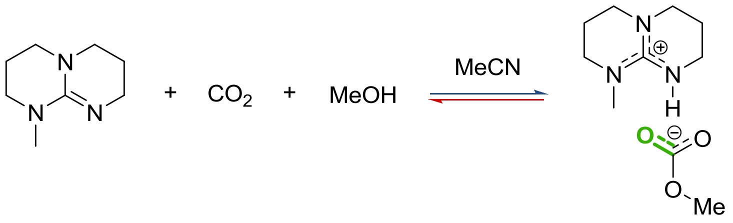

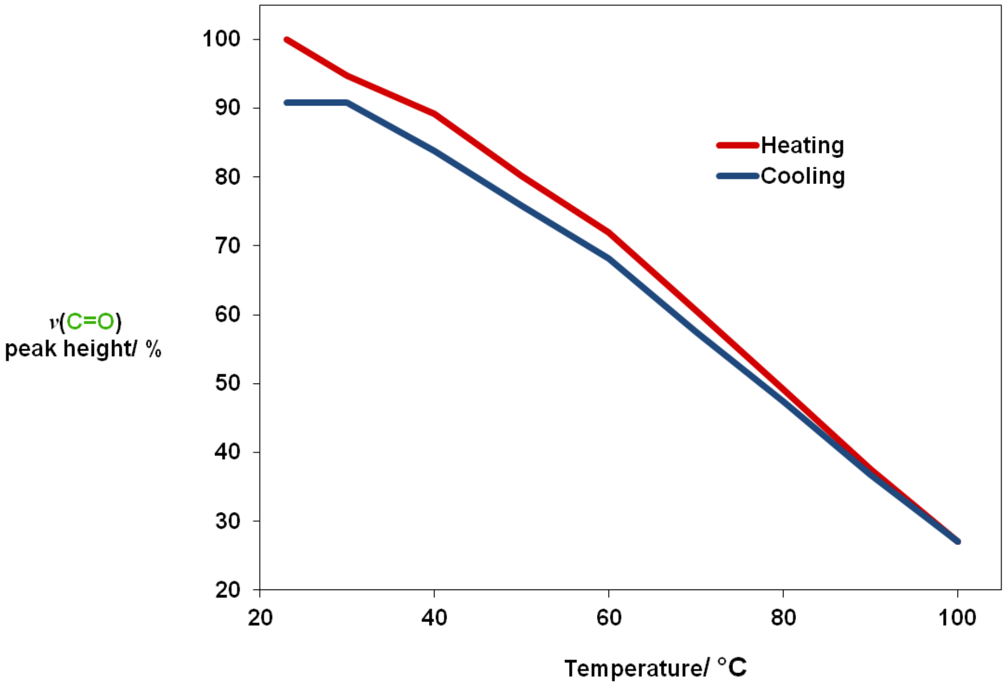

Figure 33. Plot of the methyl carbonate *ν*(C=O) peak height versus temperature for the equilibrium between the guanidinium methylcarbonate salt and MTBD/methanol/CO_2.

However, the CO_2 concentration in this experiment is of course much lower than when supercritical CO_2 is being used as solvent. The MTBD free base is soluble in $scCO_2$ and the IR spectrum of MTBD at 60°C and 24 MPa is shown in figure 34 (red). The guanidine C=N stretch can be observed at around 1620 cm^{-1}, and has a similar appearance to the peak observed in organic solvents. When a solution of MTBD in *n*-butanol in a mole ratio of 20:1 is dissolved in $scCO_2$, under the same conditions of temperature and pressure, the spectrum is not simply the sum of the spectra of MTBD and butanol (figure 34, blue). Two broad, weak peaks are all that can be observed in the region of the guanidine C=N stretch. This suggests that the equilibrium is highly shifted towards the alkylcarbonate salt, which is apparently poorly soluble in $scCO_2$.

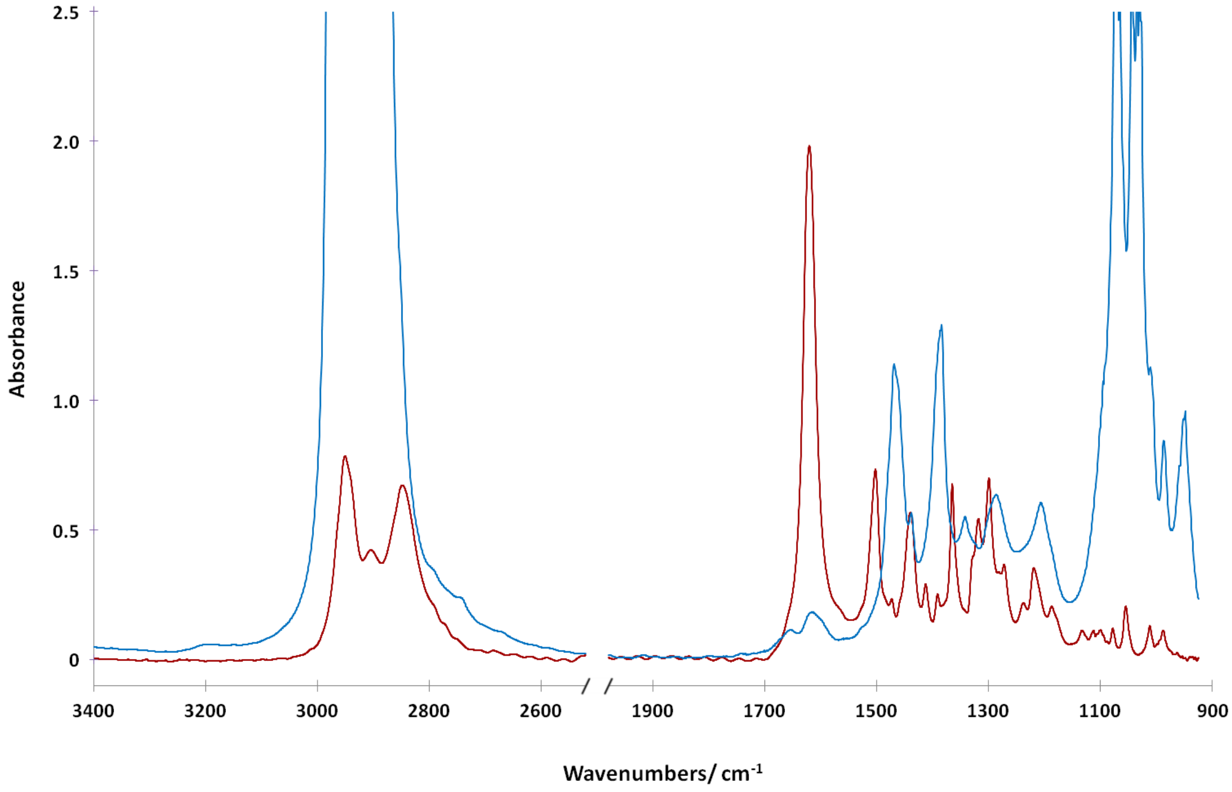

Figure 34. IR spectra recorded in $scCO_2$: MTBD ($c = 8.4 \times 10^{-3}$ mol dm^{-3} [red]) and MTBD plus *n*-butanol ($c = 8.4 \times 10^{-3}$ mol dm^{-3} and 0.17 mol dm^{-3} respectively [blue]). $P = 24$ MPa and $T = 60$°C.

II-2-9 Effect of CO_2 on the kinetics of reaction in organic solvent

In order to investigate the consequences of guanidinium alkylcarbonate salt formation on catalysis, the kinetics of the urethanisation reaction were investigated in dichloromethane solution at 24°C: conditions under which the formation of the alkylcarbonate salt is more or less quantitative under a low pressure of CO_2. The reaction between phenyl isocyanate and *n*-butanol was chosen in this case because of its simpler kinetic scheme.

A dichloromethane solution of butanol with 5 mol% MTBD was first subjected to 0.2 MPa CO_2 pressure and the formation of the guanidinium alkylcarbonate salt was verified by the expected changes in the IR spectrum. A phenyl isocyanate solution was then added to the mixture and the evolution of the reaction was followed in the same way as for the kinetic monitoring in CO_2. For comparison, the reaction was run under the same conditions in the absence of CO_2 (see figure 35).

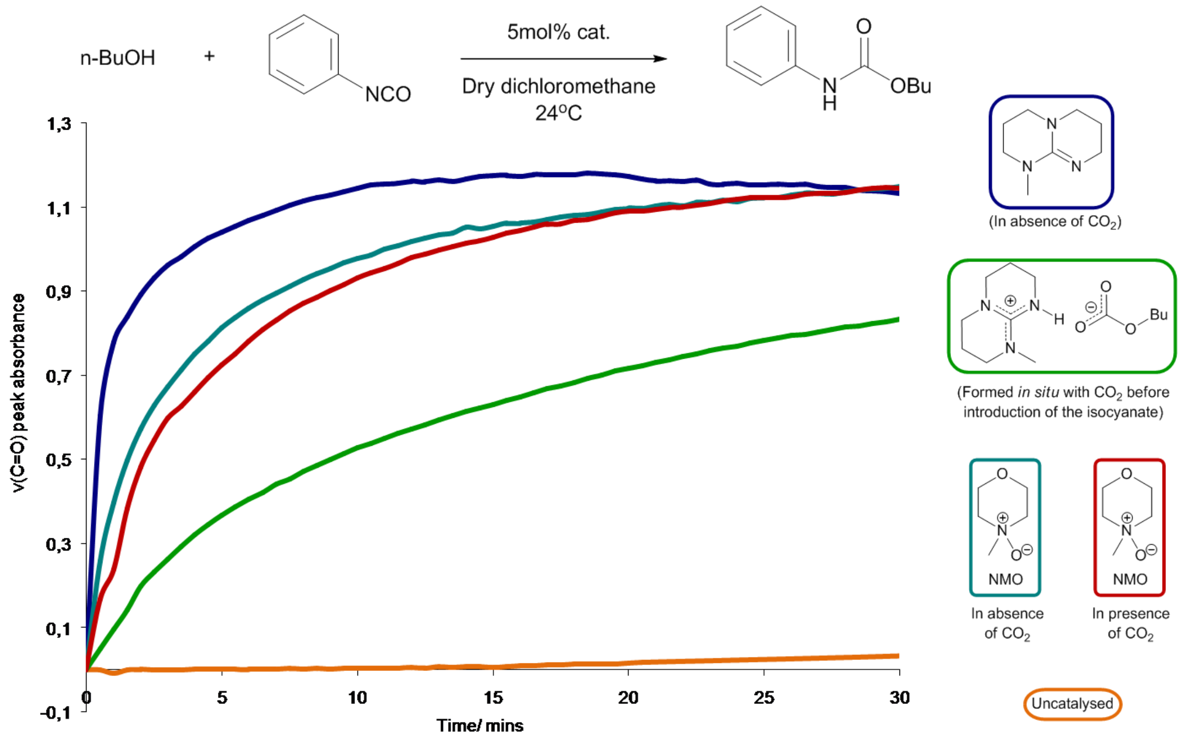

Figure 35. Kinetic curves for the reaction of phenyl isocyanate with *n*-butanol catalysed by 5 mol% MTBD or NMO in dichloromethane solution in the presence or absence of CO_2.

There was a clear difference between the MTBD catalysed reactions carried out in the presence or absence of CO_2 (green and dark blue curves respectively) with CO_2 bringing about a reduction in the rate of reaction. Given that the rate of reaction in the presence of CO_2 was still relatively rapid compared to the uncatalysed reaction (orange curve), it seems unlikely that the reaction is catalysed only by the very small equilibrium concentration of MTBD free base, and it is conceivable that a different catalytic mechanism is in operation, involving the butylcarbonate ion as either a nucleophile or base. It has been reported that the basicity of the alkylcarbonate anion is enhanced when associated with an onium cation, rendering it effective for the catalysis of Michael reactions for example.[130] Alkylcarbonate salts (with a metal or quaternary ammonium cation) have also been patented as moderately active catalysts for the preparation of polyisocyanurates or poly(urethane-isocyanurates).[131] Equally, DBU salts of weak acids have been used in polyurethane formulations.[10] The IR spectra presented in figure 34 suggest that the guanidinium alkylcarbonate salt is the *de facto* catalytic species for reactions conducted in supercritical CO_2. In the presence of water, the more stable bicarbonate salt should be favoured over the alkylcarbonate salt,[100a, 130] but it does not appear to show any catalytic activity. This difference in activity is presumably due to a difference in solubility in $scCO_2$.

It is interesting to compare these results to those of the ring-opening polymerisation of lactide in $scCO_2$. The latter reaction can be catalysed by DBU but the rate of reaction in $scCO_2$ was found to be slower than in organic solvents.[99] In addition, a narrower molecular mass distribution than in bulk polymerisation was obtained. This parallels catalysis using DBU salts of benzoic or acetic acid in organic solvents, which also lead to reduced reaction rate and narrower molecular mass distribution compared to DBU catalysed reactions.[132] It is intriguing that the DBU catalysed ROP of lactide in $scCO_2$ also works with water as initiator. This contrasting behaviour with the water sensitivity of the urethanisation reaction is perhaps due to the fact that the ROP reaction occurs in a CO_2-swollen monomer phase rather than a supercritical CO_2 phase.

The effect of CO_2 on reactions catalysed by NMO was also tested using the same procedure, but in this case there was no clear effect on the rate of reaction (red and turquoise curves).

II-3 Conclusions

In situ FTIR has proven to be a valuable method for reaction monitoring in supercritical CO_2, allowing a comparison of various organocatalysts with regards to the kinetics of urethane formation in a model reaction. Analysis of the spectra has also allowed the identification of the reaction intermediates and a comparison of the selectivity of the catalysts towards the ortho- and para-isocyanate groups of 2,4-TDI.

Guanidine and amidine catalysts MTBD and DBU clearly show higher catalytic activity for the urethanisation reaction in $scCO_2$ than traditional tertiary amine catalysts. However, their activity in $scCO_2$ seems likely to be reduced compared to reactions in organic solvents due to an equilibrium shifted towards the guanidium or amidinium alkycarbonate salts. These catalysts also show a certain sensitivity to the presence of water, which reduces their activity, and they appear to be prone to the formation of allophanate and particularly isocyanurate side-products.

On the other hand, the amine oxide catalyst NMO does not seem to be deactivated by the presence of CO_2, it is not markedly sensitive to the presence of water and it does not particularly promote the formation of side-products. Thus, although the rate of the urethanisation reaction was found to be slower with NMO than with guanidine/amidine catalysts in an organic solvent, it is faster in $scCO_2$. However, reactions with NMO fail to reach completion and result in a limited yield, particularly at low catalyst loading. The reasons for this remain unclear but the apparent deactivation of the catalyst during the course of the reaction could simply be due to precipitation.

II-4 Experimental Section

II-4-1 Infrared Set-Up

The infrared absorption measurements were performed on a ThermoOptek Nicolet 6700 FTIR spectrometer equipped with a globar as the infrared source, a KBr/Ge beamsplitter and a DTGS (Deuterated TriGlycine Sulphate) detector in order to investigate the spectral range 400-4000 cm^{-1}. Single beam spectra recorded with a 2 cm^{-1} resolution were obtained after the Fourier transformation of 32 accumulated interferograms (the resolution and number of scans were reduced during kinetic reaction monitoring in order to reduce the time required to collect each spectrum).

The infrared absorption experiments were performed using an in-house built stainless steel cell[133] (figure 36) equipped with two cylindrical silicon windows and a variable path length. The seal was obtained using the unsupported area principle. The windows were positioned on the surface of a stainless steel plug with a 100 µm Kapton® foil placed between the window and the plug to compensate for any imperfections between the two surfaces. Teflon® O-rings were used to ensure the seal between the plug and the cell body. The cell was heated using cartridge heaters disposed in the periphery of the body of the cell. Two thermocouples were used, the first one located close to a cartridge heater for the temperature regulation and the second one close to the sample area to measure the temperature of the sample with an accuracy of about 2°C. The cell was connected via a stainless steel capillary tube to a hydraulic pressurizing system which allows the pressure to be raised up to 50 MPa with an absolute uncertainty of ± 0.1 MPa and a relative error of ± 0.3%.

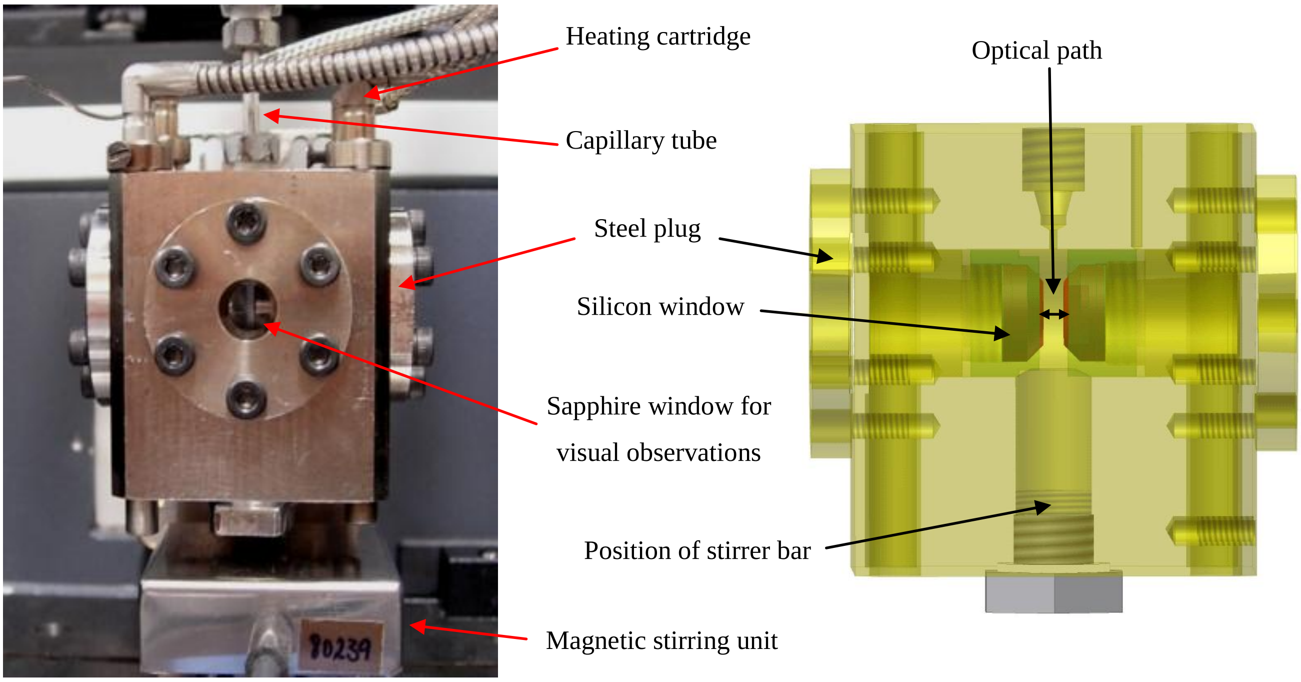
Heating cartridge
Capillary tube
Steel plug
Silicon window
Sapphire window for visual observations
Position of stirrer bar
Magnetic stirring unit
Optical path
80239

Figure 36. The high-pressure optical cell: photo (left) and schematic diagram (right) with only the side windows shown for clarity.

II-4-2 Raman Spectroscopy

The Raman measurements were performed using a Horiba Jobin-Yvon HR800-UV confocal spectrometer with a resolution of 0.7 cm^{-1} in the spectral range 200-3300 cm^{-1}. The laser excitation wavelength was 752 nm and the laser beam power was 3.7 mW. To improve the signal-to-noise ratio, each spectrum was the result of 2 accumulated spectra for typical times of 60 seconds.

II-4-3 Materials

2,4-TDI >99% (analytical standard grade) and phenyl isocyanate 98% were purchased from Sigma-Aldrich and used as received. *n*-Butanol (Sigma-Aldrich) was distilled over CaH_2 and stored over molecular sieves. CO_2 (N45 quality, <7 ppm H_2O) was supplied by Air Liquide. DBTDL 95% (Alfa Aesar), MTBD 98% (Sima-Aldrich), TBD 98% (Sima-Aldrich), DBU 99% (Alfa Aesar), triethylamine 99% (Alfa Aesar), DABCO 98% (TCI), DMAP 99% (Sima-Aldrich), 4-PPY 98% (TCI), and NMO 97% (Sima-Aldrich) were used as received.

Dichloromethane was purified through a Grubbs apparatus before use. Acetonitrile was distilled over CaH_2 before use.

II-4-4 Kinetic Monitoring in $scCO_2$

The high-pressure cell (configured with a path length of 5.05 mm) was dried by heating under vacuum then rinsed with $scCO_2$. *n*-Butanol (9.2 µL, 0.10 mmol) or a solution of catalyst in *n*-butanol (1:20 mol/mol for 5 mol% catalyst) was added into the capillary tube above the cell then injected with ~6 MPa CO_2. The temperature was increased to 60°C then the pressure increased to 20 MPa. A spectrum was recorded of the butanol/catalyst solution in $scCO_2$. 2,4-TDI (7.1 µL, 5.0×10^{-2} mmol) (or PhNCO 11.0 µL, 0.10 mmol) was then injected from a small length of capillary tube in between two valves (see figure 37) with a pressure gradient of ~10 MPa. The pressure was then adjusted to 24 MPa. A first spectrum was recorded immediately after the addition of the isocyanate. Further spectra were recorded every two minutes at the beginning of the reaction then every ten minutes up to about 17 hours reaction time. Each spectrum was the result of 4 accumulated scans with a resolution of 4 cm^{-1}.

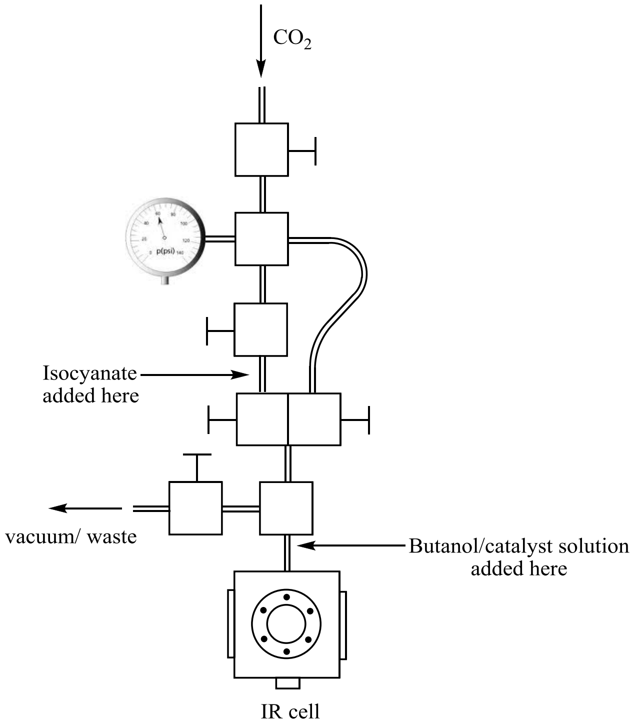

Figure 37. Experimental set-up for *in situ* reaction monitoring in supercritical CO_2.

II-4-5 NMR/Raman analysis of reaction residues

In most cases, DMSO-d_6 was added directly into the high pressure cell after cooling and depressurization. Due to its complex geometry, the cell had to be taken apart in order to recover the solution, resulting in the absorption of relatively large amounts of water into the DMSO. To obtain samples for Raman spectroscopy, the residue was collected with dichloromethane and the solvent then evaporated.

II-4-6 Kinetic monitoring in dichloromethane solution

A mixed solution of *n*-butanol and catalyst (0.50 mol dm^{-3} in butanol and 2.5 x 10^{-2} mol dm^{-3} in catalyst) and a solution of phenyl isocyanate (0.50 mol dm^{-3}) in dry dichloromethane were prepared under argon. The high-pressure cell (configured with a path length of 0.29 mm) was dried by heating under vacuum then 2.0 mL of the butanol/catalyst solution was added directly. The IR spectrum of the solution was recorded then 2.0 mL of the PhNCO solution was added and the mixture agitated with a magnetic stirrer at 24°C. Spectra were recorded every 30 seconds (5 accumulated scans with a resolution of 4 cm^{-1}).

For experiments conducted in the presence of CO_2, the butanol/catalyst solution was subjected to 0.2 MPa CO_2 pressure before the addition of the phenyl isocyanate solution. In the case of the MTBD catalysed reaction, the formation of the guanidinium butylcarbonate salt was followed by the corresponding changes to the IR spectrum.

II-4-7 CO_2 absorption experiments

A 1:1 solution of methanol and MTBD in freshly distilled acetonitrile was prepared under argon (0.15 mol dm^{-3}). The high-pressure cell (configured with a path length of 0.12 mm) was placed under vacuum, then filled with 4.0 mL of the solution. The IR spectrum of the solution was recorded then the cell was opened to 0.2 MPa CO_2 pressure and the solution agitated with a magnetic stirrer (temperature = 23°C). Further spectra were recorded every 30 seconds and CO_2 absorption was found to be complete after 90 seconds.

The closed cell (fixed volume) was heated to 30°C then up to 100°C in steps of 10°C, with the IR spectrum of the solution recorded at each temperature. Successive spectra were recorded until the spectrum stabilised. The process was then repeated while allowing the cell to cool in steps of 10°C.

Chapter III

Polymerisation in Supercritical Carbon Dioxide

Summary

III-1 Introduction 96

III-2 Precipitation Polymerisation of Polyurethanes in $scCO_2$ 96

III-2-1 Analysis of the Polyurethanes 98

III-2-1-1 ^{1}H NMR Spectroscopy 98

III-2-1-2 ATR-FTIR Spectroscopy 101

III-2-1-3 Raman Spectroscopy 102

III-2-2 Conclusions of precipitation polymerisations 103

III-3 Dispersion Polymerisation of Polyurethanes using Macromonomer 104

III-3-1 Functionalisation of PDMS-$(OH)_2$ to PDMS-$(NCO)_2$ 104

III-3-2 Polymerisation 105

III-3-2-1 ^{1}H NMR analysis of polyurethanes 113

III-3-2-2 Incorporation of PDMS 113

III-3-2-3 Raman Imaging 115

III-3-3 Conclusions of dispersion polymerisations using macromonomer 116

III-4 Dispersion Polymerisation of Polyurethanes using Catasurfs 117

III-4-1 Synthesis of Organocatasurfs 117

III-4-1-1 Synthesis using a carbonate linker 117

III-4-1-2 Synthesis via a hydrosilylation reaction 122

III-4-1-3 Thermal Stability of the Catasurfs 127

III-4-2 Polymerisation 129

III-4-2-1 Incorporation of PDMS 138

III-4-2-2 Raman Imaging 139

III-4-3 Conclusions of dispersion polymerisation using organocatasurfs 140

III-5 Summary and Outlook 140

III-6 Experimental Section 141

III-6-1 Materials 141

III-6-2 Instrumentation 142

III-6-3 High pressure reactor 143

III-6-4 Experimental Procedures 144

III-6-4-1 Synthesis of PDMS-(NCO)$_2$ 144

III-6-4-2 Synthesis of Organocatasurfs 144

III-6-4-2-1 Typical Hydrosilylation Procedure 144

III-6-4-2-2 Typical Oxidation Procedure with mCPBA 144

III-6-4-2-3 Typical Oxidation Procedure with H_2O_2 145

III-6-4-3 Precipitation Polymerisations 145

III-6-4-4 Dispersion Polymerisations with Macromonomer 146

III-6-4-5 Dispersion Polymerisations with Catasurfs 146

III-1 Introduction

In the previous chapter, kinetic studies of a model reaction allowed the identification of the most active organocatalysts for the synthesis of urethanes in supercritical CO_2. However, the formation of urethane polymers (i.e. polyurethanes) is a somewhat more complex process because the physical properties of the system change with the progression of the reaction. Catalysis will influence not only the extent of conversion but will also have an impact on factors such as the rate of particle nucleation. The following study therefore sets out to determine the effect of the nature and concentration of the catalyst on polymer properties.

While the use of macromonomer-type stabilisers has been shown to afford well defined core-shell polyurethane particles, the properties of the resulting material can be affected by the incorporated stabiliser component (e.g. PDMS). The use of non-reactive stabilisers can therefore offer an interest for the preparation of pure polyurethane materials. A second aspect of this study is thus to evaluate the combination of the catalyst and surfactant into the same molecule (a “catasurf”), which could provide polyurethanes completely free from auxiliary substances. Recycling of the catasurf should even become possible, providing a yet more sustainable process.

III-2 Precipitation Polymerisation of Polyurethanes in $scCO_2$

Some preliminary polymerisations were carried out in the absence of CO_2-soluble stabilisers (i.e. precipitation polymerisations) under conditions similar to those used during kinetic monitoring of the model reaction (scheme 30). The reactions were performed in a 120 mL stainless steel reactor with a magnetically-driven overhead stirrer. 1,4-butanediol was selected as the diol partner due to the superior results achieved with this monomer in previous studies.[20, 75b] The diol and catalyst were first dissolved in CO_2 at 60°C and 20 MPa, before addition of one equivalent of 2,4-TDI and an increase in pressure to 26 MPa. After 24 hours the vessel was cooled and depressurized, then the unreacted isocyanate groups were quenched with excess ethanol. The results of these polymerisations are presented in table 2.

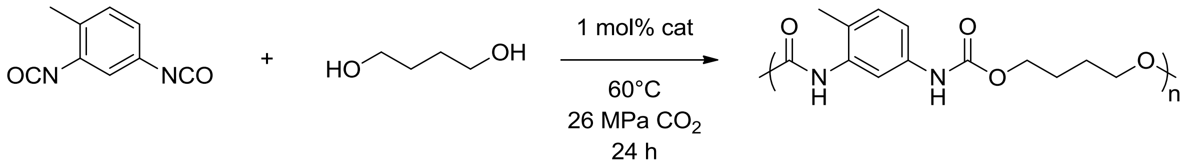

Scheme 30. Precipitation polymerisation of 2,4-TDI and 1,4-butanediol in $scCO_2$.

Catalyst	Mass Recovered (%)[a]	M_w (g mol^{-1})[b]	M_w/M_n[b]
None	61	21,600	2.7
DBTDL	99	24,500	3.4
DBU	56	35,000	3.2
MTBD	62	41,100	4.3

[a] Mass recovered after dissolution of the product in THF and evaporation of the solvent (as a percentage of the mass of monomers originally introduced). [b] Determined by SEC in DMF vs. polystyrene standards.

Table 2. Results of precipitation polymerisations between TDI and butanediol in $scCO_2$ in the presence of different catalysts.

The molecular weights of the polymers obtained were reasonably high, although the molecular weight distributions were rather large and M_w/M_n was much greater than the theoretical limit of 2 for a step growth polymerisation.[13] This is most likely due to the presence of different phases within the reaction mixture. One possibility is that once polymer chains begin to form, a dispersed phase develops which is rich in diol and growing polymer, and that further polymerisation takes place within this dispersed phase, with diffusion of isocyanate from the CO_2-rich continuous phase. This process would resemble interfacial polymerisation where high molecular weight polymer can be formed regardless of the overall conversion.[13]

It can also be seen from table 2 that the highest molecular weight polymer is not formed from the most active catalyst, DBTDL, as would be expected in a ‘normal’ step growth polymerisation where molecular weight increases as a function of conversion. This could be related to contrasting precipitation characteristics.

In the DBU catalysed reaction, a film of insoluble material was found to be adhered to the walls of the reaction vessel. The insolubility of this product suggested that it contained significant cross-linking and further analysis was carried out by ATR-FTIR and Raman spectroscopy (*vide infra*). A significant portion of insoluble material was also obtained from the MTBD catalysed reaction.

During the recovery of the reaction products, THF was used to dissolve the last portion of material remaining in the reaction vessel. Therefore, a mass recovery near 100% could be expected, but this was not always the case, partly because of the complex shape of the reactor and partly due to the presence of insoluble material which was strongly adhered to the walls of the reactor in certain reactions. The higher yield attained in the DBTDL reaction was also due in part to a higher incorporation of ethanol when the reaction was quenched (more ethyl carbamate end-groups could be observed by NMR). The moderate yields obtained suggested that some material may have been eliminated from the vessel during depressurization. This eventuality was examined by evaporating the solvent from the ethanol bath into which the CO_2 had been vented. A significant amount of residue was obtained in the case of the uncatalysed reaction, which was identified as the diethyl carbamate of TDI and corresponded to approximately 10% of the TDI originally introduced. In the catalysed reactions, only traces of this product were obtained, suggesting that the TDI had been more completely consumed. On the other hand, around 20% of the catalyst was recovered from the DBTDL catalysed reaction. This is consistent with the results of Grignard and co-workers, who showed that dibutyltin diacetate could be extracted from poly(caprolactone) using CO_2.[72] Thus, a DBTDL promoted polymerisation followed by catalyst extraction could perhaps provide an alternative ‘green’ process to organocatalysis.

III-2-1 Analysis of the Polyurethanes

III-2-1-1 ^{1}H NMR Spectroscopy

The NMR spectra of butanediol/TDI oligomers in DMSO-d_6 have been well documented.[119a, 119c] The signals corresponding to butanediol units within or at the end of the polymer chain are fairly well separated and can also be differentiated from the residual butanediol monomer (figure 38).

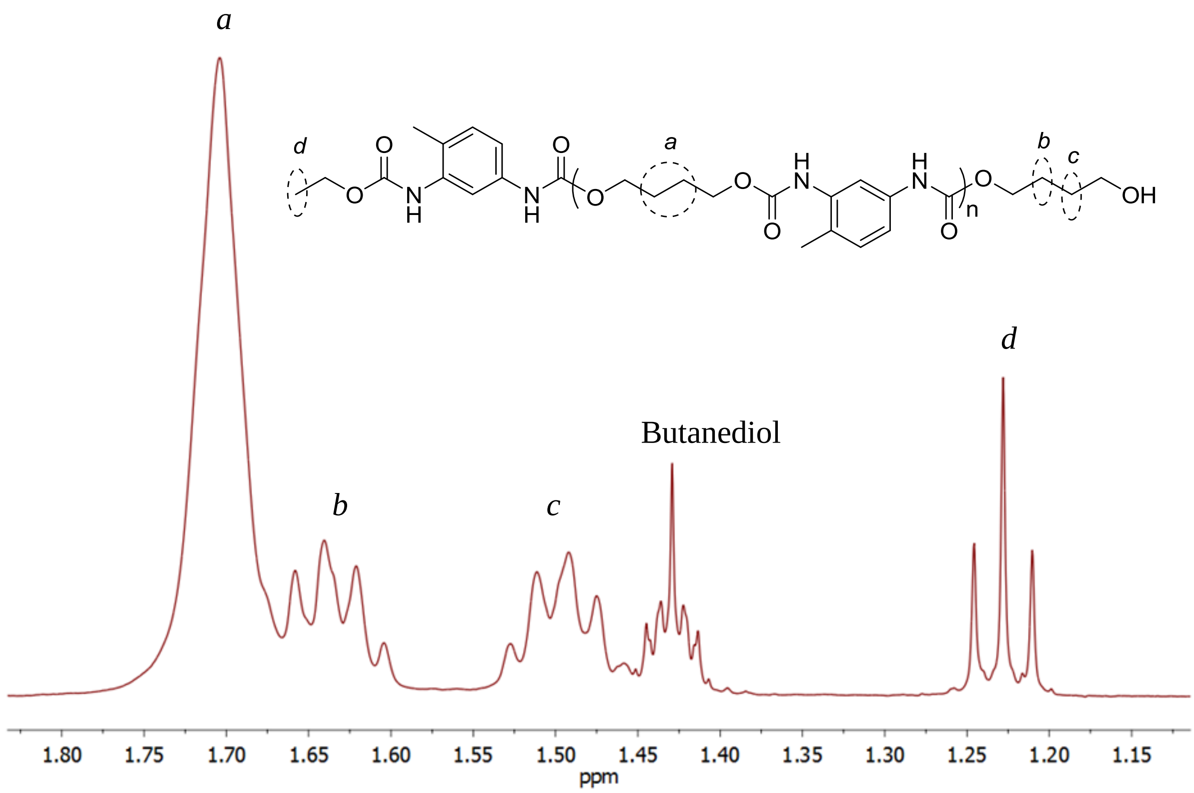

Figure 38. Aliphatic protons in the ^{1}H NMR spectrum of polyurethane from precipitation polymerisation of 2,4-TDI and 1,4-butanediol in $scCO_2$ (reaction without catalyst). Ethyl carbamate end-groups arise from the reaction quench with ethanol.

Another interesting feature of the spectra is the splitting of urethane N-H peaks according to their different environments (either within or at the end of the chain), which can reveal some information about the isocyanate reactivity. When the polymerisation reaction is quenched with excess alcohol, the unreacted isocyanate groups will be converted to terminal urethane groups. Therefore, the less reactive isocyanate groups will represent a higher proportion of terminal urethane groups. Given that the ortho- and para-urethane groups are well separated, this provides a way of assessing their relative reactivity.

The N-H signals of the polyurethanes obtained from precipitation polymerisation in CO_2 in the presence of different catalysts are shown in figure 39. First of all, in the absence of catalyst (green spectrum), there is a higher proportion of terminal urethane groups at the ortho-position compared to the para-position, which is consistent with the known order of reactivity. When the reaction is catalysed by DBTDL, the difference between the ortho- and para-positions is much greater (black spectrum), with the terminal groups appearing almost exclusively at the ortho-position. Finally, with DBU and MTBD catalysis, this difference is reduced (blue and red spectra). This demonstrates the increased selectivity of DBTDL towards the para-isocyanate group compared to DBU and MTBD and is in agreement with the results obtained from *in situ* IR spectra during kinetic monitoring of the model reaction (see chapter 2). The magnitude of the difference in reactivity between the two isocyanate groups could have consequences for the molecular weight of the polymers which are produced. In step growth polymerisations, high conversions are needed in order to attain high molecular weights. In cases where the rates of different reaction steps are not equal, the time required to achieve a high molecular weight will therefore strongly depend on the rate of the slowest reaction step.[13] In this sense, it can be more favourable to have reaction steps with similar rates in order to produce high molecular weight polymers. Unequal reactivities are also expected to affect the molecular weight distribution of the polymer. The greater the difference in reactivity, the narrower the molecular weight distribution that will be obtained (this effect is greater at low conversions, and at 100% conversion the theoretical limit of M_w/M_n is equal to two, which is the same as the case for groups with equal reactivity). However, in the current study of precipitation polymerisations, these effects are undoubtedly drowned-out to some extent by the influence of the heterogeneity of the reaction mixture.

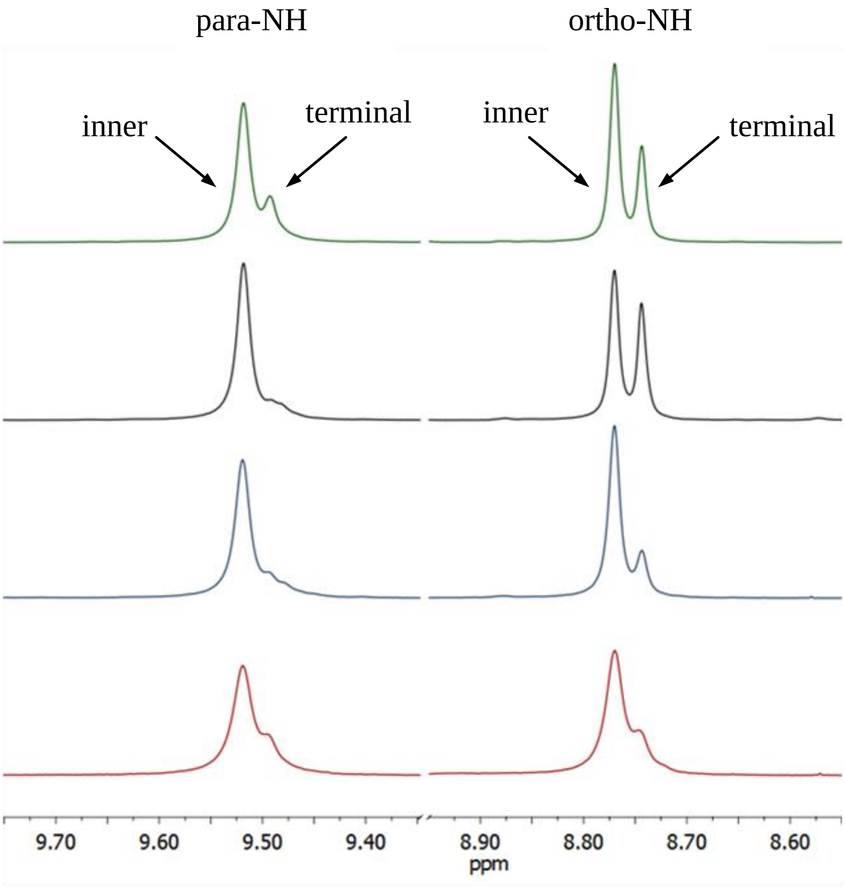

Figure 39. Urethane N-H signals in the ^{1}H NMR spectra of polyurethanes: the product of reaction without catalyst (green), with DBTDL catalyst (black), with DBU catalyst (blue), and with MTBD catalyst (red).

III-2-1-2 ATR-FTIR Spectroscopy

The ATR-FTIR spectrum of the polyurethane produced in the DBTDL catalysed reaction is shown in figure 40 (black). When a high molecular weight sample was generated by fractional precipitation, the spectrum remained essentially unchanged. The spectrum of the insoluble material from the DBU catalysed reaction (blue) was very similar, although the *ν*(C=O) peak around 1700 cm^{-1} was somewhat broader and the maximum was shifted by approximately 10 cm^{-1} to higher wavenumbers, which could indicate the presence of allophanate linkages.[134] On the other hand, in the spectrum of the insoluble material from the MTBD catalysed reaction, increased absorbance could be observed around 1407 and 756 cm^{-1} and this corresponds well to some of the strongest isocyanurate bands, which have been assigned to vibrations of the ring with E' and A_2'' symmetry respectively.[123] The attribution of allophanate and isocyanurate was supported by the fact that the product from the DBU catalysed reaction gradually dissolved in DMSO or DMF over several days (degradation of allophanate linkages, c.f. chapter 2), while the product from the MTBD catalysed reaction did not.

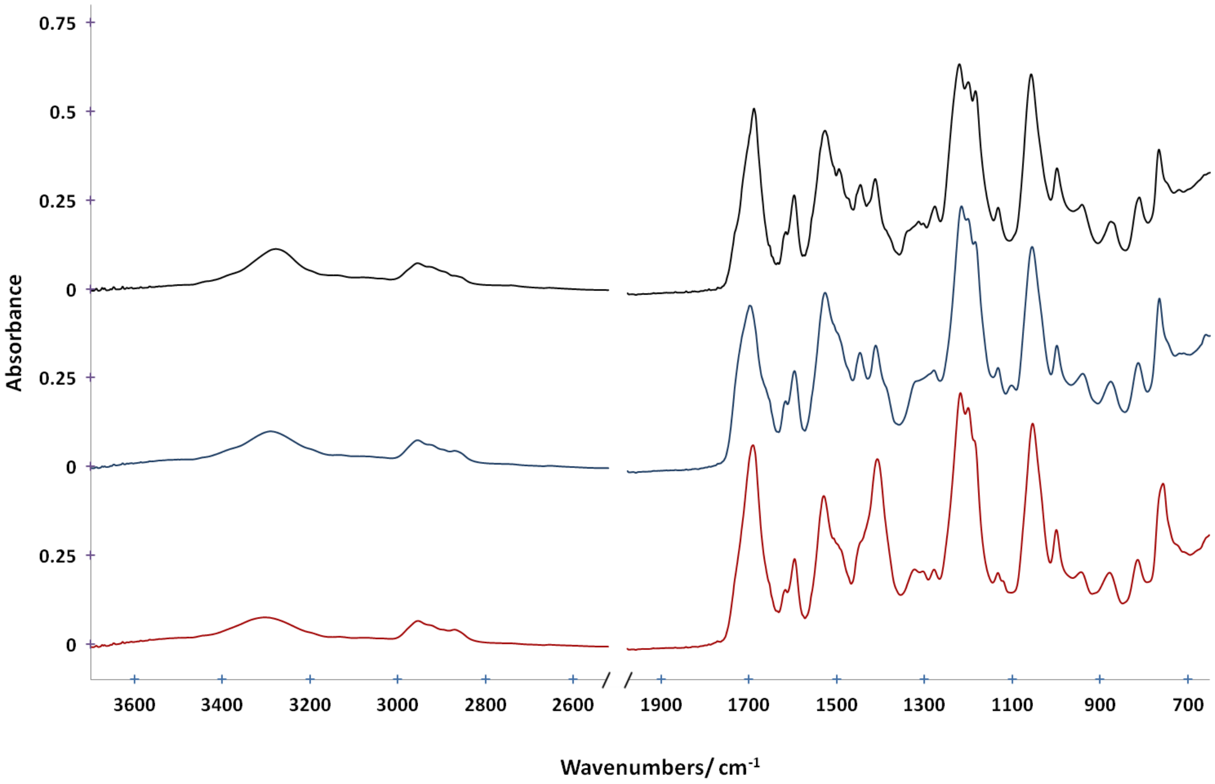

Figure 40. ATR-FTIR spectra of polyurethanes: the product of the reaction catalysed by DBTDL (black), insoluble material from the reaction catalysed by DBU (blue) and insoluble material from the reaction catalysed by MTBD (red). The region between 2000 and 2500 cm^{-1} does not contain any absorptions and has been removed for clarity.

III-2-1-3 Raman Spectroscopy

The presence of isocyanurate was more easily identified in the Raman spectra. The insoluble material from the MTBD catalysed reaction showed peaks at 1773 and 678 cm^{-1} (figure 41, red), which are not present in the spectrum of the polyurethane produced in the DBTDL catalysed reaction (black). Bands in these regions have been attributed to A_1’, ν(C=O) and γ(CNC) of isocyanurate respectively.[123] A weak peak at 1773 cm^{-1} was present in the spectrum of the insoluble material from the DBU catalysed reaction (blue) indicating a low concentration of isocyanurate groups.

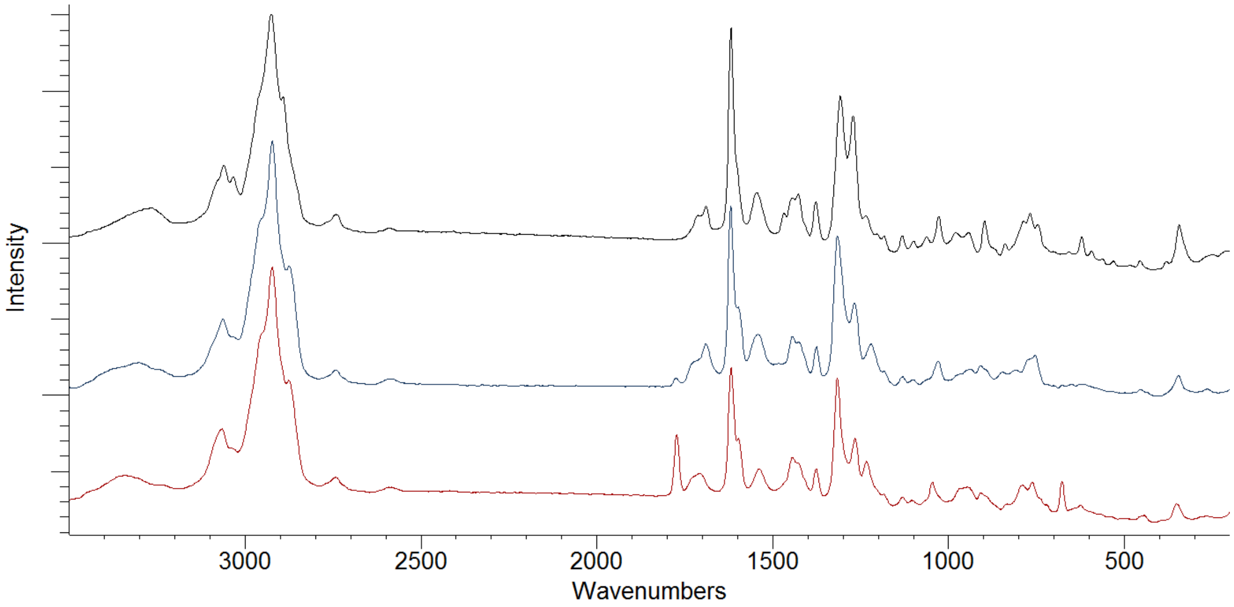

Figure 41. Raman spectra of polyurethanes: the product of the reaction catalysed by DBTDL (black), insoluble material from the reaction catalysed by DBU (blue) and insoluble material from the reaction catalysed by MTBD (red).

III-2-2 Conclusions of precipitation polymerisations

Precipitation polymerisation of polyurethanes in $scCO_2$ leads to polymers with broad molecular weight distributions, presumably due to the effects of phase separation. Higher molecular weights were achieved with MTBD and DBU organocatalysts compared to DBTDL, which could be related to the levelling of the reactivity of the two isocyanate groups in TDI, but might otherwise be an effect of contrasting precipitation characteristics. On the other hand, MTBD and DBU led to significant side-product formation, rendering the polymer difficult to remove from the reactor. Although reasonable yields and molecular weights of polyurethane can be achieved by precipitation polymerisation, the form of the products obtained makes recovery of the polymer quite impractical and may limit its utility. Dispersion polymerisation should therefore prove advantageous by producing spherical polymer particles.

III-3 Dispersion Polymerisation of Polyurethanes using Macromonomer

A series of polymerisations was carried out to determine the effect of the catalyst in a macromonomer-stabilised system. Diisocyanate functionalised PDMS macromonomer was used since it has proven to give well-defined microparticles (scheme 31).

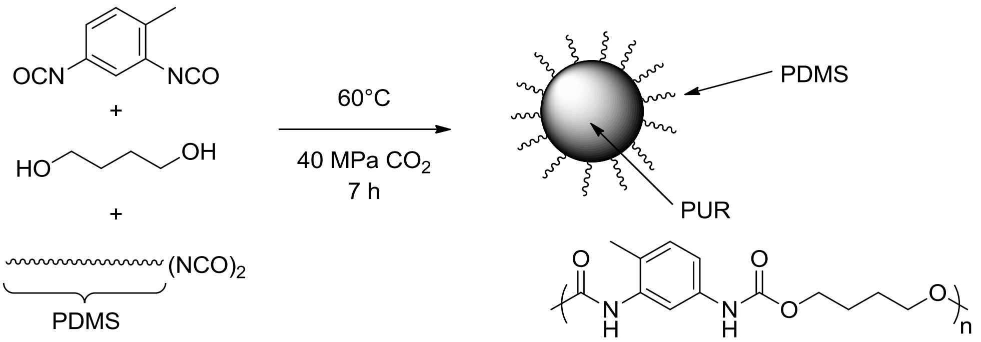

Scheme 31. Synthesis of core-shell polyurethane-PDMS particles in $scCO_2$ using a diisocyanate functionalised PDMS macromonomer.

III-3-1 Functionalisation of PDMS-$(OH)_2$ to PDMS-$(NCO)_2$

The diisocyanate functionalised PDMS stabiliser (PDMS-$(NCO)_2$) was prepared by the reaction of diol-terminated PDMS (PDMS-$(OH)_2$, M_n = 3200 g mol^{-1}) with 2,4-TDI (scheme 32). The synthesis was first carried out according to a previously reported procedure, involving dropwise addition of a solution of PDMS-$(OH)_2$ to 4 equivalents of TDI.[20, 75b] In concordance with previous findings, SEC analysis of the product showed a high molecular weight shoulder along with the main peak, which had been attributed to the coupled product (PDMS-TDI-PDMS). In an attempt to decrease the amount of coupled product obtained, the reaction was performed with an increased excess of TDI (12 equivalents in total), but this appeared to have little effect. It could be that some of the coupled product observed is actually the result of urea formation occurring in the solution prepared for SEC analysis.

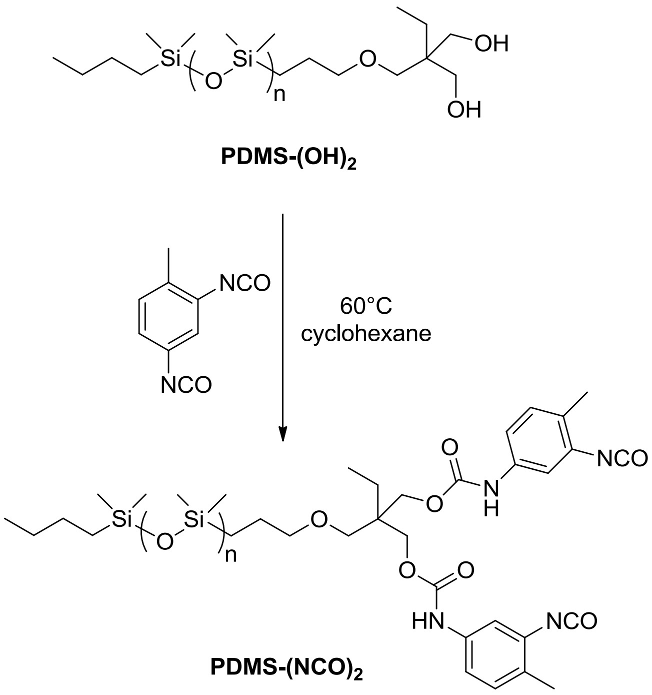

Scheme 32. Functionalisation of PDMS-(OH)$_2$ to PDMS-(NCO)$_2$ with 2,4-TDI. (*N.B.* Although the structure of PDMS-(OH)$_2$ was previously represented differently,[20, 75b] the above structure was confirmed by COSY and HSQC NMR experiments.)

III-3-2 Polymerisation

Polymerisations were carried out under conditions which had given the best results in preceding studies, with a stabiliser concentration equal to 10% of the total mass of the system and a CO_2 pressure of 40 MPa to ensure the solubility of all the reaction components (the cloud point pressure of the PDMS macromonomer is 33.5 MPa at the experimental concentration of 0.35 wt% vs. CO_2). 1,4-butanediol and the catalyst were first dissolved in CO_2 at 60°C and 20 MPa pressure. The PDMS macromonomer was then injected by differential pressure and the pressure in the reactor was increased to 30 MPa. After 30 minutes, 2,4-TDI was injected in the same manner and the pressure finally increased up to 40 MPa. After 7 hours, the reactor was cooled and depressurized, and the solid product was collected directly.

Catalysis with MTBD was investigated first, but proved to be problematic. In a reaction catalysed with 1 mol% MTBD, a large portion of the product obtained was insoluble and even the soluble part showed high levels of isocyanurate by NMR. It was very difficult to remove the entirety of the product residue from the reaction vessel and for this reason the use of guanidine/amidine catalysts in further polymerisations was abandoned. Attention was thus focused on the amine oxide catalyst NMO, and the results of NMO catalysed polymerisations are presented in table 3.

Without the presence of stabiliser, polymerisation catalysed by 1 mol% NMO produced a low molecular weight, tacky polymer product (entry 5). Spherical microparticles were obtained in all the other reactions in the presence of PDMS macromonomer, but the macroscopic form of the product varied from a fairly free-flowing powder (catalyst concentration of 1 mol% or above) to a solid that was somewhat aggregated into clumps (catalyst concentration of 0-0.2 mol%), suggesting an inhomogeneous distribution of residual PDMS or monomers in the product. The yield generally increased with increasing catalyst concentration as the consumption of the monomers was more complete. The yield also depended somewhat on the form of the product, as for example the tacky solid produced without PDMS macromonomer was more difficult to recover from the reactor.

Entry	NMO catalyst loading (mol %)[a]	Yield (%)[b]	Particle Size (µm)[c]	M_w (g mol^{-1})[d]	M_w/M_n[d]	Material recovered from ethanol bath after venting of CO_2[e]		Amount of PDMS in crude particles (wt %)[f]	Amount of PDMS in washed particles (wt %)[f,g]	Difference in PDMS before/after washing (wt % of crude particles)[h]	PDMS residue recovered from supernatant fluid (wt % of crude particles)[i]
						PDMS (wt% of system)	TDI derivatives (% of TDI introduced)				
1	0	56	0.7-180	20,000	2.1	0.5	4.3	6.5	6.6	0.0	2.3
2	0.2	68	0.4-200	23,000	2.3	1.3	10.5	7.2	2.2	5.1	8.8
3	1.0	60	0.5-60	37,000	3.1	0.5	4.9	9.8	7.9	2.1	1.8
4	5.0	77	0.5-5	36,000	2.6	0.0	0.0	6.9	5.1	1.9	7.0
5	1.0	37	Tacky solid	18,000	2.2	N/A	18.1	N/A	N/A	N/A	N/A

[a] Mol % vs. OH (= mol % vs. NCO). [b] Mass recovered from reactor divided by mass of monomers plus stabiliser. [c] Determined from optical microscope and SEM images. [d] Determined by SEC in DMF vs. polystyrene standards. [e] Material recovered from evaporation of the ethanol bath into which CO_2 was vented at the end of the reaction. PDMS and urethane derivatives were crudely separated by washing the residue with cyclohexane. [f] Determined by ^1H NMR in 1:1 THF-d_8:DMF-d_7 (see appendix). [g] After three cycles of dispersion/centrifugation in cyclohexane. [h] Calculated from $(x - y)/(1 - 0.01y)$ where x is the amount of PDMS in the crude particles and y is the amount of PDMS in the washed particles (see appendix). [i] PDMS residue obtained from evaporation of the supernatant fluid after centrifugation of the particles.

Table 3. Dispersion polymerisation of 1,4-butanediol with 2,4-TDI in $scCO_2$, in the presence of 10 wt% PDMS-$(NCO)_2$ macromonomer.

The SEM micrographs of the particles produced in the absence of catalyst or in the presence of 0.2 mol% NMO (entries 1 and 2) showed similar size distributions (figure 42 and 43). On the other hand, with 0.2 mol% NMO, particles with diameters as small as 0.4 µm could be distinguished, whereas without catalyst the smallest particles where somewhat larger, and were bound together by agglomerated material.[*] Even the largest particles appeared to be coated with this agglomerated material, whereas the particles from the reaction with NMO had a smoother appearance. Fractures were present in some of the largest particles which exposed a porous inner structure, presumably formed by some kind of foaming process. The formation of microcellular foams using high pressure CO_2 has been studied in some detail, for example by Beckman and co-workers who investigated poly(methyl methacrylate) and polyurethane foams.[135] Microcellular foams can be produced by a number of different processes that lead to phase separation of a polymer solution. In the case of a CO_2 solution, this includes an increase in the molecular weight of the polymer or a drop in pressure. The supersaturation of CO_2 in the polymer induces the nucleation of pores, which grow by diffusion of CO_2 from the polymer rich regions, or by gas expansion. The diffusion of CO_2 from the polymer into the pores also leads to an increase in the T_g of the polymer (reduction in the plasticising effect of CO_2) until it is vitrified and the foam structure is frozen-in. A non-porous skin can be formed at the polymer surface due to a higher rate of CO_2 diffusion out of the surface than into the pores.[135a] It thus seems probable that the pores observed in the large spherical particles are formed by phase separation within large droplets of CO_2-swollen polymer, occurring as a result of depressurization or growth in polymer molecular weight.

---

[*] In the literature, there is some discrepancy in the use of the terms ‘agglomerate’ and ‘aggregate’. In this text, ‘agglomerate’ is used to describe an assembly of fused or cemented particles, while ‘aggregate’ is used to describe an assembly of more weakly adhered particles.

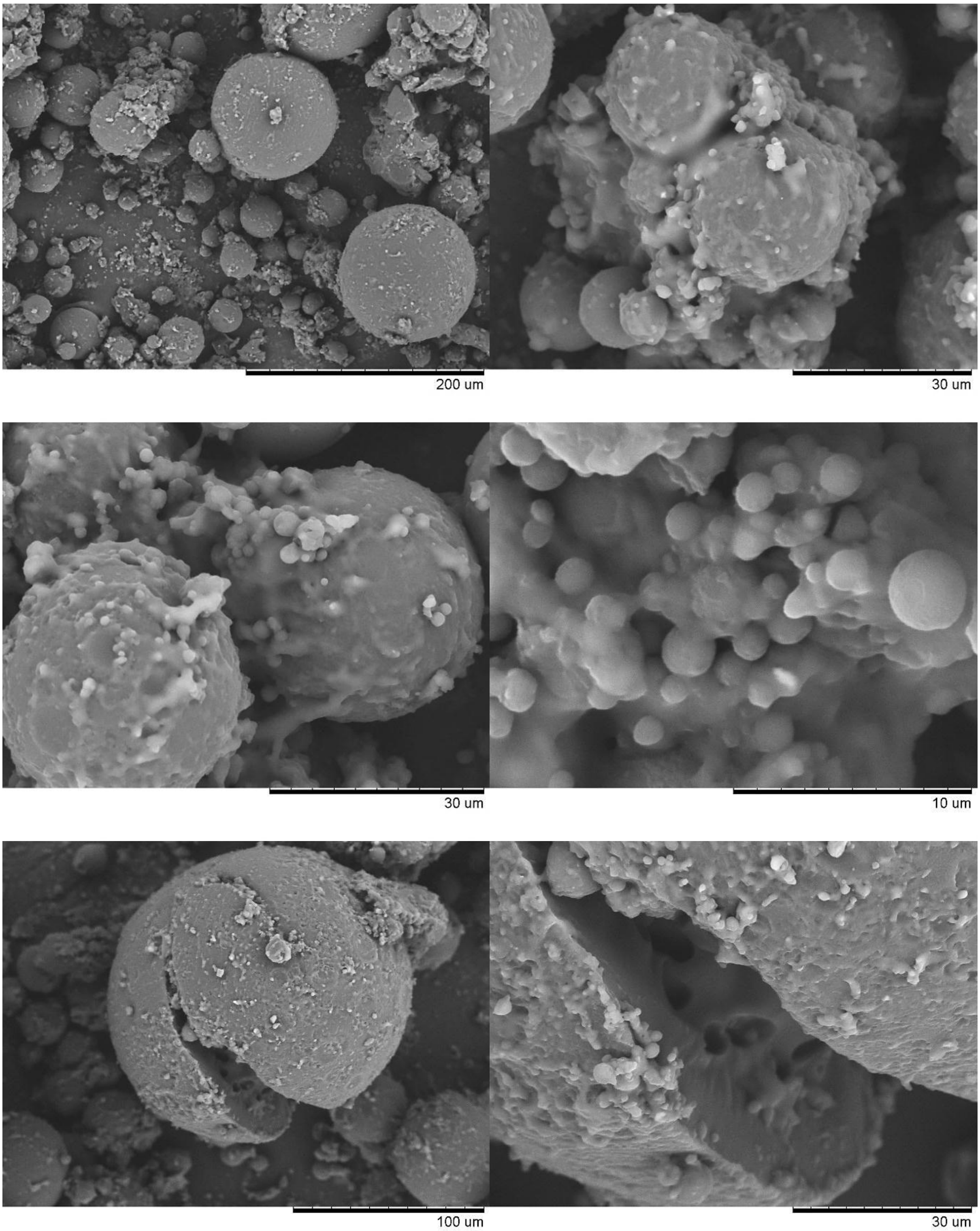
200 um
30 um
30 um
10 um
100 um
30 um

Figure 42. SEM images of polyurethane particles produced in the absence of catalyst (table 3, entry 1).

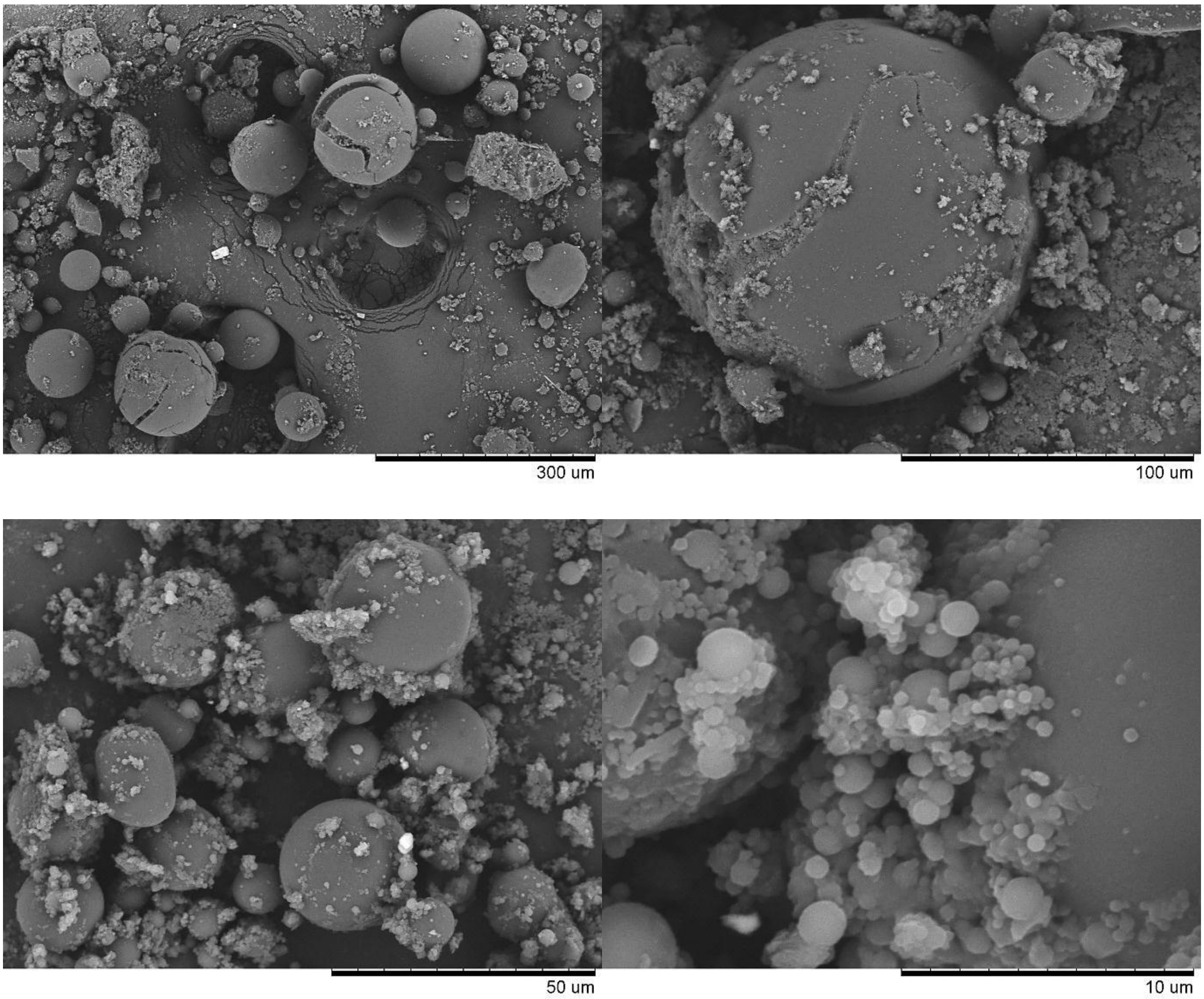

Figure 43. SEM images of polyurethane particles produced in the presence of 0.2 mol% NMO (table 3, entry 2).

In the reaction catalysed by 1 mol% NMO, the largest particles showed broad dimples in their surface or a puckered structure in the extreme case (figure 44). This could be a result of the surface collapsing into an underlying porous structure. This might occur if CO_2 can escape from the pores before vitrification of the polymer. With regard to the smaller particles, significant aggregation/agglomeration could also be observed.

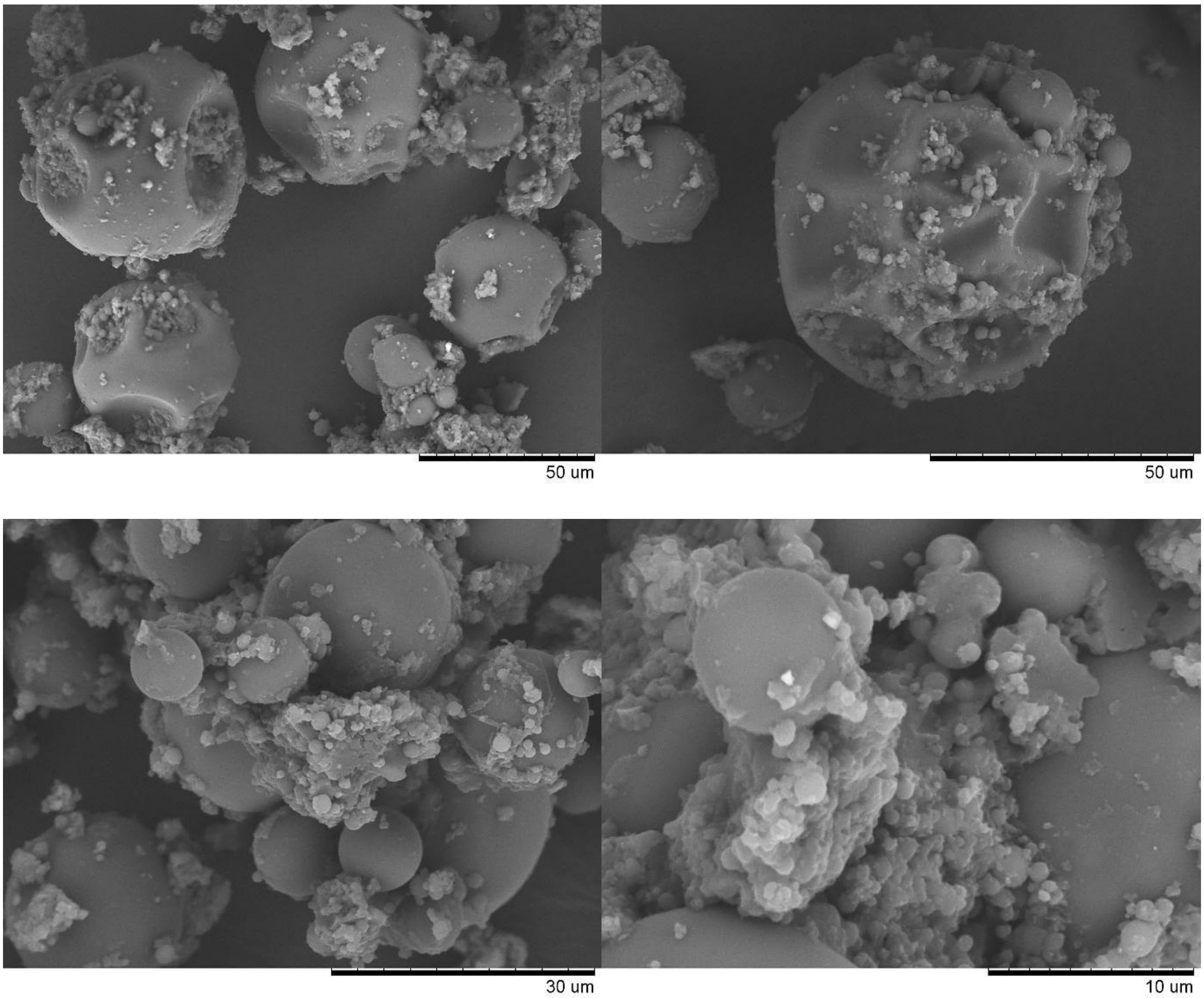

Figure 44. SEM images of polyurethane particles produced in the presence of 1 mol% NMO (table 3, entry 3).

In the reaction catalysed by 5 mol% NMO, even though the particles were quite small, they were rather irregularly shaped and often resembled the larger dimpled or puckered structures observed with 1 mol% of the catalyst. The formation of these structures from surface collapse into pores seems unlikely, considering that for such small particles diffusion of CO_2 out of the particle should be rapid (i.e. the radius of the particle is smaller than the thickness of a non-porous skin that could be formed). Once again, the particles were often highly aggregated/agglomerated.

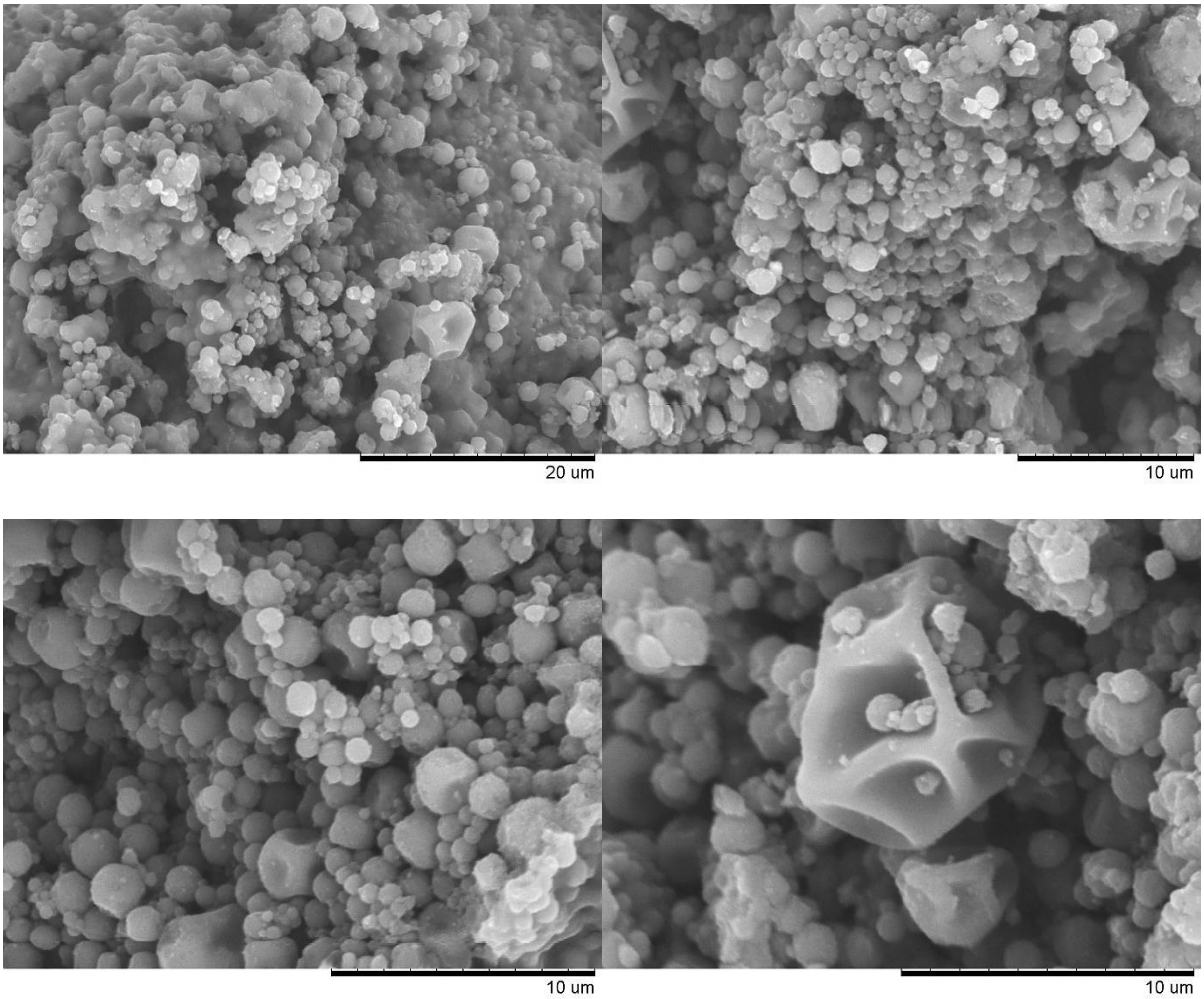

Figure 45. SEM images of polyurethane particles produced in the presence of 5 mol% NMO (table 3, entry 4).

The average size and the size distribution of the particles generally decreased with increasing catalyst concentration. Higher catalyst concentrations could be expected to increase the rate of particle nucleation, giving rise to more uniform particle growth and thus a narrower size distribution. Equally, the initiation of a larger number of nuclei would be expected to lead to smaller particle diameter, since the quantity of monomers is divided between the total number of particles.

At the same time, the molecular weight of the polymers generally increased with increasing catalyst loading, as would be expected for reactions reaching a higher extent of conversion. However, the molecular weight distributions remained fairly broad and were the broadest for the higher catalyst concentrations. M_w/M_n was particularly high for the reaction with 1 mol%

catalyst where the distribution was somewhat bimodal. This is perhaps due to concomitant catalysed and non-catalysed particle formation.

In the majority of the reactions, a significant amount of residue was collected from evaporation of the ethanol bath into which the CO_2 had been vented. This mostly corresponded to unreacted TDI and PDMS macromonomer, although in some cases a small amount of solid material was also visibly ejected from the reactor during depressurization. The PDMS was crudely separated from the urethane/polyurethane by trituration of the residue with cyclohexane. The PDMS recovered accounted for up to 13% of the PDMS originally introduced, while the TDI derivatives (mainly as the diethyl carbamate) corresponded to up to 18% of the TDI introduced. Although there was no clear-cut trend between the catalyst concentration and the amount of residue, the absence of residue from the reaction catalysed with 5 mol% NMO suggested that the TDI had been entirely consumed and that the PDMS macromonomer was perhaps more completely incorporated.

III-3-2-1 ^{1}H NMR analysis of polyurethanes

The NMR spectra in DMSO-d_6 of the polyurethanes produced in the absence of catalyst or with 0.2 mol% NMO were essentially identical. With higher amounts of catalyst, the intensity of the signals corresponding to residual butanediol and aromatic amino groups (from reaction of residual NCO groups with water) decreased, as well as the signals corresponding to butanediol end-groups. This is in line with the increasing M_n of the polymers as recorded by GPC. On the other hand, increasing levels of urea could be observed with increasing catalyst concentration. The hygroscopic nature of the catalyst is perhaps responsible for introducing higher amounts of water into the reaction.

III-3-2-2 Incorporation of PDMS

In preceding studies, the use of NMR integration to determine the level of PDMS incorporation in PUR-PDMS particles was called into question.[20] The values determined from ^{1}H spectra in DMF-d_7 were rather low and repeated analysis of the same sample gave variable results. It was suggested that this could result from the poor solubility of PDMS in DMF, since dynamic light scattering experiments indicated the formation of aggregates in DMF solution. Similar behaviour has been reported for block copolymers of PDMS with 2-dimethylaminoethyl methacrylate, since the sharp PDMS signal observed by ^{1}H NMR in

$CDCl_3$ becomes a broad signal with reduced intensity in acidified D_2O.[136] In some cases, solvent mixtures have been used to obtain NMR spectra of amphiphilic PDMS-based block copolymers, although this did not always avoid the formation of aggregates.[137]

In the present study, a 1:1 mixture of DMF and THF was used to analyse the PUR-PDMS particles. THF is a good solvent for PDMS and a moderate solvent for polyurethane. Analyses of the particles were performed before and after three cycles of dispersion/centrifugation in cyclohexane and the results are presented in table 3. The difference between the PDMS content before and after dispersion/centrifugation is also compared to the amount of PDMS residue obtained by evaporation of the supernatant fluid. Although the values obtained by the two methods are not in very good agreement, the general tendencies are reasonably consistent. There is a reduction in PDMS content with washing, the extent of which varies between the samples, but a significant amount of PDMS always remains in the product. On the other hand, there does not appear to be a clear trend between the catalyst concentration and the level of incorporation of PDMS in the particles.

The PDMS residue obtained from the supernatant fluid during dispersion/centrifugation of the particles was also analysed by NMR spectroscopy. Interestingly, only the butyl end-group of the macromonomer could be identified in the spectra, suggesting that the PDMS had perhaps been cleaved from the particles leaving the anchoring group behind.

ATR-FTIR is another technique that has been used for the quantitative determination of composition in PDMS based copolymers, using the relative intensities of the absorptions attributed to Si-C or Si-O bonds compared to absorptions characteristic of the second polymer block (this method requires some means of calibration).[137] However, when the spectra of PUR-PDMS particles were recorded, the PDMS and PUR bands showed high overlap. Furthermore, only weak changes in the peak intensities were observed compared to a pure polyurethane sample. Therefore, the development of a method of quantification from this technique does not seem feasible. Additionally, since ATR-FTIR is a surface technique, phase segregation could give rise to results which are not representative of the entire sample.

Thermogravimetric analysis (TGA) has also been used to obtain quantitative composition data.[137-138] However, given that the temperature ranges of decomposition of the different components are liable to overlap and may be affected by the presence of catalysts or impurities, the precision of this technique for determining low quantities of PDMS in PUR-PDMS particles is questionable.

Finally, elemental analysis is another possible means of determining the quantitative composition of PUR-PDMS particles. The polymer produced in the presence of 0.2 mol% NMO catalyst (table 3, entry 2) was analysed for its nitrogen, carbon and hydrogen composition, which was then used to calculate the PDMS content (see appendix). For the crude particles, the results indicated a PDMS content of 9.4% calculated from carbon content and 10.6% calculated from nitrogen content (average of two samples), while for the washed particles, the PDMS content was 5.4% calculated from carbon content and 6.5% calculated from nitrogen content. These results are only loosely in agreement with the results of NMR analyses, but confirm the general trend that a portion of PDMS is removed upon washing the particles with cyclohexane, and that a significant amount of PDMS remains in the product. One major drawback of this method is the very small sample size used (~1 mg), which may not be representative of the entire product.

III-3-2-3 Raman Imaging

In the Raman spectra of PUR-PDMS particles, the signals corresponding to polyurethane and PDMS are well resolved. Determination of the bulk concentration of PDMS should be possible by Raman scattering in the transmission geometry,[139] although this would require some method development. On the other hand, confocal Raman microscopy offers the opportunity to identify the spatial location of the polyurethane and PDMS components. The Raman images presented in figure 46B & D show a 5 µm thick cross-section through a sample of crude PUR-PDMS particles (prepared with 0.2 mol% NMO catalyst (table 3, entry 2)). Each pixel corresponds to a Raman spectrum of a spot of 5 µm diameter. Using the intensity of the polyurethane signals at 1270 and 1308 cm^{-1}, the Raman image of the polyurethane can be established (figure 46B), which matches well with the optical microscope image (figure 46A). Adding a second colour to map the intensity of the PDMS signal at 485 cm^{-1} gives the image shown in figure 46D. It can be seen that the PDMS is mostly located around the exterior of the polyurethane particles, although it is difficult to evidence a distinct core-shell structure. The large size distribution of the particles is problematic, since the cross-section which is analysed will not necessarily pass through the core of all the different particles. Comparing figure 46D to the SEM micrograph in figure 43 with a similar magnification (image with 50 µm scale bar) also suggests that the regions of high PDMS concentration could correspond to clusters of smaller particles which would be impossible to distinguish in the optical microscope image. The more evenly sized particles produced in the presence of 5 mol% NMO catalyst are unfortunately too small to be imaged by this technique, as their diameter is of the same order of magnitude as the resolution.

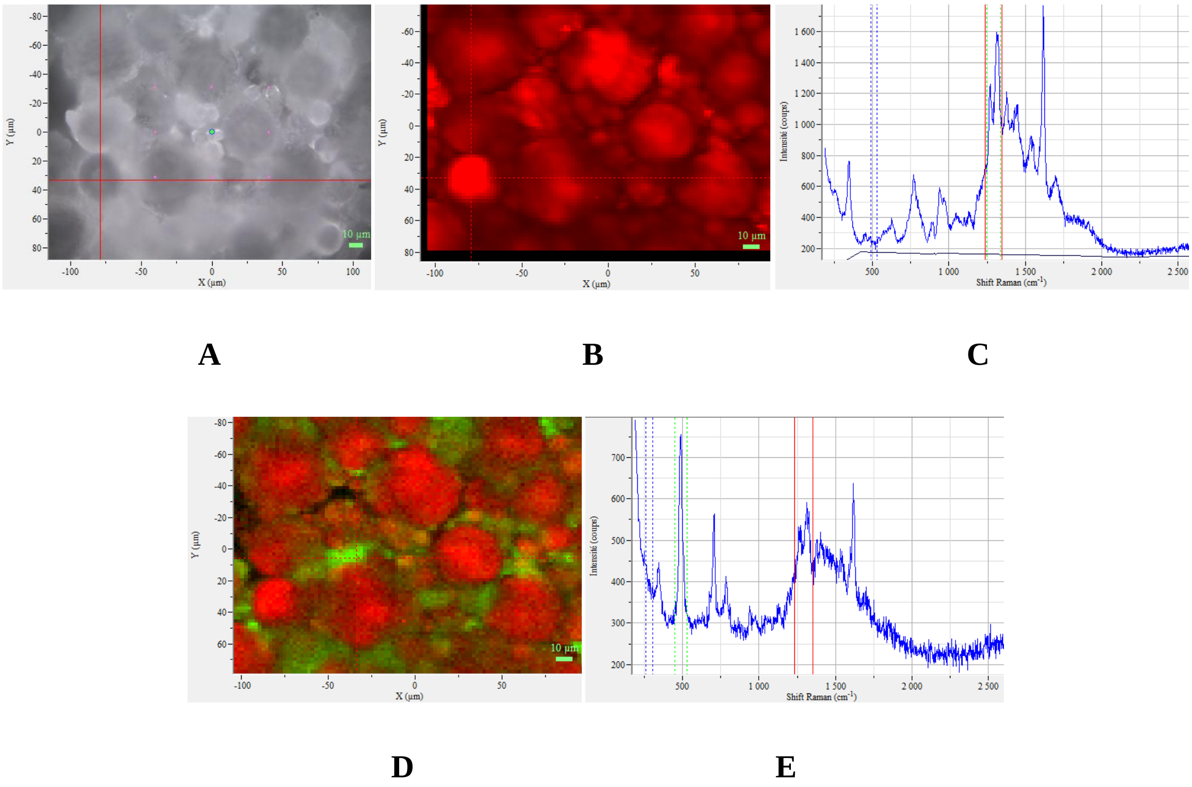

Figure 46. Raman imaging of the crude PUR-PDMS particles produced in the presence of 0.2 mol% NMO catalyst (table 3, entry 2). (A) Optical microscope image. (B) Raman image mapping the intensity of the polyurethane signals at 1270 and 1308 cm^{-1}. (C) Raman spectrum at the position marked by the cursor in images A and B. (D) Raman image mapping the intensity of the polyurethane signals at 1270 and 1308 cm^{-1} (red) and the intensity of the PDMS signal at 485 cm^{-1} (green). (E) Raman spectrum at the position marked by the cursor in image D.

III-3-3 Conclusions of dispersion polymerisations using macromonomer

Polymerisations stabilised by isocyanate functionalised PDMS macromonomer result in the formation of polymer microparticles, although these show significant levels of aggregation/agglomeration. The concentration of NMO catalyst has a clear effect on both the molecular weights of the polymers as well as the particle morphology obtained. Molecular weights increase with increasing catalyst loading while the average size of the particles decreases. The particles also appear to become less spherical with increasing catalyst concentration. The influence of the catalyst is modest at 0.2 mol% loading but becomes more significant at 1 mol%. No correlation could be identified between the catalyst concentration and the level of incorporation of the PDMS macromonomer into the polymer. A portion of the PDMS could be removed from the particles by dispersion in cyclohexane followed by centrifugation, but an appreciable amount always remained.

III-4 Dispersion Polymerisation of Polyurethanes using Catasurfs

Catalytic surfactants (‘catasurfs’) have already found applications in areas such as heterogeneous oxidation reactions[140] or the formation of silica microparticles.[141] In the dispersion polymerisation of polyurethanes, such species may be able to produce polymer particles without permanently bound auxiliary substances. Removal of the catasurf at the end of the reaction will thus afford uncontaminated polyurethane materials. The ability of a catasurf to stabilise polymer particles will presumably depend upon its interfacial activity, i.e. the relative affinity of the catalyst end-group for the dispersed and CO_2 phases. Strong interactions between the stabiliser end-group and the polymer (pseudo-grafting) would be expected to give the greatest control over particle morphology. Another consequence of combining the catalyst and stabiliser is that the spatial location of the catalytic moiety can be controlled. With a catasurf, the catalytic function should be found at the phase interface, whereas with small molecules, the catalyst may be partitioned between the two phases.

Amine oxide functionalised PDMS makes a good candidate for a catasurf, since the amine oxide function is very polar and would be expected to have a much higher affinity for the dispersed monomer/polymer phase compared to the CO_2 phase. The use of an ‘organocatasurf’ is also in keeping with the desire for a metal-free reaction.

III-4-1 Synthesis of Organocatasurfs

III-4-1-1 Synthesis using a carbonate linker

The first synthetic strategy that was envisaged for the preparation of organocatasurfs was to attach the catalyst moiety to a commercially available mono-alkoxy terminated PDMS (PDMS-OH) via a linker group. This strategy would allow fairly straightforward variation of the catalyst structure, and should facilitate purification. The carbonate group appeared to be a good choice for the linker as it does not have an isocyanate-reactive site and since a variety of tertiary amines containing a hydroxyl group are commercially available. The amine could thus be oxidised to the amine oxide before coupling to PDMS-OH through a carbonate linkage.

The strategy outlined above was first attempted starting from *N*,*N*-dimethyl-2-aminoethanol **34**. The corresponding amine oxide **35** was obtained in reasonable yield by oxidation with mCPBA (scheme 33) followed by short column chromatography on basic alumina.

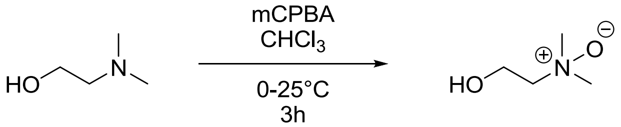

34 **35**

Scheme 33. Oxidation of *N*,*N*-dimethyl-2-aminoethanol.

Carbonyldiimadazole (CDI, **36**) was selected as the coupling agent for carbonate formation because it is easier to handle and less toxic than phosgene or related reagents and allows isolation of the intermediate imidazole carboxylic ester.[142] However, the reaction of **35** with CDI did not afford the desired compound **37** as the product underwent an intramolecular rearrangement with loss of CO_2. The rearranged product **38** was isolated in 58% yield. A similar rearrangement with a three-membered ring aziridinium intermediate has been reported for the reaction of CDI with *N*,*N*-dialkyl β-aminoalcohols.[143]

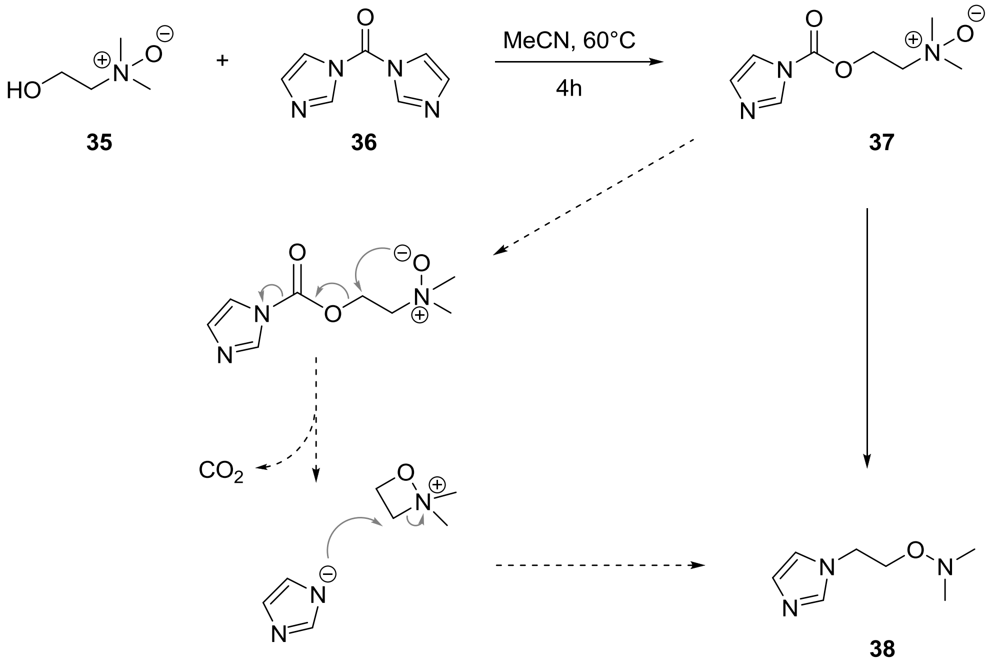

Scheme 34. Reaction of dimethylaminoethanol oxide with CDI followed by an intramolecular rearrangement with loss of CO$_2$.

The same approach was repeated starting from 4-hydroxy-1-methylpiperidine **39**, for which the rearrangement reaction in the second step would not be possible. In this case, the oxidation step led to two diastereoisomers (**40** and **41**) in approximately equal proportions (scheme 35), which could be separated by column chromatography on basic alumina followed by repeated recrystallization.

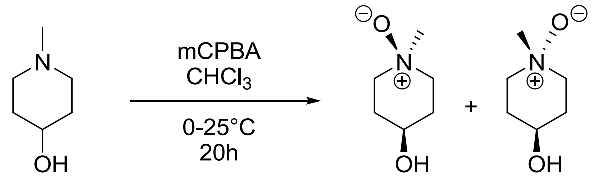

39 **40** **41**

Scheme 35. Oxidation of 4-hydroxy-1-methylpiperidine.

Once again, reaction of the amine oxide with CDI did not afford the desired product. The use of 1.5 equivalents of CDI led to low conversion, but when 2.5 equivalents were used a complex mixture of products was obtained. The only compound that could be isolated by liquid-liquid extraction showed NMR signals consistent with a *N*-(piperidinomethyl)imidazole moiety (**42**),[144] suggesting that a Polonovski-type reaction had taken place (scheme 36). *N*-(dialkylaminomethyl)imidazoles do have some practical applications[144] so an adapted procedure could perhaps be synthetically useful.

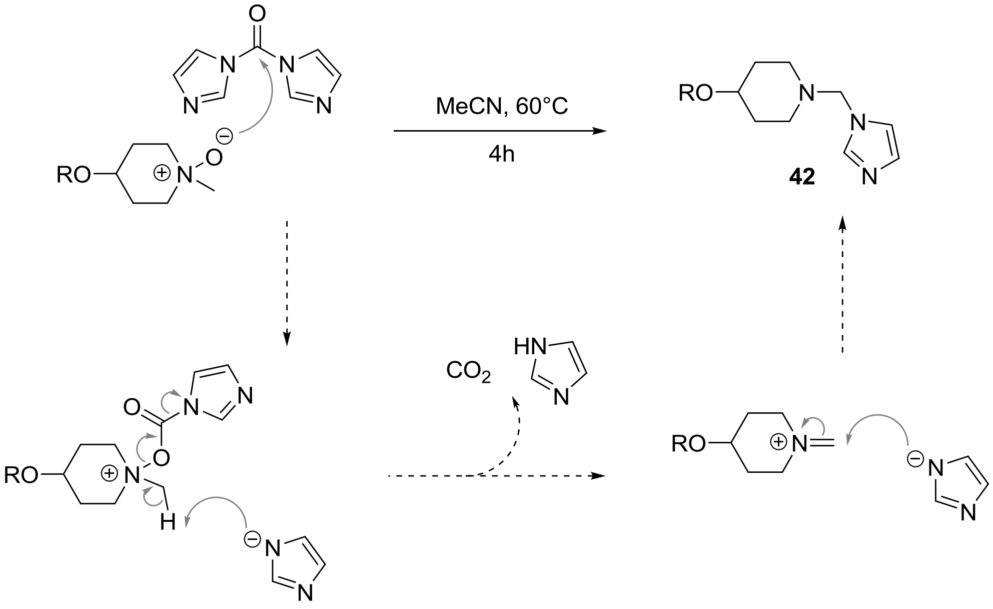

Scheme 36. Polonovski-type reaction of amine oxide with CDI.

In view of these unwanted reactions, the order of the coupling reaction was reversed so that the imidazole carboxylic ester of the PDMS could be formed first, and then reacted with the hydroxyl group of the amine oxide (scheme 37). This procedure was validated using butanol as a model for PDMS-OH, but when the reaction was performed with the latter, the change of solvent from acetonitrile to a less polar solvent (THF) meant that the amine oxide was poorly soluble and prolonged heating was required in order to reach full conversion. The PDMS product obtained was a mixture of the desired compound (**44**) and PDMS-OH, so this did not appear to be a suitable method of preparation.

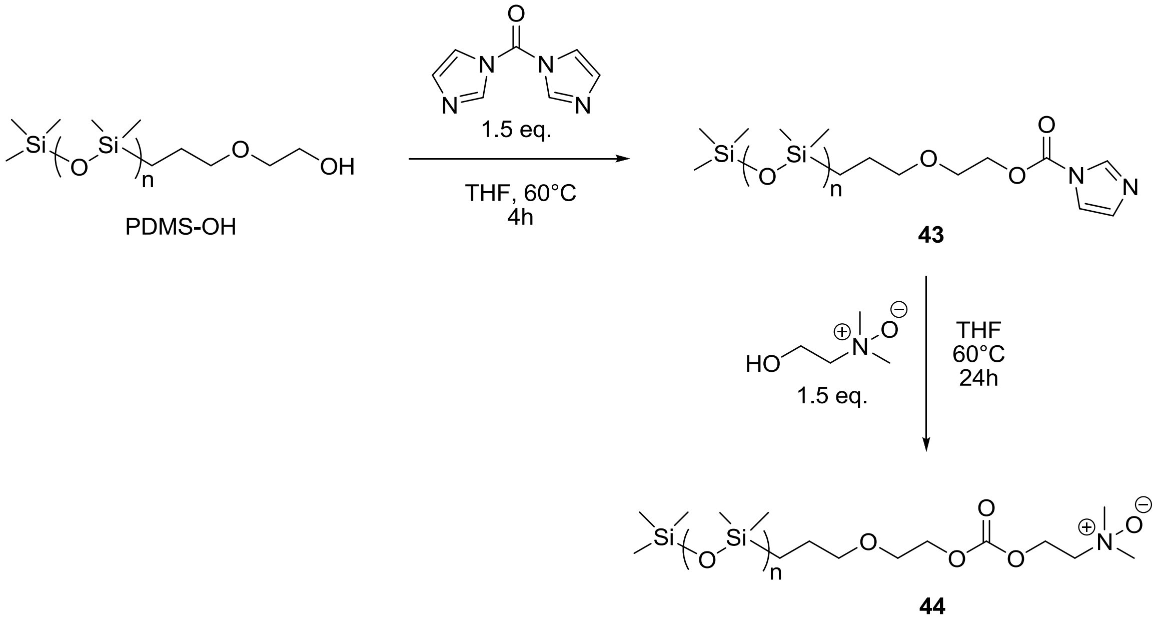

Scheme 37. Synthetic route to amine oxide terminated PDMS.

Finally, the order of the steps in the synthesis was further rearranged to form the carbonate linkage before the oxidation of the amine. The amino-terminated PDMS (**45**) was thus prepared in a one-pot, two-step procedure (scheme 38). The first step gave complete conversion to the imidazole carboxylic ester, and the second step reached approximately 94% conversion by NMR. The by-products and excess reagents were removed by washing the crude material with acetonitrile. Oxidation of the amino-terminated PDMS was then carried out using mCPBA to afford **44**. The same procedure was not attempted with 4-hydroxy-1-methylpiperidine **39** because carbonate formation with a secondary alcohol was found to require catalysis with potassium hydroxide, which is incompatible with the PDMS.

Unfortunately, compound **44** was found to degrade over time to a mixture of PDMS-OH, dimethylaminoethanol oxide (**35**) and a symmetrical di-PDMS substituted carbonate. Considering that the amino-substituted PDMS **45** remained unchanged over time, it appears that the amine oxide function catalyses the hydrolysis and transesterification of the carbonate linkage. Therefore, an alternative synthesis was sought to produce more robust organocatasurfs without using a carbonate linkage.

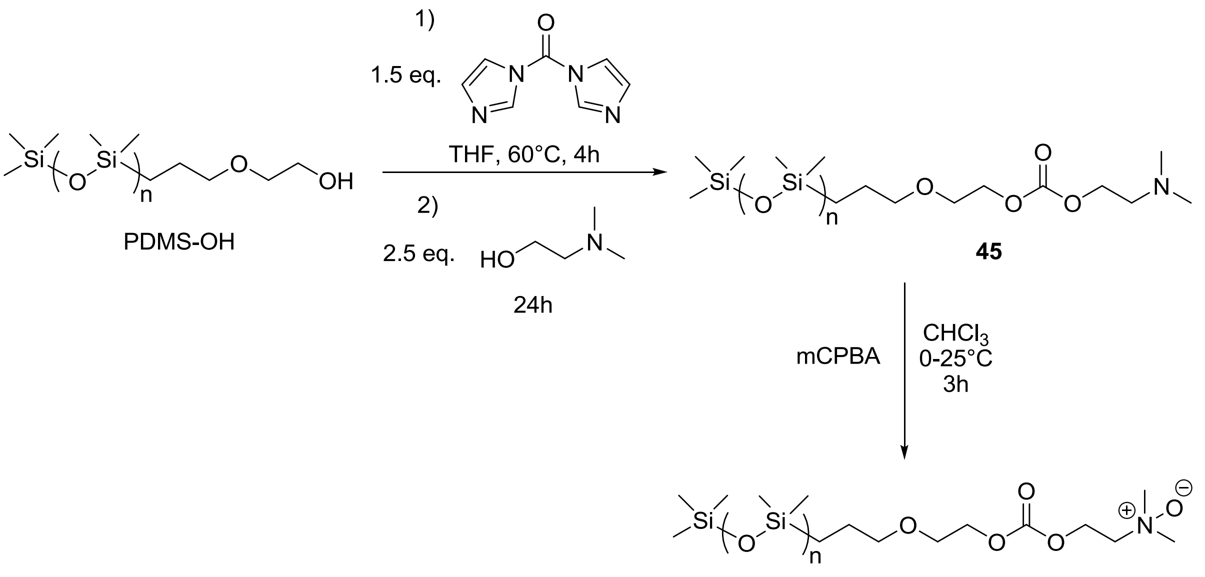

44

Scheme 38. Alternative synthetic route to amine oxide terminated PDMS.

III-4-1-2 Synthesis via a hydrosilylation reaction

The preparation of organosilicon amine oxides has been reported in the patent literature for applications such as surfactants or anti-foaming agents.[145] The principal method of synthesis described involves the attachment of a tertiary amine to a hydrosilicon compound via a hydrosilylation reaction, followed by oxidation of the amine to the amine oxide. This approach was thus applied to the synthesis of organocatasurfs starting from hydride-terminated PDMS. Several different PDMS starting materials were commercially available, which were telechelic or monohydride-terminated with different molecular weights (figure 47).

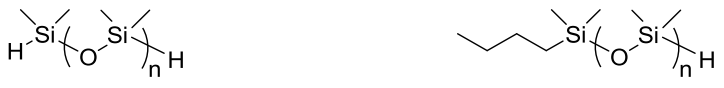

M_n = 5000-7000 g mol^{-1} (Supplier's label)
M_n = 6000 g mol^{-1} (^{1}H NMR)

46a

1) M_n = 600-800 g mol^{-1} (Supplier's label)
M_n = 1000 g mol^{-1} (^{1}H NMR)

2) M_n = 4000-6000 g mol^{-1} (Supplier's label)
M_n = 8100 g mol^{-1} (^{1}H NMR)

46b

Figure 47. Hydride-terminated PDMS starting materials.

The hydrosiloxanes were reacted with *N*,*N*-dimethylallylamine in the presence of Karstedt's catalyst, leading to complete conversion (scheme 39). The preparation of the allyl ether of 1-methyl-4-piperidinemethanol was also attempted in order to make an alternative coupling partner but purification of the product proved to be difficult. The amino terminated PDMS compounds were then oxidised with mCPBA to afford the amine oxides.

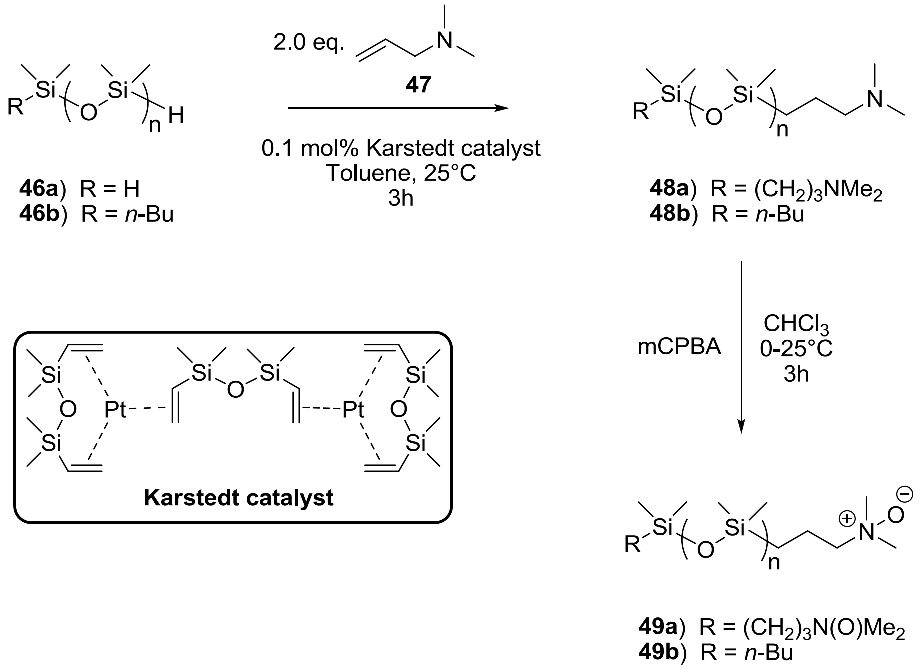
2.0 eq.
47
0.1 mol% Karstedt catalyst
Toluene, 25°C
3h
46a) R = H
46b) R = n-Bu
48a) R = (CH2)3NMe2
48b) R = n-Bu
mCPBA
CHCl3
0-25°C
3h
Karstedt catalyst
49a) R = (CH2)3N(O)Me2
49b) R = n-Bu

Scheme 39. Synthesis of amine oxide terminated PDMS via hydrosilylation.

The conversion of amine groups to amine oxide could be demonstrated clearly by ^{1}H NMR spectroscopy. In the spectrum of **49a**, the singlet corresponding to the methyl groups bonded to nitrogen is observed at a characteristic chemical shift of 3.1 ppm compared to 2.5 ppm for the amine precursor **48a** (figure 48).

The end-group functionalization of **49a** was also verified by MALDI-TOF mass spectroscopy. The mass spectrum showed isotopically split distributions separated by 74.0 Da (siloxane repeat unit), with the first peak of each distribution at m/z corresponding to (n x 74.02) + 102.09 + 160.12 (see figure 49 and 50). The isotopic splitting pattern also agreed well with theoretical intensities.

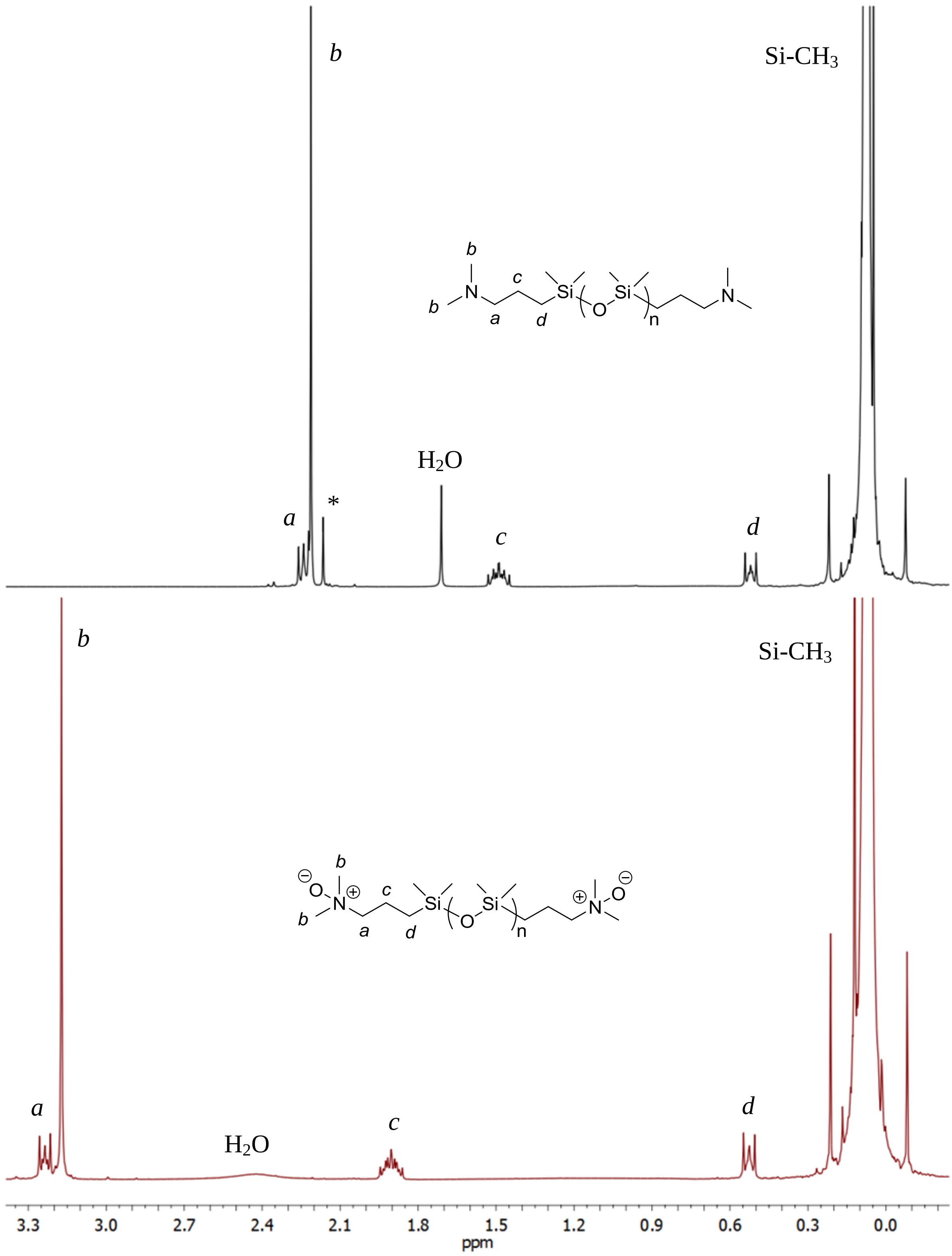

Figure 48. ^{1}H NMR spectra of the telechelic amine-oxide terminated PDMS **49a** (red) and the amine terminated precursor **48a** (black) (* impurity).

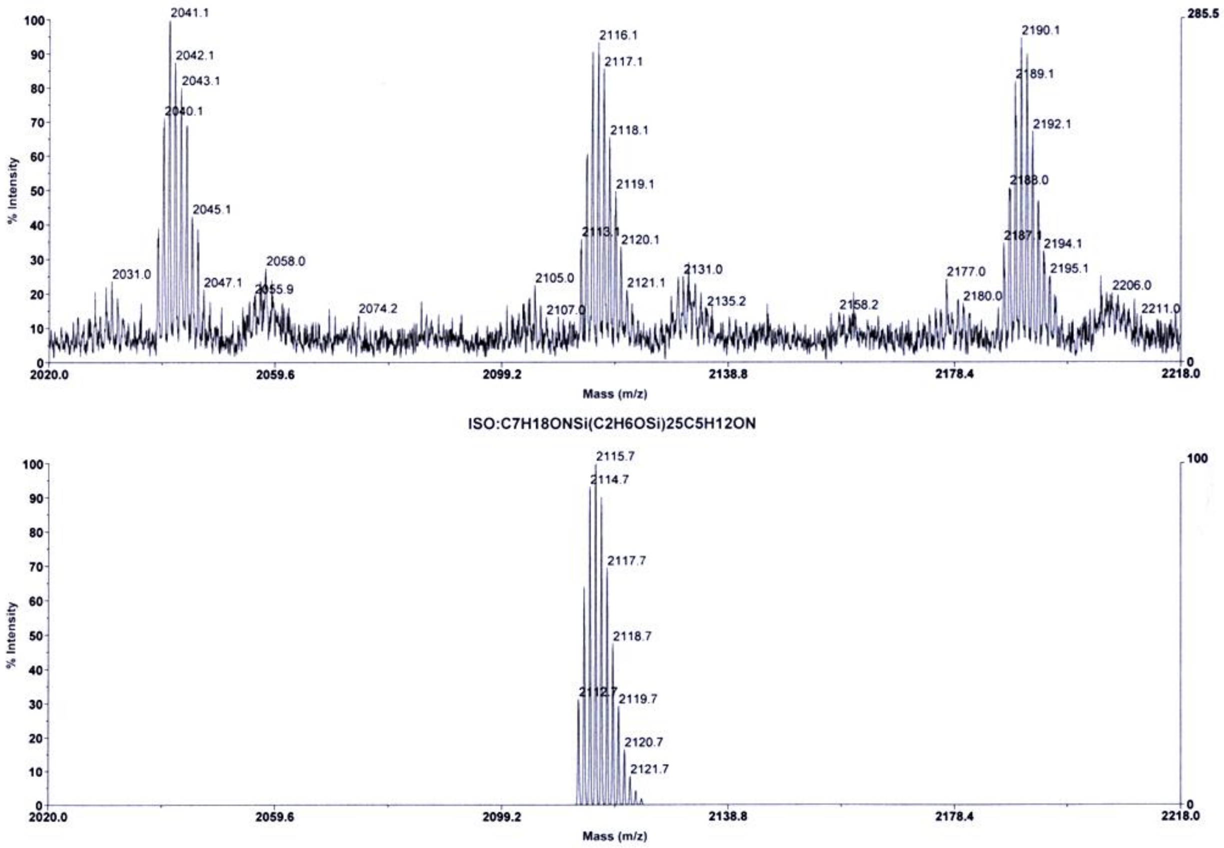

Figure 49. MALDI-TOF mass spectrum of **49a** between 2020 and 2218 m/z (top) and calculated spectum for n = 25 (bottom).

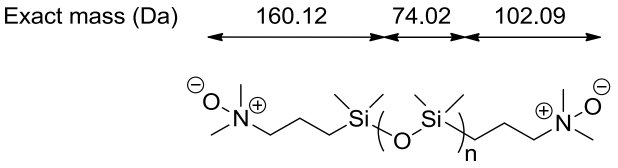

Figure 50. Exact masses of the siloxane repeat unit and amine oxide end-groups (for the most abundant isotopes).

The acid by-product of mCPBA could not be removed effectively from the amine oxide by washing with sodium hydrogen carbonate and since more basic solutions risked to decompose the product,[145b] the acid was removed via short column chromatography on basic alumina. However, this led to a significant loss of amine oxide end-groups. For example, the M_n calculated from the ^1H NMR integral of dimethylsiloxy units versus end-groups was

13,700 g mol^{-1} for the telechelic amine oxide-terminated PDMS **49a** compared to 7000 g mol^{-1} for the starting amine **48a**. The M_n was also calculated by potentiometric titration of the amine oxide groups, giving a slightly larger value of 15,900 g mol^{-1} (7900 g mol^{-1} for the starting amine). The loss of amine oxide groups is perhaps due to a decomposition reaction on alumina, similar to the one reported to occur in basic aqueous solutions (scheme 40).

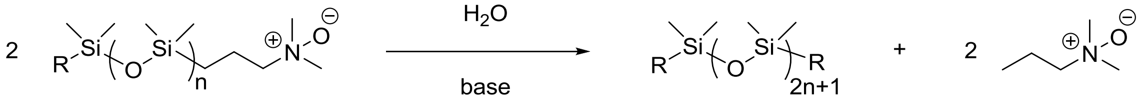

Scheme 40. Reported decomposition of amine oxide-terminated siloxanes in basic aqueous solution.

An alternative oxidation procedure was later developed using hydrogen peroxide in a biphasic mixture with chloroform. The reaction was catalysed with CO_2 via *in situ* formation of the peroxymonocarbonate ion (HCO_4^-) (scheme 41). The work-up method proved to be very important in this case because with certain procedures the isolated product decomposed within a few days (with the appearance of *N*,*N*-dimethyl-3-aminopropanol oxide in the NMR spectrum). The only work-up which avoided this decomposition was a liquid-liquid extraction using pentane and methanol. The organocatasurfs produced by this method showed the same molecular weight as the precursor amines (calculated by NMR).

Regardless of the method of preparation, the organocatasurfs **49a-b** were found to undergo gradual decomposition at room temperature (~25% reduction in amine oxide end-groups over 4 months for **49b** by ^{1}H NMR), although the products of the decomposition were difficult to identify.

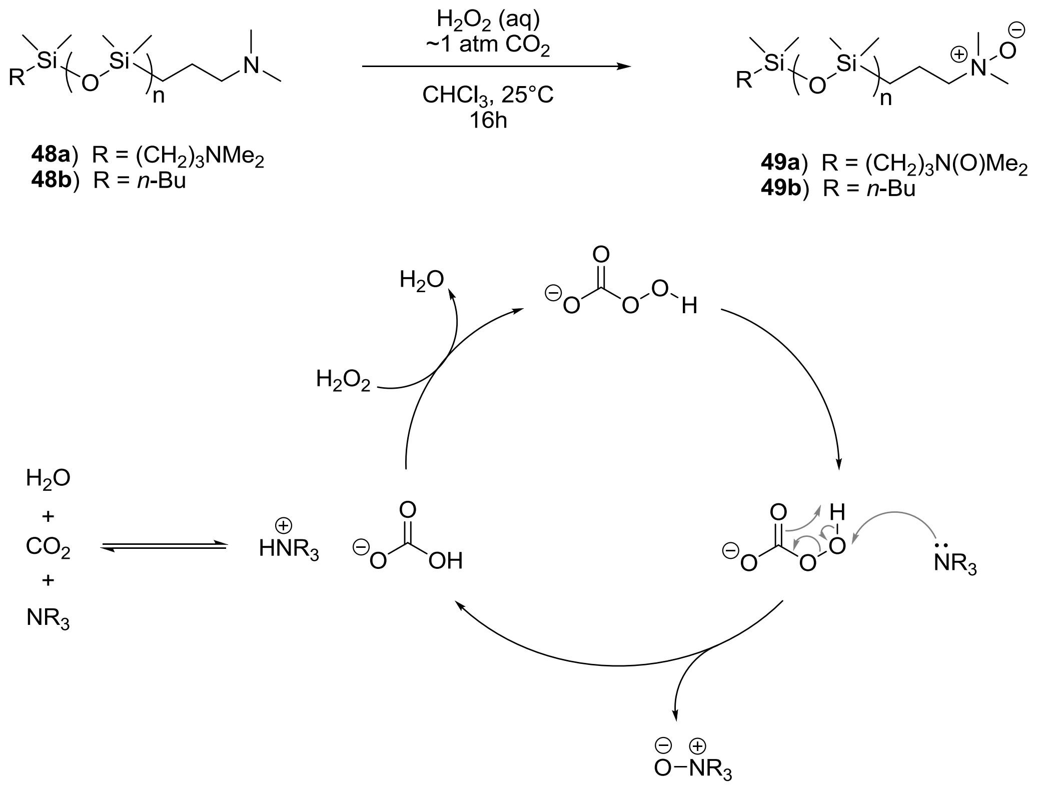

Scheme 41. CO_2 catalysed oxidation of amino-terminated PDMS with H_2O_2.

III-4-1-3 Thermal Stability of the Catasurfs

The thermal stability of amine oxides is important to consider, since amine oxides may undergo a thermally-induced elimination reaction known as the Cope elimination (scheme 42). The reaction requires a hydrogen atom in a β-position to nitrogen and is also subject to conformational constraints since *N*-methylpiperidine oxides are resistant to the intramolecular reaction. In the patent literature concerning organosilicon amine oxides, this reaction is reported to occur at temperatures above 75°C.[145a, b]

The thermal stability of the organocatasuf **49b** (M_n = 1600 g mol^{-1}) was assessed by thermogravimetric analysis (figure 51). The data was acquired with a heating rate of 5.0°C/min in a nitrogen atmosphere. For comparison, the thermal stability of **48b** was also determined. The differential thermogravimetric analysis curve (DTG curve) of **48b** shows a single broad peak for the maximum rate of weight loss centred around 300°C. This corresponds either to vaporisation of the low molecular weight PDMS or a catalysed degradation reaction, since the depolymerisation of catalyst-free, trimethylsiloxy-terminated

PDMS occurs above 420°C.[146] The DTG curve of **49b** shows the same broad peak centred around 300°C with a second fairly sharp peak between about 95 and 150°C with a maximum at 134°C. This presumably corresponds to the Cope elimination of the amine oxide end-groups. The temperature of 60°C used in the polymerisation reactions therefore appears to be sufficiently low to avoid the thermal elimination of the catalyst groups.

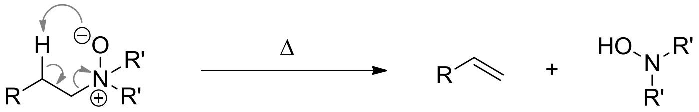

Scheme 42. Cope elimination of amine oxides.

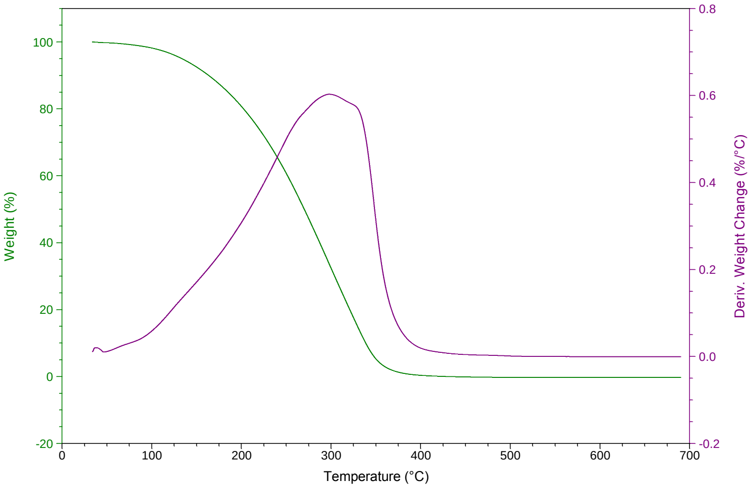

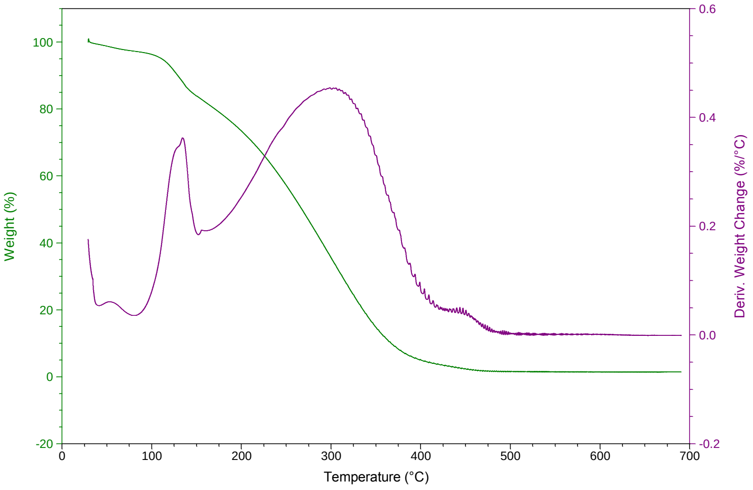

Figure 51. Thermogravimetric analysis curve (green) and differential thermogravimetric analysis curve (purple) of **48b** (top) and **49b** (bottom).

III-4-2 Polymerisation

Polymerisations were carried out under analogous conditions to the macromonomer stabilised reactions. However, in this case it was not possible to independently vary the concentration of catalytic functions, the concentration of PDMS and the PDMS molecular weight. Catalyst concentrations of 0.2 and 1 mol% were tested, giving rise to PDMS concentrations between 10 and 43 weight percent of the system, depending on the molecular weight and the functionality of the catasurf. The diol and catasurf were first dissolved in CO_2 at 60°C and 30 MPa, before addition of the diisocyanate and an increase in pressure to 40 MPa. After 7 hours, the reactor was cooled and depressurized, and the solid product was collected directly. The results of the polymerisations are presented in table 4.

Entry	Catasurf[a]	Quantity of PDMS (wt% of system)	Yield (%)[b]	Particle Size (μm)[c]	M_w (g mol^{-1})[d]	M_w/M_n[d]	Material recovered from ethanol bath after venting of CO_2[e]		Amount of PDMS in crude particles (wt %)[f]	Amount of PDMS in washed particles (wt %)[f,g]	Difference in PDMS before/after washing (wt % of crude particles)[h]	PDMS recovered from supernatant fluid (wt % of crude particles)[i]
							PDMS (wt% of system)	TDI derivatives (% of TDI introduced)				
1a	0.2 mol % **49a** (15,000 g mol^{-1})	10.2	72	0.7-650	22,000	2.5	1.1	7.5	6.2	6.1	0.1	1.4
1b	0.2 mol % **49a** (15,000 g mol^{-1})	10.2	72	1.0-450	25,000	2.7	0.9	6.3	4.7	5.4	0.0	2.0
2	0.2 mol % **49a** (12,000 g mol^{-1})	8.3	75	0.6-1000	28,000	2.9	0.6	9.6	7.9	6.9	1.1	1.5
3	0.2 mol % **49b** (10,000 g mol^{-1})	13.1	72	1.0-700	25,000	2.4	2.4	10.4	6.6	1.8	4.9	10.9
4	1.0 mol % **49b** (1600 g mol^{-1})	10.7	58	No particles	16,000	1.8	5.3	8.7	2.8	1.7	1.2	1.4
5	1.0 mol % **49b** (1600 g mol^{-1})	18.8	73	0.4-130	28,000	2.4	6.0	4.5	8.8	5.9	3.2	4.7
6	1.0 mol % **48a** (7500 g mol^{-1})	22.1	60	0.4-250 & 1-2 mm	14,000	2.2	5.5	22.9	6.4	1.5	5.0	16.3
7	1.0 mol % **49a** (12,000 g mol^{-1})	31.2	84	0.5-35	39,000	1.9	2.5	0.2	23.6	14.3	10.9	10.5
8	1.0 mol % **49b** (10,000 g mol^{-1})	43.1	77	0.8-150	41,000	2.3	2.9	0.2	15.6	1.5	14.3	38.0

[a] Mol % catalyst groups vs. OH (= mol % vs. NCO). [b] Mass recovered from reactor divided by mass of monomers plus catasurf. [c] Determined from optical microscope and SEM images. [d] Determined by SEC in DMF vs. polystyrene standards. [e] Material recovered from evaporation of the ethanol bath into which CO_2 was vented at the end of the reaction. PDMS and urethane derivatives were crudely separated by washing the residue with cyclohexane. [f] Determined by ^{1}H NMR in 1:1 THF-d_8:DMF-d_7 (see appendix). [g] After three cycles of dispersion/centrifugation in cyclohexane. [h] Calculated from $(x - y)/(1 - 0.01y)$ where x is the amount of PDMS in the crude particles and y is the amount of PDMS in the washed particles (see appendix). [i] PDMS residue obtained from evaporation of the supernatant fluid after centrifugation of the particles.

Table 4. Dispersion polymerisation of 1,4-butanediol with 2,4-TDI in $scCO_2$, in the presence of organocatasurfs.

Using 0.2 mol% of the telechelic catasurf **49a** with a molecular weight of 15,000 g mol^{-1} (entry 1a & b), the yield and molecular weight of the polyurethane obtained were comparable to that achieved with 0.2 mol% NMO in the presence of the PDMS macromonomer (table 3, entry 2). On the other hand, the molecular weight distribution and the characteristics of the particles showed a clear contrast. In the case of the catasurf, the molecular weight distribution was bimodal, while there was an enormous variation in the size of the particles with diameters ranging from about 0.7 to 650 µm (figure 52). The very large particles could be crudely separated from the smaller ones by filtering a cyclohexane dispersion through a 100 µm mesh filter. Further analysis showed that the two populations correlated to the two peaks in the molecular weight distribution, with the smaller particles corresponding to the higher molecular weights. The large particles accounted for the majority of the mass of the product.

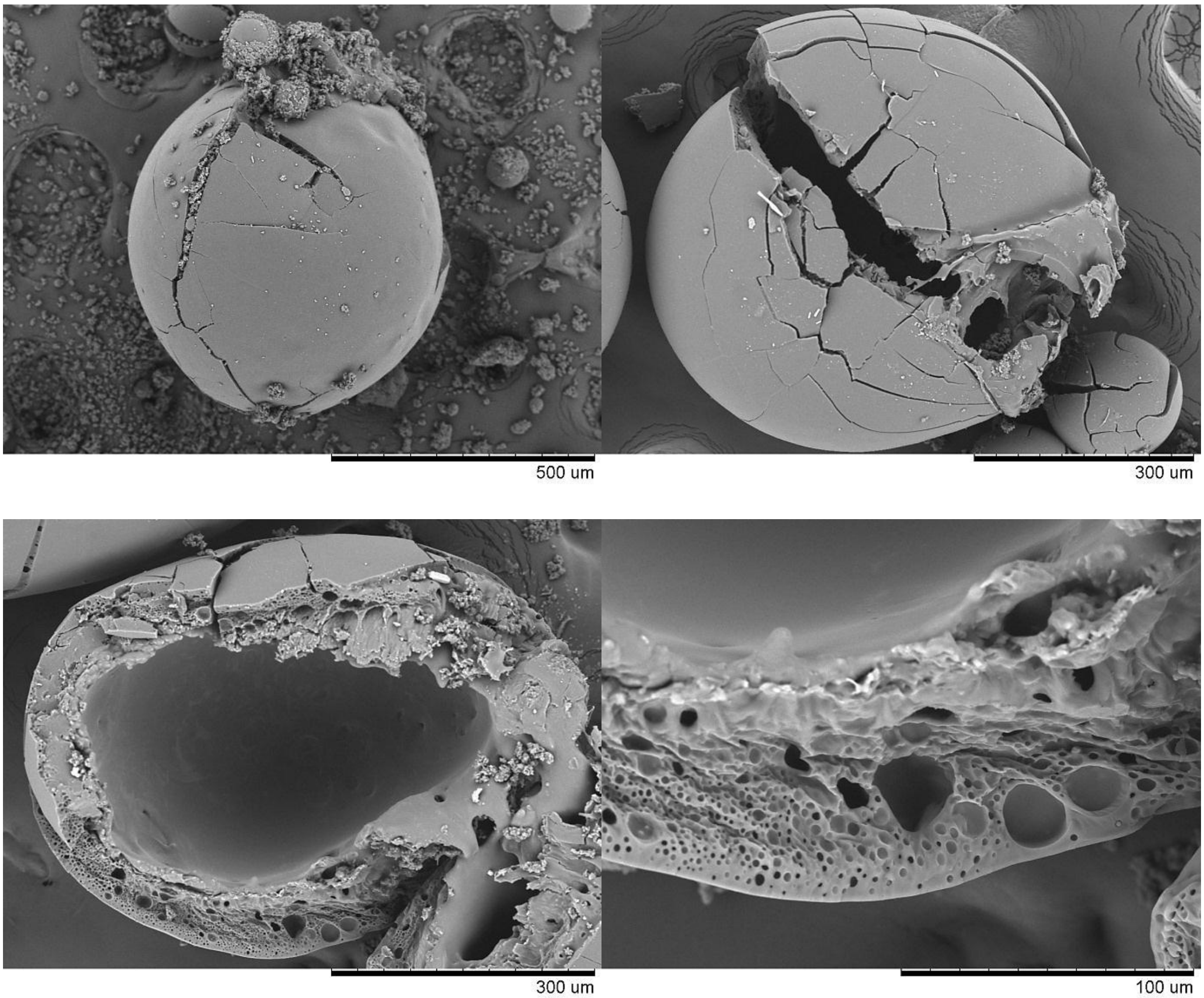

Figure 52. SEM images of polyurethane particles produced in the presence of 0.2 mol% telechelic catasurf **49a** with an M_n of 15,000 g mol^{-1} (entry 1a). (continues on next page)

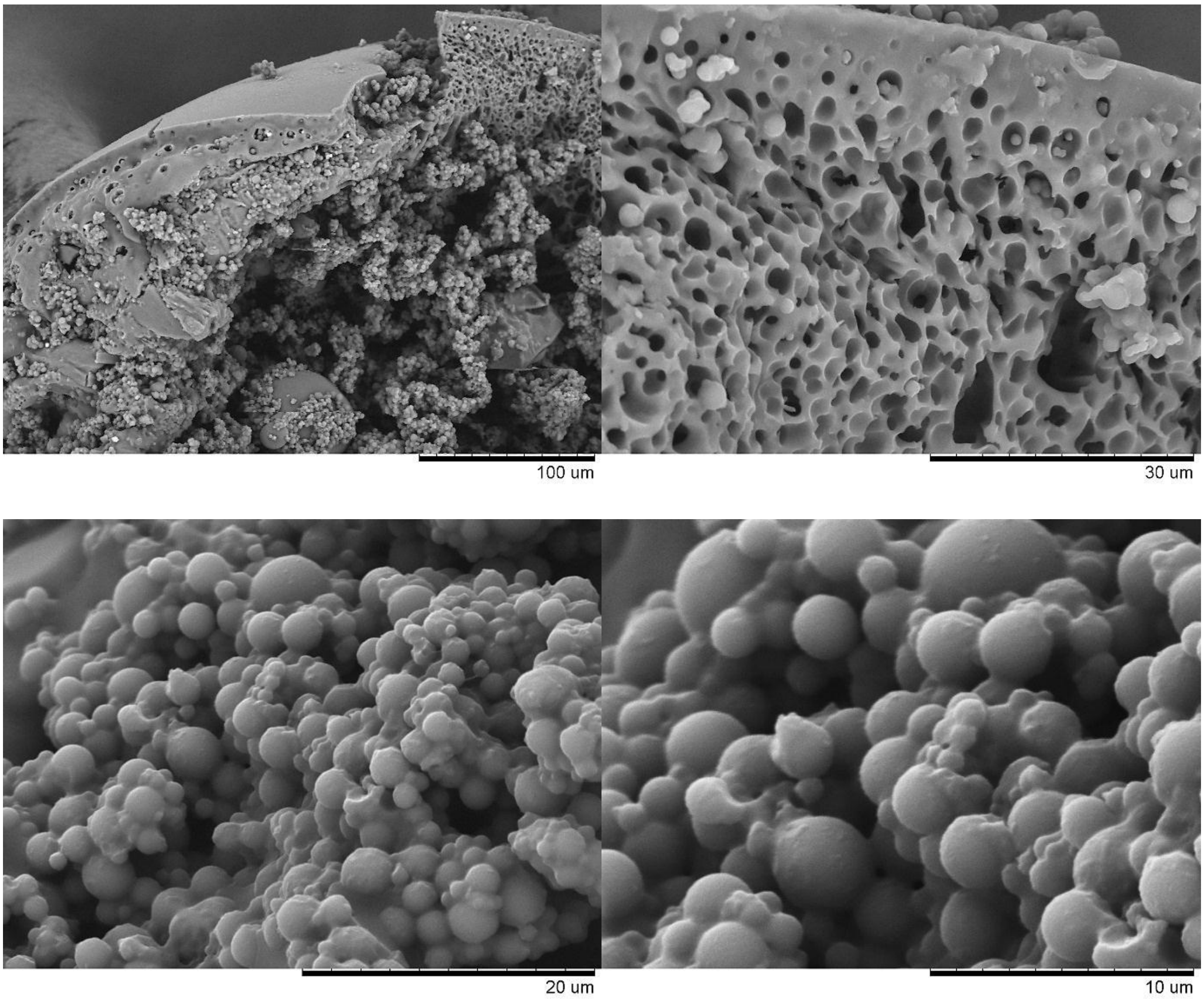

Figure 52 (continued). SEM images of polyurethane particles produced in the presence of 0.2 mol% telechelic catasurf **49a** with an M_n of 15,000 g mol^{-1} (entry 1a).

The large particles were quite fragile, and the SEM micrographs of those which had shattered showed pronounced internal structure. This consisted of a hollow inner-core, a microcellular shell, and a non-porous skin. Such structure presumably results from the formation of a reverse vesicle type aggregate, with polymerisation occurring within the vesicle shell (figure 53). The hollow interior may then expand by the same processes that lead to the growth of pores in microcellular foams. The correlation between the size of the particles and the polymer molecular weight is perhaps explained in that only the low molecular weight polymer has a sufficiently low T_g for the expansion process to occur. The formation of vesicles rather than micelle-type structures is usually rationalised in terms of the critical packing parameter (p) of the amphiphile, which describes the ratio of the cross-sectional areas of the head group and tail. A conically shaped amphiphile leads to micelles, while a cylindrically shaped amphiphile ($p \approx 1$) leads to vesicles.[147]

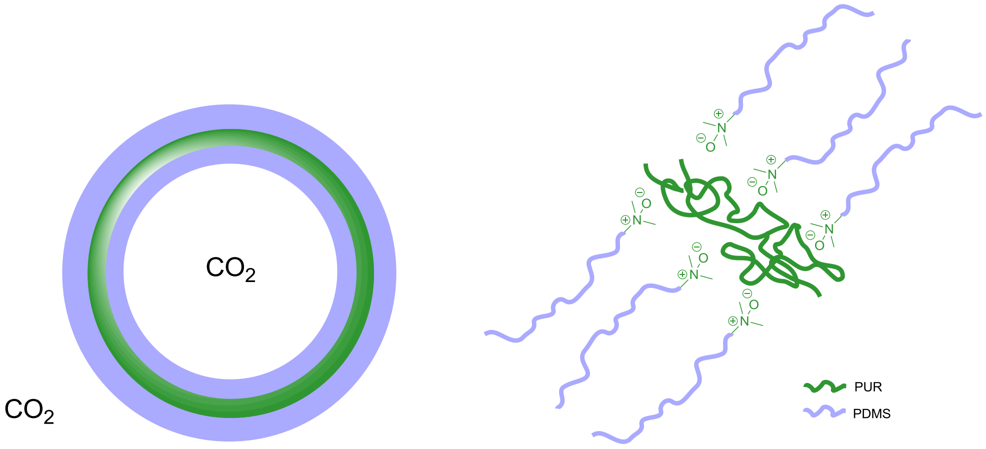

Figure 53. Schematic diagram of reverse vesicles in CO_2. The shell is formed from polyurethane and catasurf end-groups, while PDMS chains extend into the CO_2 phase both inside and outside the vesicle.

At an equivalent concentration of catalyst groups (0.2 mol%), polymerisation in the presence of a second batch of the telechelic catasurf with a slightly lower molecular weight of PDMS (entry 2) or a monofunctional catasurf with an M_n of 10,000 g mol^{-1} (entry 3) gave very similar results, although with the monofunctional catasurf the small particles were less agglomerated.

In contrast, at an equivalent concentration of PDMS, 1 mol% of monofunctional catasurf **49b** with a much lower M_n (1600 g mol^{-1}) did not produce spherical particles (entry 4). The product was obtained as fragments of microcellular foam, which showed a large surface area of non-porous skin (figure 54). These did not appear to be fragments of spherical particles and it seems likely that the foam was formed within the mould of the reactor and was then shattered by the stirrer. Therefore, the PDMS chain of this catasurf is apparently too short to impart effective stabilisation. The yield and molecular weight of the polymer were also relatively low. Microparticles were produced when this catasurf was used in combination with the PDMS macromonomer (entry 5), although the results were no better than those achieved with 1 mol% NMO (table 3, entry 3), suggesting that the short PDMS tail presents no particular advantage for catalysis or for controlling particle morphology.

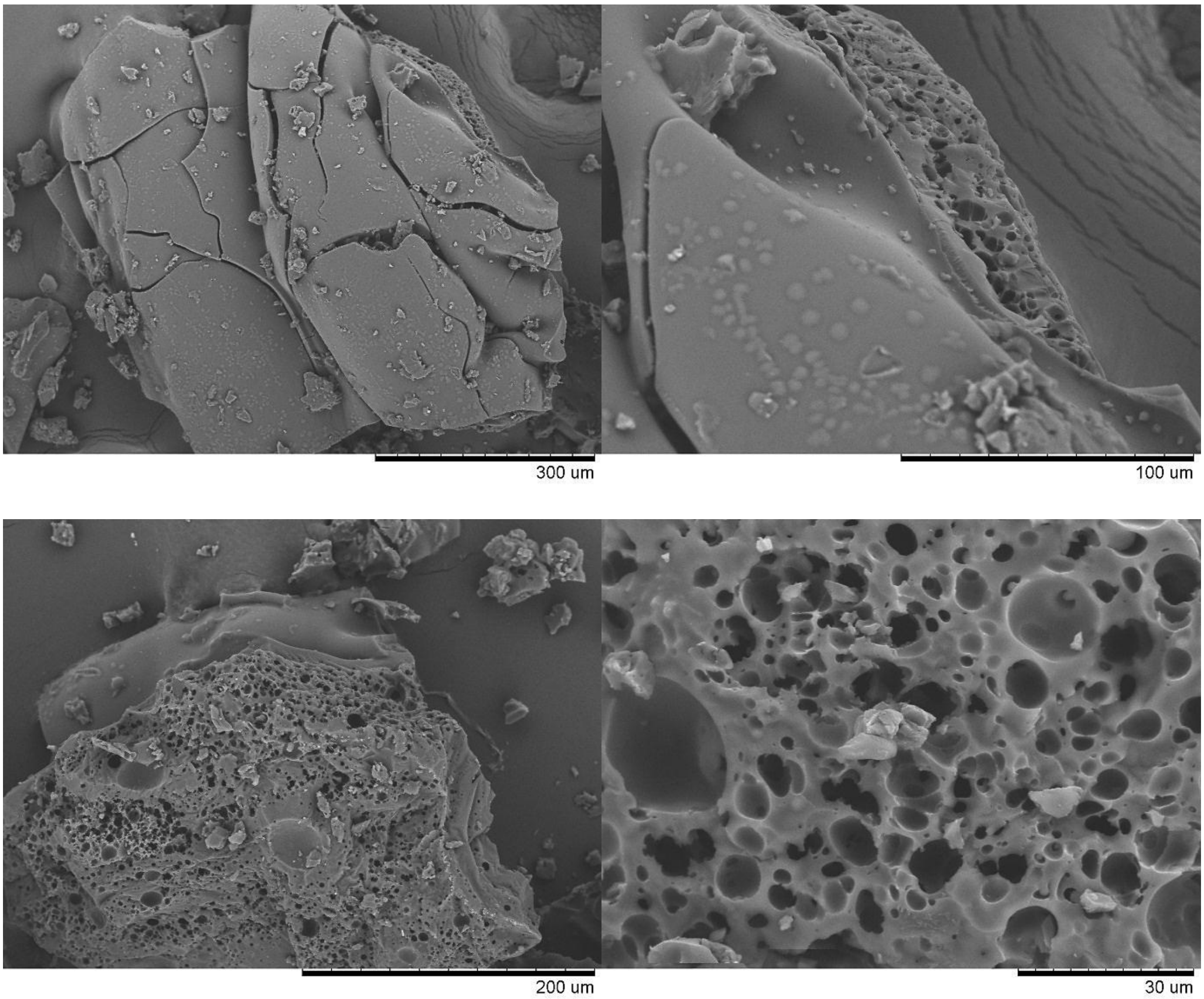

Figure 54. SEM images of polyurethane microcellular foam produced in the presence of monofunctional catasurf **49b** with an M_n of 1600 g mol^{-1} (entry 4).

The amino functionalised PDMS **48a** (amine oxide precursor) was also tested for its ability to act as a catasurf. With 1 mol% of this compound (M_n = 7500 g mol^{-1}), only low molecular weight polymer could be obtained (entry 6). The product was recovered in the form of soft, spheroidal beads with diameters in the range of 1-2 mm (figure 55), which completely coalesced when the product was centrifuged in cyclohexane. A small portion of microparticles, similar to those produced with amine oxide catasurfs, were also present within the sample (figure 56). The inferior results achieved with amine compared to amine oxide functions are presumably due to the reduced interfacial activity of the catasurf as well as its reduced catalytic activity, since more uniform microparticles were obtained even in the absence of catalyst with the PDMS macromonomer (table 3, entry 1). The poor stabilising ability of the catasurf might be a result of more favourable interactions between tertiary amine groups and CO_2.[88a]

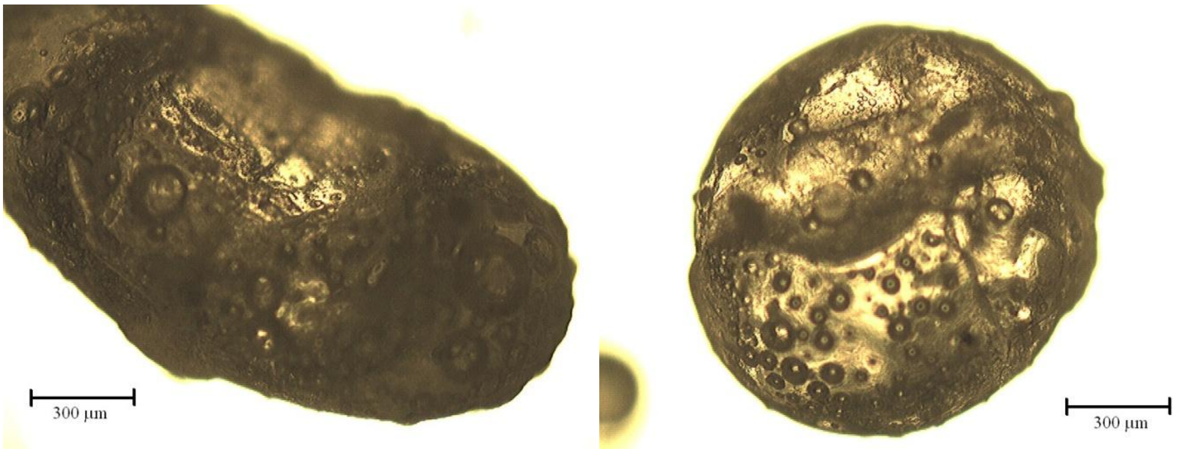

Figure 55. Optical microscope images of the large spheriodal beads produced with 1.0 mol% amino-terminated PDMS catasurf **48a** (entry 6).

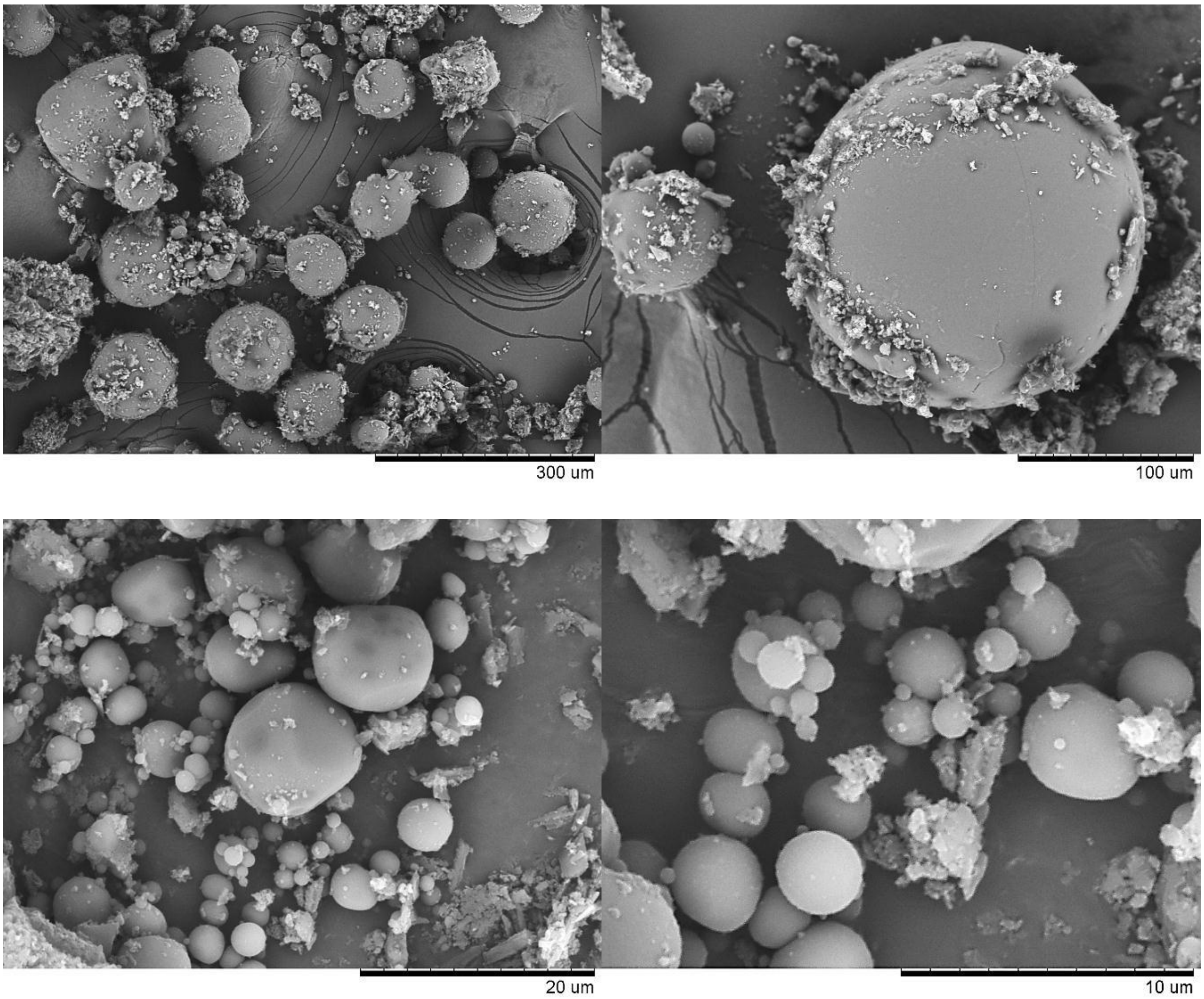

Figure 56. SEM images of polyurethane particles produced in the presence of 1.0 mol% amino-terminated PDMS catasurf **48a** (entry 6).

Much better results were finally achieved using 1 mol% of the amine oxide catasurfs **49a** and **49b** with long PDMS chains (entries 7 and 8). The molecular weights of the polyurethane obtained were relatively high and the molecular weight distributions remained fairly narrow. Unlike for the lower catasurf concentrations, no very large particles were produced. There was however, a significant difference in the form of the products produced with the two different catasurfs. With the telechelic catasurf **49a**, a very low density solid was produced, while with the monofunctional catasurf **49b**, the product was a viscous paste consisting of the solid polyurethane dispersed in the liquid PDMS. The SEM images of the particles produced with **49a** showed many highly agglomerated clusters, as well as some more weakly aggregated clusters (figure 57). The low density of the product could perhaps be explained by large void spaces within the agglomerated structure. In contrast, the particles produced with

49b showed very little aggregation or agglomeration (figure 58). Although the telechelic catasurf might be expected to fold over on itself to form a ‘loop’ protruding from the surface of the polyurethane particles, it could also possibly form a bridge between particles, leading to less effective stabilisation. With the monofunctional catasurf **49b**, the range of particle diameters was large, but the vast majority of the particles were fairly uniform with diameters between 0.8-2 µm.

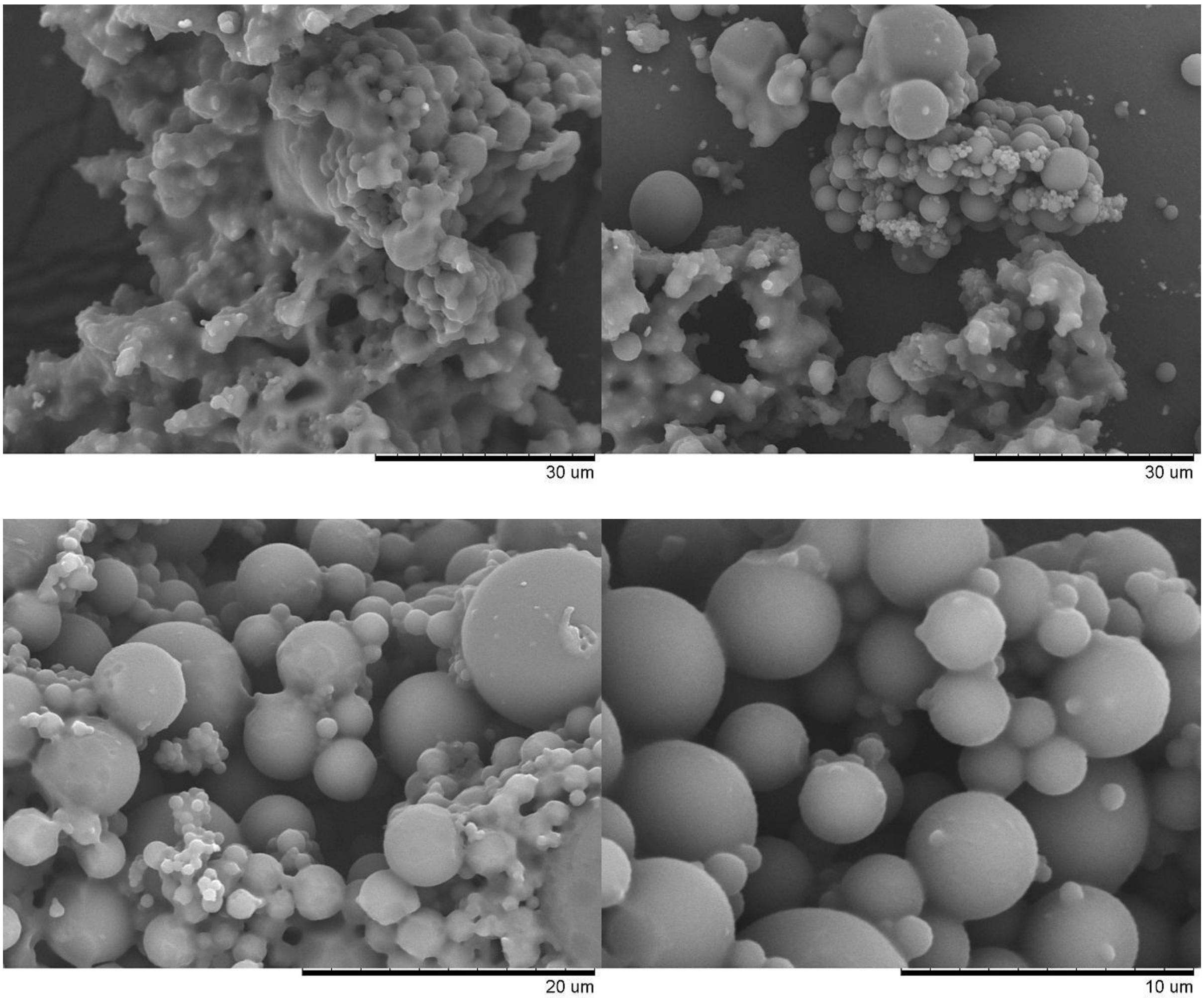

Figure 57. SEM images of polyurethane particles produced in the presence of 1.0 mol% telechelic catasurf **49a** with an M_n of 12,000 g mol^{-1} (entry 7).

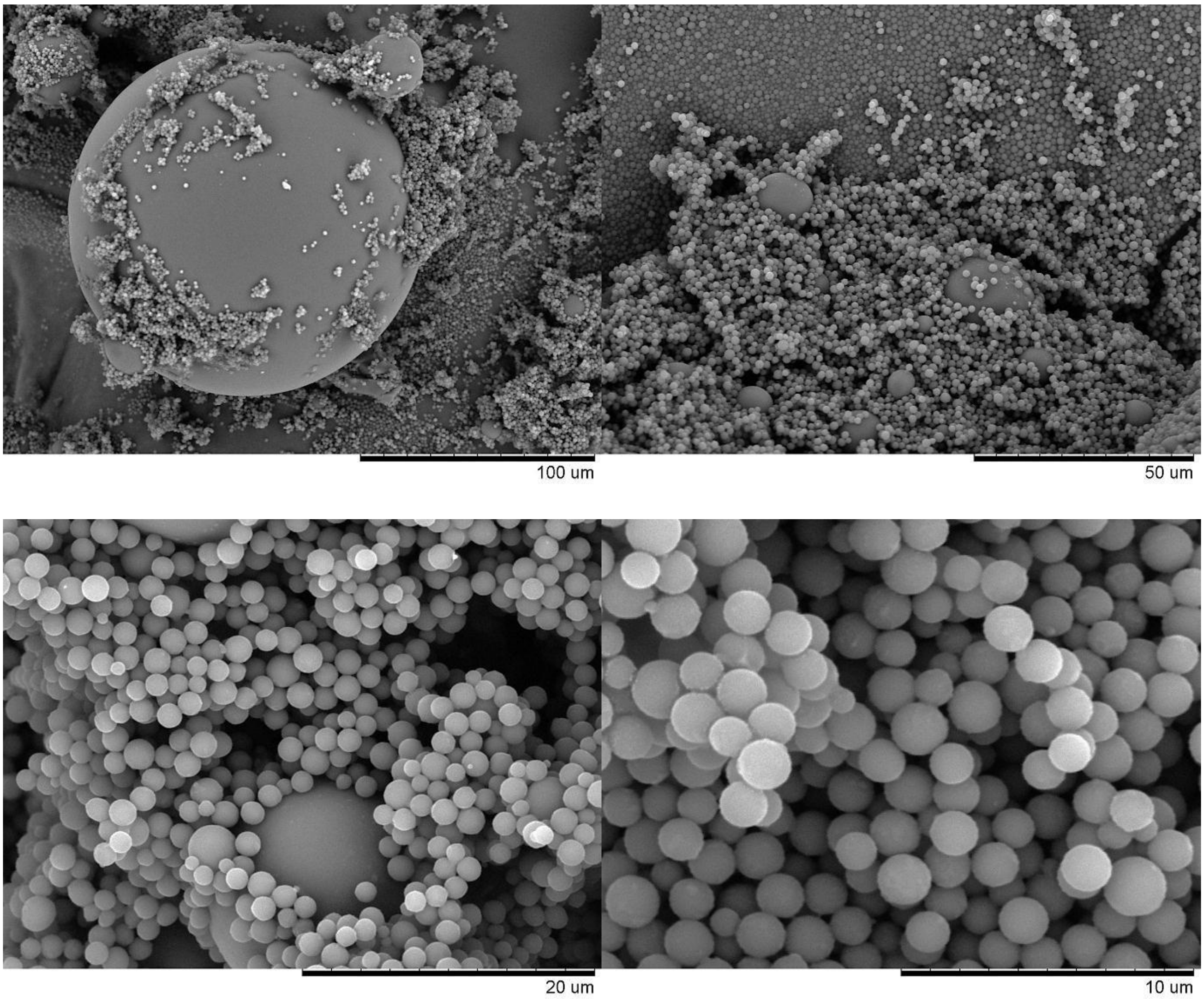

Figure 58. SEM images of polyurethane particles produced in the presence of 1.0 mol% monofunctional catasurf **49b** with an M_n of 10,000 g mol^{-1} (entry 8).

III-4-2-1 Incorporation of PDMS

The level of incorporation of PDMS in the product was once again analysed by NMR using a solvent mixture of DMF and THF (table 4). Some of the samples with a high concentration of PDMS formed turbid solutions (e.g. entries 6 and 8) and the calculated PDMS content is undoubtedly underestimated. The amount of PDMS residue obtained by evaporation of the solvent from the supernatant fluid after dispersion/centrifugation in cyclohexane was also recorded and the residues were analysed by NMR.

It is clear that the monofunctional catasurf **49b** is much more readily removed from the product than the telechelic catasurf **49a**. The presence of two rather than one amine oxide moieties may significantly increase the strength with which the catasurf binds to the polyurethane particles. An alternative explanation could be that a greater amount of the telechelic catasurf is trapped in the sample due to agglomeration of the particles. The short PDMS chain catasurf and the amino functionalised PDMS **48a** appeared to be the most easily removed from the polyurethane, since significant quantities were extracted during venting of the CO_2 from the reactor (entries 4 and 6). In all cases, at least 1.5-2 wt% PDMS remained in the samples after washing and was perhaps trapped within the particles.

Amine oxide groups could not be identified in the NMR spectra of the PDMS residues, and it seems possible that the catalyst group remains imprisoned within the particles and is cleaved from the PDMS chain. In consequence, there appears to be little chance of recycling the catasurf. This contrasted with the amino functionalised PDMS, which was recovered unchanged and could presumably be recycled.

III-4-2-2 Raman Imaging

A Raman image of the crude polyurethane particles produced in the presence of 1 mol% **49a** (entry 7) is shown in figure 59. As for the particles prepared with the PDMS macromonomer, the PDMS appears to be mostly located around the exterior of the particles, although in this case the PDMS appears to be more concentrated into a few zones. These zones might correspond to clusters of smaller particles, but an SEM image of the same area would be necessary to confirm this.

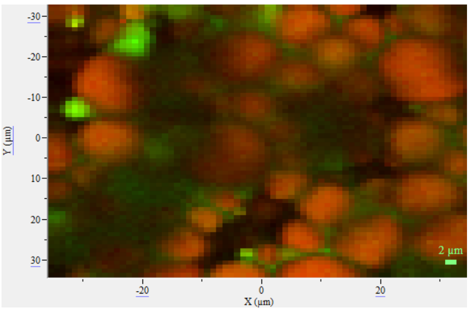

Figure 59. Raman image of the crude polyurethane particles produced in the presence of 1 mol% catasurf **49a** (entry 7). The image maps the intensity of the polyurethane signals at 1270 and 1308 cm^{-1} (red) and the intensity of the PDMS signal at 485 cm^{-1} (green).

Raman imaging of the crude particles produced in the presence of 1 mol% **49b** (entry 8) was not carried out, since the PDMS formed a liquid paste with the particles.

III-4-3 Conclusions of dispersion polymerisation using organocatasurfs

The use of amine oxide terminated PDMS catasurfs in dispersion polymerisation afforded polyurethane particles with specific morphologies. A catasurf with a short PDMS chain (M_n of 1600 g mol^{-1}) did not impart sufficient steric stabilisation to induce the formation of microparticles and a microcellular foam morphology was produced instead. The use of catasurfs with longer PDMS chains (10,000-15,000 g mol^{-1}) led to spherical particles, although the nature of these particles varied according to the concentration of the catasurf. At a loading of 0.2 mol% (~10 wt% of the system), both small particles and large, hollow spheres were produced, while with a loading of 1.0 mol% (31-43 wt% of the system) the latter were absent. The monofunctional catasurf proved to be superior to the telechelic analogue in producing less agglomerated particles, and could also be more easily removed from the product. However, the catasurf did not appear to be recovered intact and therefore it would not be reusable. In addition, the amine oxide catasurfs seemed to be inherently subject to slow decomposition. On the other hand, an amine terminated PDMS catasurf produced low molecular weight polymer with poorly controlled morphology, but it could be recovered unchanged from the product.

III-5 Summary and Outlook

Precipitation polymerisations were only of limited use in evaluating organocatalysts for the formation of polyurethanes in $scCO_2$, but did highlight the problems associated with side-reactions promoted by MTBD and DBU catalysts. Dispersion polymerisation with an isocyanate terminated PDMS macromonomer gave greater insight, and it was found that increasing concentrations of amine oxide catalyst led to higher molecular weight polymer and decreasing particle size, although significant agglomeration was often observed. The principal of combining catalyst and surfactant into the same molecule (a catasurf) has proven to be viable, and the results achieved with catasurfs sometimes offered an improvement over the macromonomer stabilised system. The best results were achieved with 1 mol% of a monofunctional amine oxide terminated catasurf (M_n = 10,000 g mol^{-1}), where polyurethane with a reasonably high molecular weight was produced in the form of well-defined microparticles. However, the results failed to match the narrow particle size dispersity reported for the system combining DBTDL with the PDMS-$(NCO)_2$ macromonomer.[20, 75b]

One drawback with the relatively long PDMS chain catasurfs is that for 1 mol% catalyst loading the PDMS concentration is excessively high. One way of increasing the ratio of catalyst groups to PDMS would be to use a copolymer with catalytic side chains (figure 60), but this would also have an impact on the manner in which the catasurf coordinates to polymer particles and would probably increase the difficulty of separation.

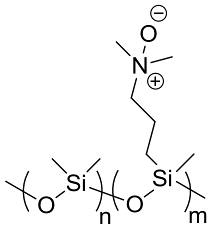

Figure 60. PDMS copolymer with catalytic side chains.

The combination of DBTDL with amine functionalised catasurfs could perhaps provide an interesting alternative system, since both of these components have shown substantial extractability with CO_2. The high catalytic activity of DBTDL might counterbalance the moderate stabilising ability of the amine-based catasurf to encourage the formation of microparticles. A synergistic effect between tin compounds and tertiary amine catalysts has also been reported,[1a, 17] which could present an additional advantage.

III-6 Experimental Section

III-6-1 Materials

2,4-TDI 98% (TCI), anhydrous n-butanol (Sigma-Aldrich), 1,4-butanediol 98% (Fluka), DBTDL 95% (Alfa Aesar), MTBD 98% (Sima-Aldrich), DBU 99% (Alfa Aesar), NMO 97% (Sima-Aldrich), 1,1’-carbonyldiimadazole 97% (Sigma-Aldrich), *N*,*N*-dimethylaminoethanol 99% (Sigma-Aldrich), 4-hydroxy-1-methylpiperidine 98% (Alfa Aesar), *N*,*N*-dimethylallylamine 98% (TCI), Karstedt catalyst (xylene solution, 2.1-2.4% Pt, ABCR) and hydrogen peroxide 35% (Sigma-Aldrich) were used as received. mCPBA ≤77% (Sigma-Aldrich) was washed with phosphate-buffered saline (PBS) 1x solution then distilled water and dried under vacuum before use. PDMS-OH (M_n 4670 g mol^{-1}) was purchased from

Sigma-Aldrich, PDMS-$(OH)_2$ (M_n 3200 g mol^{-1}) was kindly donated by Shin-Etsu, and hydride terminated PDMS 95% (telechelic, 100 cSt; monofunctional, 5-9 cSt & 100 cSt) was purchased from ABCR. Acetonitrile, cyclohexane and toluene were dried over molecular sieves before use. THF was distilled over sodium and benzophenone. Ethanol, methanol and chloroform were used without further purification. CO_2 (N45 quality, <7 ppm H_2O) was supplied by Air Liquide.

III-6-2 Instrumentation

NMR spectra were recorded on a Bruker AC-400 spectrometer (^{1}H 400.2 MHz, ^{13}C 100.6 MHz) using $CDCl_3$ as internal reference. The chemical shifts (δ) and coupling constants (J) are expressed in ppm and Hz respectively.

Size exclusion chromatography (SEC) analyses were performed in DMF at 80 °C with 1g/L LiBr and a flow rate of 0.8 mL/min. The setup consisted of a PL-GPC 50 Plus integrated GPC (Polymer Laboratories, Varian) with a series of three PLgel 5 μm MIXED-D columns. The elution of the filtered samples was monitored using simultaneous UV and refractive index detectors. The elution times were converted to molar mass using a calibration curve based on low dispersity (M_w/M_n) polystyrene standards.

Mass spectrometry measurements were carried out at the Centre d'Etude Structurale et d'Analyse des Molécules Organiques (CESAMO), Bordeaux. MALDI-TOF mass spectra were recorded on an Applied Biosystems Voyager spectrometer with a pulsed nitrogen laser at 337 nm. High resolution mass spectra were recorded on an Applied Biosystems Qstar spectrometer operating in the electrospray ionisation (ESI) mode with a Q-TOF analyser. Elemental analyses were performed on a Flash 2000 instrument (ThermoFisher Scientific) at the CESAMO.

SEM analyses were performed on a Hitachi TM-1000 tabletop microscope. The polymer samples (after three cycles of dispersion/centrifugation in cyclohexane) were mounted on a metal stud with carbon adhesive and sputtered with gold before analysis.

Thermogravimetric analyses were performed on a Q50 TGA (TA instruments) with a heating rate of 5.0°C/min under a nitrogen flow rate of 60 ml/min.

ATR-IR spectra were recorded on a ThermoOptek Nexus 670 FTIR spectrometer with a golden gate accessory (globar as the infrared source, KBr/Ge beamsplitter and MCT

[Mercury Cadmium Telluride] detector). Spectra were recorded in the range 650-4000 cm^{-1}. Single beam spectra recorded with a 4 cm^{-1} resolution were obtained after the Fourier transformation of 200 accumulated interferograms.

Raman spectra were recorded with a Horiba Jobin-Yvon HR800-UV confocal spectrometer with a spectral resolution of 0.7 cm^{-1} in the range 200-3300 cm^{-1}. The laser excitation wavelength was 752 nm and the laser beam power was 3.7 mW. To improve the signal-to-noise ratio, each spectrum was the result of 2 accumulated spectra for typical times of 60 seconds.

Raman imaging was carried out on a Horiba Jobin-Yvon XploRA confocal spectrometer equipped with a grating of 600 lines/mm giving access to the spectral range 200-2400 cm^{-1} with a spectral resolution of 9 cm^{-1}. A microscope objective (X50) was used to focus the laser beam of a laser diode on the sample and to collect the Raman scattered light. The confocal hole was set at 100 µm so that the extension of the sampling volume was estimated to be a cylinder of roughly 5 µm diameter and 5 µm height. Raman spectra were collected point by point with a spatial resolution of 2 µm and an acquisition time of 0.2 seconds for each spectrum. The laser excitation wavelength was 784.5 nm and the laser beam power was approximately 10 mW at the sample.

III-6-3 High pressure reactor

The high pressure reactor (Top Industrie) was a stainless steel (1.4571) autoclave with a volume of 118 mL, fitted with a magnetically-coupled overhead stirrer and a digital pressure gauge (ASCO). The temperature was controlled via an electrical heating jacket with a regulating thermocouple in contact with the body of the vessel. The internal temperature was monitored with a thermocouple placed inside a thermowell which descended into the centre of the reactor. The seal between the head and body of the reactor was ensured by a Teflon O-ring. Liquid CO_2 was cooled with a minichiller then compressed to the desired pressure with a Dosapro Miltonroy pump. The liquid reactants were added from a 15 mL stainless steel addition cell, connected to the reactor via a stainless steel capillary tube. The addition cell was fitted with a low pressure CO_2 inlet to allow the addition of reactants under a flow of CO_2.

III-6-4 Experimental Procedures

III-6-4-1 Synthesis of PDMS-$(NCO)_2$

A solution of PDMS-$(OH)_2$ (3.8 mL, 1.15 mmol) in 120 mL cyclohexane was added dropwise over 5 hours to a solution of 2,4-TDI (2.0 mL, 13.8 mmol) in 10 mL cyclohexane at 60°C under a nitrogen atmosphere. After complete addition, the mixture was stirred for a further 2 hours at 60°C. The solvent was then evaporated and the crude product was washed with 4 x 10 mL acetonitrile. The product was dried under vacuum to give a clear, colourless oil (3.75 g, 92% yield), which was stored under nitrogen.

^{1}H NMR ($CDCl_3$, 400 MHz): δ = 7.21 (br s, 1H), 7.07 (d, J = 8 Hz, 1H), 6.99 (dd, J = 8 Hz, J = 2 Hz, 1H), 6.63 (br s, 1H), 4.21-4.10 (m, 4H) 3.40-3.26 (m, 4H), 2.25 (s, 6H), 1.62-1.44 (m, 4H), 1.37-1.25 (m, 4H), 0.95-0.85 (m, 6H), 0.57-0.47 (m, 4H), 0.07 (s), 0.04 ppm (s).

III-6-4-2 Synthesis of Organocatasurfs

III-6-4-2-1 Typical Hydrosilylation Procedure

N,*N*-dimethylallylamine (0.91 mL, 7.68 mmol) was added to a solution of monohydride terminated PDMS (20 mL, ~3.84 mmol) in 20 mL toluene under a nitrogen atmosphere. Karstedt's catalyst solution (37 µl, ~3.84 x 10^{-3} mmol) was then added and the mixture stirred for 3.5 hours. The product was precipitated into 50 mL methanol then dried under vacuum (pale yellow oil, 18.13 g, 93% yield).

^{1}H NMR ($CDCl_3$, 400 MHz): δ = 2.27-2.21 (m, 2H), 2.21 (s, 6H), 1.54-1.44 (m, 2H), 1.37-1.25 (m, 4H), 0.91-0.85 (m, 3H), 0.57-0.49 (m, 4H), 0.07 (s), 0.05 (s), 0.04 ppm (s).

^{13}C NMR ($CDCl_3$, 100 MHz): δ = 63.4, 45.6, 26.5, 25.6, 21.6, 18.1, 15.9, 13.9, 1.3, 1.2, 0.3, 0.3 ppm.

III-6-4-2-2 Typical Oxidation Procedure with mCPBA

A solution of mCPBA (0.786 g, 4.55 mmol) in 15 mL chloroform was added over 15 minutes to an ice-cooled solution of telechelic amino terminated PDMS (9.11 g, ~1.52 mmol) in 9 mL chloroform under a nitrogen atmosphere. The solution was stirred for a further 3 hours, during which the temperature was allowed to warm up to room temperature. Excess mCPBA was then destroyed by stirring the mixture with activated carbon (0.75 g) for 1 hour. The mixture was filtered through celite then the acid by-product was removed by passage through a short column of basic alumina. Fine particles of alumina were removed by filtration through a 0.4 μm PTFE filter, then the solvent was evaporated and the product was dried under vacuum (colourless oil, 7.95 g, 87% yield).

^{1}H NMR ($CDCl_3$, 400 MHz): δ = 3.27-3.21 (m, 4H), 3.17 (s, 12H), 1.96-1.86 (m, 4H), 0.57-0.50 (m, 4H), 0.12 (s), 0.07 ppm (s).

^{13}C NMR ($CDCl_3$, 100 MHz): δ = 74.7, 58.7, 18.1, 15.0, 1.3, 1.2, 0.3 ppm.

III-6-4-2-3 Typical Oxidation Procedure with H_2O_2

5 mL H_2O_2 (35%) was added to a solution of mono-amino terminated PDMS (5.0 g, ~0.628 mmol) in 10 mL chloroform. CO_2 was bubbled through the mixture for 15 minutes then the reaction was left stirring under an atmosphere of CO_2 for 16 hours. The solvent was evaporated and the residue was dissolved in 100 mL 1:1 methanol:pentane. The methanol layer was discarded and the pentane layer was washed with a further 2 x 25 mL methanol. The solvent was then evaporated and the product was dried under vacuum (colourless oil, 4.92 g, 98% yield).

^{1}H NMR ($CDCl_3$, 400 MHz): δ = 3.27-3.21 (m, 2H), 3.17 (s, 6H), 1.96-1.86 (m, 2H), 1.37-1.25 (m, 4H), 0.91-0.85 (m, 3H), 0.57-0.50 (m, 4H), 0.12 (s), 0.07 (s), 0.04 ppm (s).

^{13}C NMR ($CDCl_3$, 100 MHz): δ = 74.7, 58.7, 26.5, 25.6, 18.1, 18.1, 15.0, 13.9, 1.3, 1.3, 1.2, 0.3, 0.3 ppm.

III-6-4-3 Precipitation Polymerisations

The reactor was heated to 60°C and purged with three cycles of vacuum/CO_2, then flushed with supercritical CO_2. 1,4-butanediol (0.89 mL, 10 mmol) and the catalyst (0.20 mmol) were placed in the addition cell and injected into the reactor with CO_2 at the bottle pressure (~5.5 MPa). The pressure was then increased to 20 MPa and the stirrer set in motion (500 rpm). After 30 minutes, 2,4-TDI (1.43 mL, 10 mmol) was injected from the addition cell by differential pressure and the overall pressure increased to 26 MPa. After 24 hours reaction time, the vessel was cooled with a flow of compressed air. The CO_2 was vented over several hours via a cannula plunged into a bath of ethanol. 30 mL ethanol was then added to the reactor and the mixture left to stir for ~16 hours. The ethanol/product mixture was removed from the vessel and the remaining product was recovered by dissolution in THF. The solvent was then evaporated and the product dried under vacuum.

III-6-4-4 Dispersion Polymerisations with Macromonomer

1,4-butanediol and the catalyst (0-1.0 mmol) were first dissolved in CO_2 at 60°C and 20 MPa pressure as above. The PDMS macromonomer (0.29 g, 10 wt% of the system [monomers + macromonomer]) was then injected by differential pressure and the pressure in the reactor was increased to 30 MPa. After 30 minutes, 2,4-TDI was injected in the same manner and the pressure finally increased up to 40 MPa. After 7 hours, the reactor was cooled, the CO_2 was vented, and the solid product was collected directly.

A 0.5 g portion of the product was subjected to three cycles of dispersion/centrifugation in 40 mL cyclohexane. The solvent was evaporated from the supernatant fluid after filtration through a 0.4 µm PTFE filter, and the residue was analysed by NMR spectroscopy.

III-6-4-5 Dispersion Polymerisations with Catasurfs

A similar procedure was followed as above, except that 1,4-butanediol and the catasurf (0.02-0.2 mmol) were first dissolved in CO_2 at 60°C and 30 MPa, before addition of the diisocyanate after 30 minutes and an increase in pressure to 40 MPa. After 7 hours, the reactor was cooled, the CO_2 was vented, and the solid product was collected directly.

A portion of the product was washed with cyclohexane as above.

Conclusions Générales

L'ambition à l'origine de cette thèse était d'élaborer des matériaux polymères par des procédés respectueux de l'environnement et de la santé humaine. A cet effet, la synthèse de polyuréthanes de morphologie spécifique a été réalisée en remplaçant les solvants organiques par le dioxyde de carbone supercritique. Ces travaux ont débuté par un criblage d'organo-catalyseurs qui pourraient remplacer les catalyseurs à base d'étain dont la toxicité est une préoccupation actuelle.

Afin de réaliser cette étude, la réaction entre le toluène-2,4-diisocyanate et le *n*-butanol dans le $scCO_2$ a été choisie comme réaction modèle. Son suivi *in situ* par FTIR a permis l'identification des organo-catalyseurs les plus efficaces dans ce milieu. Les guanidines et amidines bicycliques (MTBD et DBU) se sont montrées relativement actives bien qu'une perte de performance ait été mise en évidence. Cette baisse d'activité s'explique par la présence d'une interaction du catalyseur avec l'alcool et le CO_2. De plus, ces catalyseurs ont deux inconvénients : d'une part, la présence de CO_2 entraine une sensibilité de ces catalyseurs à l'humidité. D'autre part, ces composés favorisent des réactions secondaires de l'isocyanate. Le criblage montre aussi que la NMO (catalyseur de type amine-oxyde) a une activité catalytique appréciable. Toutefois, si la cinétique initiale de la réaction est comparable à celle du catalyseur de référence à base d'étain (DBTDL), son rendement final est moindre. La NMO est relativement peu sensible à la présence d'eau et ne semble pas entrainer de réaction secondaire.

L'examen des spectres FTIR a permis de mettre en évidence que la sélectivité entre les groupements isocyanates est modulée en fonction des catalyseurs employés. Le DBTDL et dans une moindre mesure la NMO, favorisent la réaction sur l'isocyanate en position para, alors que le MTBD et le DBU atténue la différence entre les deux vitesses de réaction.

Cette sélection d'organo-catalyseurs a ensuite été utilisée dans des polymérisations par polyaddition du toluène-2,4-diisocyanate avec le 1,4-butanediol dans le $scCO_2$. Une étude préliminaire de polymérisation par précipitation a mis en évidence des problèmes de réticulation dus aux réactions secondaires observées avec les catalyseurs MTBD et DBU. Afin d'obtenir des particules de géométrie contrôlée, un macromonomère de PDMS terminé par un groupement isocyanate a été choisi comme stabilisant. Ces polymérisations par dispersion ont conduit à l'obtention de particules sphériques de polyuréthanes. Dans ces réactions, l'augmentation de la concentration du catalyseur NMO donne lieu à des polymères de plus grandes masses molaires et des particules de plus petits diamètres.

Enfin, pour obtenir un matériau sans résidu, le catalyseur et le surfactant ont été combinés au sein d'un même composé « un catasurf ». Cette approche originale a permis la production de particules relativement uniformes. Le catasurf monofonctionnel conduit à un meilleur contrôle de la géométrie des particules par rapport au catasurf téléchélique. Le catasurf monofonctionnel a pu être éliminé des particules, ce qui pourrait élargir le champ d'application de ces matériaux.

Dans l'avenir, il serait intéressant d'optimiser les catasurfs dans le but de contrôler les caractéristiques des matériaux obtenus : la masse molaire du PDMS ainsi que la position des groupements catalytiques (en ramification plutôt qu'en bout de chaîne) pourraient modifier à la fois la taille des particules et les masses molaires des polyuréthanes.

D'autre part, les catasurfs développés ne sont pas, à ce jour, réutilisables : un changement de la nature même des groupements catalytiques pourrait permettre de les rendre plus robuste et donc potentiellement recyclable.

De plus, dans l'optique des synthèses de polyuréthanes plus respectueuses de l'environnement, notre équipe s'intéresse déjà à l'utilisation de monomères bio-sourcés. Une transposition au $scCO_2$ des résultats obtenus serait alors une étape supplémentaire pour un procédé « vert ».

Enfin, il faut souligner que les perspectives d'utilisation du dioxyde de carbone pour la synthèse de polyuréthanes restent nombreuses. L'incorporation du CO_2 lui-même au sein du polymère est probablement le meilleur moyen d'augmenter la valeur ajoutée d'un procédé dans le CO_2. En effet, des réactions où le CO_2 est un réactif existent déjà : la copolymérisation des époxydes avec le CO_2 pour former des diols de type poly(éther carbonate) est depuis peu employée par l'industrie des polyuréthanes.[11] Le dioxyde de carbone est aussi vu comme un potentiel remplaçant du phosgène (composé hautement toxique et corrosif utilisé pour la production des isocyanates).[148] Ainsi, la mise en réaction du CO_2 pourrait avoir une portée environnementale supplémentaire par la diminution des émissions des gaz à effet de serre et par le remplacement des composés carbonés issus de la pétrochimie.

Appendix

Summary

A-1 Synthesis of model compounds 156

A-2 Calculation of PDMS content in polyurethane particles by NMR 161

A-3 Calculation of PDMS content in polyurethane particles by elemental analysis 161

A-4 Calculation of the difference in PDMS content after dispersion/centrifugation in cyclohexane 162

A-1 Synthesis of model compounds

Materials

2,4-TDI 98% (TCI), anhydrous *n*-butanol (Sigma-Aldrich), DBTDL 95% (Alfa Aesar), MTBD 98% (Sima-Aldrich), Co(II) 2-ethylhexanoate solution 65 wt% in mineral spirits (Sigma-Aldrich), 2-methyl-5-nitrophenyl isocyanate 97% (Alfa Aesar) and 4-methyl-3-nitrophenyl isocyanate 98% (Sigma-Aldrich) were used as received. Toluene was dried over molecular sieves before use. THF was distilled over sodium and benzophenone. Methanol and ethyl acetate were used without further purification. The reactions were performed under a dry nitrogen atmosphere unless otherwise stated.

Instrumentation

NMR spectra were recorded on a Bruker AC-400 spectrometer (^{1}H 400.2 MHz, ^{13}C 100.6 MHz) using $CDCl_3$ or DMSO-d_6 as internal reference. The chemical shifts (δ) and coupling constants (J) are expressed in ppm and Hz respectively.

Experimental Procedures

Dibutyl 4-methyl-1,3-phenylenedicarbamate (20)

2,4-TDI (0.50 mL, 3.50 mmol) was added dropwise over 30 minutes to 5 mL *n*-butanol in a water bath at ambient temperature. The mixture was then stirred for a further 2 hours. The excess butanol was evaporated and the product was recrystallised from ethanol (large colourless crystals, 0.709 g, 63 % yield).

^{1}H NMR (DMSO, 400 MHz): δ = 9.48 (s, 1H), 8.74 (s, 1H), 7.49 (d, J = 2 Hz, 1H), 7.15 (dd, J = 8 Hz, J = 2 Hz, 1H), 7.05 (d, J = 8 Hz, 1H), 4.08-4.02 (m, 4H), 2.11 (s, 3H), 1.63-1.55 (m, 4H), 1.43-1.32 (m, 4H), 0.91 ppm (t, J = 7 Hz, 6H).

Butyl 2-methyl-5-nitrophenylcarbamate

0.34 mL *n*-butanol (3.70 mmol) and 10.0 µL DBTDL (1.68×10^{-2} mmol) were added to a solution of 2-methyl-5-nitrophenyl isocyanate (0.60 g, 3.37 mmol) in 6 mL THF. The mixture was stirred for 1.5 hours at room temperature. The solvent was then evaporated, the residue was taken up in ethyl acetate, filtered though a plug of celite and the product crystallised by vapour diffusion of pentane into the solution (white needles, 0.65 g, 77% yield).

^{1}H NMR (DMSO, 400 MHz): δ = 9.21 (s, 1H), 8.40 (d, J = 2 Hz, 1H), 7.88 (dd, J = 8 Hz, J = 2 Hz, 1H), 7.46 (d, J = 8 Hz, 1H), 4.12 (t, J = 7 Hz, 2H), 2.34 (s, 3H), 1.67-1.59 (m, 2H), 1.45-1.34 (m, 2H), 0.92 ppm (t, J = 7 Hz, 3H).

^{13}C NMR (DMSO, 100 MHz): δ = 154.3, 145.9, 138.4, 137.7, 131.3, 118.6, 117.3, 64.4, 30.5, 18.6, 18.1, 13.6 ppm.

Butyl 4-methyl-3-nitrophenylcarbamate

A similar procedure was followed as for butyl 2-methyl-5-nitrophenylcarbamate, starting from 4-methyl-3-nitrophenyl isocyanate. The product was obtained as yellow plates (75% yield).

^{1}H NMR (DMSO, 400 MHz): δ = 10.00 (s, 1H), 8.20 (d, J = 2 Hz, 1H), 7.61 (dd, J = 8 Hz, J = 2 Hz, 1H), 7.39 (d, J = 8 Hz, 1H), 4.10 (t, J = 7 Hz, 2H), 2.44 (s, 3H), 1.65-1.56 (m, 2H), 1.43-1.32 (m, 2H), 0.91 ppm (t, J = 7 Hz, 3H).

^{13}C NMR (DMSO, 100 MHz): δ = 153.6, 148.7, 138.3, 133.1, 126.1, 122.7, 113.1, 64.3, 30.5, 19.0, 18.6, 13.5 ppm.

Butyl 5-amino-2-methylphenylcarbamate (26)

Butyl 2-methyl-5-nitrophenylcarbamate (0.40 g, 1.59 mmol) and Pd/C (10 wt%, 0.155 g, 7.93 x 10^{-2} mmol) in 16 mL 2:1 vol/vol ethyl acetate/methanol were cycled though vacuum/nitrogen three times then vacuum/hydrogen twice. The mixture was then left stirring for 24 hours under a hydrogen atmosphere provided from a rubber balloon. The catalyst was removed by filtration through celite then the solvent was evaporated and the product was dried under vacuum (pinkish white solid, 0.350 g, 99% yield).

^{1}H NMR (DMSO, 400 MHz): δ = 8.47 (s, 1H), 6.78 (d, J = 8 Hz, 1H), 6.60 (d, J = 2 Hz, 1H), 6.28 (dd, J = 8 Hz, J = 2 Hz, 1H), 4.82 (s, 2H), 4.03 (t, J = 7 Hz, 2H), 2.01 (s, 3H), 1.63-1.53 (m, 2H), 1.42-1.31 (m, 2H), 0.91 ppm (t, J = 7 Hz, 3H).

^{13}C NMR (DMSO, 100 MHz): δ = 154.4, 146.8, 136.6, 130.3, 118.4, 111.0, 110.6, 63.6, 30.7, 18.6, 16.8, 13.6 ppm.

Butyl 3-amino-4-methylphenylcarbamate (27)

A similar procedure was followed as for **26**, starting from butyl 4-methyl-3-nitrophenylcarbamate. The product was obtained as a greenish viscous oil (99% yield).

^{1}H NMR ($CDCl_3$, 400 MHz): δ = 6.99-6.89 (m, 2H), 6.53 (dd, *J* = 8 Hz, *J* = 2 Hz, 1H), 6.46 (br s, 1H), 4.14 (t, *J* = 7 Hz, 2H), 3.62 (br s, 2H), 2.11 (s, 3H), 1.69-1.59 (m, 2H), 1.47-1.36 (m, 2H), 0.95 ppm (t, *J* = 7 Hz, 3H).

Urea 28

A solution of *n*-butanol (0.32 mL, 3.50 mmol) in 5 mL THF was added dropwise over 25 minutes to a solution of 2,4-TDI (0.50 mL, 3.50 mmol) and DBTDL (10 µL, 1.75 x 10^{-2} mmol) in 2 mL THF. The mixture was stirred for 1 hour at room temperature before the addition of 63 µL H_2O (3.50 mmol). The mixture was then stirred for a further 17 hours during which a solid precipitated. The mixture was diluted with heptane then filtered. The product was washed from the filter with DCM/MeOH leaving behind insoluble impurities. The solvent was then evaporated and the product recrystallised from toluene/MeOH (white agglomerates, 0.424 g, 51% yield).

^{1}H NMR (DMSO, 400 MHz): δ = 9.45 (s, 2H), 8.16 (s, 2H), 7.93 (d, *J* = 2 Hz, 2H), 7.10-7.02 (m, 4H), 4.05 (t, *J* = 7 Hz, 4H), 2.19 (s, 6H), 1.63-1.55 (m, 4H), 1.43-1.32 (m, 4H), 0.91 ppm (t, *J* = 7 Hz, 6H).

^{13}C NMR (DMSO, 100 MHz): δ = 153.6, 152.6, 137.5, 137.3, 130.0, 121.9, 113.2, 112.2, 63.6, 30.6, 18.6, 17.4, 13.6 ppm.

Urea 29

A solution of H_2O (32 µL, 1.75 mmol) in 5 mL THF was added dropwise over 25 minutes to a solution of 2,4-TDI (0.50 mL, 3.50 mmol) and DBTDL (10 µL, 1.75 x 10^{-2} mmol) in 2 mL THF. The mixture was stirred for 1 hour at room temperature before the addition of *n*-butanol (0.64 mL, 7.01 mmol). The mixture was then stirred for a further 15 hours at room temperature before precipitation into 100 mL heptane. The crude product was purified by column chromatography (DCM/ 2% MeOH) but co-eluted with compound **30** (white powder, 0.448 g, 54% yield [**29** + **30**]).

^{1}H NMR (DMSO, 400 MHz): δ = 8.73 (s, 2H), 8.50 (s, 2H), 7.50 (d, J = 2 Hz, 2H), 7.13 (dd, J = 8 Hz, J = 2 Hz, 2H), 7.05 (d, J = 8 Hz, 2H), 4.06 (t, J = 7 Hz, 4H), 2.12 (s, 6H), 1.65-1.56 (m, 4H), 1.44-1.33 (m, 4H), 0.92 ppm (t, J = 7 Hz, 6H).

^{13}C NMR (DMSO, 100 MHz): δ = 154.4, 152.4, 137.7, 136.6, 130.2, 124.6, 114.7, 114.4, 63.8, 30.7, 18.6, 17.1, 13.6 ppm.

Urea 30

A solution of *n*-butanol (49 µL, 0.531 mmol) in 1.0 mL THF was added dropwise over 15 minutes to a solution of 2,4-TDI (76 µL, 0.531 mmol) and DBTDL (3.2 µL, 5.31 x 10^{-3} mmol) in 0.5 mL THF. The mixture was stirred for 1 hour at room temperature before the addition of a solution of **26** (0.118 g, 0.531 mmol) in 1.0 mL THF. The mixture was then stirred for a further 17 hours at room temperature before precipitation into 30 mL heptane (white powder, 0.200 g, 80% yield).

^{1}H NMR (DMSO, 400 MHz): δ = 9.43 (s, 1H), 8.94 (s, 1H), 8.74 (s, 1H), 8.00 (d, J = 2 Hz, 1H), 7.77 (s, 1H), 7.52 (d, J = 2 Hz, 1H), 7.19 (dd, J = 8 Hz, J = 2 Hz, 1H), 7.10-7.01 (m, 3H), 4.06 (m, 4H), 2.16 (s, 3H), 2.13 (s, 3H), 1.65-1.55 (m, 4H), 1.44-1.33 (m, 4H), 0.92 (t, J = 7 Hz, 3H), 0.92 ppm (t, J = 7 Hz, 3H).

^{13}C NMR (DMSO, 100 MHz): δ = 154.4, 153.6, 152.4, 137.9, 137.5, 137.3, 136.6, 130.3, 130.0, 124.3, 121.3, 114.3, 114.0, 112.9, 111.5, 63.8, 63.6, 30.7, 30.6, 18.6, 17.2, 17.1, 13.6, 13.6 ppm.

Allophanates 31 & 32

n-butanol (0.67 mL, 7.36 mmol) was added dropwise to 2,4-TDI (0.70 mL, 4.90 mmol) in a water bath at ambient temperature. 13.0 µL Co(II) 2-ethylhexanoate solution (65 wt% in mineral spirits, 2.45 x 10^{-2} mmol) was then added and the mixture was stirred for 22 hours in an oil bath at 90°C. The crude reaction mixture was separated by column chromatography (5:1 heptane/ethyl acetate). Compound **31** was the major allophanate isomer obtained and was recrystallised by vapour diffusion of pentane into an ethyl acetate solution (white raspberry-like crystals, 0.334 g, 24% yield). The structure was confirmed by ROESY NMR spectroscopy (CD_3CN).

^{1}H NMR ($CDCl_3$, 400 MHz): δ = 10.86 (s, 1H), 7.91 (d, J = 2 Hz, 1H), 7.36 (br s, 1H), 7.29 (br s, 1H), 7.24-7.10 (m, 3H), 6.68 (br s, 1H), 6.51 (br s, 1H), 4.23-4.06 (m, 6H), 2.33 (s, 3H), 2.13 (s, 3H), 1.68-1.57 (m, 4H), 1.55-1.46 (m, 2H), 1.45-1.32 (m, 4H), 1.23-1.13 (m, 2H), 0.97-0.89 (m, 6H), 0.82 ppm (t, *J* = 7 Hz, 3H).

^{13}C NMR ($CDCl_3$, 100 MHz): δ = 156.1, 153.9, 153.7, 151.1, 136.8, 136.7, 136.7, 136.6, 130.8, 130.8, 122.5, 118.9, 114.5, 111.5, 67.4, 65.2, 65.1, 31.1, 31.1, 30.5, 19.2, 18.9, 17.6, 16.9, 13.8, 13.6 ppm.

Compound **32** was isolated after further column chromatography of mixed fractions (DCM/ 1% MeOH) and was recrystallised by vapour diffusion of pentane into an ethyl acetate solution (white raspberry-like crystals, 0.025 g, 1.8% yield). The structure was confirmed by ROESY NMR spectroscopy ($CDCl_3$).

^{1}H NMR ($CDCl_3$, 400 MHz): δ = 10.83 (s, 1H), 7.90 (br s, 1H) , 7.37 (dd, *J* = 8 Hz, *J* = 2 Hz, 1H), 7.27-7.21 (m, 2H), 7.18-7.13 (m, 1H), 7.08 (d, *J* = 8 Hz, 1H), 6.65 (br s, 1H), 6.35 (br s, 1H), 4.22-4.04 (m, 6H), 2.20 (s, 3H), 2.12 (s, 3H), 1.70-1.59 (m, 4H), 1.55-1.46 (m, 2H), 1.46-1.34 (m, 4H), 1.24-1.13 (m, 2H), 0.98-0.91 (m, 6H), 0.82 ppm (t, *J* = 7 Hz, 3H).

^{13}C NMR ($CDCl_3$, 100 MHz): δ = 155.9, 154.0, 153.7, 151.1, 136.8, 136.6, 136.6, 136.3, 130.9, 130.8, 130.8, 118.9, 116.0, 113.1, 67.3, 65.4, 65.2, 31.1, 31.1, 30.5, 19.2, 19.2, 18.9, 17.2, 16.9, 13.9, 13.8, 13.6 ppm.

Isocyanurate 33

A solution of MTBD (5.0 µL, 3.50 x 10^{-2} mmol) in 2.5 mL toluene was added in one portion with vigorous stirring to a solution of 2,4-TDI (0.50 mL, 3.50 mmol) in 2.5 mL toluene. After 60 seconds, *n*-butanol (0.64 mL, 7.01 mmol) was added and the mixture was stirred for a further 2 hours at room temperature. The mixture was then precipitated into 50 mL heptane. The crude product was purified by column chromatography (DCM/ ethyl acetate) (white powder, 0.190 g, 22% yield).

^{1}H NMR (DMSO, 400 MHz): δ = 8.91 (s, 3H), 7.54 (d, *J* = 2 Hz, 3H), 7.26 (d, *J* = 8 Hz, 3H), 7.09 (dd, *J* = 8 Hz, *J* = 2 Hz, 3H), 4.07 (t, *J* = 7 Hz, 6H), 2.24 (s, 9H), 1.64-1.55 (m, 6H), 1.43-1.32 (m, 6H), 0.91 ppm (t, *J* = 7 Hz, 9H).

A-2 Calculation of PDMS content in polyurethane particles by NMR

The weight fraction of PDMS in the polyurethane particles was calculated from the ^{1}H NMR integrals of the peak corresponding to methyl units in PDMS at δ = 0.07 ppm and the peak corresponding to the aromatic methyl groups in the polyurethane at δ = 2.11 ppm.

The mole fraction of PDMS is:

$$f_{(mol)\,PDMS} = \frac{\int 0.07ppm/6}{(\int 2.11ppm/3) + (\int 0.07ppm/6)} \tag{4}$$

The mass fraction of PDMS is:

$$f_{(wt)\,PDMS} = \frac{f_{(mol)\,PDMS} \times M_{PDMS}}{\left(f_{(mol)\,PDMS} \times M_{PDMS}\right) + \left(f_{(mol)\,PUR} \times M_{PUR}\right)} \tag{5}$$

$$= \frac{f_{(mol)\,PDMS} \times M_{PDMS}}{\left(f_{(mol)\,PDMS} \times M_{PDMS}\right) + (1 - f_{(mol)\,PDMS} \times M_{PUR})} \tag{6}$$

$$= \frac{f_{(mol)\,PDMS}}{f_{(mol)\,PDMS} + ([1 - f_{(mol)\,PDMS}]\, M_{PUR}/M_{PDMS})} \tag{7}$$

A-3 Calculation of PDMS content in polyurethane particles by elemental analysis

The nitrogen and carbon content in the polyurethane repeat unit are 10.60 and 59.08 wt% respectively. The nitrogen and carbon content in the PDMS repeat unit are 0 and 32.39 wt% respectively.

The weight fraction of PDMS in the sample was thus calculated from nitrogen content by:

$$f_{(wt)}PDMS \;=\; 1 - \frac{f_{(wt\%)\,N}}{10.60} \tag{8}$$

or calculated from carbon content by:

$$f_{(wt)}PDMS = \frac{59.08 - f_{(wt\%)\,C}}{59.08 - 32.39} \tag{9}$$

A-4 Calculation of the difference in PDMS content after dispersion/centrifugation in cyclohexane

The difference in PDMS content after centrifugation/dispersion in cyclohexane (*i.e.* the amount of PDMS removed from the crude particles) was calculated by comparison of the NMR values of the PDMS content in the crude *vs.* washed particles.

At a first glance, this could be calculated by subtracting the value for the washed particles from the value for the crude particles. However, this is not strictly correct, since the PDMS content in the washed particles is calculated as a percentage of the material remaining after the wash and not as a percentage of the crude material.

Thus, in order to calculate the percentage of PDMS removed from the crude particles the following formula can be used:

$$f_{(wt\%)\,removed} = \frac{f_{(wt\%)\,crude} - f_{(wt\%)\,washed}}{1 - (f_{(wt\%)\,washed}/100)} \tag{10}$$

References

1. (a) Silva, A. L.; Bordado, J. C. *Catal. Rev. - Sci. Eng.* **2004,** *46* (2), 31-51; (b) Blank, W. J.; He, Z. A.; Hessell, E. T. *Prog. Org. Coat.* **1999,** *35* (1-4), 19-29.
2. (a) *Revised assessment of the risks to health and the environment associated with the use of the four organotin compounds TBT, DBT, DOT and TPT*; The Scientific Committee on Health and Environmental Risks (SCHER): 2006; (b) *Toxicological Profile for Tin and Tin compounds*; ATSDR (Agency for Toxic Substances and Disease Registry): 2005.
3. EC 782/2003.
4. Kiesewetter, M. K.; Shin, E. J.; Hedrick, J. L.; Waymouth, R. M. *Macromolecules* **2010,** *43* (5), 2093-2107.
5. Zimmerman, R. L.; Renken, T. L. *J. Cell. Plast.* **1989,** *25* (3), 259-269.
6. Daniels, E. S.; Sudol, E. D.; El-Aasser, M. S. in *Polymer Colloids*, ACS Symposium Series: 2001; Vol. 801, pp 1-12.
7. *Plastics – the Facts 2012 An analysis of European plastics production, demand and waste data for 2011*; PlasticsEurope: 2012.
8. Bayer, O.; Siefken, W.; Rinke, H.; Orthner, L.; Schild, H., DRP 728981, 1937.
9. Król, P. *Prog. Mater. Sci.* **2007,** *52* (6), 915-1015.
10. Hashimoto, S. in *International Progress in Urethanes*, Ashida, K.; Frisch, K. C., Eds. Technomic Publishing Co.: Westport, 1981; Vol. 3, pp 43-82.
11. Haider, K. W.; McDaniel, K. G.; Hayes, J. E.; Shen, J., US 7977501, 2011.
12. (a) Schwetlick, K.; Noack, R. *J. Chem. Soc., Perkin Trans. 2* **1995,** (2), 395-402; (b) Spirkova, M.; Kubin, M.; Dusek, K. *J. Macromol. Sci., Chem.* **1987,** *A24* (10), 1151-1166.
13. Odian, G., *Principles of Polymerization*. 4th ed.; Wiley-Interscience: Hoboken, 2004.
14. Kogon, I. C. *J. Org. Chem.* **1959,** *24* (1), 83-86.
15. Kogon, I. C. *J. Org. Chem.* **1961,** *26* (8), 3004-3005.
16. (a) Arnold, R. G.; Nelson, J. A.; Verbanc, J. J. *Chem. Rev.* **1957,** *57* (1), 47-76; (b) Tiger, R. P.; Sarynina, L. I.; Entelis, S. G. *Russ. Chem. Rev.* **1972,** *41* (9), 774.
17. Wegener, G.; Brandt, M.; Duda, L.; Hofmann, J.; Klesczewski, B.; Koch, D.; Kumpf, R. J.; Orzesek, H.; Pirkl, H. G.; Six, C.; Steinlein, C.; Weisbeck, M. *Appl. Catal., A* **2001,** *221* (1-2), 303-335.
18. (a) Flynn, K. G.; Nenortas, D. R. *J. Org. Chem.* **1963,** *28* (12), 3527-3530; (b) Bertoldo, M.; Cappelli, C.; Catanorchi, S.; Liuzzo, V.; Bronco, S. *Macromolecules* **2005,** *38* (4), 1385-1394; (c) Alsarraf, J.; Ammar, Y. A.; Robert, F.; Cloutet, E.; Cramail, H.; Landais, Y. *Macromolecules* **2012,** *45* (5), 2249-2256.
19. Schwetlick, K.; Noack, R.; Stebner, F. *J. Chem. Soc., Perkin Trans. 2* **1994,** (3), 599-608.
20. Renault, B. Elaboration de particules de polyuréthane dans le dioxyde de carbone supercritique: de l'étude des interactions moléculaires à la polymérisation. Ph. D. Thesis, University of Bordeaux I, Bordeaux, 2007.
21. (a) Geoghegan, J. T.; Roth, R. W. *J. Appl. Polym. Sci.* **1965,** *9* (3), 1089-1093; (b) Ulrich, H.; Reymore Jr, H. E.; Sayigh, A. A. R. *J. Polym. Sci. Polym. Chem. Ed.* **1975,** *13* (9), 2031-2033.
22. Katsamberis, D.; Pappas, P. S. *J. Appl. Polym. Sci.* **1990,** *41* (9-10), 2059-2065.

23. Kashio, M.; Sugizaki, T.; Yamamoto, S. i.; Matsuoka, T.; Moriya, O. *Polymer* **2008,** *49* (15), 3250-3255.
24. (a) Richter, R. *Tetrahedron Lett.* **1968,** *9* (48), 5037-5039; (b) Richter, R. *Chem. Ber.* **1968,** *101* (9), 3002; (c) Richter, R.; Trautwein, W. P. *Chem. Ber.* **1969,** *102* (3), 931-937; (d) Arya, V. P.; Shenoy, S. J. *Indian J. Chem., Sect. B: Org. Chem. Incl. Med. Chem.* **1976,** *14B* (10), 763-765.
25. (a) Burkus, J. *J. Org. Chem.* **1962,** *27* (2), 474-476; (b) Titskii, G. D.; Garkusha-Bozhko, I. P. *Ukr. Khim. Zh.* **1993,** *59* (3), 94; (c) Adams, R. K.; Cooper, J. R., US 3173896, 1965; (d) Frauendorfer, E. E.; Klockemann, W. B., US 2003/0144453 A1, 2003.
26. Matsuoka, T.; Harano, K. *Tetrahedron* **1995,** *51* (23), 6451-6458.
27. Monagle, J. J. *J. Org. Chem.* **1962,** *27* (11), 3851-3855.
28. Coutelier, O.; El Ezzi, M.; Destarac, M.; Bonnette, F.; Kato, T.; Baceiredo, A.; Sivasankarapillai, G.; Gnanou, Y.; Taton, D. *Polym. Chem.* **2012,** *3* (3), 605-608.
29. (a) Bantu, B.; Pawar, G. M.; Decker, U.; Wurst, K.; Schmidt, A. M.; Buchmeiser, M. R. *Chem. Eur. J.* **2009,** *15* (13), 3103-3109; (b) Bantu, B.; Pawar, G. M.; Wurst, K.; Decker, U.; Schmidt, A. M.; Buchmeiser, M. R. *Eur. J. Inorg. Chem.* **2009,** (13), 1970-1976; (c) Duong, H. A.; Cross, M. J.; Louie, J. *Org. Lett.* **2004,** *6* (25), 4679-4681.
30. Kemmere, M. F. in *Supercritical Carbon Dioxide in Polymer Reaction Engineering*, Kemmere, M. F.; Meyer, T., Eds. Wiley-VCH: Weinheim, 2005; pp 1-14.
31. (a) Kendall, J. L.; Canelas, D. A.; Young, J. L.; DeSimone, J. M. *Chem. Rev.* **1999,** *99* (2-3), 543-563; (b) Cooper, A. I. *J. Mater. Chem.* **2000,** *10* (2), 207-234.
32. Jessop, P. G.; Leitner, W. in *Chemical Synthesis Using Supercritical Fluids*, Jessop, P. G.; Leitner, W., Eds. Wiley-VCH: Weinheim, 1999; pp 1-36.
33. Baldyga, J.; Henczka, M.; Shekunov, B. Y. in *Supercritical Fluid Technology for Drug Product Development*, York, P.; Kompella, U. B.; Shekunov, B. Y., Eds. Marcel Dekker: New York, 2004; pp 87-150.
34. (a) Lavanchy, F.; Fourcade, E.; de Koeijer, E.; Wijers, J.; Meyer, T.; Keurentjes, J. T. F. in *Supercritical Carbon Dioxide in Polymer Reaction Engineering*, Kemmere, M. F.; Meyer, T., Eds. Wiley-VCH: Weinheim, 2005; pp 37-54; (b) Zetterlund, P. B.; Aldabbagh, F.; Okubo, M. *J. Polym. Sci., Part A: Polym. Chem.* **2009,** *47* (15), 3711-3728.
35. Kirby, C. F.; McHugh, M. A. *Chem. Rev.* **1999,** *99* (2), 565-602.
36. Beckman, E. J. *Chem. Commun.* **2004,** *10* (17), 1885-1888.
37. Sarbu, T.; Styranec, T.; Beckman, E. J. *Nature* **2000,** *405* (6783), 165-168.
38. Sadowski, G. in *Supercritical Carbon Dioxide in Polymer Reaction Engineering*, Kemmere, M. F.; Meyer, T., Eds. Wiley-VCH: Weinheim, 2005; pp 15-35.
39. (a) Girard, E.; Tassaing, T.; Marty, J. D.; Destarac, M. *Polym. Chem.* **2011,** *2* (10), 2222-2230; (b) Chen, J. G.; Liu, X.; Liu, Z. W.; Hu, D. D.; Zhang, C.; Xue, D.; Xiao, J.; Liu, Z. T. *Macromolecules* **2012,** *45* (11), 4907-4919.
40. Bray, C. L.; Tan, B.; Wood, C. D.; Cooper, A. I. *J. Mater. Chem.* **2005,** *15* (4), 456-459.
41. Tuminello, W. H.; Dee, G. T.; McHugh, M. A. *Macromolecules* **1995,** *28* (5), 1506-1510.
42. Fink, R.; Beckman, E. J. *J. Supercrit. Fluids* **2000,** *18* (2), 101-110.
43. (a) Xiong, Y.; Kiran, E. *Polymer* **1995,** *36* (25), 4817-4826; (b) Melnichenko, Y. B.; Kiran, E.; Wignall, G. D.; Heath, K. D.; Salaniwal, S.; Cochran, H. D.; Stamm, M. *Macromolecules* **1999,** *32*, 5344-5347; (c) Liu, K.; Kiran, E. *J. Supercrit. Fluids* **1999,** *16* (1), 59-79; (d) Bayraktar, Z.; Kiran, E. *J. Appl. Polym. Sci.* **2000,** *75*, 1397-1403.

44. (a) Shen, Z.; McHugh, M. A.; Xu, J.; Belardi, J.; Kilic, S.; Mesiano, A.; Bane, S.; Karnikas, C.; Beckman, E.; Enick, R. *Polymer* **2003,** *44*, 1491-1498; (b) Rindfleisch, F.; DiNoia, T. P.; McHugh, M. A. *J. Phys. Chem.* **1996,** *100*, 15581-15587.
45. Lee, H.; Terry, E.; Zong, M.; Arrowsmith, N.; Perrier, S.; Thurecht, K. J.; Howdle, S. M. *J. Am. Chem. Soc.* **2008,** *130* (37), 12242-12243.
46. Lee, H.; Pack, J. W.; Wang, W.; Thurecht, K. J.; Howdle, S. M. *Macromolecules* **2010,** *43* (5), 2276-2282.
47. Birkin, N. A.; Arrowsmith, N. J.; Park, E. J.; Richez, A. P.; Howdle, S. M. *Polym. Chem.* **2011,** *2* (6), 1293-1299.
48. (a) Stoychev, I.; Galy, J.; Fournel, B.; Lacroix-Desmazes, P.; Kleiner, M.; Sadowski, G. *J. Chem. Eng. Data* **2009,** *54* (5), 1551-1559; (b) Galy, J.; Sawada, K.; Fournel, B.; Lacroix-Desmazes, P.; Lagerge, S.; Persin, M. *J. Supercrit. Fluids* **2007,** *42* (1), 69-79.
49. (a) Kazarian, S. G.; Vincent, M. F.; Bright, F. V.; Liotta, C. L.; Eckert, C. A. *J. Am. Chem. Soc.* **1996,** *118*, 1729-1736; (b) Yuan, Y.; Teja, A. S. *J. Supercrit. Fluids* **2011,** *56* (2), 208-212; (c) Dobrowolski, J. C.; Jamroz, M. H. *J. Mol. Struct.* **1992,** *275*, 211-219; (d) Reilly, J. T.; Bokis, C. P.; Donohue, M. D. *Int. J. Thermophys.* **1995,** *16* (3), 599-610.
50. (a) Wang, Y.; Hong, L.; Tapriyal, D.; Kim, I. C.; Paik, I. H.; Crosthwaite, J. M.; Hamilton, A. D.; Thies, M. C.; Beckman, E. J.; Enick, R. M.; Johnson, J. K. *J. Phys. Chem. B* **2009,** *113* (45), 14971-14980; (b) Kilic, S.; Michalik, S.; Wang, Y.; Johnson, J. K.; Enick, R. M.; Beckman, E. J. *Macromolecules* **2007,** *40* (4), 1332-1341; (c) Nelson, M. R.; Borkman, R. F. *J. Phys. Chem. A* **1998,** *102*, 7860-7863; (d) Raveendran, P.; Wallen, S. L. *J. Am. Chem. Soc.* **2002,** *124* (42), 12590-12599.
51. Tan, B.; Woods, H. M.; Licence, P.; Howdle, S. M.; Cooper, A. I. *Macromolecules* **2005,** *38* (5), 1691-1698.
52. Bray, C. L.; Tan, B.; Higgins, S.; Cooper, A. I. *Macromolecules* **2010,** *43* (22), 9426-9433.
53. Tan, B.; Bray, C. L.; Cooper, A. I. *Macromolecules* **2009,** *42* (20), 7945-7952.
54. (a) Ganapathy, H. S.; Hwang, H. S.; Jeong, Y. T.; Lee, W. K.; Lim, K. T. *Eur. Polym. J.* **2007,** *43* (1), 119-126; (b) Hile, D. D.; Pishko, M. V. *J. Polym. Sci., Part A: Polym. Chem.* **2001,** *39* (4), 562-570; (c) Bratton, D.; Brown, M.; Howdle, S. M. *Macromolecules* **2003,** *36* (16), 5908-5911.
55. Thurecht, K. J.; Howdle, S. M. *Aust. J. Chem.* **2009,** *62* (8), 786-789.
56. Mueller, P. A.; Bonavoglia, B.; Storti, G.; Morbidelli, M. in *Supercritical Carbon Dioxide in Polymer Reaction Engineering*, Kemmere, M. F.; Meyer, T., Eds. Wiley-VCH: Weinheim, 2005; pp 105-138.
57. Consani, K. A.; Smith, R. D. *J. Supercrit. Fluids* **1990,** *3* (2), 51-65.
58. Park, E. J.; Richez, A. P.; Birkin, N. A.; Lee, H.; Arrowsmith, N.; Thurecht, K. J.; Howdle, S. M. *Polymer* **2011,** *52* (24), 5403-5409.
59. (a) O'Neill, M. L.; Yates, M. Z.; Johnston, K. P.; Smith, C. D.; Wilkinson, S. P. *Macromolecules* **1998,** *31* (9), 2838-2847; (b) O'Neill, M. L.; Yates, M. Z.; Johnston, K. P.; Smith, C. D.; Wilkinson, S. P. *Macromolecules* **1998,** *31* (9), 2848-2856; (c) Li, G.; Yates, M. Z.; Johnston, K. P.; Howdle, S. M. *Macromolecules* **2000,** *33* (11), 4008-4014.
60. Yates, M. Z.; Shah, P. S.; Johnston, K. P.; Lim, K. T.; Webber, S. *J. Colloid Interface Sci.* **2000,** *227* (1), 176-184.
61. Canelas, D. A.; DeSimone, J. M. *Macromolecules* **1997,** *30* (19), 5673-5682.
62. DeSimone, J. M.; Maury, E. E.; Menceloglu, Y. Z.; McLain, J. B.; Romack, T. J.; Combes, J. R. *Science* **1994,** *265* (15 July), 356-359.

63. (a) Shaffer, K. A.; Jones, T. A.; Canelas, D. A.; DeSimone, J. M.; Wilkinson, S. P. *Macromolecules* **1996,** *29* (7), 2704-2706; (b) Giles, M. R.; Hay, J. N.; Howdle, S. M.; Winder, R. J. *Polymer* **2000,** *41* (18), 6715-6721.
64. Christian, P.; Howdle, S. M.; Irvine, D. J. *Macromolecules* **2000,** *33* (2), 237-239.
65. Baran, N.; Deniz, S.; Akgün, M.; Uzun, I. N.; Dinçer, S. *Eur. Polym. J.* **2005,** *41* (5), 1159-1167.
66. Rosell, A.; Storti, G.; Morbidelli, M.; Bratton, D.; Howdle, S. M. *Macromolecules* **2004,** *37* (8), 2996-3004.
67. Okubo, M.; Fujii, S.; Maenaka, H.; Minami, H. *Colloid Polym. Sci.* **2002,** *280* (2), 183-187.
68. Minami, H.; Kagawa, Y.; Kuwahara, S.; Shigematsu, J.; Fujii, S.; Okubo, M. *Des. Monomers Polym.* **2004,** *7* (6 SPEC. ISS.), 553-562.
69. Fujii, S.; Minami, H.; Okubo, M. *Colloid Polym. Sci.* **2004,** *282* (6), 569-574.
70. Ryan, J.; Aldabbagh, F.; Zetterlund, P. B.; Okubo, M. *Polymer* **2005,** *46* (23), 9769-9777.
71. McHale, R.; Aldabbagh, F.; Zetterlund, P. B.; Okubo, M. *Macromol. Rapid Commun.* **2006,** *27* (17), 1465-1471.
72. Grignard, B.; Stassin, F.; Calberg, C.; Jérôme, R.; Jérôme, C. *Biomacromolecules* **2008,** *9* (11), 3141-3149.
73. (a) Radhakrishnan, B.; Cloutet, E.; Cramail, H. *Colloid Polym. Sci.* **2002,** *280* (12), 1122-1130; (b) Cloutet, E.; Radhakrishnan, B.; Cramail, H. *Polym. Int.* **2002,** *51* (10), 978-985; (c) Chambon, P.; Radhakrishnan, B.; Cloutet, E.; Papon, E.; Cramail, H. *Macromol. Symp.* **2003,** *199,* 47-57; (d) Radhakrishnan, B.; Chambon, P.; Cloutet, E.; Cramail, H. *Colloid Polym. Sci.* **2003,** *281* (6), 516-530.
74. (a) Chambon, P.; Cloutet, E.; Cramail, H. *Macromolecules* **2004,** *37* (16), 5856-5859; (b) Chambon, P.; Cloutet, E.; Cramail, H.; Tassaing, T.; Besnard, M. *Polymer* **2005,** *46* (4), 1057-1066.
75. (a) Renault, B.; Cloutet, E.; Cramail, H.; Tassaing, T.; Besnard, M. *J. Phys. Chem. A* **2007,** *111* (20), 4181-4187; (b) Renault, B.; Tassaing, T.; Cloutet, E.; Cramail, H. *J. Polym. Sci., Part A: Polym. Chem.* **2007,** *45* (23), 5649-5661; (c) Renault, B.; Cloutet, E.; Cramail, H.; Hannachi, Y.; Tassaing, T. *J. Phys. Chem. A* **2008,** *112* (36), 8379-8386; (d) Renault, B.; Cloutet, E.; Lacroix-Desmazes, P.; Cramail, H. *Macromol. Chem. Phys.* **2008,** *209* (5), 535-543.
76. Jessop, P. G. *J. Supercrit. Fluids* **2006,** *38* (2), 211-231.
77. Hobbs, H. R.; Thomas, N. R. *Chem. Rev.* **2007,** *107* (6), 2786-2820.
78. (a) Kobayashi, S.; Makino, A. *Chem. Rev.* **2009,** *109* (11), 5288-5353; (b) Villarroya, S.; Thurecht, K. J.; Heise, A.; Howdle, S. M. *Chem. Commun.* **2007,** (37), 3805-3813; (c) Jérôme, C.; Lecomte, P. *Adv. Drug Delivery Rev.* **2008,** *60* (9), 1056-1076.
79. Abbott, A. P.; Corr, S.; Durling, N. E.; Hope, E. G. *J. Phys. Chem. B* **2004,** *108* (15), 4922-4926.
80. Harmer, M. A.; Hutchenson, K. W. *Chem. Commun.* **2002,** (1), 18-19.
81. Wang, S.; Kienzle, F. *Ind. Eng. Chem. Res.* **2000,** *39* (12), 4487-4490.
82. Chateauneuf, J. E.; Nie, K. *Adv. Environ. Res.* **2000,** *4* (4), 307-312.
83. (a) Vieville, C.; Mouloungui, Z.; Gaset, A. *Ind. Eng. Chem. Res.* **1993,** *32* (9), 2065-2068; (b) Hou, Z.; Han, B.; Zhang, X.; Zhang, H.; Liu, Z. *J. Phys. Chem. B* **2001,** *105* (19), 4510-4513.
84. Shi, M.; Chen, Y.; Xu, B.; Tang, J. *Green Chem.* **2003,** *5* (1), 85-88.
85. Parratt, A. J.; Adams, D. J.; Clifford, A. A.; Rayner, C. M. *Chem. Commun.* **2004,** (23), 2720-2721.
86. Rose, P. M.; Clifford, A. A.; Rayner, C. M. *Chem. Commun.* **2002,** (9), 968-969.

87. Jessop, P. G. in *Supercritical Fluid Technology for Drug Product Development*, York, P.; Kompella, U. B.; Shekunov, B. Y., Eds. Marcel Dekker: New York, 2004; pp 461-496.
88. (a) Kilic, S.; Wang, Y.; Johnson, J. K.; Beckman, E. J.; Enick, R. M. *Polymer* **2009,** *50* (11), 2436-2444; (b) Meredith, J. C.; Johnston, K. P.; Seminario, J. M.; Kazarian, S. G.; Eckert, C. A. *J. Phys. Chem.* **1996,** *100*, 10837.
89. Nigmatov, A. G.; Kuchurov, I. V.; Siyutkin, D. E.; Zlotin, S. G. *Tetrahedron Lett.* **2012,** *53* (27), 3502-3505.
90. Peppel, W. J. *Ind. Eng. Chem.* **1958,** *50* (5), 767-770.
91. (a) Xie, H.; Duan, H.; Li, S.; Zhang, S. *New. J. Chem.* **2005,** *29*, 1199; (b) Dou, X.-Y.; Wang, J.-Q.; Du, Y.; Wang, E.; He, L.-N. *Synlett* **2007**, 3058.
92. He, L. N.; Yasuda, H.; Sakakura, T. *Green Chem.* **2003,** *5* (1), 92-94.
93. Kayaki, Y.; Yamamoto, M.; Ikariya, T. *Angew. Chem., Int. Ed.* **2009,** *48* (23), 4194-4197.
94. Della Ca', N.; Gabriele, B.; Ruffolo, G.; Veltri, L.; Zanetta, T.; Costa, M. *Adv. Synth. Catal.* **2011,** *353* (1), 133-146.
95. Kayaki, Y.; Yamamoto, M.; Ikariya, T. *J. Org. Chem.* **2007,** *72* (2), 647-649.
96. (a) Mizuno, T.; Iwai, T.; Ishino, Y. *Tetrahedron Lett.* **2004,** *45* (38), 7073-7075; (b) Gao, J.; He, L. N.; Miao, C. X.; Chanfreau, S. *Tetrahedron* **2010,** *66* (23), 4063-4067.
97. Patil, Y. P.; Tambade, P. J.; Deshmukh, K. M.; Bhanage, B. M. *Catal. Today* **2009,** *148* (3-4), 355-360.
98. Yoda, S.; Bratton, D.; Howdle, S. M. *Polymer* **2004,** *45* (23), 7839-7843.
99. Blakey, I.; Yu, A.; Howdle, S. M.; Whittaker, A. K.; Thurecht, K. J. *Green Chem.* **2011,** *13* (8), 2032-2037.
100. (a) Heldebrant, D. J.; Yonker, C. R.; Jessop, P. G.; Phan, L. *Energy Environ. Sci.* **2008,** (1), 487-493; (b) Heldebrant, D. J.; Jessop, P. G.; Thomas, C. A.; Eckert, C. A.; Liotta, C. L. *J. Org. Chem.* **2005,** *70* (13), 5335-5338; (c) Jessop, P. G.; Heldebrant, D. J.; Li, X.; Eckert, C. A.; Liotta, C. L. *Nature* **2005,** *436* (7054), 1102.
101. Caraculacu, A. A.; Coseri, S. *Prog. Polym. Sci.* **2001,** *26* (5), 799-851.
102. (a) Moravek, S. J.; Storey, R. F. *J. Appl. Polym. Sci.* **2008,** *109* (5), 3101-3107; (b) Sahre, K.; Elrehim, M. H. A.; Eichhorn, K. J.; Voit, B. *Macromol. Mater. Eng.* **2006,** *291* (5), 470-476.
103. (a) Xu, L.; Li, C.; Ng, K. Y. S. *J. Phys. Chem. A* **2000,** *104* (17), 3952-3957; (b) Parnell, S.; Min, K.; Cakmak, M. *Polymer* **2003,** *44* (18), 5137-5144.
104. (a) Yang, P. F.; Han, Y. D.; Li, T. D.; Li, J. Y. *Chin. Chem. Lett.* **2010,** *21* (7), 853-855; (b) Boitsov, E. N.; Trub, E. P. *Kinet. Catal.* **1984,** *25* (2 pt 1), 221-224.
105. Grepinet, B.; Pla, F.; Hobbes, P.; Swaels, P.; Monge, T. *J. Appl. Polym. Sci.* **2000,** *75* (5), 705-712.
106. Di Giacomo, A. *J. Phys. Chem.* **1961,** *65* (4), 696-697.
107. Renault, B.; Tassaing, T.; Cloutet, E.; Cramail, H. *J. Polym. Sci. A* **2007,** *45*, 5649 - 5661.
108. Suzuki, T.; Tsuge, N.; Nagahama, K. *Fluid Phase Equilib.* **1991,** *67*, 213-226.
109. Höfle, G.; Steglich, W.; Vorbrüggen, H. *Angew. Chem., Int. Ed. Engl.* **1978,** *17* (8), 569-583.
110. (a) Andreev, V. *Russ. J. Org. Chem.* **2009,** *45* (7), 1061-1069; (b) Soo Kim, S.; Rajagopal, G.; Won Kim, D.; Ho Song, D. *Synth. Commun.* **2004,** *34* (16), 2973 - 2980; (c) Liu, X.; Lin, L.; Feng, X. *Acc. Chem. Res.* **2011,** *44* (8), 574-587.
111. Lohmeijer, B. G. G.; Pratt, R. C.; Leibfarth, F.; Logan, J. W.; Long, D. A.; Dove, A. P.; Nederberg, F.; Choi, J.; Wade, C.; Waymouth, R. M.; Hedrick, J. L. *Macromolecules* **2006,** *39* (25), 8574-8583.

112. Baker, J. W.; Davies, M. M.; Gaunt, J. *J. Chem. Soc.* **1949**, 24-27.
113. Arnaud, V.; Le Questel, J. Y.; Mathé-Allainmat, M.; Lebreton, J.; Berthelot, M. *J. Phys. Chem. A* **2004,** *108* (48), 10740-10748.
114. Laurence, C.; Brameld, K. A.; Graton, J.; Le Questel, J. Y.; Renault, E. *J. Med. Chem.* **2009,** *52* (14), 4073-4086.
115. Kondyurin, A.; Klyachkin, Y. *J. Appl. Polym. Sci.* **1994,** *54* (10), 1385-1393.
116. Suchkova, G. G.; Maklakov, L. I. *Vib. Spectrosc.* **2009,** *51* (2), 333-339.
117. (a) Parker, J. A.; Thomas, J. J.; Zeise, C. L. *J. Org. Chem.* **1957,** *22* (5), 594-596; (b) Bailey, M. E.; Kirss, V.; Spaunburgh, R. G. *Ind. Eng. Chem.* **1956,** *48* (4), 794-797; (c) Simons, D. M.; Arnold, R. G. *J. Am. Chem. Soc.* **1956,** *78* (8), 1658-1659.
118. Çoban, M.; Konuklar, F. A. S. *Comput. Theor. Chem.* **2011,** *963* (1), 168-175.
119. (a) Lesar, M.; Zigon, M.; Malavasic, T. *J. Appl. Polym. Sci.* **1993,** *47* (5), 805-814; (b) Kricheldorf, H. R.; Hull, W. E. *Makromol. Chem.* **1981,** *182* (4), 1177-1196; (c) Fu, B.; Feger, C.; MacKnight, W. J.; Schneider, N. S. *Polymer* **1985,** *26* (6), 889-894; (d) Sumi, M.; Chokki, Y.; Nakai, Y.; Nakabayashi, M.; Kanzawa, T. *Makromol. Chem.* **1964,** *78* (1), 146-156.
120. Okuto, H. *Makromol. Chem.* **1966,** *98* (1), 148-163.
121. Furukawa, M.; Yokoyama, T. *J. Polym. Sci. B Polym. Lett. Ed.* **1979,** *17* (4), 175-180.
122. Spirkova, M.; Kubin, M.; Dusek, K. *J. Macromol. Sci., Chem.* **1990,** *A27* (4), 509-522.
123. Vorotyntseva, V. D.; Roginskaya, T. N.; Moleva, V. P.; Tikhonova, T. N.; Finkel'shtein, A. I.; Zagranichnyi, V. I. *J. Appl. Spectrosc.* **1974,** *17* (4), 1317-1320.
124. (a) Barbarini, A.; Maggi, R.; Mazzacani, A.; Mori, G.; Sartori, G.; Sartorio, R. *Tetrahedron Lett.* **2003,** *44* (14), 2931-2934; (b) Pereira, F. S.; deAzevedo, E. R.; da Silva, E. F.; Bonagamba, T. J.; da Silva Agostíni, D. L.; Magalhães, A.; Job, A. E.; Pérez González, E. R. *Tetrahedron* **2008,** *64* (43), 10097-10106; (c) Pérez, E. R.; Da Silva, M. O.; Costa, V. C.; Rodrigues-Filho, U. P.; Franco, D. W. *Tetrahedron Lett.* **2002,** *43* (22), 4091-4093; (d) Pérez, E. R.; Santos, R. H. A.; Gambardella, M. T. P.; De Macedo, L. G. M.; Rodrigues-Filho, U. P.; Launay, J. C.; Franco, D. W. *J. Org. Chem.* **2004,** *69* (23), 8005-8011.
125. Villiers, C.; Dognon, J.-P.; Pollet, R.; Thuéry, P.; Ephritikhine, M. *Angew. Chem., Int. Ed.* **2010,** *49* (20), 3465-3468.
126. Phan, L.; Chiu, D.; Heldebrant, D. J.; Huttenhower, H.; John, E.; Li, X.; Pollet, P.; Wang, R.; Eckert, C. A.; Liotta, C. L.; Jessop, P. G. *Ind. Eng. Chem. Res.* **2008,** *47* (3), 539-545.
127. Huang, S.; Ma, J.; Li, J.; Zhao, N.; Wei, W.; Sun, Y. *Catal. Commun.* **2008,** *9* (2), 276-280.
128. Brzezinski, B.; Schroeder, G.; Rybachenko, V. I.; Kozhevin, L. I. *Spectrochim. Acta, Part A* **2001,** *57* (3), 405-410.
129. (a) Brzezinski, B.; Zundel, G. *J. Mol. Struct.* **1996,** *380* (3), 195-204; (b) Glowiak, T.; Majerz, I.; Sobczyk, L.; Brzezinski, B.; Wojciechowski, G.; Grech, E. *J. Mol. Struct.* **2000,** *526* (1-3), 177-184; (c) Przybylski, P.; Wojciechowski, G.; Brzezinski, B.; Zundel, G.; Bartl, F. *J. Mol. Struct.* **2003,** *661-662* (1-3), 171-182.
130. Fabris, M.; Lucchini, V.; Noè, M.; Perosa, A.; Selva, M. *Chem. Eur. J.* **2009,** *15* (45), 12273-12282.
131. Allen, M. G.; Van Dyke Tiers, G., US Patent 3817939, 1974.
132. Coady, D. J.; Fukushima, K.; Horn, H. W.; Rice, J. E.; Hedrick, J. L. *Chem. Commun.* **2011,** *47* (11), 3105-3107.
133. Martinez, V.; Mecking, S.; Tassaing, T.; Besnard, M.; Moisan, S.; Cansell, F.; Aymonier, C. *Macromolecules* **2006,** *39*, 3978-3979.
134. Kopusov, L. I.; Zharkov, V. V. *J. Appl. Spectrosc.* **1966,** *5* (1), 95-97.

135. (a) Goel, S. K.; Beckman, E. J. *Polym. Eng. Sci.* **1994,** *34* (14), 1137-1147; (b) Goel, S. K.; Beckman, E. J. *Polym. Eng. Sci.* **1994,** *34* (14), 1148-1156; (c) Parks, K. L.; Beckman, E. J. *Polym. Eng. Sci.* **1996,** *36* (19), 2404-2416; (d) Parks, K. L.; Beckman, E. J. *Polym. Eng. Sci.* **1996,** *36* (19), 2417-2431.
136. Huan, K.; Bes, L.; Haddleton, D. M.; Khoshdel, E. *J. Polym. Sci., Part A: Polym. Chem.* **2001,** *39* (11), 1833-1842.
137. Bomfim, J. A. S.; Mincheva, R.; Beigbeder, A.; Persenaire, O.; Dubois, P. *e-Polymers* **2009**, no. 35.
138. Yeh, J. T.; Shu, Y. C. *J. Appl. Polym. Sci.* **2010,** *115* (5), 2616-2628.
139. Matousek, P.; Parker, A. W. *Appl. Spectrosc.* **2006,** *60* (12), 1353-1357.
140. Nardello-Rataj, V.; Caron, L.; Borde, C.; Aubry, J. M. *J. Am. Chem. Soc.* **2008,** *130* (45), 14914-14915.
141. Rajendra, V.; Gonzaga, F.; Brook, M. A. *Langmuir* **2012,** *28* (2), 1470-1477.
142. Rannard, S. P.; Davis, N. J. *Org. Lett.* **1999,** *1* (6), 933-936.
143. Tang, Y.; Dong, Y.; Vennerstrom, J. L. *Synthesis* **2004,** (15), 2540-2544.
144. Love, B. E. *J. Org. Chem.* **2007,** *72* (2), 630-632.
145. (a) Pike, R. A., US2955127, 1960; (b) Jonas, D. A.; Owen, W. J., FR2022318, 1970; (c) Morehouse, E. L., US3402191, 1968.
146. Thomas, T. H.; Kendrick, T. C. *J. Polym. Sci. A-2 Polym. Phys.* **1969,** *7* (3), 537-549.
147. Tung, S. H.; Lee, H. Y.; Raghavan, S. R. *J. Am. Chem. Soc.* **2008,** *130* (27), 8813-8817.
148. (a) Abla, M.; Choi, J. C.; Sakakura, T. *Chem. Commun.* **2001,** (21), 2238-2239; (b) Abla, M.; Choi, J. C.; Sakakura, T. *Green Chem.* **2004,** *6* (10), 524-525; (c) Ion, A.; Van Doorslaer, C.; Parvulescu, V.; Jacobs, P.; De Vos, D. *Green Chem.* **2008,** *10* (1), 111-116.

SYNTHÈSE DE POLYURÉTHANES PAR ORGANO-CATALYSE DANS LE DIOXYDE DE CARBONE SUPERCRITIQUE

Resumé :

La synthèse de particules polyuréthane par organo-catalyse dans le dioxyde de carbone supercritique a été étudiée. Des réactions modèles ont été préalablement conduites et suivies par spectroscopie infrarouge *in situ* dans le CO_2 supercritique afin d'identifier les catalyseurs organiques de réaction d'uréthanisation les plus efficients. Une série de polymères siliconés CO_2-phile, porteurs de la fonction organo-catalytique en bout de chaîne (organo-catasurfs), a ensuite été préparée et testée dans le CO_2 supercritique pour la polymérisation en dispersion de polyuréthane.

Mots-clés : *polyuréthane, dioxyde de carbone supercritique, organo-catalyse, polymérisation en milieu dispersé, polymérisation par étapes, spectroscopie infrarouge in situ, polydimethylsiloxane, catasurfs*

ORGANOCATALYSED SYNTHESIS OF POLYURETHANES IN SUPERCRITICAL CARBON DIOXIDE

Summary:

The organocatalysed synthesis of polyurethane particles in supercritical carbon dioxide has been studied. Model reactions were first carried out in supercritical CO_2 and monitored by *in situ* infrared spectroscopy in order to indentify the most efficient catalysts for the urethanisation reaction. A series of CO_2-philic silicone polymers, end-functionalised with the organocatalytic group (organocatasurfs), were then synthesised and tested in supercritical CO_2 for the dispersion polymerisation of polyurethane.

Keywords: *polyurethane, supercritical carbon dioxide, organocatalysis, dispersion polymerisation, step-growth polymerisation, in situ infrared spectroscopy, polydimethylsiloxane, catasurfs*

Laboratoire de Chimie des Polymères Organiques (LCPO), UMR 5629

Institut des Sciences Moléculaires (ISM), UMR 5255